UNIVERSITY OF SOUTHAMPTON

FACULTY OF ENGINEERING AND THE ENVIRONMENT
School of Civil Engineering and the Environment
Environmental Engineering

Synthesis and Use of Magnetic Nanoparticles for the Adsorption of Mercury from Water

By
Othman M. Hakami

Supervisors
Prof. Charles J. Banks and Dr. Yue Zhang

Thesis for the degree of Doctor of philosophy

June 2012

University of Southampton
Abstract
Faculty of Engineering and the Environment
Civil Engineering and the Environment
Environmental Engineering
Doctor of Philosophy

Synthesis and Use of Magnetic Nanoparticles for the Adsorption of Mercury from Water

By
Othman M. Hakami

This study used magnetite (Fe_3O_4) nanoparticles (NPs), mesoporous silica coated magnetite NPs (SCMNPs) and thiol functionalised silica-coated magnetite nanoparticles (SH-SCMNPs) for Hg(II) removal and recovery from water. The Fe_3O_4 NPs were prepared via conventional co-precipitation methods. Mesoporous silica coating was created on dense liquid-silica coated magnetite NPs (DLSC-Fe_3O_4 NPs) using cetyltri-methyl-ammonium chloride (CTAC) as molecular templates and followed by a sol-gel reaction. SCMNPs were functionalised with 3-MPTMS using the co-condensation method. Functionalisation of SCMNPs with this specific organic group was performed to enhance the selectivity of the magnetic NPs towards Hg(II). The characteristics of these particles were assessed at different stages in the production process. The hydrodynamic particle size distribution increased from an average diameter of ~75 nm for Fe_3O_4 NPs to ~105 nm after silica coating, and was found to be ~111 nm after functionalisation with thiol. The particles were found to be almost spherical with a uniform mesoporous structure with a pore size of ~2.1 nm. The particles were strongly responsive to an external magnetic field making separation from solution possible in less than 1 minute using a permanent magnet.

Batch tests were used to evaluate the feasibility of the prepared NPs for the adsorption and desorption of Hg (II) from synthetic wastewater. SH-SCMNPs displayed a high removal efficiency for Hg(II) uptake, with 90% of Hg(II) removed during the first 5 minutes and equilibrium in less than 15 minutes. The adsorption efficiency was highly pH dependant. Adsorption was not affected by the majority of coexisting cations and anions under the conditions tested. 3 M HCl and thiourea in a 3 M HCl solution was an effective eluent for the desorption of adsorbed-Hg on SCMNPs and SH-SCMNPs respectively. This did not result in the destruction of the nanoparticles and they could subsequently be reused, without loss of their activity, in further adsorption tests. The adsorption characteristics of the particles were quantified in a series of isotherm experiments using Hg(II) solution concentrations of between 40 and 1000 $\mu g\ L^{-1}$ at adsorbent concentrations of 4 and 8 $mg\ L^{-1}$. The adsorption capacity was higher than for other commonly used adsorbents. Both the Langmuir and Freundlich isotherm models were applied to the isotherm data and the maximum adsorption capacity was achieved when the ratio of adsorbent to adsorbate was low.

A semi-continuous method for using the process at a lab scale was developed and was found to be successful in the removal and recovery of Hg(II) and confirmed the results of the batch experiments.

Key words: Mercury, Magnetite NPs, Mesoporous, SH-SCMNPs, Adsorption, Desorption.

List of Contents

List of Tables

List of Figures

DECLARTION of AUTHORSHIP

I, Othman M. Hakami declare that the thesis entitled:

Synthesis and Use of Magnetic Nanoparticles for the Adsorption of Mercury from Water

and the work presented in the thesis are both my own, and have been generated by me as the result of my own original research. I confirm that:

- this work was done wholly or mainly while in candidature for a research degree at this University;
- where any parts of this thesis previously submitted for a degree or any other qualification at this University or any other institution, this has been clearly stated;
- where I have consulted the published work of others, this is always clearly attributed;
- where I have quoted from the works of others, the source is always given. With the exception of such quotations, this thesis is entirely my own work,
- I have acknowledged all main sources of help;
- where the thesis is based on work done by myself jointly with others, I have made clear exactly what was done by others and what I have contributed myself;
- Parts of this work has been published before submission as following:
    1. HAKAMI, O., ZHANG, Y. & BANKS, C. J. 2010. Mercury(II) Ion Adsorption onto Thiol-Functionalized Silica Coated Magnetite Nanoparticles 10th *UK YWP conference, April 2010* University of Cranfield, UK.
    2. HAKAMI, O., ZHANG, Y. & BANKS, C. J. 2010. Synthesis and Characterisation of Magnetite Nanoparticles for Mercury Removal and Recovery from Industrial Effluent. *Postgraduate Research Showcase, Faculty of Engineering, Science and Mathematics. May 2010* University of Southampton.
    3. HAKAMI, O., ZHANG, Y. & BANKS, C. J. 2011. Thiol- functionalised mesoporous silica coated magnetite nanoparticles for high efficient removal and recovery of Hg(II) in synthetic wastewater. *International Water Association Conference: Nano and Water*. Ascona, Switzerland.
    4. HAKAMI, O., ZHANG, Y. & BANKS, C. J. 2012. Thiol-functionalised mesoporous silica-coated magnetite nanoparticles for high efficiency removal and recovery of Hg from water. *Water Research,* 46**,** 3913-3922.

Signed: ……..

Date: …….

Acknowledgments

I would like to thank my supervisors, Prof. Charles J. Banks and Dr. Yue Zhang for their encouragement and help during the last three and a half years. I would not have been able to produce this work without their lively, enthusiastic and energetic approach to research. They led me into the world of nanotechnology for water and wastewater treatment and guided me throughout this research endeavour. They have also been very supportive and have given me the freedom to pursue various ideas without objection. What I learned from them will benefit me throughout my life. I would also like to give thanks to Prof. Trevor W. Tanton and Prof. John Zhou, professor of Environmental Engineering at LSBU for their fruitful discussions and very positive comments during final viva. I am also grateful to Dr. Sonia Heaven for her valuable advices and support.

Special thanks must be given to Dr. Alan G. Howard, ex-senior lecturer in the School of Chemistry for his help and comments during the preparation of nanoparticles. I am grateful to Pillar Pascual-Hidalgo for her technical assistance and advice during my research period in the environmental laboratories and to Dr. Shuncai Wang for operating the TEM and SEM apparatus. I would also like to thank Dr. Maurits de Palenque and Dr. Harold Chong from the Nano Research Group at ECS for their technical support on using the Zetasizer Nano and Raman spectroscopy. Mr. Ross Williams from the NOC has graciously helped in XRD and FTIR spectroscopy measurements. I would also like to thank Mr. Khalid Hassan for his help and assistance in the operation of the BET surface area analyser. Special thanks to Dr. Jamil Renno for proofreading various drafts of this work. I am grateful for the help and support of all the members in the Bio-energy and organic recourses group, past and present, for making my time there so enjoyable.

I would like to acknowledge the Ministry of Higher Education of the Kingdom of Saudi Arabia (University of Jazan) for funding and supporting this PhD work.

Finally, special thanks are due to my immediate family. My wife, Taharh, and my son, Mohannad, provided an endless source of motivation throughout my PhD work. From the bottom of my heart, I would like to thank them for their constant support and unconditional love. Despite the long distance between us, my mother, brothers and sisters have always supported me in whatever and wherever I decided to do and go, therefore, I forever indebted to them. Special thanks go to my brother, Ali, for his advice and support. Much appreciation goes to my sister, Salma for her constant encouragement. I would finally like to thank my late father, Mousa, whose life was not long enough to see this day. Mousa's life has been a constant source of inspiration for me: he never told me how to live, he lived let me watch him. There is no way I can thank him enough except by raising Mohannad the way he raised me.

List of Units and Abbreviations

AA	Atomic absorption
AAS	Atomic absorption spectroscopy
AC	Activated carbon
AFS	Atomic fluorescence spectroscopy
ASTM	The American Society for Testing and Materials
BET	Brunauer- Emmet -Teller
BJH	Barrette-Joyner- Halenda
CTAC	Cetyl-trimethyl-ammonium chloride
CVAFS	Cold vapour atomic fluorescence spectroscopy
DLSC	Dense liquid silica coating
D.W	Deionised water
Hg(II)	Divalent mercury
DLS	Dynamic Light Scattering
ED	Electron Diffraction
EDX	Energy Dispersive X-ray analysis
EPA	Environmental Protection Agency
Hg^0	Elemental mercury
FCC	Face Centered Cubic
FTIR	Fourier transform infrared spectroscopy
HSAB	Hard and soft acids and bases
HAADF	High-angle annular dark field
HRTEM	High Resolution TEM
ICP-MS	Inductively coupled plasma mass spectrometry
ICP-OES	Inductively coupled plasma optical emission spectrometry
IUPAC	International union of pure and applied chemistry
IEP	Isoelectric point
JCPDS	Joint Committee on Powder Diffraction Standards
LCT	Liquid crystal templating
Fe_3O_4	Magnetite
MPTMS	Mercaptopropytrimethoxysilane
Hg	Mercury
$HgCl_2$	Mercuric chloride
HgS	Mercuric sulfide
Hg_2Cl_2	Mercurous chloride
CH_3Hg^+	Methyl mercury
MeHg	Methylation
$\mu g\ L^{-1}$	Microgram per litre

mg L^{-1}	Milligram per litre
mmol	Milimolar
Hg(I)	Monovalent mercury
ng L^{-1}	Nanogram per litre
nm	Nanometer
NPs	Nanoparticles
nZVI	Nanoscale zero-valent iron
pH_{pzc}	Point of zero charge
Pdi	Polydispersity Index
PET	Polyethylene terephthalate
rpm	Revolutions per minute
SCMNPs	Silica-coated magnetite nanoparticles
SEM	Scanning electron microscopy
STEM	Scanning transmission electron microscopy
SPIO	Superparamagnetic Iron Oxide Particles
TEOS	Tetraethoxysilane
TGA	Thermo Gravimetric Analysis
TMOS	Tetramethoxysilane
SH-SCMNPs	Thiol-functionalised mesoporous silica coated magnetite nanoparticles
TEM	Transmission electron microscopy
VSM	Vibrating sample magnetometer
v/v	Volume by volume
WQC	Water quality criteria
XRD	X-ray diffractometer

Chapter 1

Introduction

1.1 Research Background

Mercury (Hg) is a naturally occurring element which is found in air, water and soil, and is one of the most hazardous metals found in the environment. It is also frequently found in wastewater originating from chemical manufacturing, chlor-alkali plants, electrical wiring devices and switches, mining, painting and coating, dental works, nuclear and other industries (Clarkson, 1998; Black and Corporation, 2010) and also by agricultural sources (Veiga et al., 1994). Hg exists in several forms: elemental mercury, inorganic mercury, and organic mercury compounds (Clarkson, 1998). Very low concentration of Hg in water has been recognised as a primary problem that can cause severe physiological and health effects because it can easily pass through the skin and damage the central nervous and endocrine systems (Wu et al., 2007; Wang et al., 2010a). The limit of a maximum guideline concentration of Hg in drinking water and discharge to water are summarised in Table 1.1 which is a comparison between values in the EU drinking water directive (98/83/EC) (Directive, 1998), the WHO guideline values for drinking water quality regulation (WHO, 2006), and the EU discharge to inland surfaces waters directive (2000/60/EEC) (Commission, 2006). The regulated levels of Hg ions in drinking water and wastewater discharges are extremely low and it is a major challenge to decrease the level of Hg to these levels in the large volumes of water in a cost effective manner. For this reason already contaminated ground water resources may not be available for abstraction or use and may also continue to pose an environmental risk.

Table 1.1: Health impacts of Hg, contaminant sources and maximum guideline concentration of mercury in drinking water and wastewater discharges.

Potential health effects from ingestion of water	Short term exposure: gastrointestinal distress Long term exposure: nervous system or kidney damage *	
Sources of contaminant in drinking water	Erosion of natural deposits, discharge from refineries and factories, runoff from landfills and croplands *	
Hg emission (t y^{-1})	Natural sources 2500-3000**	Anthropogenic sources 6000***
	Mercury Regulatory limit (μg L^{-1})	
EU (98/83/EC) 1	WHO 2	EU (2000/60/EEC) 5
Information sources	*Information retrieved on August 12, 2012, from USEPA, (EPA, 2012) ** (Rye, 2010) *** (Pirrone et al., 2009)	

A number of approaches, such as chemical precipitation, volatilisation, electrochemical deposition, oxidation reduction, ion exchange, membrane technologies, and mechanical filtration, have already been employed for the removal of Hg from industrial effluent (Pacheco et al., 2006; Mattigod et al., 2007). Unlike other heavy metals, however, Hg can be recovered through biological treatment by converting Hg^{2+} to Hg^{0}, which can then be removed by adsorption (Otto and Bajpai, 2007). Although the effectiveness of these processes has been sufficiently proved, they present many difficulties and limitations due to high energy requirements, complex operation, incomplete metal removal, and a large volume of sludge production (Xu et al., 2003). Furthermore, increasingly stringent environmental regulations pertaining to discharges containing mercury necessitate the development of technically and economically feasible processes for the removal of mercury from wastewater (Spiegel and Veiga, 2010)

One of the most promising technologies for the removal of low concentrations of heavy metals from water and wastewater is adsorption. This technique has been used for many years and the effectiveness of various adsorbents has been demonstrated in different water and wastewater applications (Babel and Kurniawan, 2003; Brown et al., 2001).

Chapter 1

Adsorption is widely used for the removal of Hg from industrial effluent due to its high performance and low cost (Rezaee et al., 2005). In principle, adsorption can be used not only for the removal of Hg from industrial effluents, but also to recover and recycle Hg back to industrial processes (Paez-Hernandez et al., 2005). For an industrial separation process to work efficiently, whether bulk separation or purification, it is vital for the adsorbent material to possess a high internal volume that is accessible to the elements extracted from the fluid. Moreover, it is essential that the adsorbent have several strong mechanical properties, such as durability and resistance to attrition, and good kinetic properties – that is, it must be capable of transferring adsorbing molecules rapidly to the adsorption sites. In most applications, the adsorbent must be regenerated after use and it is therefore desirable that regeneration be carried out efficiently and without damage to mechanical and adsorptive properties. Finally, in order to compete with other commercially available separation processes, the raw materials and techniques for producing adsorbents must be cost-effective (Bailey et al., 1999; Celis et al., 2000; Thomas and Crittenden, 1998).

Activated carbon (AC) is one of the most common industrial adsorbents used for mercury removal (Bailey et al., 1999; Kurniawan et al., 2006; Namasivayam and Kadirvelu, 1999), yet various studies have shown practical limitations to this method. Even in a well-operated system, regeneration of the carbon may result in a loss of ~15% of the original material; this coupled with the use of complexing agents to improve performance can result in substantial waste generation (Babel and Kurniawan, 2003; Bailey et al., 1999). Fly ash (Rio and Delebarre, 2003), clay (Senevirathna et al., 2011) , Zeolite (Chojnacki et al., 2004) and peat moss (Brown et al., 2001) have also been used as adsorbents because their structure provides sufficient surface area for adsorption. In all cases, however, the presence of an ill-defined pore structure (Hahn et al., 1996; Yoshitake et al., 2002) has a hindering effect on diffusion, which may lead to a decrease in the adsorption rate and the available capacity (Hu et al., 2006). Ideally, the pores of an adsorbent should facilitate the transport of molecules and provide free access. This can be achieved through interlinked pores with a near uniform size distribution (Yoshitake et al., 2002).

Chapter 1

Recently, nanotechnology has been identified as a promising technology for solving many problems and as having an important role in water purification and quality (Diallo and Savage, 2005). The American Society for Testing and Materials (ASTM) defined nanotechnology as "a term referring to a wide range of technologies that measure, manipulate or incorporate materials and or features with at least one dimension between approximately 1 and 100 nanometer (nm)" (ASTM, 2006). Given increase in the methods for environmental remediation and water treatment techniques related to removal that rely on adsorption at the solid-liquid interface, it is only logical to explore a new generations of adsorbent based on nanotechnology for the removal of heavy metals. In comparison with conventional adsorbents and their bulk or micron-scale analogue, nanoparticles (NPs) demonstrate greater specific surface area. This can be translated for more reactive sites with faster kinetics for uptake (Tratnyek and Johnson, 2006). Although nanomaterials may provide better immediate results compared to other water and wastewater techniques, our knowledge of the environmental fate, transport and toxicity of nanomaterials is still in its infancy (Colvin, 2003). It is thus necessary to study the regeneration process of nanomaterials in order to decrease any environmental pollution that may follow their release. There are four classes of nanoscale materials with potential for water purification: (i) metal-containing nanoparticles, (ii) carbonaceous nanomaterials, (iii) zeolite and (iv) dendrimers. These have a broad range of physico-chemical properties that make them particularly attractive for the separation process or as reactive media for water purification (Tiwari et al., 2008). Diallo and Savage (2005) conducted a brief review of the application nanoscale adsorbents in water purification for mitigation of heavy metals. Many kinds of nanomaterials are in various stages of research and development, each possessing a unique functionality that makes them potentially applicable to the remediation of industrial effluents, groundwater, surface water and drinking water. As a result of these developments, nanomaterials that have become available include: nano-sorbent, nanocatalysts, bioactive nanoparticles, nanostructured catalytic membranes, submicron, nanopowder, nanotubes, magnetic nanoparticles, granules, flake, high surface area metals particles supramolecular assemblies with characteristic length scales of 1-100 nm, including clusters,

micromolecules and colloids; all of these could in the future have a significant impact on improving water quality in the natural environment (Diallo and Savage, 2005).

Magnetic (Fe_3O_4) nanoparticles (NPs) have unique properties, such as small size, large surface area, magnetic properties and a high number of active surface sites on Fe_3O_4 NPs. These properties can also lead to an enhancement in adsorption capacities of this sorbent material. These characteristics all contribute to a high adsorption efficiency, high removal rate, and easy and rapidly facilitated separation of the adsorbent from the solution using a magnetic field (Oliveira et al., 2003; Hu et al., 2004). Magnetic composite particles can be designed to have specific physical, chemical and surface properties that allow the selective attachment of ions, molecules, macromolecules, cells, colloidal particles or liquid phases (Warner et al., 2009; Xu and Dong, 2008). Once the target has attached, the use of a magnet provides a very simple and effective method of separating the particles along with their targeted specific group from the aqueous phase. The manufacture of these magnetic composite particles first requires the creation of the nanoparticles and then modification of the surface to match the requirements and constraints of the proposed end use (Hu et al., 2006; Williams, 1994). However, magnetic separation could solve many of the issues associated with conventional methods, such as filtration, centrifugation or gravitational separation, which requires much less energy to achieve a given level of separation (Shipley et al., 2009).

Since discovery in 1992 (Kresge et al., 1992), micro and mesoporous nanomaterials have had a great focus of scientific and technological interest. Due to their high surface area, high porosity, and extremely good catalytic properties, there has been a huge effort to show their potential for applications in many fields, such as materials science, chemistry, medical and biomedical sciences and bioengineering (Kanel and Nepal, 2008). Nanoporous materials have numerous applications in environmental research, as these have good chemical and physical properties, such as a high surface area and high porosity (Kanel et al., 2005); this coupled with high reactivity makes them useful as adsorbents in water and wastewater treatment. Functionalised nanoporous adsorbents are therefore now being studied with respect to their possible use in the removal of

heavy metals from aqueous media (Mamadou et al., 2008; Da'na and Sayari, 2011; Shahbazi et al., 2010; Brown et al., 2000). Among the types examined, those with thiol-functionalised groups have been found to be most efficient for the removal of Hg(II) (Walcarius and Delacôte, 2005). However, the majority of related reports, such as those of Bibby and Mercier (2002), Mattigod et al. (2007), Delacôte et al. (2009a), and Yamauchi et al. (2009) focused on the application of adsorption of Hg(II) onto the modification silica. The sorption mechanism of adsorption of Hg(II) onto thiol-functionalised silica was not examined. With all unique properties of nanoporous materials, mesoporous silica coated magnetite particle can offer simple and rapid separation of Hg loaded magnetic NPs from treated water using an external magnetic field (Dong et al., 2008).

While the application of magnetic nano-sorbent for removing heavy metals is still in its very early stages, new developments are rapidly coming to the surface as the area of nanotechnology is growing fast. Most of these previous studies focus on the adsorption process for the removal of heavy metals from contaminated water, and little exists on factors leading to a decrease of adsorption, such as dissolution, types of eluents and the effect of pH on these ideal sorbents. Studying these factors, along with understanding of the mechanism of adsorption of Hg(II), could lead to the establishment of a good knowledge based on adsorption behaviours and provide the foundation for further studies.

1.2 Research Aim and Objectives

The aim of the research was to develop an adsorption system for the removal and recovery of mercury from water using nanoparticles formed from magnetite. This goal was sought by achieving the following objectives.

1. To syntheses Fe_3O_4 NPs through conventional co-precipitation method and coat them with mesoporous silica (SCMNPs) to obtain in a magnetic nano-sorbent with a large surface area, uniform pores and high magnetic properties. Finally, to functionalise these SCMNPs with a thiol functional group by co-condensation and thus enhance their selectivity towards Hg(II) ions.

2. To study their physical and chemical properties through various physical and chemical instrumental techniques.
3. To identify practical operating conditions for achieving the maximum Hg(II) adsorption and desorption using batch tests.
4. To examine the reusability of the prepared adsorbents.
5. To understand the mechanism of mercury adsorption onto magnetic NPs, including the action and behaviour of any functional chemical groups.
6. To test if the adsorbent could work in real application by developing a semi-continuous system.

1.3 Thesis Overview

The thesis is divided into eight chapters

- Chapter 1(Introduction): briefly presents the background and scope of this work.
- Chapter 2 (Literature review): reviews the literature relating to potential health and environmental impacts of mercury. This chapter also introduces conventional technologies for mercury removal from water and wastewater, along with a summary of fundamental adsorption principles and a state-of-the-art of the mercury removal using adsorption technique. The conventional methods for nanoparticles production, surface modification and their application in environmental protection are also discussed.
- Chapter 3 (Experimental Materials and Methods): describes the methods used in this study for the preparation of Fe_3O_4 NPs, SCMNPs and SCMNPs and SH-SCMNPs. Advanced methods for NPs characterisation are described as well as the analytical method for Hg and other metals ion's determination. The experimental design and batch test procedures are also described.
- Chapter 4 (Characterisation of NPs): the crystallinity and mineral composition, size, morphology, magnetisation and surface charge of Fe_3O_4 NPs, SCMNPs and SH-SCMNPs is described in this chapter.
- Chapter 5 (Adsorption and Desorption of Hg): discusses the application of prepared NPs for the removal and recovery of Hg and the optimising of the operational conditions for mercury removal and recovery in batch system.

- Chapter 6 (Mechanism of Adsorption): mechanism of adsorption is analysed in this chapter using the Langmuir and Freundlich isotherms and advanced analytical techniques.
- Chapter 7 (Semi-Continuous System for Adsorption and Desorption of Hg): taking into account real applications, the semi-continuous system presented the potential application of SH-SCMNPs for the removal and recovery of mercury.
- Chapter 8 (Conclusions and Future Work): the results of this study are summarised in this chapter, and proposals for possible future work are offered.

Chapter 2

Literature Review

2.1 Characteristics of Mercury and its Environmental Impact

2.1.1 Introduction

Mercury (Hg), a highly toxic element, is a major environmental concern (EPA, 2009). Hg is released both naturally into the environment and through human activities. Hg has been used intensively for a number of industrial purposes due to its chemical and physical properties. Hg contamination of the environment by mining activities and industrial wastewater has resulted in the pollution of large areas of soils and sediments worldwide. This is the result of improper disposal or discharge of processed waste streams from abandoned Hg mines, gold mines where Hg is used in an amalgamation process, and where Hg has been released as a by-product of a chemical process. In all cases, these wastewater effluents often contain mercury ions at concentrations above local discharge limits (Tchounwou et al., 2003; Pacheco et al., 2006). There are still many uses of mercury, including the production of chlor-alkali, in electrical wiring devices and switches, measuring and control devices, lighting and dental works. As a result of industrial, domestic and medical activities, the amount of total mercury in the environment is increasing (Hissler and Probst, 2006). The amount of Hg introduced to the earth's atmosphere every year is approximately 5000 tons (Ram et al., 2009).

2.1.1.1 Forms and sources of mercury

Three forms of Hg occur in the environment: elemental (Hg^0), inorganic (Hg (I) and Hg(II) and organic compounds. The physical and chemical properties of Hg compounds are summarised in Table 2.1. Elemental Hg is of considerable importance toxicologically due to its high water solubility (20 mg L^{-1}) and high vapour pressure. Because of its high surface tension, it forms small compact spherical droplets when released into the environment.

Table 2.1: Physical and chemical properties of Hg compounds (Atwood, 2006; EPA, 2007).

Compound	Elemental Mercury	Mercuric Chloride	Mercurous Chloride	Methyl-mercuric Chloride
Molecular formula	Hg^0	$HgCl_2$	Hg_2Cl_2	CH_3HgCl
Molecular weight	200.59	271.52	472.09	251.1
Solubility	20 mg L^{-1} at 25 ˚C	74 g L^{-1} at 20 ˚C	2.0 mg L^{-1} at 25 ˚C	100 mg L^{-1} at 21 ˚C
Density	13.534 g cm^{-3} at 25 ˚C	5.4 g cm^{-3} at 25 ˚C	7.15 g cm^3 at 19 ˚C	4.06 g cm^{-3} at 20 ˚C
Boiling point (˚C)	357	302	384	Not available
Melting point (˚C)	-39	277	302	170
Oxidation state	0	+2	+1	+2

Hg also exists in the inorganic form Hg(I) (mercurous salts) and Hg(II) (mercuric salts) (WHO, 1991). In its most prevalent state, Hg(II), Hg can be ligated to a variety of counterions, including hydroxide, chloride, sulphide. The most common natural form of mercury is mercuric sulphide (HgS - commercially known as cinnabar ore), which has the least water solubility of 10 ng L^{-1} (Atwood, 2006). The most important salts are mercuric chloride ($HgCl_2$), a poison that is highly soluble in water (74 g L^{-1} at 20 ˚C), and mercurous chloride (Hg_2Cl_2), which has low water solubility (2.0 mg L^{-1} at 20 ˚C) (Ullrich et al., 2001; Otto and Bajpai, 2007).

The last form of Hg is organic Hg compounds, which consist of diverse chemical structures in which Hg forms a covalent bond with carbon. Organic Hg compounds include three main groups: 1) alkalimercurials, such methylmercury (CH_3Hg^+) and ethylmercury ($C_2H_5Hg^+$); 2) artylmercurials, such as phenylmercury ($C_6H_5Hg^+$) and 3) the family of alkoxyalkali mercury diuretics (Otto and Bajpai, 2007).

Hg is emitted by both anthropogenic and natural processes. Approximately 80% of the Hg released into the environment comes from human activities, including the burning of fossils, compost incinerators, mining and extraction of Hg from cinnabar, the chlor-alkali industries, pulp and paper industries, paints, fungicides, electrical equipments, instrumentation, amalgamation and dental use. Recent human activities, such as metal smelting, chemical synthesis, medical devices and waste deposal also produce a

considerable amount of Hg emission into atmosphere. The emissions of Hg associated with various anthropogenic activities are summarised in Figure 2.1.

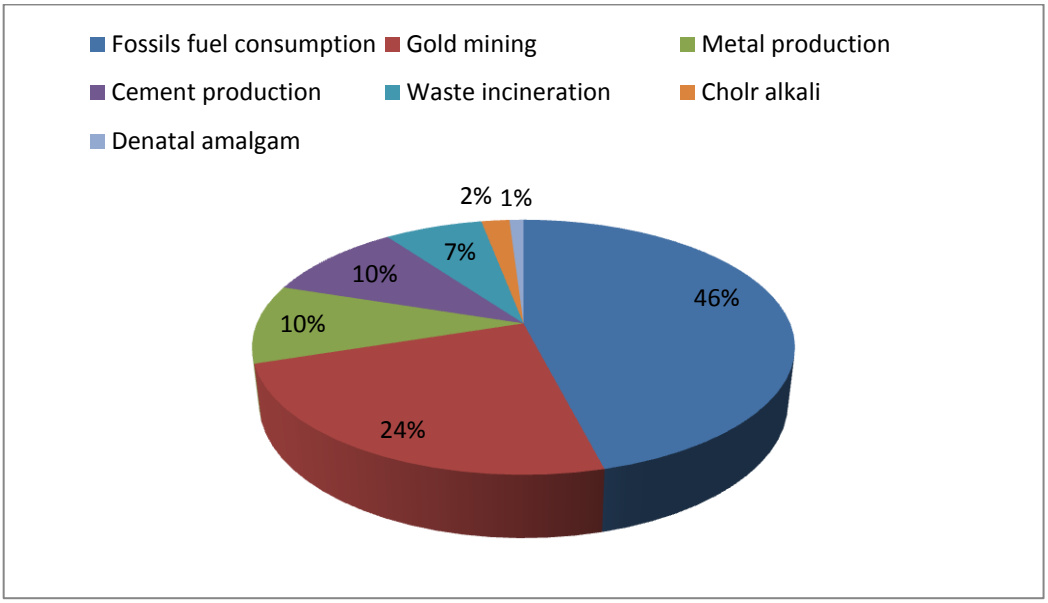

Figure 2.1: Estimated proportion of global anthropogenic mercury emissions in 2008 from different sources (Pacyna et al., 2010).

The earth's crust naturally contains 0.5 parts per million of mercury. This amount is released slowly from rocks and minerals as they erode under normal weathering conditions or volcanic activities (Clarkson, 1998).

2.1.1.2 Transformation of mercury

Hg occurs naturally in the environment and can be found in air, soil and water. It is rarely found as pure liquid metal mercury in nature but rather within compounds and inorganic salts. Its chemistry is complex being present in a number of chemical forms that can be readily transformed from one to another. The transformation into different chemicals forms allows Hg to be transferred between soils, water and air. This mobility has resulted in Hg becoming one of the most global spread pollutants (EPA, 2009).

Due to its chemical properties, Hg can move through various environments and possibly change from one form to another during this process. Three main types of reaction in the Hg cycle determine the Hg transformation between the various forms: oxidation-reduction and methylation- demethylation (Atwood, 2006; Khatoon-Abadi et al., 2008;

Adeniji et al., 2004). In oxidation and reduction reactions, Hg is oxidized to a higher valence state, for example from Hg^0 to Hg^{2+}, and conversely Hg^{2+} is reduced to low valence state. The process to convert inorganic Hg to the toxic methylmercury is called Hg methylation (MeHg). MeHg occurs by bioreaction under aerobic or anaerobic conditions, such as by sulphate-reducing bacteria (SRB). The MeHg occurrence depends on bacteria activity and some chemical factors, such as pH, inorganic Hg concentration in sediments, concentration of dissolved oxygen (DO), temperature and availability of chemical precursor or methyl donor. Normally, methylation takes place in the bottom of sediments but it can also occur in water columns near the oxycline area. The most intense MeHg occurs in transitional oxidising anaerobic zones of natural sediments. Demethylation is a chemical process resulting in the removal of a methyl group (CH_3) from a molecule in biochemical systems. Demethylation can occur under aerobic and anaerobic conditions (EPA, 1997). The Hg transport in the environment is illustrated in Figure 2.2.

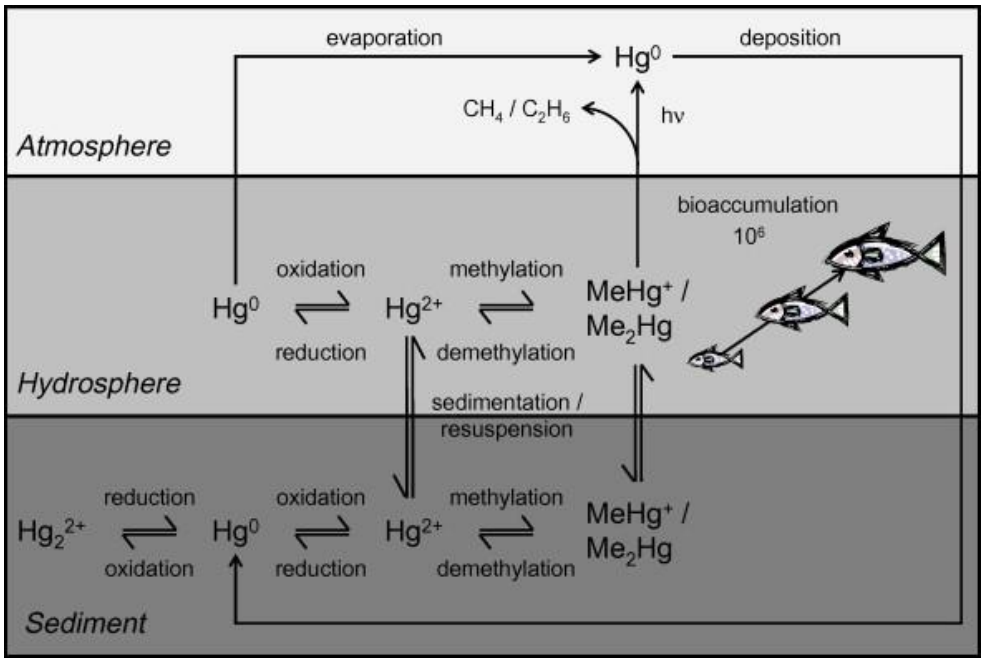

Figure 2.2: Mercury cycle (Leopold et al., 2009).

2.1.1.3 Toxicity of mercury

Hg is one of the most hazardous contaminants that can be found in aquatic environments. High levels of exposure to Hg may lead to neural and brain damage. Brain damage occurs more usually in children than adults due to parental or postnatal exposure (Bittner et al., 1998). The ecological and toxicological impacts of Hg are strongly dependant on its chemical form (Ullrich et al., 2007). The WHO suggested that the intake for adults should be less than 0.3 mg total Hg per person per week, of which no more than 0.2 mg should be methylmercury (O'Neill, 1998).

There are two pathways to the human exposure to Hg; these are: 1) in consumption as methylmercury (CH_3Hg^+) or by breathing vaporous mercury (Hg^0) emitted from various sources, such as metallic mercury, dental amalgams and ambient air; 2) Elemental mercury (Hg^0) itself can be toxic, especially if inhaled, but this element can also be methylated by microorganisms in aquatic systems into its most toxic organic form, methylmercury (CH_3Hg^+), which biomagnifies through the food chain, especially in fish tissue (Malm et al., 1995). In the following, the most common exposure of Hg will be briefly reviewed (Nüßlein et al., 1995):

- Direct :
  1. Inhalation of airborne gases and particles.
  2. Incidental ingestion of contaminated soils.
  3. Ingestion of contaminated drinking water.
  4. Contact with contaminated sediments.
- Indirect:
  1. Ingestion of locally grown vegetables.
  2. Ingestion of locally produced dairy products, such as milk.
  3. Ingestion of meat and fish.

Chronic toxicity is the toxicity impact that lingers or continues for a relatively long period of time.

An improved understanding of the toxic health effects of Hg and its bioaccumulative properties has led to greater regulatory control. For example, the WHO recommends a

maximum mercury level of 2.0 μg L^{-1} in drinking water, although the guidelines in developing countries are still based on US guidelines of 5.0 μg L^{-1} , which is listed under the Clean Water Act (CWA) (EPA, 2007). Also, under the CWA, the US EPA has established ambient water quality criteria (WQC) for Hg and has issued technology based standards for specific industries to control Hg discharge into rivers, streams, lakes and wet lands (Otto and Bajpai, 2007). The EU maximum levels of Hg ions in drinking water is 1.0 μg L^{-1} (Directive, 1998).

2.2 Currently Used Methods for Mercury Removal

2.2.1 Mercury Removal Technologies

The problem of disposing of industrial wastewater is as old as industry itself. Industrial wastes often cause serious water, air and soil pollution. Hg is frequently found from electrolytic production of chlorine and caustic soda in mercury cells (chlor-alkali industry), nuclear, pulp and paper industries, paints, fungicides, electrical equipments, manufacturing of wiring devices and switches, and many other industries (Xu and Dong, 2008). These industries still generate wastewater containing mercury at different concentrations and in different forms. Sometimes, the concentration could be as high as 10 mg L^{-1} (Von Canstein et al., 1999) . It is necessary for these industries to reduce their mercury pollution load to an acceptable level before discharge into the municipal sewer (Paez-Hernandez et al., 2005).

In order to remove Hg contamination from contaminated soil, water and wastewater streams, several technologies have already been employed, including chemical precipitation, volatilisation, electrochemical deposition, oxidation reduction, ion exchange, membrane technology, and mechanical filtration (Paez-Hernandez et al., 2005). However, these methods tend to be either ineffective or extremely expensive when used to remove low metal concentrations in general. Nine technologies have been identified as being able to treat Hg contaminated soil, waste, water and wastewater (as shown in Table 2.2), but only five out of the nine methods have been recommended to remove Hg from water and wastewater. These include: precipitation/co-precipitation,

adsorption, ion exchange membrane filtration and bioremediation (EPA, 2007). Different factors should be considered before choosing a method to remove mercury from aqueous environment. The first important factor in choosing a method is that it must not leave toxic residue that may release Hg in the future and must later be removed by another method. Localisation of the water stream under treatment is very important from an efficiency and cost-saving perspective, and it is necessary to have low-cost materials to treat large volumes of wastewater (Atwood, 2006). Therefore, a selection of the most appropriate treatment for any given waste system, whether consisting of one or more individual metal removal processes, requires accurate determination of the volume and characteristics of the effluent along with bench-scale treatability studies.

Table 2.2: Applicability of mercury treatment technologies (EPA, 2007).

Technology	Soil [a]	Waste [b]	Water	
			Ground & surface water [c]	Wastewater [d]
Solidification/Stabilisation	●	●		
Soil Washing and Acid Extraction	●	●		
Thermal Treatment	●	●		
Vitrification	●	●		
Precipitation/Coprecipitation			●	●
Adsorption			●	●
Ion exchange			●	●
Membrane Filtration				●
Biological Treatment				●

Notes:

[a] Soil includes soil, debris, sludge, sediments and other solid-phase environmental media.

[b] Waste includes nonhazardous and hazardous solid waste generated by industry.

[c] Ground and surface water also includes mine drainage.

[d] Wastewater includes nonhazardous and hazardous industrial wastewater and leaches.

Below, a brief presentation of the five methods currently used to remove toxic heavy metals, including mercury, from water and wastewater.

2.2.1.1 Chemical precipitation process

The conventional technology for the removal of toxic heavy metals, such as Pb, Cu, Zn and Hg, in large industrial plants is chemical precipitation. Metals precipitate from the solution by adding alkali to raise the pH, as shown in Figure 2.3, and the settled sludge is then collected and dewatered before its ultimate disposal (Kamara et al., 1989). Sulphide precipitation is considered the most common precipitation method to remove inorganic Hg from wastewater (EPA, 1998). Precipitation technologies can reduce Hg concentrations to less than 2.0 μg L^{-1}. However, some systems, such as those based on activated carbon polishing, have to use multiple precipitation steps and additional technologies as pre-treatments to reach this level (EPA, 2007).

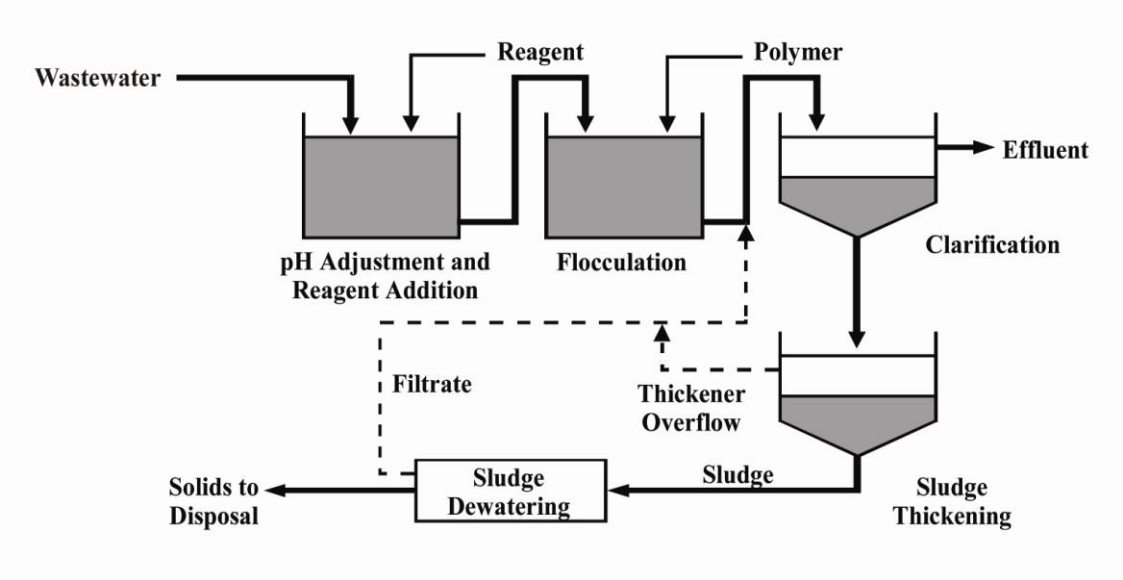

Figure 2.3: Model of precipitation system (EPA, 2007).

As it is very simple and highly efficient technique for removing large quantities of Hg from contaminated water, this method is widely used in industry. However, the presence of other contaminants, both dissolved, colloidal and suspended, may affect precipitation and therefore need to be removed through other processes (Randtke, 1988). The main problems associated with precipitation processes is that they are often

followed by solid/liquid separation processes as a secondary step, low density of solids and the ultimate disposal of the voluminous sludge which often contains a high content of water. The inappropriate disposal of unstable precipitates may cause secondary contaminate of water because metal ions can be leached out from the sludge, returning to the aqueous environment. In addition, a polishing step is required for most precipitation processes in order to achieve low residual levels of metal ions in the processed water (Dong et al., 2008; EPA, 2007).

2.2.1.2 Ion exchange process

Ion exchange is used as a non-consumptive method for selective removal and recovery of heavy metals. The ions are removed from wastewater and concentrated on the exchange resin (Baes et al., 1997). Then, the resin is regenerated. This method is a simple and highly efficient technique for removing even traces of impurities from the solution. Such a process includes the removal of Pb(II), Hg(II), Zn(II), Cd(II) and Cr(III) and Cr(VI) from water and industrial wastewater (Dabrowski et al., 2004). The ion exchange process continues until the solution being treated exhausts the resin exchange capacity. The exhausted resin must be regenerated by other chemicals that replace the ions captured in the ion exchange operation, thus converting the resin back to its original composition for reuse in the next cycle (Xu and Dong, 2008). Generally, ion exchange has many problems for the removal of heavy metals, such as poor wettability, small surface area, poor selectivity, slow adsorption rate and challenges in regeneration (Nam et al., 2003). The presence of suspended solids may affect the effectiveness of ion exchange process. However, in practice for wastewater treatment, ion exchange could not achieve the treatment goal and prefiltration is required to remove suspended solids that might mechanically clog the resin bed (Xu and Dong, 2008).

It is possible to remove Hg(II) from water and industrial wastewater using several types of ion exchangers, such as strongly acidic cation exchangers, weakly and strongly basis anion exchangers as well as selective ion exchangers of various types. However, these methods are particularly useful when treating large volumes of a diluted solution (Larson and Wiencek, 1992). Among many types of ion exchange resins used, total mercury removal (TMR), which was developed by Akazo in 1976 (Dujardin et al.,

2000), was found to be the most efficient for mercury removal (Atwood, 2006). Western European industries have applied the selective ion exchange Imac TMR to remove Hg(II) ions from technological solutions, especially from electrolytic brines (Dabrowski et al., 2004). In order to enhance the affinity of ion exchangers towards Hg(II), the ion exchangers are functionalised with thiocarbamate functional groups. This has the capability to improve the reduction of the ions level from 20 mg L^{-1} to less than 2.0 µg L^{-1}.

2.2.1.3 Membrane filtration process

Membranes are a selective barrier, allowing some constituents to pass while blocking the passage of others. There are four types of membrane filtration techniques, which are classified by pore size: (1) microfiltration (MF), (2) ultrafiltration (UF), (3) nanofiltration (NF), and (4) reverse osmosis (RO) (AWWA, 2005).

For Hg removal, a pre-treatment step should be used to form mercury precipitates that can be more effectively removed by this technology. Then, membranes can reduce concentrations of mercury to less than 2.0 µg L^{-1} (EPA, 2007). Suspended solid, organic compounds and other contaminants can cause membrane fouling during mercury removal operations (Uludag et al., 1997). In order to enhance separation of mercury from aqueous waste, modern membranes are incorporated with functional materials or applied electric current. Generally, membrane filtration is used less than frequently because it tends to produce larger volumes of residual than other mercury treatment technologies (Otto and Bajpai, 2007).

2.2.1.4 Biological treatment process

Although biological treatment has been successfully applied to degrade organic contaminants, it is not applicable to the treatment of Hg contamination of wastewater. It can, however, be used as a treatment by converting soluble ionic mercury (Hg(II)) into element or metallic mercury (Hg^0) that is retained on the biomass where it is more easily removed from the water by another technology, such as adsorption or precipitation (Wagner-Dobler et al., 2000). The simplified model of a biological treatment system is shown in Figure 2.4. In this type of process, pre-treatment should be applied to adjust

the pH of the solution to be in the optimal range at 6.5 to 7.5 using sodium hydroxide and phosphoric acid as optimal for aerobic biotreatment process (EPA, 2007).

The problem associated with biological treatment is that a high concentration of Hg may be toxic to microorganisms used in biological treatment. Also, the presence of sufficient amount of nutrients, such as sucrose and yeast extract, is crucial to the performance of a biological system because nutrients are essential for the growth of microorganisms (Wagner-Dobler et al., 2000; Mattigod et al., 2007). Also, this technique requires an extensive rector setup and for this reason is not suitable for in situ remediation.

Figure 2.4: Model for a biological treatment system (EPA, 2007).

This technique had been used in chlor-alkali plants (Wagner-Dobler et al., 2000; Wagner-Döbler, 2003). They found that after water had remained in the reactor for approximately three hrs, this technique could not achieve the minimum level for discharge and passed through an activated carbon filter to remove any mercury not captured by the bacteria. The other drawback is that the Hg concentration in the incoming wastewater must be regulated, as if it grows too high, the Hg will overwhelm the bacteria and kill them.

2.2.1.5 Adsorption process

Various studies have shown that adsorption techniques are highly efficient in removing heavy metals from water and industrial wastewater without discharging any harmful by-products to the treated water. Effective recovery of adsorbed Hg can also be expected from an adsorption system (Bailey et al., 1999; Babel and Kurniawan, 2003; Pérez-Quintanilla et al., 2006; Nam et al., 2003). Adsorption takes places in most natural, physical, biological and chemical systems and adsorption operations employing solids, such as activated carbon (Skubal and Meshkov, 2002; Ruthven, 1984). The choice of an adsorbent for mercury removal is governed by three criteria: (1) mercury adsorption must be thermodynamically possible, (2) kinetic limitations must not prevent it even at a very low contact time, and (3) in biosorption process, the adsorbent must not lead to the growth of bacteria (Pacheco et al., 2006).

Adsorption of molecules can be represented as a physical or chemical reaction:

$$A + B \leftrightarrow A.B$$

where A is the adsorbate (contaminant), B is the adsorbent and $A.B$ is the adsorbed compound. The most common adsorbents widely used for the removal of Hg from wastewater are activated carbon fly ash and clay (Namasivayam and Kadirvelu, 1999; Babel and Kurniawan, 2003). The common adsorbents for removal of Hg(II) will be discussed in details in following section.

The effectiveness of adsorption is sensitive to many kinds of contaminants in the untreated water. The presence of suspended solids, organic compounds and biological growth can cause fouling and plugging. Pre-treatment using flocculation or filtration is commonly used to reduce organic compounds and suspended solids and enhance adsorption characterization (EPA, 2007).

2.2.1.5.1 Common Hg adsorbents

Apart from the criteria mentioned in the Chapter 1 (Section 1.1), other factors must be considered before choosing an adsorbent for removing Hg from an aqueous environment. One of the most important requirements when making such a choice is that the toxic residue should not generate a new contaminant that will need to be

removed later by another method. Highly efficient and low-cost materials are necessary in the remediation process. For an industrial separation process to work efficiently, whether this be a bulk separation or purification, it is vital for the adsorbent material to possess a high internal volume that is accessible to the elements extracted from the fluid. Moreover, it is essential that the adsorbent must have several strong mechanical properties, such as durability and resistance to attrition, and good kinetic properties – that is, it must be capable of transferring adsorbing molecules rapidly to the adsorption sites. In most applications, the adsorbent must be regenerated after use and it is therefore desirable that regeneration be carried out efficiently and without damage to mechanical and adsorptive properties. It is important to regenerate the adsorbent after most uses, which in turn makes it essential that the regeneration process be conducted efficiently, preventing any damage to the mechanical and adsorptive properties. Most importantly, in order to compete with other commercially available separation processes, the raw materials and techniques used for producing adsorbents must be cost-effective. Finally, the environmental regulations governing the discharge of treated wastewater should be considered, and the amount of sludge or residue generated and their disposal costs (Thomas and Crittenden, 1998; Bailey et al., 1999; Celis et al., 2000). There are many types of adsorbents that have already been investigated, including activated carbon, chitosan, fly ash, clay, natural zeolites and agricultural waste for removing mercury from industrial effluent (Babel and Kurniawan, 2003; Kurniawan et al., 2006; Atwood, 2006). However, most published works using conventional adsorbents have dealt with high and environmentally unrealistic concentrations of mercury (usually more than 20 mg L^{-1}) (Girginova et al., 2010), even knowing that the average mercury concentration from industrial wastewater discharge is less than 10 mg L^{-1} (Von Canstein et al., 1999; Wagner-Döbler, 2003) and that pharmaceutical wastewater contains mercury with average of 3.8 mg L^{-1} (Cyr et al., 2002). This is mostly because the determination of Hg at low concentrations of less than 100 μg L^{-1} is a difficult task. Therefore, the development of new adsorbents with high efficiency for removal of Hg at low concentrations is an extremely important task in wastewater treatment. Below, a brief presentation of the common adsorbents used to remove Hg from water and wastewater is presented.

Activated carbon (AC) has been widely used in industrial applications for Hg removal. AC is classified into four types based on shape and size: powder (PAC), granular (GAC), fibrous (ACF), and clothe (ACC). Due to the different sources of raw materials, the extent of chemical activation, and the physicochemical characteristics, each type of activated carbon has its specific application as well as inherent advantages and disadvantages in wastewater treatment (Lewinsky, 2007). Although a significant number of low-cost adsorbents from various materials have been investigated, commercially activated carbon (CAC) is still the standard sorbent of Hg. Many researchers are continuing to develop and investigate the use of AC for Hg removal (Babel and Kurniawan, 2003). Various studies have reported that the removal efficiency of Hg using GAC was more 60% of total Hg at the range of Hg concentrations 1-30 μg L^{-1} at pH 7.0 (Patterson and Stein, 1997). The equilibrium time for the removal of mercury was more than two hrs and GAC generally cannot be regenerated (Namasivayam and Kadirvelu, 1999). However, some results showed that its regeneration process is complicated (Zhang et al., 1991). PAC is not widely used for removal of mercury as GAC due to low efficiency and the fact that it cannot be regenerated for reuse (Warhurst et al., 1997). As a result of intensive applications of activated carbon, activated carbon has become an expensive material. Another disadvantage is that activated carbon requires complexing agents to improve its removal performance of inorganic Hg (Babel and Kurniawan, 2003). Therefore, the cost-effectiveness of this material is reduced. Recently, activated carbon has ceased to be attractive in small-scale industries because of cost-inefficiency reasons (Dias et al., 2007).

Fly ash is an industrial solid material generated from thermal power plants, such as those located in India during coal combustion. Generally, it is one of the most conventional and cheapest adsorbents having an excellent ability for mercury removal (Patterson and Stein, 1997; El-Mogazi et al., 1988). The disadvantage of using fly ash is that it was reported in many published studies that the adsorption's capacity is generally low, usually between 2.5-6 mg Hg g^{-1}, and also required a large amount of fly ash, which cannot be replaced (Sen and De, 1987; Babel and Kurniawan, 2003).

Peat moss, originally from plants, mainly contains lignin and cellulose as major components. It is widely available and commonly used as a sorbent that has adsorption capabilities for mercury removal. Peat moss is a porous material with a large surface area (>200 m^2 g^{-1}) and can be modified to improve its sorption capacity, so that high efficiency for binding heavy metals can be achieved. Peat moss materials are also relatively inexpensive sorbents and are widely commercially available with an average cost of about US$ 0.023/Kg (Bailey et al., 1999; Babel and Kurniawan, 2003). The peak adsorption of Hg(II) onto peat moss was found at pH ranges between 3.5 and 6.5, and the maximum capacity obtained was 16.2 mg Hg g^{-1}. However, peat moss, like any kind of biosorbent, requires drying and chemical pre-treatment either with acid or alkali to enhance effective performance (Sharma and Forster, 1993).

Clay minerals, such as micas, montmoillonite and kaolinite, have been widely used in mercury removal (Guerra et al., 2009). The adsorption capabilities of clay minerals are the result of a net charge on the structure of very fine-grain silicate minerals. Another factor that contributes to the enhancement of adsorption capabilities is the high surface area of clay minerals (~800 m^2 g^{-1}) (Cadena et al., 1990). In comparison with conventional adsorbents, the adsorption capacity of clay for Hg is very low, usually less than 1 mg g^{-1} (Viraraghavan and Kapoor, 1994; Wang et al., 1985) at Hg concentrations 1000 μg L^{-1}. However, the uptake and adsorption capacity of Hg(II) was enhanced when clay was modified with thiol organic groups (Senevirathna et al., 2011; Manohar et al., 2002). Clay minerals require a high temperature to achieve their adsorption, which increases the cost-effectiveness of this sorbent (Manohar et al., 2002; Brigatti et al., 2005).

Zeolites are naturally occurring as microporous crystalline aluminosilicates consisting of a framework of tetrahedral molecules, linked with each other by oxygen atoms. Zeolites are generally cheap adsorbents and their price is about US$ 0.03-0.12/kg, according to quality (Lin and Juang, 2009). The surface area of zeolites is around 70 m^2 g^{-1}. The mechanism of adsorption is not only physical, but is also based on ion-exchange, where cations bind to negatively charged groups on the sorbent surface (Chojnacki et al.,

2004). Zeolites cannot be regenerated for reuse (Komarowski and Yu, 1997; Lin and Juang, 2009).

Although the above methods have been widely used for removal of Hg from aqueous solutions, most of these materials suffer from inherent problems such as low removal capacity, low selectivity, long equilibrium time or mechanical and thermal instability. Therefore, the development of new sorbents should be governed by the following criteria: the ideal adsorbent should have great stability against coagulation and consist of an insoluble porous material with large active sites. It should be modified with organic groups that can interact with target pollutants. It should achieve fast adsorption with high capacity and good reusability.

2.2.1.5.2 Mechanism of adsorption

Adsorption is the 'process by which liquid or gaseous molecules are concentrated on the surface of a solid' (Seader and Henley, 2012). In some ways, it is like *absorption*, except the liquid-phase *abs*orbent is replaced with a solid-phase *ads*orbent. In the absorption process the solid is captured via surface tension or non-selective penetration, or in other words *absorption* is the 'process by which atoms, molecules or ions enter a bulk phase (liquid, gas, or solid)'. For example, granules used to absorb oil that has spilled on a floor. When a solid exhibits selective uptake, this process is called an *adsorption*.(Albright, 2008). Sorption is a term introduced by J.W. McBain (McBain, 1909), includes selective transfer to the surface and/or into the bulk of a solid or liquid.

Several mechanisms can be involved in adsorption process, such as physical adsorption involving Van der Waals forces and chemical adsorption (Thomas and Crittenden, 1998). The *Adsorbate* is the substance that is removed from liquid phase during the interface. *Adsorbent* is the solid, liquid or gas phase onto which the adsorbate accumulates. Adsorption processes include the attachment of the materials to be adsorbed to the adsorbent at an available adsorption site (Tchobanoglous et al., 2003).

In an adsorption process, molecules, ions or atoms, as shown in Figure 2.5, in a gas or liquid diffuse to the surface of a solid where they bound with the solid surface or are held by intermolecular forces. To achieve a large adsorption surface per unit volume, porous solid particles, such as micro or mesoporous, with small-diameter less than 50

nm, interconnected pores are used. In porous adsorbents, the adsorption occurs on the surface of the active sites of the pores as shown in Figure 2.6.

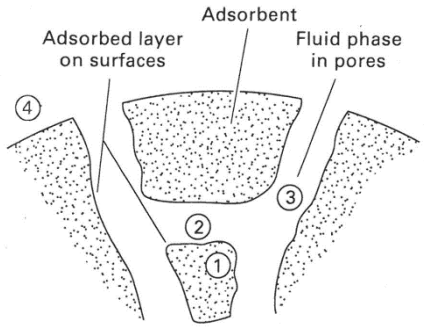

Figure 2.5: Adsorption process on the solid-particles adsorbents (Seader and Henley, 2012) .

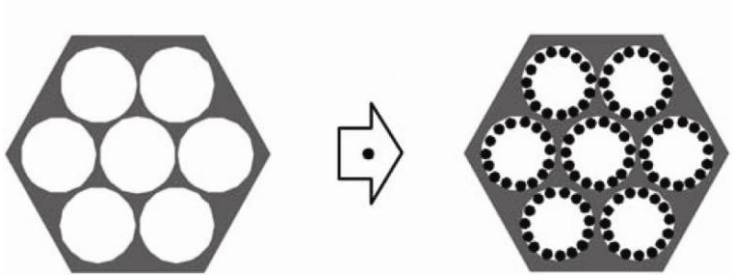

Figure 2.6: Adsorption of metal ions into uniform pore morphology of hexagonal mesoporous silica leads to a grafted material with unrestricted access of ions to all of the functional sites (Walcarius and Mercier, 2010).

The adsorption phenomenon at a surface is essentially an attraction of adsorbate molecules (gaseous or liquid) to the adsorbent surface. The interaction between the adsorbate and the adsorbent is largely the result of binding forces between the individual atoms, ions, or molecules of an adsorbate and the adsorbent surface; all of these forces having their origin in electromagnetic interactions. Adsorption includes physical adsorption, ion exchange and chemical adsorption, depending on the attraction force between adsorbent and adsorbate (Thomas and Crittenden, 1998).

Physical adsorption results from the action of Van der Waals forces, which are comprised of both London dispersion forces and classical electrostatic forces between the solid and the adsorbate. Physical adsorption is relatively non-specific and the adsorbed ions are hence relatively easy to desorb into water phase depending on their

affinity for solids. Exchange adsorption, or ion-exchange, involves electrostatic attachment of ionic species to sites of opposite charge at the surface of an adsorbent, with subsequent displacement of these species by other ionic adsorbates of greater electrostatic affinity. Chemical adsorption, or chemisorptions, involves a reaction between an adsorbate and an adsorbent resulting in a change in the chemical form of the adsorbate. The resulting chemisorptive bond is usually stronger than that derived from the physical Van der Waals forces (Rodrigues et al., 1989; Thomas and Crittenden, 1998). Attachment of adsorbate molecules at functional groups on adsorbent surfaces can also result from specific interactions that do not result in adsorbate transformation. These interactions, designated as "specific adsorptions," exhibit a range of binding energies commonly associated with physical adsorption, electrostatic, chemisorptive, and functional-group interactions. Such interactions broadly define the affinity of an adsorbent for a specific adsorbate. Moreover, the propensity of a given metal bind within a given ligand can be explained by the theory of hard and soft acids and bases (HSAB). Heavy metals are divided into soft acids, such as Hg(II), Pb(II) and Cd(II), or borderline acids, such as Cu(II), Ni(II), Zn(II) based on the HSAB principles of Pearson (Pearson, 1968).

In recent years, the increasing interest in developing new sorbents has meant that surface functionalisation methods have generated much research attention. The key advantage of this method is that the surface of sorbents can be modified to acquire very distinctive properties through the choice of different functional groups, while maintaining the substrate properties (Aguado et al., 2005; Xu and Dong, 2008). Among the types of functional organic groups, Hg is perfectly adsorbed on thiol groups (Mattigod et al., 2007). A new approach for making Hg ions adsorbent is based on the covalent grafting of thiol groups to the framework pore walls of mesoporous NPs molecular sieves with respect to hydroxyl group densities, channel dimensions and morphologies (Kanel and Nepal, 2008). Moreover, the mechanism and capabilities of Hg adsorption of the resulting thiol-functionalised derivatives depend on two factors: the organic groups loading, and the accessibility of Hg(II) to the internal adsorption site (Jal et al., 2004; Aguado et al., 2008). It is well known that soft acids and bases are largely covalent

bound (Pearson, 1963; Pearson, 1968; Nalewajski, 1984). Hg(II) tends to form covalent bonds with reduced sulphur (Hesterberg et al., 2001). The structure of thiol functionalised mesoporous silica after Hg adsorption is illustrated Figure 2.7, as around 50% of silicon centres are functionalised with SH groups and become available for binding to Hg; it is likely that extended Hg-S chains could form within the pores through the bridging of thiol ligands to two mercury centres (Billinge et al., 1997).

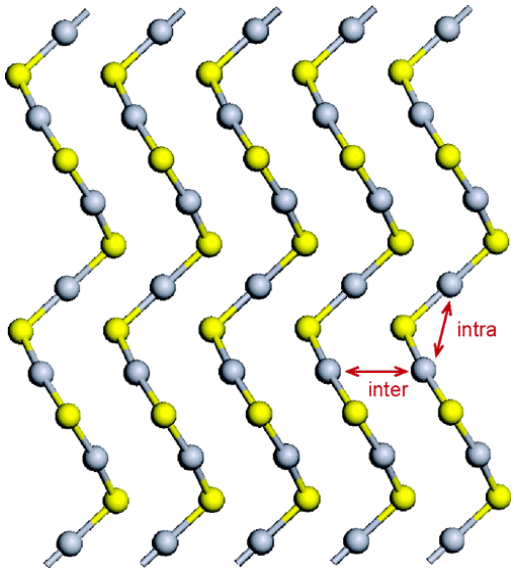

Figure 2.7: Schematic of HgS structure after adsorption (Yellow: S, Grey: Hg) (Billinge et al., 1997).

The mechanism of adsorption of Hg(II) onto SH-SCMNPs will be investigated in this study (Chapter 6) based on HSAB theory and the information obtained from zeta potential, Raman and FTIR spectroscopic study.

2.2.1.5.3 Adsorption isotherm

In order to successfully represent the dynamic adsorptive behaviour of any substance from the fluid to the solid phase, it is important to have a satisfactory description of the equilibrium state between the two phases composing the adsorption system. Generally, the amount of material adsorbed as a function of the concentration of this material remained in the solution at a constant temperature and the resulting function is called an adsorption isotherm (Tchobanoglous et al., 2003). The isotherm plays a crucial

functional role in predictive modeling procedures for analysis and design of adsorption systems.

A variety of isotherm models have been proposed; some of them have a theoretical foundation and some are of a more empirical nature. The Langmuir isotherm model and Freundlich isotherm model have been widely applied. Many criteria give them advantages to be widely used, including simple application and a good description of experimental behaviour in a large range of operating conditions. Furthermore, these isotherm model are characterised by a limited number of adjustable parameters (Thomas and Crittenden, 1998). Below, a brief presentation of the two common adsorption isotherms is presented.

Langmuir isotherm

In the years 1916 to 1918, Langmuir established the adsorption theory to describe gaseous adsorption on planer surfaces (Langmuir, 1918). The Langmuir adsorption isotherm assumes all adsorbates have equal opportunity to adsorb on the surface of the adsorbent and that each adsorbent adsorbs to only one site.

The derivation of the Langmuir adsorption isotherm involves three implicit assumptions:

- The adsorption occurs at a fixed number of definite, localised sites.
- Monolayer adsorption is formed on the surface of the adsorbent.
- The surface of the adsorbent is homogeneous.

There is no lateral interaction between the adsorbate's molecules.

The commonly quoted form is

$$q_e = \frac{Q_e b C_e}{1 + b C_e}, \quad (2.1)$$

and its linear form is

$$\frac{C_e}{q_e} = \frac{1}{Q_0 b} + \frac{C_e}{Q_0}, \quad (2.2)$$

where C_e is the equilibrium concentration (mg L^{-1}), q_e is the amount of metals adsorbed at equilibrium (mg g^{-1}), Q_0 and b are Langmuir constants related to the adsorption capacity and energy, respectively.

The Langmuir isotherm may be modified to describe multiple adsorbate competition as well as adsorbents containing sites with particular affinities (Stumm and Morgan, 1996; Sawyer et al., 2002). Data fitting can be performed using linear and nonlinear regression methods. Caveats do exist for concentration extremes; if the concentration is very high (e.g. $bC_e >> 1$), the q_e will eventually become equal to Q_e. This is denoted by a straight line on the isotherm curve. For very low concentrations (e.g. $bC_e << 1$), the curve is initially a straight line, and q_e increases linearly with C_e.

Deviations often occur from the Langmuir correlation due to the formation of multi-layers at higher adsorbate surface concentrations. Freundlich developed a model that can overcome this limitation by including the effect of heterogeneous adsorption that allows for the formation of multilayer adsorbates (Perry et al., 2008).

The Hg(II) adsorption isotherm of thiol-functionalised mesoporous silica adsorbents usually exhibited typical Langmuir behaviour that is characteristic of chemical adsorption (Chen et al., 1999; Brown et al., 2000; Aguado et al., 2005; Aguado et al., 2008). This observation suggests the adsorption of a monolayer on independent binding sites. However, the adsorbed quantities of Hg(II) were higher than the available thiols (Hg/SH ratio > 1) when experiments were performed with excess Hg. This could be the result of another adsorption as well as binding mechanism that may not be simply predicted. Thus, several investigations were attempted to elucidate this point and techniques such as X-ray absorption spectroscopy (XAS) (Chen et al., 2004), X-ray absorption fine structure spectroscopy (XAFS) (Feng et al., 1997; Kemner et al., 1999) and atomic pair distribution function (PDF) analysis of synchrotron X-ray Powder diffraction data (Billinge et al., 1997) were used to understand the coordination state of Hg(II) once immobilised on the materials. Several forms of monodentate, bidentate and multilayer structure have been reported in the literature depending on the condition used in adsorption experiments. Note that Hg(II) species are also likely to interact with silanol groups located on the silica surface (to form –Si–O–Hg complexes) (Walcarius and Delacôte, 2003), and though the adsorbed Hg(II) quantities via this process remain low, they can contribute to explaining the observation of immobilised mercury in amounts that are higher than the available thiols (Hg/SH ratio > 1).

Freundlich isotherm

The equilibrium relation isotherm is often used to describe adsorption to multi-site or heterogeneous surface across a wide range of adsorbate concentrations (Noll et al., 1991).

The Freundlich isotherm is expressed as

$$q_e = KCe^{\frac{1}{n}} \quad (2.3)$$

and its linear form is given as

$$\log(q_e) = \log(K_f) + n^{-1}\log(C_e) \quad (2.4)$$

where K_f are Freundlich constants incorporating all the factors that affect the adsorption process such as capacity and intensity, and n^{-1} is the Freundlich exponent representing adsorbate change in affinity as adsorption density changes, usually ranging 0.7 to 1.2. This is typically plotted as log (C_e/q_e) versus log (C_e). A good adsorbent is considered to have a Freundlich exponent, n, such that $0.2 < n^{-1} < 0.8$, with smaller values indicating strong adsorbate-adsorbent bonds and consequently, better adsorption (Albright, 2008).

The Freundlich equation is an empirical expression that encompasses the heterogeneity of the surface and the exponential distribution of adsorption sites and their energies (Faust and Aly, 1998). The Freundlich isotherm often provides a better fit for collected data as it accounts for the heterogeneity of the adsorbents, therefore allowing multilayer adsorption on the sorbent. However, it has also drawbacks: it is nonlinear at low concentrations and does not reach the plateau behaviour that can be achieved by using the Langmuir isotherm. Therefore, it is best used for intermediate concentrations (Sawyer et al., 2002). In general, a large number of the experimental results in the field of Van der Waals adsorption can be expressed by means of the Freundlich equation in the medium concentration range (Noll et al., 1991).

The process of the adsorption of Hg(II) from the aqueous phase using Fe_3O_4 NPs can be described as a heterogeneous reaction between solids and liquids (Bayramoğlu and

Arica, 2007). Therefore, the Freundlich isotherm was deemed appropriate to describe the adsorption of mercury on Fe_3O_4 as it accounts for the initial surface adsorption followed by a condensation effect resulting from extremely strong solute-solute interaction.

2.3 Application of Nanoparticles (NPs)

2.3.1 Application of Non-Magnetic NPs for Environmental Protection

Nanotechnology does not just concern the manufacturing of very small structured materials but, more importantly, how these can be used to perform a specific task. In the case of the proposed research, nanomaterials will be used in solving environmental problems. This will be achieved through their utilisation in controlling the emissions from industrial sources discharging mercury. Other example applications in the environmental field are given below.

NPs have been widely used for the treatment of contaminated soils, sediments, water and solid waste using many kinds of non-magnetic NPs (Zhang, 2003), and only three major classes of NPs are widely used for water and wastewater treatment, which include metal containing (ceramic) NPs, Zeolites NPs, and carbonaceous NPs such as, carbon nanotube (CNTs).

Due to their unique properties, CNTs have attracted much research attention. For example, Yue and Economy (2005) used CNTs for the removal of trace contaminants, such as humic acid and aromatic hydrocarbons (benzene, toluene and ρ-Xylane). CNTs have been used for the removal of heavy metal ions such as Pb(II) (Li et al., 2002), Cu(II) (Stafiej and Pyrzynska, 2007), Hg(II) (Tawabini et al., 2010) and Cd(II) (Li et al., 2003) and its capacity was found to be three times higher than that of GAC. Although CNTs have shown good potential in water purification technology, CNTs are not widely used as adsorbents due to their high cost (Harris et al., 2004). Metal NPs are widely used for environmental protection due to their low cost and unique physico-chemical properties and can easily be modified with a variety of organic functional groups. Zero valent iron particles (nZVI) and titanium dioxide (TiO_2) have been intensively used in

environmental protection (Zhang, 2003). nZVI have been used for degrading chlorinated organic through reduction because its reduction speed is faster than natural rates, however, it still can take days (Tratnyek and Johnson, 2006). Although most studies on nZVI focused on the degradation of chlorinated compounds in water, such as trichloroethylene (TCE) or perchloroethylene (PCBs) (He and Zhao, 2005; Kim and Carraway, 2000), there has been some interest in using nZVI for the adsorption of heavy metals such as As(V) (Kanel et al., 2005), AS(III) (Su and Puls, 2001) and Cu(II) (Xiao et al., 2011). The low surface area and presence of dissolved Fe during the adsorption processes at low pH are disadvantages of using nZVI for the adsorption of heavy metals (Ku and Chen, 1992). Another drawback is its sensitivity to oxidation in air and aqueous media (Faraji et al., 2010). Titanium dioxide (TiO_2) NPs have been intensively used for the removal of organic contaminants from various media via oxidation and reduction (Jiang et al., 2007), such as chlorinated alkanes and benzene, dioxins and polychlorinated biphenyls (PCBs) (Obare and Meyer, 2004; Asahi et al., 2001). Due to the toxicity concerns of the TiO_2 NPs and their fate and transport in environment not being well understood at the time (Farré et al., 2009; Farré et al., 2011), TiO_2 NPs were not considered a promising sorbent for the removal of heavy metals. To enhance its separation from a treated water stream using an external magnetic field, TiO_2 NPs was coated with magnetic NPs (Álvarez et al., 2010; Wu et al., 2011). Although porous aluminium oxide (Al_2O_3) NPs with surface area of ~200 $m^2 g^{-1}$ is widely used as adsorbent for filtering contaminates in drinking water (Shan et al., 2009), it did not show a good effect for removal of Hg . In general, Al_2O_3 NPs have ill-defined pore structure, and thus have low adsorption capacities and act in a kinetic manner (Kanel and Nepal, 2008).

Since the discovery of mesoporous silicas, many efforts have been devoted to synthesising mesoporous silica of high surface area and defined size and pore diameter for removing heavy metals from aqueous media. For sorbent preparation, the mesoporous silica is used as a supporting phase to immobilize the extraction agent. The selectivity of the sorbent relies strongly on the affinity of the surface-coated functional ligand for specific pollutants (Xu and Dong, 2008).

Chapter 2

The removal of heavy metals from wastewater using modified mesoporous silicas particles is an interesting subject for many researchers. The surface of mesoporous silica was modified with many organic chelating agents for environmental applications. For instance, mesoporous silica was modified with 3-MPTMS and used for the removal of Hg(II), Cu(II), Zn(II), and Ni(II) from wastewaters. It was found that the adsorption capacity of the metals was not only proportional to the concentration of the thiol (-SH) groups on the surface but was also strongly based on pore size (Aguado et al., 2005; Mattigod et al., 2007; Aguado et al., 2008). Organic chains are adsorbed onto the internal silica structure through C-Si covalent bonding from a monolayer of a functional group. Consequently, it is likely to enhance and control the superficial properties in order to obtain specific sites. These mixtures between organic and inorganic materials have found a range of applications in the adsorption of heavy metals.

There are several studies on the application of functionalised mesoporous silica for the removal of heavy metals from water. The uptake of these cations is based on functional groups fixed on mesoporous silica. Using a batch technique, mercapto-mesoporous silica showed higher affinity for adsorption of Hg(II) from an aqueous solution (Brown et al., 1999; Brown et al., 2000; Chen et al., 1999; Aguado et al., 2008), whereas another divalent cations such as, Cu(II), Zn(II), Cr(VI) and Ni(II) present in wastewater are preferably adsorbed on amino functionalised (-NH) (Lee et al., 2001; Xue and Li, 2008; Aguado et al., 2009). Experimental results showed that the materials are highly efficient for the adsorption of heavy metals at low concentration.

In summary, functionalised mesoporous silica is one of the most widely used adsorbents for removal of heavy metals due to its large surface area and narrow pore distribution. Although the effectiveness of this nano-sorbent has been sufficiently proved, the present high production cost is a major disadvantage (Han et al., 2003), as, importantly, is its surface area, which rapidly decreases with increasing pore size (Deere et al., 2002). Currently, functionalised mesoporous silica coated magnetite NPs with tailored surface functionalities is an ideal candidate for the adsorption of heavy metals due its unique properties; this will be discussed in the following section.

2.3.2 Application of Magnetic NPs for Environmental Protection

Recently, magnetite has come to be of great interest to researchers from a wide range of disciplines, including those working on magnetic fluid catalysis, biotechnology, magnetic resonance imaging and environmental remediation (Schutte and Focke, 2007). Magnetic separation is an effective technique to separate target magnetic particles from aqueous systems. The design of the physical, chemical and surface properties of magnetic composites particles will enable selective attachment of ions, molecules, macromolecules, cells, colloidal particles or liquid phases onto magnetite particles. Therefore, it is obvious that the application of these particles in separation technology offers great flexibility. A key-lock relation in potential application of magnetic composite particles is shown in Figure 2.8, which summarises the various applications of magnetic nanocomposites. The lock varies from metal or toxic species for their potential to solve environmental problems to antigen and streptavidin, as in biological application, while the key could be a specific functional group, antibody or biotin (Xu and Dong, 2008). Engineering magnetic composite particles is an interdisciplinary subject, which requires an integrated approach involving the manufacture and surface modification of appropriate composites with careful attention to the constraints imposed by end users. The properties of these particles are of critical importance to the successful application of the technology (Williams, 1994).

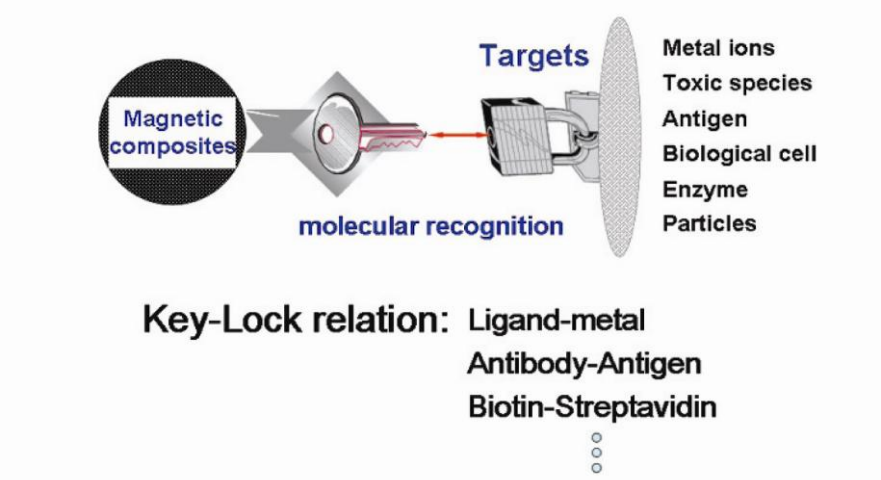

Figure 2.8: Key-lock relation in potential application of magnetic composite particles (Xu and Dong, 2008).

Magnetite (Fe_3O_4) NPs ensure an easy and cheap separation using a strong magnetic field. Due to its magnetic field property, a magnetite is not only an adsorbent for toxic metals removal from a solution, as shown in Figure 2.9, but also a magnetically energizable element for attracting and retaining paramagnetic NPs that can be removed from solution (Hu et al., 2006; Xu and Dong, 2008). Moreover, the toxic metals loaded on the isolated magnetic particles can be stripped off by, for example, acid eluent and the NPs can then be reused.

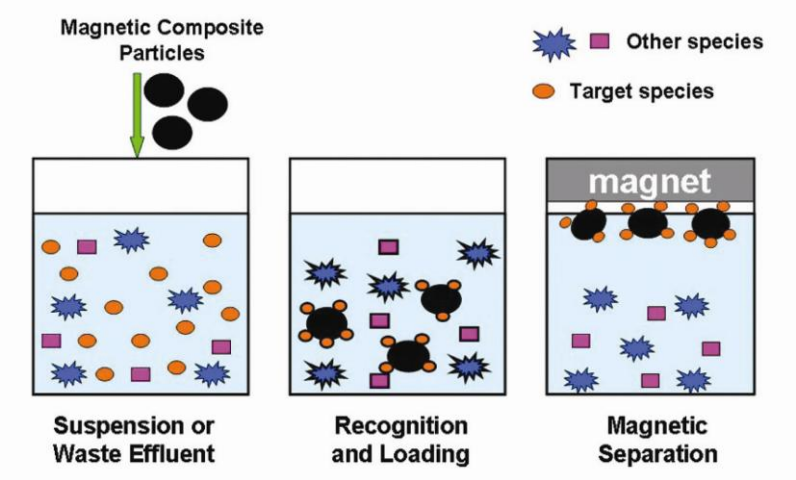

Figure 2.9: Illustration of magnetic separation technology in metal removal from aqueous media (Xu and Dong, 2008).

There are many advantages of using magnetic NPs as an adsorbent: (1) adsorption capacity of magnetite NPs is comparatively high due to its large surface area, (2) simple and rapid separation of metal-loaded magnetic adsorbent from treated water can be achieved via an external magnetic field, (3) no secondary pollutants are produced, (4) the amount of chemicals used is diminished, and (5) magnetite NPs are available commercially and can also be easily synthesised (Tuutijärvi et al., 2009).

Magnetite NPs have been tested and found to be effective in removing and recovering ions of heavy metals, such as Cu(II), Zn(II), Ni(II) and Hg(II) from water and industrial wastewater (Bruce et al., 2004; Hu et al., 2005a; Huang and Hu, 2008; Wang et al., 2010b). Magnetic NPs with added functional groups may have an even greater potential application in industrial wastewater (Figueira et al., 2011; Dong and Xu, 2009). A

number of researchers have used magnetic NPs for the removal of heavy metals from water and wastewater. These have advantages because of their large surface area, which leads to a high adsorption efficiency, fast removal rates, and easy separation from the solution by a magnetic field. The heavy metals can also subsequently be removed from the magnetic particles so that these can be reused and the metal recovered (Oliveira et al., 2003). Hu et al. (2005a) used unmodified magnetite NPs (Fe_3O_4) NPs for the removal of Cr(VI) from industrial wastewater. These NPs were synthesised via sol-gel method and the average diameter of the nanoparticles was ~10 nm. Yean et al. (2005) and Mayo et al. (2007) used magnetic NPs as an adsorbent for the removal and recovery of both As(III) and As(V). The NPs in these cases had a small diameter of ~ 10 nm and showed a high capacity and efficiency for removal of As(III) and As(V). Tuutijärvi et al. (2009) applied three types of magnetic nanoparticles (commercially available, sol-gel prepared, and monochemical made) for the removal of As(V) from water. Adsorption experiments were carried out with different particle sizes varying from 3 nm to 8 nm. These particles were not easily collected with an external magnetic field.

The characteristics of magnetic nanocomposite can be enhanced by silanation to form particles with different functional groups, such as –SH, NH_2 and COOH. These functional groups are selected to be effective for enhanced or selective removal and recovery of pollutants. These include functional groups targeted at heavy metals ions, such as Cu, Zn, Ni and Hg from aqueous solutions (Huang and Hu, 2008; Hu et al., 2005b). In the following section, a brief presentation of the adsorption and desorption of Hg(II) using different kinds of NPs is provided.

2.3.3 Application of NPs for Hg Adsorption

The aim of this brief is to give the current standpoint and trends in the development of NPs for the removal of Hg from aqueous media. Numerous research activities in this area were focused on design and synthesis of NPs with unique structure and chemistry to achieve superior properties in comparison to conventional adsorbent.

A new class of high-performance NPs is silica-based nanoporous functionalised sorbent materials. A number of good reviews have appeared in the literature dealing with the application of these superior adsorbents in the field of water treatment (Adebajo et al.,

2003; Diallo and Savage, 2005; Logar and Kaucic, 2006). Generally, for Hg removal the effort has been mostly concentrated on the incorporation of –SH groups to the mesostructure silica nanomaterials (Aguado et al., 2005). This brief focuses on the most exciting application of this adsorbent for Hg(II) removal. Brown et al. (2000) demonstrated one step synthesis of thiol-functionalised mesoporous structure with pore diameter of about 2.5 nm. The maximum Hg(II) loading capacity was 206 mg Hg g^{-1}. It was found that the rate of Hg(II) uptake was very slow and equilibrium condition was achieved within 24 hrs. Treating Hg-laden adsorbent with 12.1M HCl was found to recover only 60% of Hg(II) ions. Mattigod (2007) developed novel materials by combining synthetic nanoporous substrate with tailored pore size (2-5 nm) and high surface area (approximately 1000 m^2 g^{-1}) with self-assembled monolayers of well ordered thiol functional groups. The maximum capacity was approximately 300 mg Hg g^{-1} of sorbent with very fast kinetic (more than 95% of Hg was adsorption in less than 10 minutes of contact time). Brown (1999) has described the interesting point that the mesoporous silica structure modified with –SH organic groups are apparently characterised by a better selectively for Hg(II) binding (with respect to other metal species) than corresponding amorphous sorbent. A tentative explanation for such an unexpected behaviour was proposed as being on a thermodynamic basis, suggesting the lack of ability of metal cations other than Hg(II) to coordinate within the confined spaces of the regular pore channels. Yoshitake et al. (2002) investigated the efficiency of functionalised mono-layer ($Si{-}CH_2{-}CH_2{-}CH_2{-}SH$) for mercury adsorption. It was found that functionalised mono-layer were extremely efficient in removing mercury. pH has played a key role in removal Hg(II) by silica NPs; however, on the basis of the above mentioned literature, the experiments were usually performed at between pH 4-6. However, thiol-functionalised mesoporous silica has been intensively used for Hg(II) removal and showed high efficiency as summarised in Table 2.3.

Table 2.3: Comparison data for Hg(II) binding to thiol-functionalised mesoporous silica.

Mesoporous materials type	Functionalised methods	Hg(II) adsorption capacity (mg g^{-1})	Equilibrium time (hr)	References
FMMS	SAMMS	234	24	Chen et al., (1999)
HMS	Grafting	20	18	Mercier and Pinnavaia (1997)
	Co-condensation	130.4	24	Brown et al., (1999)
	Co-condensation	172	10	Lee et al.,(2001)
	Co-condensation	170	24	Nooney et al., (2000)
MCM-41	Grafting	48.1	24	Mercier and Pinnavaia, (1998b)
	Co-condensation	160.4	18	Walcarius et al., (2003)
MCM-48	Co-condensation	481.4	48	Delacôte et al., (2009b)
	Grafting	115	24	Gaslain et al.,(2007)
MSU	Co-condensation	104.3	24	Bibby and Mercier(2002),
SBA-15	Co-condensation	52.1	24	Lesaint et al., (2005)
	Co-condensation	148.4	18	Mercier and Pinnavaia,(1998a)

***Abbreviations*:**
FMMS: Functionalised Monolayer on Ordered Mesoporous Silica; HMS: Hexagonal Mesoporous Silica; MCM: Mobil Composition of Matter; MSU: Michigan State University; SBA: Santa Barbara Amorphous; SAMMS: Self-Assembled on Mesoporous Silica.

Magnetic separation is an easy yet effective technique to separate target magnetic particles from complex multiphase systems. As discussed in Section 2.3.2, magnetic NPs can also offer high surface volume ratio, simple methods for the preparation and possibility for surface modification. Although the Fe_3O_4 NPs can be used effectively in the removal of some kinds of heavy metals without further modification, in the case of Hg(II) adsorption it is necessary to modify the surface of Fe_3O_4 NPs with functional organic groups to enhance their adsorption performance (Wee and Bai, 2008). Huang and Hu (2008) described the synthesis procedure for making non-porous structure SCMNPs modified with 3-MPTMS for Hg(II) removal. This NPs shows an equilibrium

Hg(II) adsorption capacity of 83.8 mg Hg g^{-1} at pH 6.0 and rapid adsorption kinetics. Fe_3O_4 NPs modified with humic acid were used for removal of heavy metals including Hg(II). Sorption of the Hg(II) to Fe_3O_4/HA reached equilibrium in less than 15 min. More than 90% of 1 mg L^{-1} Hg(II) was adsorbed using 50 mg L^{-1} of adsorbent at pH 6.0 (Liu et al., 2008). Girginova et al. (2010) synthesised and tested non-porous SCMNPs for Hg(II) removal from water. This sorbent was not quite sufficient, with removal of 74% of Hg(II) at the initial concentration of 50 μg L^{-1}. Donia et al. (2008) tested prepared magnetic chitosan resin modified with thiourea for Hg(II) adsorption, and their result shows that about 90% of Hg(II) removal was achieved within 70 min and maximum uptake was 261.6 mg Hg g^{-1}.

Nevertheless, magnetic and non-magnetic NPs have had a tremendous impact on the adsorption of Hg(II) due to their large surface area, higher reactivity and other described unique properties. The following points need further investigation:

- Regeneration of nano-adsorbents is not widely investigated. A promising nano-sorbent should be regenerated for multiple cycles without a significant decrease in performance in successive runs.
- The optimal uptake conditions for engineering application, such as pH, effect of temperature and effect of shaking speed, should be evaluated in order to enhance the performance of prepared NPs for treatment of real effluents with different chemical composition.
- Although some previous studies have shown an excellent performance of Hg(II) adsorption using NPs, all of them were carried out in a batch operation system for each experimental run. Therefore, in order for these findings to be implemented in industrial applications, all the operation conditions should be used to design a scaled-up continuous system for the continual removal and recovery of Hg(II).
- Although modified mesoporous silica nano-sorbent has been well applied in Hg(II) removal, functionalised mesoporous SCMNPs were not well investigated, and most previous studies indicate disadvantages, such as low adsorption

capacity, slow kinetics and inefficient reuse. All of these drawbacks will limit their practical application.

- The mechanism of the adsorption of Hg(II) onto thiol functionalised mesoporous SCMNPs using sophisticated analytical instruments will assist in the establishment of a good understanding of the behaviour of Hg(II) sorption on this adsorbent.

2.3.4 Desorption and Regeneration of NPs

The raw material conservation and problems of discharge disposal led to the concept of recovery, recycle or reuse of waste materials. Also, the industrial discharge in the environment causes environmental pollution, which is strictly prohibited, and this resulted in the waste treatment concept. There are two main elements that have an impact on the recovery process, economics and technology. The former is the most crucial factor, as uneconomical processes will not be feasible for the industrialists and its implementation will become difficult. Disposal would be favoured when the adsorbent is of low cost, or if it is very difficult to regenerate in case of strong chemical interaction between adsorbates and adsorbents. In the majority of process applications, the disposal of adsorbents as waste is not an economic option and therefore regeneration processes should be carried out either in situ or externally to the adsorption vessel to an extent sufficient that the adsorbent can be reused (Nemerow and Agardy, 1998; Noll et al., 1985).

The research conducted by Diallo and Savage (2005) showed that incorporation of nano-particles and nano-porous particles with water treatment facilities is possible, but one of the major hurdles of nanotechnology application is the cost effective availability of a sufficient amount of high quality nanoparticles. There is a lack of suppliers that can provide this facility, and the unavailability of the nano-material is also due to insufficient awareness in public about its transportation and toxicity in the environment (Colvin, 2003; Lecoanet et al., 2004). This suggests that there is a need to conduct study of the regeneration process of nano-materials so that environmental pollution after their release can be decreased.

Saturation point is ultimately attained by most of the adsorbents, and when there is no regeneration or recycling process, a solid mass of exhausted adsorbents starts accumulating and needs to be disposed of by some means. Regeneration is of significant importance as it helps in the recovery of spent adsorbents, which overall makes the industrial process more economical and allows metals recovered in the process to be exploited in the future for some useful purpose. A high quality adsorbent with an almost 90% efficient regeneration process can be reused for water treatment (Manju et al., 2002). As a result of the strong association of metals with adsorbent, it is possible that a small fraction of metals will be retained inside adsorbent and cannot be regenerated by the regeneration process, which can cause reduction in the sorption capacity in further adsorption process (Billinge et al., 1997; Brown et al., 2000; Walcarius and Delacôte, 2005; Feng et al., 1997).

Practically, a combination of different parameters is employed for the desorption and regeneration of the adsorbent, and it entails high temperature, decreased partial pressure, decreased concentration, washing with inert fluid, replacement of adsorbent with some other strong adsorbent, and alteration in the chemical ambiance such as pH change. It has been noticed that temperature alteration is more effective in bringing a thermodynamic potential change compared to the pressure and selection of regeneration approach based on the economics and technology of the process used (Thomas and Crittenden, 1998). Mineral acids are commonly used in most of desorption processes as a pre-treatment agent (Stirk and Staden, 2002). Hydrochloric acid is commonly used for the elution of metal ions, including Hg(II), from adsorbents due to their high solubility, its common usage in industry and its relatively low cost (Naja and Volesky, 2010).

Nanotechnology research shows promising results in effectively treating metal contaminants to adhere to government regulatory standards. Multiple studies of nanoparticles adsorption of metal contaminants have shown impressive results. Unfortunately, there is less work on the nano-particle recovery and regeneration, which renders this approach unappealing to industrialists. In contrast, traditional adsorbents and bulk media components can be efficiently recovered by the established recovery

methods. It has been found that Fe_3O_4 can be generated over five- cycles of adsorption-desperation using 0.01M NaOH with the recovery of 82.5% of Cr(VI) at the end of the fifth cycle (Hu et al., 2004; Hu et al., 2005b). It was reported that regenerated SCMNPs have 90% of original Cr(VI) retention capacity (Wang and Lo, 2009). HNO_3 (0.1M) and Fe_3O_4 NPs can be consistently used, having no negative impact on Pb(II) adsorption potential (Nassar, 2010). With the use of nanoparticles, the lifetime of adsorbents is observed to be extended, and this ultimately reduces their cost. A new type of adsorbent has been introduced in which functionalized mesoporous particles have been employed, and these particles have a strong chemical association with thiol organic group and Hg(II). This consequently reduces the desorption efficiency of the system (Feng et al., 1997). Some studies have shown that mesoporous particles can be regenerated. According to (Walcarius and Delacôte, 2005; Huang and Hu, 2008), Hg(II) adsorbed on SH groups cannot be quantitatively eluted without thiourea. In Hg(II) laden NH_4 functionalized magnetic mesoporous silica (AMMS), an aqueous basic solution with pH 8.5 was employed for the desorption purposes (Liu and Du, 2011). Regeneration of AMMA adsorbents can be performed using slightly basic environment with a little decrement in the efficiency almost 15%.

2.4 Production of Magnetic NPs

The choice of the Fe_3O_4NPs has three advantages: (1) the synthesis technique can be easily scaled up to produce large quantity of NPs, (2) The highly magnetic properties allow an external magnetic field to be used to bring about rapid separation of the metal-loaded particles from treated water, (3) Fe_3O_4NPs have a large surface area which gives a high number of adsorption sites and a high adsorption.

2.4.1 Physical Synthesising Techniques

Three physical methods are currently commonly used for synthesis and commercial productions of nanomaterials, as briefly reviewed below.

2.4.1.1 High-energy ball milling

High-energy ball milling utilises conventional mechanical grained techniques to break coarse metal grains into micro or nanoscale particles. This is referred to as an "up to down: or top-down" (Li et al., 2006) approach. The heavy deformation of coarser materials is attested by means of a high-energy mill or a high energy shear process. Although this method is very useful in generating commercial quantities of the material, it presents many disadvantages. These include poly-dispersed NPs, small surface area and chemical impurity (Li et al., 2006). The diameter of the produced NPs ranges from 10 to 200 nm (Pilloni et al., 2010) .

2.4.1.2 Inert-gas condensation

Producing NPs by Inert Gas Condensation (IGC) from supersaturated vapours is a conventional technique. The system consists of a vapor source inside a vacuum chamber containing an inert gas, usually argon or helium, mixed with another gas that is selected on the basis of the material to be prepared. The process is generally divided into two steps: first, a metallic nano-phase powder is condensed under inert convention gas after a supersaturated vapour of the metal is obtained inside the chamber. Secondly, the powder obtained is oxidised by mixing another gas in the chamber with it (Baker et al., 2008). IGC has been investigated by many researchers (Nakayama and Yamamoto, 1999; Wang et al., 2004). Sanchez-Lopez et al. (1997) were the first researchers to syntheses nanoscale iron particles through IGC and these had an average diameter of 17 nm. More recently, researchers using the IGC technique to produce magnetic NPs have achieved an average size of between 8 and 25 nm (Li et al., 2006). The high cost is the disadvantage of this method (Wang et al., 2004).

2.4.1.3 Severe plastic deformation

Severe plastic deformation (SPD) was introduced by Bridgman in 1952 (Sus-Ryszkowska et al., 2004). SPD methods provide significant deformations at relatively low temperatures under the high pressures employed. SPD is an efficient technique in producing very fine nanocrystaline structure materials (Pippan et al., 2010), including ultra-fine-grained structures containing mostly high-angle grain boundaries. This method is able to produce magnetic NPs with an average size of between 5 and 30 nm.

This method has the advantage of being versatile and easy to perform and analyse the particles. The main disadvantage of this method is its high cost (Li et al., 2006).

2.4.2 Chemical Synthesising Techniques

Chemistry has played a key role in developing materials with novel and technologically important properties. The advantage of chemical synthesis is its versatility in designing and producing new materials that can be refined into the final product. Chemical methods are not, however, always perfect and there are difficulties in chemical processing to high specifications (Xu and Dong, 2008).

There are eight types of chemical methods for the synthesis of magnetic nanoparticles; these include: sono-chemical, reverse micelle, precipitation, silica-gel, chemical vapour condensation, pulse electro-deposition, liquid flame spray and liquid-phase reduction. However, only four out the aforementioned methods are most commonly used; these are summarised below:

2.4.2.1 Sono-chemical method

This method is expensive and complicated (Grinstaff et al., 1993). Ultrasonic techniques have been used in chemical synthesis of nanostructured materials and rely on high energy sono-chemical reactions that are driven by the formation, growth and collapse of bubbles in a liquid. Nanostructure particles for catalytic applications were sono-chemically synthesised using a volatile organometallic method. This method has been applied to enhance the characterization of nanostructured particles (Vijayakumar et al., 2000). The sonochemical method has the advantage of producing a wide range of particle size (Li et al., 2006).

2.4.2.2 Reverse micelle (or micromulsion) method

The reverse micelle method has been applied to prepare nanoparticles with a very narrow size distribution and highly uniform morphology (Carpenter, 2001). Wiggins et al. (2000) used this method to prepare nanoparticles coated by a thin layer of gold with an average diameter of between 7-25 nm and a uniform size distribution. Some materials, such as dolycol, benzene, sulfonate, styrene and ammonium peroxydisulfate, were applied to improve the stability of this method and produce pure materials of NPs.

(Song et al., 2004). NPs produced by the reverse micelle method have several disadvantages, such as extensive agglomerated NPs that are often generated, poorly crystalline NPs. Producing NPs is not an efficient process with large amounts of solvent often used to yield small quantities (Lee et al., 2005; Narita et al., 2009).

2.4.2.3 Precipitation method

Precipitation is one of the most conventional methods for preparing magnetite NPs (Kang et al., 1996). The advantages of this method are that reaction time is relatively low, water can be used as a solvent and it is easy to obtain high yields by scale-up. The disadvantage of this method is that it is difficult to control the size, size distribution and shape of the formed oxide particles (Mizukoshi et al., 2009). The surface area obtained using this method is relatively high compared to other methods (Guo et al., 2004).

2.4.2.4 Sol-gel method

The sol-gel technology is a commonly used method for producing NPs with a great variety of scientific possibilities and industrial applications. This method was introduced by Iler in 1959 to coat titania with a silica layer from a supersaturated silica solution (Xu and Dong, 2008). This method is useful to prepare a variety of nanomaterials with high purity and low-cost (Zhang, 2003). One disadvantage of this method is the difficulty of controlling the particle size and size distribution (Li et al., 2006). Sol-gel materials can be prepared using alcohol as a solvent with a suitable silica precursor. In this study, sol-gel reaction was used for coating Fe_3O_4 NPs by silica. The most commonly used metal alkoxide resources in the sol-gel processing of silicate are tetraethoxysilane (TEOS) and tetramethoxysilane (TMOS) (Wright and Sommerdijk, 2001).

However, the choice of the sol-gel technique for coating of Fe_3O_4 NPs by silica in this research project was motivated by certain specific advantages: (1) the sol-gel method can produce a large quantity of Fe_3O_4 NPs, (2) the NPs that are obtained from the sol-gel method have a large surface area and high proportion of active surface sites as the density of the hydroxyl group on the NPs is increased and hence improve silane

coupling reaction with the organic group (Hu et al., 2005a; Dong and Xu, 2009) and (3) the chemicals used in the sol-gel reaction are economically favourable.

Coating with the silica-layer is very important as it improves the stability of the NPs and prevents their coagulation with each other. It also prevents the NPs from dissolving in acidic environments, without any crucial change of their magnetic properties (Liang et al., 2009).

2.5 Nanoporous Materials

Ordered nanoporous materials offer huge potential in various fields, such as catalysis, sensors, biological molecular isolation and molecular engineering application. Recently, these materials have generated much research attention for application in water and wastewater treatment as adsorbents, ion exchange media and nano-membrane. This is due to their large surface area, good catalytic properties and high porosity (Crini, 2005; Logar and Kaucic, 2006). The porous structures come from the aggregation or intergrowth of small grains into solid particles, resulting in pores between these grains. In addition, using templating materials during the growth of the particles leads to the generation of pores after the template is removed. Thus, different materials with a variety of pore sizes can be obtained, according to the method of preparation (Sing et al., 1985). The International Union of Pure and Applied Chemistry (IUPAC) has classified porous materials into three groups based on their average size distribution (Davis, 2002):

- Microporous materials, having pore diameters in the range of 2 nm and below.
- Mesoporous materials, having pore diameters in the range of 2 nm to 50 nm.
- Macroporous materials, having pore diameters above 50 nm.

As discussed in Section 2.3.3, micro and mesoporous materials have a strong influence in water and wastewater treatment. Common methods for the preparation of nanoporous materials and their properties are summarised in the following sections.

2.5.1 Microporous Materials

Microporous materials are widely used as adsorbents and catalysts in industry and they have an annual global usage of about 1.6 million tons per year (Norell et al., 1997). Zeolite is the largest and most important subclass of these materials. Zeolites are aluminosilicates riddled with a regular arrays of micropores, and occur naturally in geology (Ozin et al., 2009). Natural zeolite microporous are used intensively in a wide range of environmental protection including water treatment, with an emphasis on heavy metals removal. Due to the large surface area, micropores are particularly useful in the field of the adsorption (Logar and Kaucic, 2006). Fumed silica (Corma, 1997) and Stöber-silica methods (Stober et al., 1968) are the most common methods used for preparing silica microporous materials. The solvent thermal technique at temperature between 100-250 ˚C is the conventional method for the preparation of zeolite micropores (Cundy and Cox, 2005).

2.5.2 Mesoporous Materials

The first successful synthesis of mesoporous materials was in 1992 by Kresge and co-workers at the Mobil Oil Corporation (Kresge et al., 1992). The aim of the general procedure was to examine the efficiency of surfactant supermolecular assemblies as a template for producing mesoporous silica. The general preparation of mesoporous materials are divided into three general steps: synthesis, drying and template removal. Synthesis of silica is the most important step among the three, as the silica characteristics are based on it. Thus, choosing the type of reagent and the reaction conditions is significant in controlling the size and pore diameters of the particles. Five reagents are normally required to synthesize mesoporous silica: a silica precursor, a surfactant, water, alcohol and a catalyst. All the materials except the silica precursor are mixed together to form a micellar. A silica precursor, which is usually TMOS or TEOS, is added to the micellar solution in order to form a mesoporous phase. Three types of pure silica mesophase structures can be formed: hexagonal, which is a 1-d system of hexagonally arrayed cylindrical pores; cubic, which consists of a biocontinuous system of pores; and lamellar, which is a 2-d system of metal oxide sheets interleaved by surfactant bilayers. These are shown in Figure 2.10 (Beck et al., 1992; Raman et al., 1996).

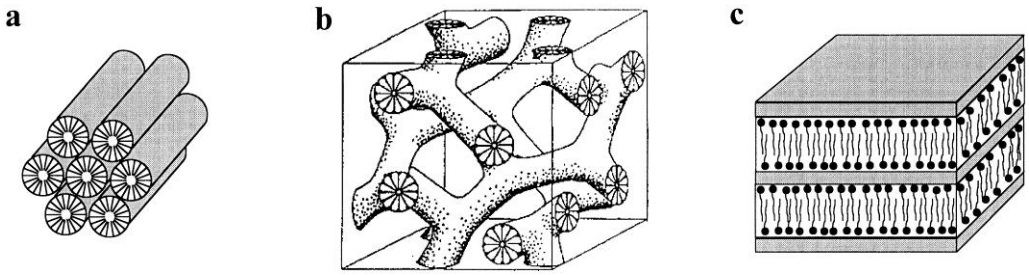

Figure 2.10: The silica-surfactant mesophases structure: (a) hexagonal, (b) cubic bicontinuous, (c) lamellar (Raman et al., 1996).

A dry process then takes place at temperatures between 25 ºC and 45 ºC (Raman et al., 1996). The final step to obtain the microporous structure is the removal of the template. The method and condition for removal of the template can affect pore size and surface area of the product. Among the methods for the removal of the template, the calcination at high temperature in the presence of oxygen and nitrogen was found to be the best method (He et al., 2003). The removal of the template by calcination at very high temperature could lead to a decrease in both pore size and surface area and result in the collapse of the mesoporous channel (Kundu et al., 1998; Hozumi et al., 2000). Thus, it is advisable when removing the surfactant by thermal treatment to keep the calcination temperature lower than 650 ºC, to avoid the collapse of the mesoporous structure.

2.5.3 Nanoporous Materials as Ideal Adsorbents

Nanoporous materials with unique properties have attracted researchers seeking for new kinds of adsorbents. Different kinds of nanoporous materials with varying surface areas, pore sizes (0.03-50 nm) and surface properties have shown a good performance for the adsorption of heavy metals including Hg. The following are the criteria for the best adsorbents, obtained from the research study of Yang (2003), Logar and Kaucic (2006), Ng and Mintova (2008), Theron (2008) and Lu and Zhao (2011):

- Adsorption capacity should be high for an ideal adsorbent, and is affected by the following parameters: surface area, functional group for strong chemical bonds and pore size. Nanoporous materials have all of these unique properties, which lead to a higher adsorption capacity.

- Adsorbate selectivity in a multicomponent mixture is another issue and high selection potential for a particular adsorbate is required in such conditions. The use of different functional groups on the surface of the nanoparticles designed on the theory of HSAB (Hard and soft acids and bases) (for heavy metals) can resolve this issue and improved selectivity for different particles can be attained in comparison with non-porous NPs.
- It is well known that adsorption kinetics are determined by particle pore size (macro, meso and microprosity) of adsorbent. Binder type and amount would also affect the intraparticle transport, and thus the global adsorption process kinetics. The presence of an ill-defined pore structure has a hindering effect on diffusion, which may lead to a decrease in the adsorption rate and the available capacity (Yoshitake et al., 2002). Nanoporous materials have an accessible interlinked pore structure, with uniform size distribution, and this unique structure helps to facilitate the transport of molecules and provide free access. Therefore, no pore blocking occurs during adsorption, which minimizes transport resistance (Campos et al., 2000; Rengaraj et al., 2004).
- Adsorbent material should be stable when exposed to harsh acidic or basic conditions and it should also show stability for high thermal and pressure changes. The adsorbent that shows consistency in its performance even if exposed to harsh ambiance is the ideal one and this assures its extended lifetime. Nanoparticles of Fe_3O_4 that are affected by dipolar magnetism and Van der Waal's forces produce NP agglomeration, which decreases monodispersity and it is unwanted situation in the adsorption process. To overcome such conditions, surfactant is coated on the surface of material as a stabilizing agent, which prevents NP agglomeration and thus improves efficiency of the system.
- Mechanical characteristics of the adsorbent also affect its efficiency and adsorbent material should be resistant to attrition, erosion and crushing when present in adsorption column. Normally, a good adsorbent must have augmented crushing strength, high bulk density and attrition resistant.

In summary, Hg is an extremely toxic substance; a very low concentration of Hg in water has been recognised as a primary problem. Current treatment technologies do not sufficiently remove Hg from aqueous solutions, are expensive, and may need secondary step to enhance their removal. NPs have been identified as having an important role in a promising technology for removal of heavy metals. This research aims to evaluate the effectiveness of Fe_3O_4 NPs, SCMNPs and SH-SCMNPs for Hg(II) removal and recovery at trace level found in industrial wastewater. It is expected that this research will provide understanding for the removal of Hg(II) onto this kind of NPs.

2.6 Physical and Chemical Characterisation Testing of NPs Structure and Function

Techniques that can be used include: (1) X-ray powder diffraction (XRD), (2) fourier transform infrared spectroscopy (FTIR), (3) transmission electron microscopy (TEM) and scanning electron microscopy (SEM), (4) Brunauer, Emmett and Teller (BET) methods (5) vibrating sample magnetometer (VSM), (6), nano-sizer for particle size distribution and zeta potential (7) thermo gravimetric analysis (TGA), and (8) Raman spectroscopy.

2.6.1 X-ray Powder Diffraction (XRD)

Powder X-Ray diffraction (PXRD) is an important and indispensable method in materials science, physics and chemistry. XRD has been recently used to characterise nanomaterials (Jérôme Rose and Brant, 2007). In this study, the XRD technique was employed to analyse quantities of phases present in the sample, the crystallographic unit cell, the crystal structure and the crystallographic texture.

XRD results are obtained by examining the interaction between X-rays and the electrons of atoms. Depending on the atomic arrangement, interferences between the scattered rays are constructive when the path difference between two diffracted rays differs by an integral number of wavelengths. This selective condition is described by the Bragg law:

$$n\lambda = 2d\sin\theta \quad (2.5)$$

where n is an integer, λ is the wavelength of the incident wave, d is the spacing between the planes in the atomic lattice, and θ is the angle between the incident ray and the scattering planes.

2.6.2 Fourier Transform Infrared Spectroscopy (FTIR)

Infrared (IR) radiation refers broadly to a range of the electromagnetic spectrum between the visible and the microwave regions. Generally, the wavelength of organic compounds are located between 400-4000 cm^{-1} (Silverstein et al., 2005). IR spectroscopy is widely used in determining the chemical structure of organic molecules. This technique is based on the absorption of IR radiation by molecules, which causes a change in the vibrational and rotational energy states of the molecules. IR spectroscopy can provide molecular vibrations with frequency in the IR range, identify unknown chemicals by matching the spectra with a known database, determine chemical groups in a specific compound and give optical or electronic properties in the IR range (Schneider et al., 1998).

FT-IR was also used to investigate the mechanism of adsorption, as this is a powerful technique used to identify the iron oxides and oxyhydroxide, which are usually presented in amorphous form. This technique could also provide information about the vibrational state of adsorbed molecules (particularly anions) and hence the nature of the surfaces complex (Wang and Lo, 2009). For a simple molecule, the amount of energy required to change the vibrational energy level from one state to another is related to the molecular vibrational frequency (ν) by Planck's Law:

$$E = h\nu \quad (2.6)$$

where h is Planck's constant and E is energy.

2.6.3 Electron Microscopy (SEM and TEM)

In electron microscopy, a narrow beam of high energy electron is directed at a specimen. Images are formed either by electrons passing through a thin sample via transmission electron microscopy (TEM), or by secondary emission from the surface of a thick sample using so called scanning electron microscopy (SEM) (Goldstein, 2007). Both SEM and TEM are commonly used to study the size, shape and chemical composition of nano-materials. Electron beams generated in electron microscopes have a much shorter

wavelength than light and therefore provide high resolutions images (~ 1 nm). Electron microscopy also provides further information about the chemical composition and crystallography of the material under study (Hoyt, 2007). There are some similarities between the two techniques as both are based on electron microscopy, both provide the possibility of seeing and examining subatomic particles and both allow examining the composition of samples. Images produced from these instruments are highly magnified and have high resolution. However, SEM and TEM also share some differences which are summarised in Table 2.4.

Table 2.4: Difference between SEM and TEM (Goldstein, 2007).

	SEM	TEM
Electron Image	Based on scattered electrons Produce the image of samples after the microscope collects and counts the scattered electrons.	Based on transmitted electrons Electrons are directly pointed towards the sample.
Focus	Only on the sample's surface	On the sample's surface and inside or beyond the surface.
Dimensional	Provides three-dimensional image	Provides two-dimensional image
Magnification	Offers 2 million as a maximum magnification level	Up to a 50 million magnification level

2.6.4 BET Methods

Historically, this method was named after the three scientists who calculated surface area based on the volume which adsorbs to the surface of a given sample (Hoyt, 2007). Isotherm nitrogen adsorption analysis is the most common technique for analysing the surface area of the sample. In addition, this method gives information about the porosity and pore size which are very important for nanoporous materials. The method of evaluating these values involves studying the adsorption and desorption of an inert gas such as nitrogen onto the surface of the solid at liquid temperature and the relative pressure (P/P_0) ranging from 0.05-1, highlighting P_0 as a vapour pressure above a layer of nitrogen that is more than one molecule thick, essentially thought of as a pure bulk liquid.

The BET method is governed by the following equation:

$$\frac{1}{v\left(\frac{p}{p_0}\right)-1} = \frac{c-1}{2a}\left(\frac{p}{p_0}\right)+\frac{1}{v_m c} \quad (2.7)$$

where P and P_0 are the equilibrium and saturation pressure of the adsorbates at the temperature of adsorption, respectively, υ is the volume of the adsorbed gas, a is the weight of adsorbed species, v_m is the volume of the monolayer adsorbed gas and c is the BET constant.

This method is widely used in surface science for the calculation of the surface area of the solid material. The total surface area S_{total} and the specific surface area and S are calculated by the following equations:

$$S_{BET,total} = \left(\frac{v_m N_s}{V}\right) \quad (2.8)$$

$$S_{BET} = \frac{S_{total}}{M} \quad (2.9)$$

where N is Avagadro's number, S is the adsorption cross section and V *is* the molar volume of the adsorbent gas and M is the mass of adsorbent (g).

2.6.5 The Vibrating Sample Magnetometer (VSM)

The vibrating sample magnetometer (VSM) is used to measure the magnetic properties or magnetic behaviour of a magnetic field (Nanomagnetic, 2009). The VSM produces an alternating magnetic field when a sample vibrates in a magnetic field. The alternating magnetic field generates an electric field in the pick-up coils and the flowing current corresponds to the magnetisation of the sample.

2.6.6 Dynamic Light Scattering (DLS) Measurements

DLS is also known as Photon Correlation Spectroscopy, Quasi-elastic Light Scattering (QELS), and Diffusing Wave Spectroscopy (Finsy, 1994). This technique is commonly used to determine the particle size distribution of solid liquid dispersions. Particle size

measurement is an extremely important parameter across most branches of industry. The stability, chemical reactivity, opacity, flow-ability and material strength of many materials are affected by the size and characteristics of the particles within them.

DLS measurements are used to analyse the velocity distribution of particle movement by measuring the dynamic fluctuations of light scattering intensity caused by the Brownian motion of the particle (Murdock et al., 2008). This technique yields a hydrodynamic radius, or diameter, to be calculated via the Stokes-Einstein equation from the aforementioned measurements.

$$D = \frac{K_B T}{6\pi\eta r} \quad (2.10)$$

Where D is the diffusion constant, q is the electrical charge, K_B is Boltzmann's constant, T is the absolute temperature, η is viscosity and r is the radius of the spherical particle.

This eventually yields an overall measurement of the particle perpendicular to the light source at that instant.

2.6.7 Thermo Gravimetric Analysis (TGA)

Thermo gravimetric analysis (TGA) is a technique by which the physicochemical properties (moisture, crystalline water, and/ or volatile components) of a substrate and/or surface reaction products can be probed as a function of temperature, whilst the substrate is subjected to a controlled heating rate. The mass of the sample in a controlled atmosphere is recorded continuously as a function of temperature or time during the heating process. The amount and the rate of weight loss at elevated temperatures are related to the chemical structure and composition of the given samples. In general, a higher temperature is required to decompose more stable materials.

2.6.8 Raman Spectroscopic Study

Raman spectroscopy is a technique that was discovered by the Indian physicist C. Raman in 1928. It is commonly used to study the internal structure of nano crystalline materials. Raman's technique provides accurate information about the molecular pattern, spacing and bonding in solid bulk materials (Jérôme Rose and Brant, 2007).

Materials and Methods

3.1 Chemicals

All chemicals used in Table 3.1 were at least of analytical reagent grade and were used as received without any further purification.

3.2 Synthesis of Nanoparticles

Magnetite (Fe_3O_4) nanoparticles (NPs) were prepared using the conventional co-precipitation method (Kang et al., 1996; Qu et al., 1999). A mesoporous silica coating was synthesised using cetyl-trimethyl-ammonium chloride (CTAC) as a molecular template followed by a sol-gel process (Liu et al., 1998; Wu and Xu, 2005). A 3-mercaptopropytri-methoxysilane (3-MPTMS) functional group was then attached through a silanation reaction (Huang and Hu, 2008). This procedure was divided into four steps as described below and outlined in Figure 3.1 and Figure 3.2. The schematic diagram and corresponding photo of the setup for the synthesis of the NPs are shown in Figure 3.3.

3.2.1 Synthesis of Fe_3O_4 Nanoparticles

The magnetite (Fe_3O_4) NPs were prepared using the co-precipitation method described by Kang et al. (1996) and Qu et al. (1999) with some modifications; the basic reaction is shown below:

$$2Fe^{3+} + Fe^{2+} + 8NH_3 + 4H_2O \rightarrow Fe_3O_4(s) + 8NH_4^+ \qquad (3.1)$$

The procedure was as follows: In a 500 mL round bottomed flask fitted with a condenser and a thermometer, 11.68 g of $FeCl_3 \cdot 6H_2O$ and 4.31 g of $FeCl_2 \cdot 6H_2O$ (Figure 3.1a) were dissolved over a 30-minute period into 200 mL of deionised water which was maintained at 85˚C whilst being vigorously stirred and bubbled with nitrogen gas. After dissolving the ferric and ferrous chloride, and while bubbling nitrogen, ~20 mL of 30% w/v aqueous NH_3 solution was added dropwise into the iron mixture until the colour of

the bulk solution changed from orange to black and the pH increased to 8.0 (checked using broad range universal indicator paper). The nitrogen flow was then turned off to allow the magnetite to precipitate and settle gradually. An external magnetic field was then applied and the black magnetite precipitate was immobilised while the supernatant was removed by decantation. The Fe_3O_4 NPs precipitate was then washed three times with deionised water (3x100 mL), twice with 0.1M NaCl (2x100 mL) and again with deionised water. The Fe_3O_4 NPs were isolated using an external magnetic field and the residual solvent was removed using a freeze drier (VirTis Bench Top 6K, UK). The sample was then dried overnight at 20 m Torr. This yielded a black powder (~ 5.10 g). Finally, the Fe_3O_4 NPs were stored in 125 mL of deionised water. The purity of Fe_3O_4 NPs was verified by the X-ray powder diffractometer (XRPD) and this will be described in Chapter 4 (section 4.2.1).

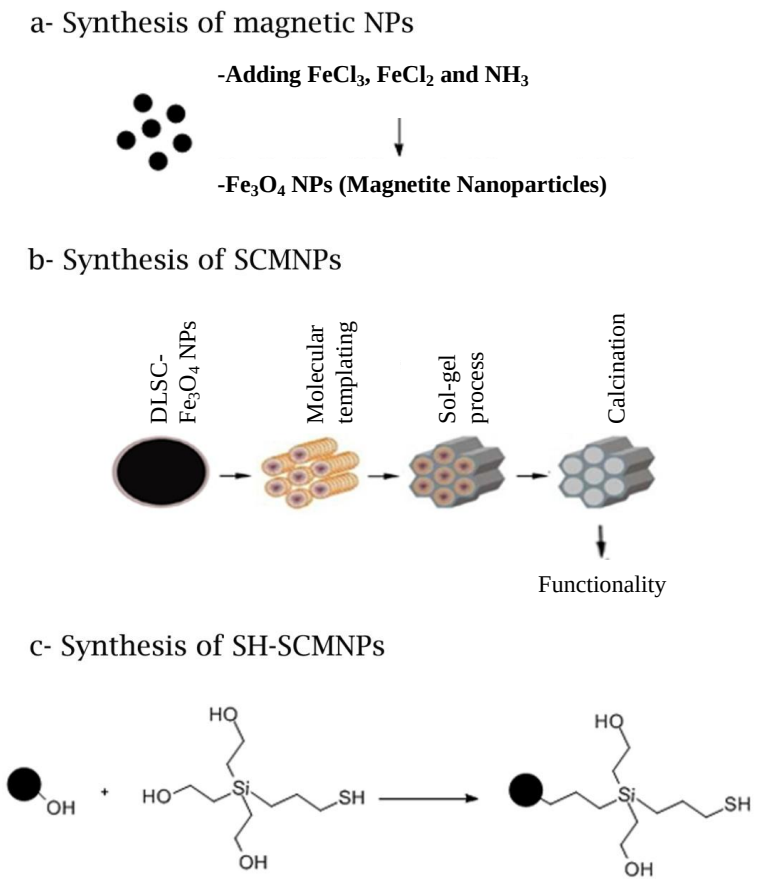

Figure 3.1: Synthesis procedure of (a) Fe_3O_4 NPs, (b) silica coated magnetite nanoparticles (SCMNPs), and (c) thiol-functionalised silica coated magnetite nanoparticles SH- SCMNPs.

Table 3.1: Chemicals and their molecular formulas.

Chemical Compound	Formula	Supplier	Purpose
Ferrous chloride tetrahydrate	$FeCl_2.4H_2O$	Sigma-Aldrich	1
Ferric chloride hexahydrate	$FeCl_3.6H_2O$		1
Ammonia solution	NH_3		1
Glacial acetic acid	CH_3CO_2H	Fisher	1,2,3
Hydrochloric acid	HCl		1
Sodium chloride	NaCl		1
Tetraethoxysilane	$C_8H_{20}O_4Si$	Sigma-Aldrich	1
3-mercaptopropytrimethoxysilane	$HS(CH_2)_3Si(OCH_3)_3$		1
Sodium Silicate	Na_2SiO_3		1
Cetyl-trimethyl-ammonium chloride (25 wt. % in H_2O)	$CH_3(CH_2)_{15}N(Cl)(CH_3)_3$		1
Glycerol	$HOCH_2CH(OH)CH_2OH$	Fisher	1
Methanol	CH_3OH		
Ethanol	CH_3CH_2OH		
Toluene	$C_6H_5CH_3$		
Mercury(II) chloride solution in 10% HNO_3	$HgCl_2$	Fisher	2
Copper (II) nitrate trihydrate solution in 10% HNO_3	$Cu(NO_3)_2.3H_2O$		2
Zinc(II) nitrate hexahydrate solution in 10% HNO_3	$Zn(NO_3)_2.6H_2O$		2
Nickel (II) nitrate hexahydrate solution in 10% HNO_3	$Ni(NO_3)_2.6H_2O$		2
Lead(II) nitrate solution in 10% HNO_3	$Pb(NO_3)_2$		1,2,3
Nitric acid	HNO_3		2,3
Thiourea	NH_2CSNH_2	Sigma-Aldrich	2
Sodium nitrate	$NaNO_3$		1,2,3
Sodium hydroxide	NaOH	Fisher	1,2.3
Potassium bromate	$KBrO_3$	Sigma-Aldrich	3
Potassium bromide	KBr		
Hydroxylamine hydrochloride	$NH_2OH.HCl$		
Tin(II) Chloride	$SnCl_2$		

Purpose:

1- Synthesis
2- Adsorption tests and recovery
3- Total Hg determination

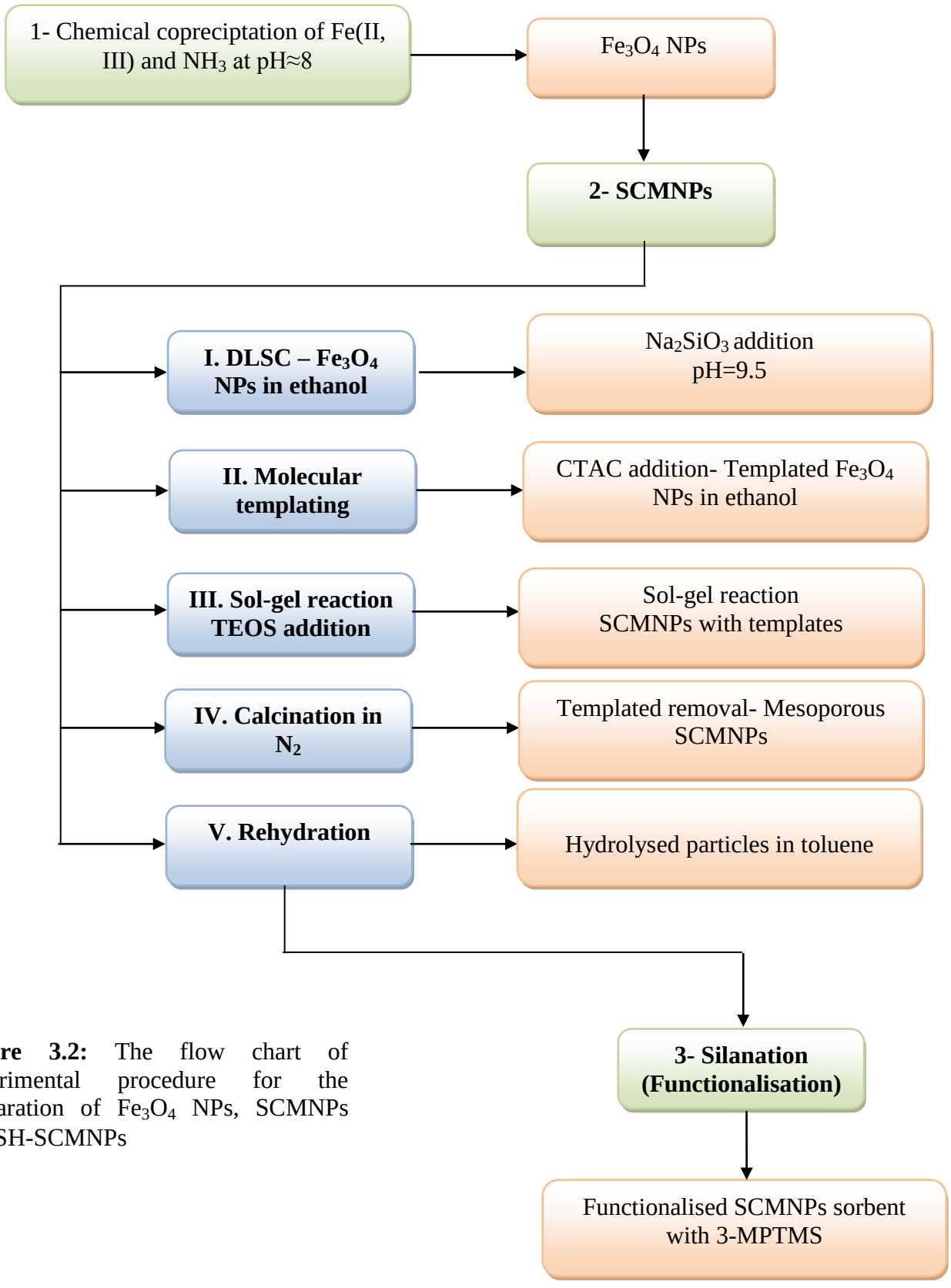

Figure 3.2: The flow chart of experimental procedure for the preparation of Fe_3O_4 NPs, SCMNPs and SH-SCMNPs

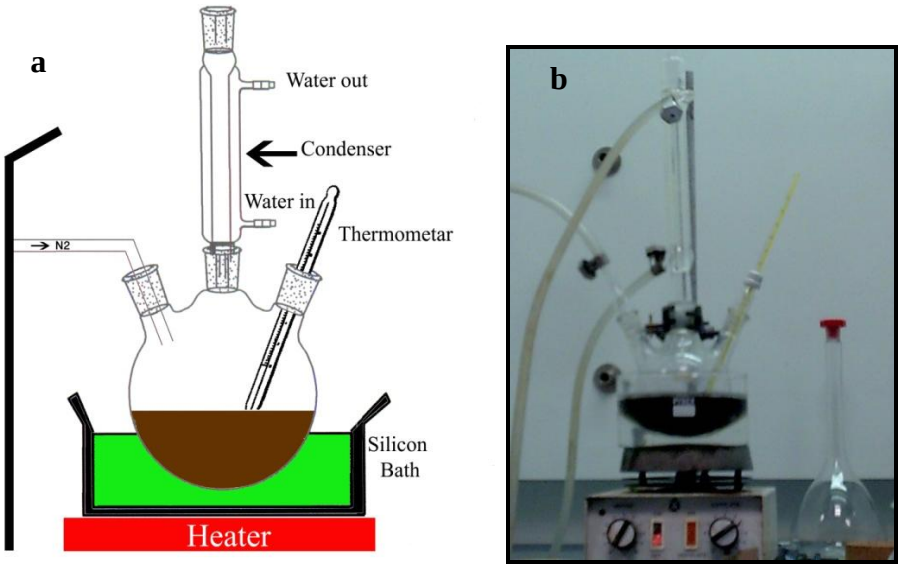

Figure 3.3: Experimental setup: (a) schematic diagram, and (b) photograph of the reactor for NPs synthesis.

3.2.2 Synthesis of Silica Coated Magnetite Nanoparticles

3.2.2.1 Stage 1: Dense liquid silica coating

Dense liquid silica coated magnetite NPs (DLSC-Fe_3O_4 NPs) were prepared by re-suspending 4 g Fe_3O_4 NPs in 150 mL of deionised water in a 500 mL 3-necked round bottomed flask with the contents agitated by immersion in an ultrasonic bath (Crest Ultrasonic CP1100, UK) for 15 minutes. The pH of the Fe_3O_4 NPs suspension was then raised to 9.5 ± 0.1 by adding 0.1 M NaOH, and the solution was stirred and heated at 90˚C for 2 hrs under a nitrogen atmosphere. Then, 10 mL of aqueous silica solution (Na_2SiO_3) were added. The suspension pH, monitored by a pH meter (FE20, Mettler Toledo, UK), was kept at 9.5 by the addition of 0.1 mol L^{-1} HNO_3. The addition of strong alkaline silica solution would increase the pH of the suspension to undersaturation condition if acid were not added during this stage. The reaction continued for 1 hr. The heater and nitrogen flow were then turned off to allow the magnetite precipitate to gradually settle and cool at room temperature. The coated particles were then isolated by applying an external magnetic field and the supernatant was removed by decantation. The magnetite precipitate was then washed three times with deionised water (3x100 mL). Finally, the DLSC-Fe_3O_4 NPs were dried overnight at pressure of 20 m Torr using a freeze drier.

3.2.2.2 Stage 2: Molecular templating of the silica coated nanoparticles

For molecular templating, 3 g of DLSC magnetite NPs were added to 100 mL of ethanol and then stirred for 30 minutes, followed by adding 75 mmol L^{-1} of cetyl-trimethyl-ammonium chloride (CTAC) aqueous solution. The mixture was allowed to react at room temperature for 3 hrs while mixing continued. The particles were finally collected from the suspension by using an external magnetic field and then used directly in the sol-gel process without washing or drying.

3.2.2.3 Stage 3: Sol-gel reaction

CTAC templated particles were mixed with 100 mL of ethanol while vigorously stirring for 1 hr in a 500 mL 3-necked round bottomed flask fitted with a nitrogen bubbling tube. Then, 80 mL of 10% (v/v) of tetraethoxysilane (TEOS) were added and stirred for further 5 hrs at room temperature. The ethanol was used as a reaction medium in the sol-gel process in order to ensure miscibility of the TEOS and to better control the hydrolysis of alkoxide. Then, 60 mL of glycerol were added and the pH was adjusted to 4.6 using glacial acetic acid and a drop of ammonia solution was added to act as a catalyst. The mixture was then stirred for further 3 hrs under a nitrogen atmosphere to ensure complete dehydration and the formation of a silica network (Figure 3.4). The mixture was washed three times with deionised water (3x100 mL) and two additional times with methanol (2x100 mL). Finally, the silica magnetite particles were collected from the suspension using an external magnetic field and then used directly in the next step.

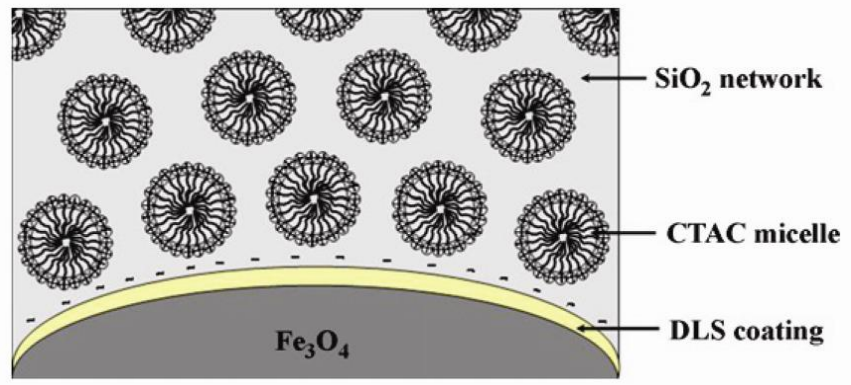

Figure 3.4: Schematic diagram of the sol-gel coated DLSC- Fe_3O_4 NPs with templates (Kim et al., 2003).

3.2.2.4 Stage 4: Calcination

The advantage of removing the surfactant using calcination is that the mesophase structure does not shrink. Therefore, the pore size does not change and the mesostructure could be easily maintained after extraction. Additionally, it is possible to remove the template without changing the concentration of silanol groups. Heating the mesoporous material at more than 900˚C causes the collapse of its framework as discussed by Chen et al. (1993). In this case, the calcination temperature is kept at a temperature lower than 600˚C to avoid the collapse of the mesostructure of the materials and the condensation of the silanation groups.

The SCMNPs at this stage are mesoporous, but their pores are filled with the surfactant. To remove these, as the fourth stage in the treatment, the SCMNPs were calcinated at temperature between 120 and 540˚C in a tube furnace with nitrogen flow for 4 hrs. The results of calcination of SCMNPs are summarised in Table 3.2.

Table 3.2: Calcination processes at different temperatures.

Temperature range (˚C)	**Weight lost (%)**	**Reason**
120-200	1.8%	Removal of residual solvents and physically adsorbed water.
200-540	No Weight lost	Since the physisorbed water and of residual solvents have been removed during preheating of the samples at 120 – 200 °C, there was no weight loss of the SCMNPs over the studied temperature range.
540	2.9%	Attributed to the removal of CTAC templates.
540-600	No Weight lost	This was indicating the completion of templates removal.
In order to avoid the collapse of the mesostructure of SCMNPs, no measurements were recorded above 600˚C.		

3.2.3 Rehydration

Before the third stage of adding a functional group to the coating, 3 g of mesoporous SCMNPs were hydrolysed in 100 mL of toluene. The suspension was stirred for 2 hrs under a nitrogen atmosphere. The particles were collected from the suspension by using

an external magnetic field and then washed three times with 200 mL of deionised water. Finally, the mesoporous SCMNPs were stored in deionised water for the next reaction.

The objective of the steam rehydration pre-treatment of the mesoporous SCMNPs is to increase the density of the hydroxyl group on the surfaces of the SCMNPs and hence improves the silane coupling reaction with the 3-MPTMS.

3.2.4 Addition of a Functional Group

To enhance the affinity of the magnetite NPs towards mercury ions, 3-MPTMS was used to functionalise the mesoporous SCMNPs, this followed the procedure developed by Huang and Hu (2008) with some modifications.

25 mL of SCMNPs were washed with ethanol (2x100 mL) and then diluted in 150 mL with 1% 3-MPTMS in 95% ethanol followed by adding 16 mmol L^{-1} acetic acid to adjust the pH to 4.5. The suspension was then transferred to a 500 mL 3-necked, round bottomed flask and stirred and heated at 60˚C for 2 hrs under nitrogen atmosphere. The particles were then washed three times with 100 mL deionised water, twice with 100 mL of methanol and the sample was dried overnight at pressure of 20 m Torr.

3.2.5 NPs Suspension

Suspending magnetic NPs in deionised water could prevent their agglomeration. However, Shan et al. (2005) and Khan (2008) found that magnetic NPs and modified magnetic NPs did not settle spontaneously in deionised water. In this work, a NPs stock suspension at a final concentration of 50 mg mL^{-1} was prepared by adding 50 mg of nano-powder to 1 mL of deionised water, forming a homogenous dark brown/black suspension. The suspensions were sonicated and stored at 4 ˚C as shown in Figure 3.5b. For the adsorption experiments, sonication (40 kHz, Crest Ultrasonic CP1100, UK) were employed to re-suspend the NPs before using them in adsorption experiments.

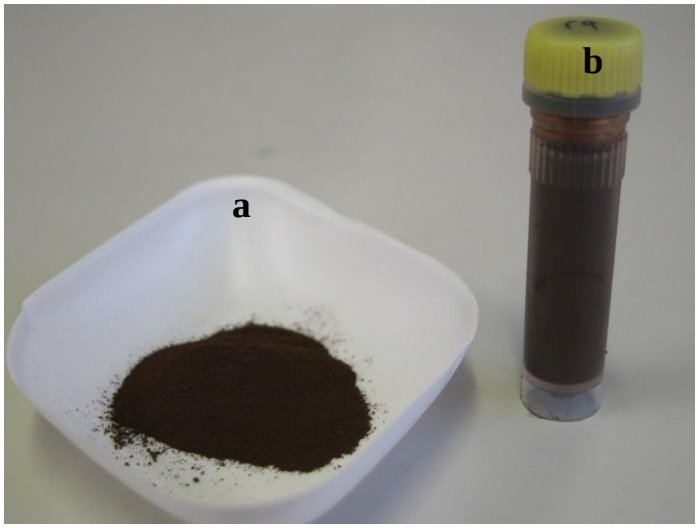

Figure 3.5: Final production, (a) magnetic nano-powder and (b) suspension of NPs in water.

3.3 Characterisation of Nanoparticles

All the prepared NPs in this study were characterised using the following methods:

1. X-ray powder diffractometer (XRPD) for crystal identification. XRD provides information about crystal size and perfection and chemical composition.
2. Fourier transform infrared spectroscopy (FTIR) for determining the chemical structure of organic molecules.
3. Size and morphology investigations through transmission electron microscopy (TEM) and scanning electron microscopy (SEM).
4. Brunauer, Emmett and Teller (BET) methods for surface area measurement and pore size distribution.
5. Dynamic light scattering (DLS) for particle size measurement and zeta potential.
6. Vibrating Sample Magnetometer (VSM) for magnetic behaviour analysis. VSM has been extensively used with magnetic materials to measure saturation, remanence, coercivity, anisotropy fields.

3.3.1 X-ray Diffraction

About 15 mg of fine ground magnetic NP samples were placed into an aluminium sample holder (11×20 mm sample area) and then the material was gently pressed against unglazed paper to minimise the preferred orientation. Samples prepared in this way had

a flat surface which appeared, to the naked eye, homogeneous and almost smooth. XRD data were obtained using Cu Kα radiation (λ= 1.5406 Å, 40 kV & 40 mA) and a Philips X'Pert Pro vertical goniometer equipped with a 1˚ divergence slit, a 0.2 mm receiving slit, a 1˚ scatter slit, a diffracted-beam graphite monochromator, and a proportional detector. The XRD patterns were obtained by step scanning from 2˚ to 76˚ (2θ) at 0.02˚ or 0.01˚ increments using a counting time of 10 S per increment. The maximum counting rate was less than 4000 counts/second so no dead-time correction was necessary. The raw data was interpreted using Philips propriety software SuperQ from Philips X'Pert and the database of the Joint Committee on Powder Diffraction Standards (JCPDS).

3.3.2 Fourier Transform Infrared Spectroscopy (FTIR)

IR spectroscopy was carried out using a Nicolet Protégé 460 FTIR spectrometer equipped with a Nic Plan IR microscope. The sample was prepared as follows. A very small amount of samples (~10 mg) was mixed with 25 to 30 times its volume of KBr in an agate pestle and mortar (mixing and grinding it at the same time). The samples were pressed in a die at 3000 kg cm^{-1} for about 3 minutes. The produced disc was run on a Nic Plan IR microscope, set at 256 scans with a resolution of 8 cm^{-1} followed by removing the background at the same settings. The range scanned was from 400 to 4000 cm^{-1}.

3.3.3 Electron Microscopy (SEM)

A bright field of SEM (JSM6500F) was used at 15 keV to observe the morphology and size of the prepared NPs. Energy Dispersive X-ray (EDX) microanalysis was also used for chemical composition analysis. The specimens for the SEM study were prepared by direct deposition of NPs on an aluminium holder which was covered by a carbon grid and then sputter coating with a thin layer of gold (~ 10 nm thick film) under high vacuum, using gold sputter coating (JEOL, 5010) to provide a homogeneous surface for analysis and imaging. The JEOL sputtering system was employed using the conditions summarised in Table 3.3. After gold coating, the sample was placed inside the SEM sample chamber and the SEM was operated under high vacuum with an accelerating voltage of 15 keV and a secondary electron (SE).

Table 3.3: The parameters employed for gold coating.

Parameters	Value
Gas employed	Argon 5 psi
Current	~ 15 mA
Time of coating	2 minutes

3.3.4 Electron Microscopy (TEM)

The particle size and morphology were analysed using JEM 3010, operating at 300 keV, with a point resolution of 2.1 Å and a magnification of $1.5x10^6$. It was also equipped with a high-angle annular dark field (HAADF) detector for the scanning transmission electron microscopy (STEM) and the EDX detector. This instrument is capable of detecting even very small metal particles (< 1 nm) by Z contrast and of analysing selected points by EDX spectroscopy.

Approximately 10 mg of particles were first dispersed in ethanol for 45 minutes using sonication (Crest Ultrasonic CP1100, UK) and then transferred to a cooper grid (Carbon Films, 200 Mesh Cu Grids, AGAR). The samples were then left to dry in a vacuum desiccator for 24 hrs before commencing the measurements.

3.3.5 BET Method

The surface area and pore size distribution of the prepared NPs was measured using a Micromeritics Gemmini 2375 surface area analyser. For sample preparation, about 20 mg of particles were placed into clean and dry tubes for gas preparation, and then the temperature was raised to 200˚C and degassed for the required time (usually between 2-3 hrs) using Vac Prep 061 (Micromeritics, UK). The weight of the sample was noted before and after degassing. Surface area was measured at liquid nitrogen temperature (77˚ K) using a conventional gas adsorption apparatus. The BET method was carried out under a relatively high vacuum and measured primarily the external area of particles and aggregates. The pore size distribution of magnetite NPs was calculated from the desorption branch of the nitrogen adsorption-desorption isotherm using the Barrett-Joyner-Halenda (BJH) model. The BJH method for calculating pore size distribution is based on a model of adsorbent as a collection of cylindrical pores. The method accounts

for capillary condensation in the pores using the classical Kelvin equation (Barrett et al., 1951)

$$\ln \frac{p}{p_o} = \frac{2\gamma M_v}{rR_cT} \quad (3.2)$$

where p is the actual vapour pressure, p_o is saturation vapour pressure, γ is the surface tension, M_v is the molar volume, R_c is the universal gas constant and r is the radius of the droplet.

3.3.6 Vibrating Sample Magnetometer (VSM)

The wet magnetic NPs samples were freeze-dried and then prepared for the magnetisation measurements with a vibrating sample magnetometer (VSM, Oxford Instruments Aerosonic 3001). About 50 mg of NPs samples were placed on the typhlone holder that was covered by white PVC insulating tape, so that the powders do not contaminate the VSM system. Hysteresis measurements were performed at 300˚ K with magnetic fields up to 0.9 T to achieve demagnetisation corrections. The magnet samples were fabricated with the right circular cylinder geometry. They were oriented such that the cylinder axis was at a right angle with the applied magnetic field. The resulting changes in the magnetic flux induced a voltage in the sensing coils and this was proportional to the magnetic moment of the sample.

3.3.7 Dynamic Light Scattering (DLS) Measurements

ME11Zetasizer Nano ZS (Malvern Instruments Ltd, UK) was used to measure the particle size in this work. The measurements were performed at 25°C and analysed in multiple narrow modes (ensuring a high resolution). Before commencing the DLS measurements, the NPs suspensions were diluted to a concentration of about 8 mg L^{-1}. The DLS of NPs were determined using a Folded Capillary cell (DTS1060), (Malvern Instrument, UK).

The Malvern Zetasizer Nano-ZS uses the Zeta sizer NIBS Software (V6.01) for data collection and analysis. The software collects and interprets data for the particle size and zeta potential. For the particle sizing in the solution, the software gives multiple aspects,

interpretations and representations of the acquired data such as intensity, volume, number distribution graphs as well as statistical analysis for each property. The mean particle diameter is directly calculated by the software from the particle distributions measured, and the resulting polydispersity index (PdI) is a measure of the size ranges present in the solution (MME11ZS-NANO, 2008).

3.3.8 Thermo Gravimetric Analysis (TGA)

TGA analysis was carried out on a Mettler Toledo TGA/SDTA85le instrument, from 25° to 900°C under N_2 gas (flow rate of 50 ml min^{-1}) at a heating rate of 10° C min^{-1}.

3.4 Total Mercury Determination and Other Metals

3.4.1 Mercury Determination

In this study, the concentration of total mercury was measured by PSA Millennium Merlin atomic fluorescence spectrometry (AFS) (PSA Millennium Merlin, P S Analytical Ltd, UK). This instrument uses a cold vapour fluorescence (CVAFS) technique in which free mercury atoms in an argon gas carrier gas are excited by a collimated ultraviolet light source at 253.7 nm. The excited atoms re-radiate their absorbed energy (fluoresce) at this same wavelength and are detected using a photomultiplier tube or UV photodiode. Using this equipment, mercury can be detected in parts per trillion (EPA, 2005). The minimum level of quantisation (ML) was established as 1.0 ng L^{-1}.

The procedure for Hg determination includes: (1) preparation of solutions for Hg analysis, (Table 3.4), (2) calibration of PSA Millennium Merlin AFS and then the Hg (II) concentration of each sample can be determined from the calibration curves of a series of standard mercury solutions prior to each analysis, and (3) analysis of the samples. All daily solutions had 7.5 mL of 33% v/v HCl and 1 mL 0.03 M $KBr/KBrO_3$ per 50 mL. The samples were kept in upright position overnight for no longer than 7 days. Before the analysis, 15 µL of 12% $NH_2OH.HCl$ were added into the samples. After digestion, all the mercury (Hg^{2+}) in the extract was reduced to Hg^0 by using acid reductant 2% m/v $SnCl_2$ in 10% v/v HCl. Hg^0 was measured by CVAFS, PSA 10.035

Millennium Merlin system following the analytical procedure developed by PSA Co., Ltd: (based on USEPA Method 1631, Revision C: Mercury in Water by Oxidation, Purge and Trap, and CVAFS).

Table 3.4: Daily, weekly and monthly analysis of Hg solutions.

Solution	Purposes	Daily	Weekly	Monthly
Hg standard	calibration	√		
$KBrO_3$	For sample digestion (preservation)		√	
KBr	For sample digestion (preservation)			√
$NH_2OH.HCl$	For removal excess bromine which indicated by the disappearance of yellow colour from the samples.		√	
$SnCl_2$	For removal all traces of Hg.		√	
Reagent Blank solution	Blank and for washing	√		
2% m/v $SnCl_2$ in 10% v/v HCl	Acid reductant	√		

3.4.2 Other Heavy Metals Determination

The concentration of metal ions (Cu(II), Ni(II), Pb(II) and Zn(II)) were measured using atomic absorption spectrometry (AAS) (SpectrAA-200, Varian Australia).

The instrument was set up according to the expected range of metal concentration in the samples as stated in the operator's manual. The employed measurement parameters are shown in Table 3.5. The AAS was first calibrated with a range of solutions with known concentrations prepared by diluting standard stock solution (Fisher Scientific, UK) to derive the calibration curve against which unknown samples were compared and their concentrations were then displayed automatically. Control metal solutions in the absence of NPs were always run in parallel with each experiment and under the same experimental conditions. All the experiments were conducted at least in triplicates and the average values were presented.

Table 3.5: The AAS parameters for metals ions analysis.

Element	Slit width (nm)	Wavelength (nm)	Lamp current (mA)
Cu	0.5	324.7	4
Ni	0.2	232	4
Pb	1.0	217	5
ZN	1.0	213.9	5

3.4.3 Determination of Iron and Silicon

All the metals dissolved in the solutions were measured by using an inductively coupled plasma-atomic emission spectrometer (Agilent 7500ce ICP-MS for total Si and Varian Vista Pro ICP-OES For total Fe) at Severn Trent Laboratories, Coventry, UK. The standard method (WAS049) was applied to determine the total concentration of Fe in the solutions. The validity range of this method is between 0.19 and 2000 mg L^{-1}. The total concentrations of Fe were determined by ICP-OES after dissolution in the presence of nitric acid. The pre-treatment ensures that any metals in suspended or colloidal forms are converted to the soluble form. The total concentration of Si was measured via WAS060 standard method. ICP-MS was then used to determine the total concentration of Si after dissolution, via the action of microwaves, in the presence of nitric acid. The digestion pre-treatment ensured that any suspended or colloidal forms were converted to soluble forms. Filtered (otherwise known as dissolved or soluble) metals were also determined by filtration through a 0.45 μm membrane filter, prior to acidification with nitric acid. The range of applicability of this method is between 10 - 2000 μg L^{-1}.

3.5 Preparation of Adsorbate Stock Solution

For batch tests, the adsorbate stock solution of Hg(II) was prepared using a Hg atomic absorption standard stock solution (1000 ppm Hg in 10% HNO_3) from (Fisher Scientific Co, UK). This standard solution was diluted as required for the adsorption experiments to obtain the target concentration of Hg with high purity deionised water (18.2 MΩ-cm). The daily working Hg solutions were prepared freshly before use. Polyethylene terephthalate (PET) containers were used to store the mercury or as reaction vessels due to their very low mercury adsorption characteristics (Copeland et al., 1996; Fadini and Jardim, 2000). Finally, a background electrolyte 0.1M $NaNO_3$ was added to the adsorbate working solution to maintain its ionic strength.

For the adsorption experiments, the stock solutions (1000 ppm, Cu, Ni, Pb and Zn in 10% HNO_3) were used to prepare the synthetic wastewater by diluting them to target concentration with high purity deionised water.

3.6 Batch Adsorption Tests

Adsorption experiments were carried out by mixing Fe_3O_4 NPs, SCMNPs and SH-SCMNPs with 50 mL of a Hg(II) solution. This solution was prepared at different concentrations in 0.1 M $NaNO_3$ to keep the ionic strength relatively constant. The initial pH was adjusted by adding either 0.1 M NaOH or 0.1 M HNO_3. All the sorption experiments were carried out in 100 mL polyethylene terephthalate (PET) bottles placed in an orbital incubator rotating at 200 rpm for 1 hr at 22.5˚C unless otherwise stated. The NPs were isolated and separated by applying an external magnetic field at the end of the test. The final concentration of Hg(II) was determined using the PSA Millennium Merlin atomic fluorescence spectrometry. All the experiments were conducted at least in duplicates and the average values are presented.

All the PET bottles used in this study were soaked in 20% v/v HNO_3 for at least 24 hrs, and rinsed using high purity deionised water (18.2 MΩ-cm).

For the control experiments, 50 mL of 10 and 80 µg L^{-1} Hg(II) were agitated in the absence of NPs for 24 hrs at 22.5˚C at a rate of 200 rpm. A volume of 10 mL sample was taken for measurement before shaking. To ensure accuracy and reliability of the results, the experiments were carried out in four replicates and the average values are presented.

The same experiments were performed for Cu(II), Ni(II), Pb(II) and Zn(II) at initial concentrations of 2 and 10 mg L^{-1} using polypropylene (PP) plastic containers.

3.6.1 Adsorption Kinetic Experiments

Kinetic studies were carried out at pH 6.0 using Hg(II) concentration 80 µg L^{-1} in a 160 mL solution to which was added a known quantity of 1.2 mg of concentrated NPs (Fe_3O_4 NPs, SCMNPs and SH-SCMNPs) suspensions to give NPs concentrations of 8 mg L^{-1}. The mixture was agitated in the orbital incubator at 200 rpm and 22.5˚C. A volume of 10 mL sample was taken for measurement at specific time intervals of 1, 2, 5, 10, 20, 30, 40, 50, 60, 80, 100, 120, 180 and 240 minutes. The samples were transferred into a PET bottle and then an external magnetic field immediately was immediately used

to separate the magnetic NPs out of the mercury solution within less than 2 minutes. The final concentration of Hg(II) was determined by PSA Millennium Merlin AFS.

3.6.2 Adsorption Isotherm Determination

The adsorption isotherm was determined by carrying out batch tests at pH 6.0 using Hg(II) concentrations of 40, 80, 200, 500, 800 and 1000 μg L^{-1} in a 50 mL solution to which a known quantity of either 0.20 or 0.40 mg of a concentrated NPs (Fe_3O_4 NPs, SCMNPs and SH-SCMNPs) suspension were added to give NPs of concentrations ~ 4 and ~ 8 mg L^{-1}. The NPs reacted for 1 hr to reach equilibrium. The mixture was separated via an external magnetic field and PSA Millennium Merlin AFS was used to determine the final concentration of Hg(II). Langmuir and Freundlich isotherms were employed to conduct the thermodynamic analysis. Experimental C_{eq} and q_{eq} data were used to evaluate the constant of each model, according to the least squares fitting method.

The Langmuir isotherm (Langmuir, 1916) was taken as:

$$\frac{C_e}{q_e} = \frac{1}{Q_0 b} + \frac{C_e}{Q_0} \quad (3.3)$$

where C_e is the equilibrium concentration (mg L^{-1}) after adsorption, Q_0 and b are Langmuir constants related to the maximum adsorption capacity and energy of adsorption respectively, and q_e is the amount of Hg(II) adsorbed at equilibrium (mg g^{-1}).

The Freundlich isotherm (Freundlich, 1926) was taken as:

$$\log q_e = \log K_f + n^{-1} \log C_e \quad (3.4)$$

where q_e is the concentration of Hg(II) adsorbed at equilibrium (mg g^{-1}), C_e is the equilibrium concentration (mg L^{-1}) after adsorption, and K_f and n^{-1} are Freundlich constants.

As described earlier in Chapter 2 (section 2.2.1.5.3), the process of the adsorption of Hg(II) from the aqueous phase using Fe_3O_4 NPs can be described as a heterogeneous reaction between solid and liquid. The Hg(II) adsorption isotherm of thiol-functionalised mesoporous silica adsorbents usually exhibited typical Langmuir behaviour that

correlated better than the Freundlich isotherm, suggesting a monolayer adsorption. However, some previous studies reported that the adsorbed quantities Hg(II) ions were higher than the available thiols sites, suggesting another mechanism of adsorption.

In the present study, although SH-SCMNPs were functionalised with thiol groups and the adsorption sites may have the same activity, the adsorption mechanism for Hg(II) may involve not only the Hg chelation by SH complexing functions, but also the surface complexation by OH or Si-OH sites which remained uncovered. Therefore, the Langmuir and Freundlich isotherm models were applied to the experimental data in this study in order to get a deeper insight into the adsorption mechanism.

3.6.3 Effect of Physical and Chemical Environmental Factors

3.6.3.1 Effect of pH

The effect of the solution's pH on the adsorption of Hg(II) was investigated to find the optimal pH for removing Hg(II). Batch tests used 50 mL of 80 μg L^{-1} Hg solutions with pH adjustment using 0.1 M NaOH and 0.1 M HNO_3 to give a range from 2.0 to 9.0. Approximately 8 μl of NP suspension (~ 0.4 mg) was spiked into the above solutions at different values of pH, and then the solution was agitated at 22.5˚C for 1 hr to reach equilibrium. The mixture was separated via an external magnetic field and PSA Millennium Merlin AFS was use to determine the final concentration of metal ions.

3.6.3.2 Effect of temperature

The removal efficiency of Hg(II) from 100 mL of 160 μg L^{-1} Hg solution by SH-SCMNPs at a concentration of 6 mg L^{-1} was tested at 10, 22.5 and 35 ˚C. The pH was adjusted at 6.0 and then agitated at 200 rpm. At specific time intervals of 1, 5, 10, 20, 30, 40, 50 and 60 minutes, 10 mL samples were taken for analysis. After separating the particles, the Hg(II) content in the supernatant was measured by PSA Millennium Merlin AFS.

3.6.3.3 Effect of shaking speed

A mixing rate ranging from 50-200 rpm was tested. This test was conducted by mixing 12 μL of NPs suspension (~ 0.60 mg) with 100 mL of 80 μg L^{-1} Hg(II) solutions at pH

6.0. The solutions were agitated at 50, 100, 200 rpm and 22.5˚C. A 10 mL sample was taken at specific time intervals of 0, 5, 10, 20, 30, 40, 50 and 60 minutes to determine the Hg(II) concentration. After separating the NPs using an external magnetic field, the final concentration of metal ions was determined by PSA Millennium Merlin AFS.

3.6.3.4 Effect of common ions

The effect of common cations was explored in binary and cocktail components adsorption. Binary experiments were carried out at fixed mass concentrations by mixing 200 μg L^{-1} of Hg(II) with each of the above cations at a ratio of 1:10, and the mixture was interacted with 16 μL of SH-SCMNPs suspensions (0.8 mg) for 1 hr at 22.5˚C to reach equilibrium. For completeness, 50 mL of 200 μg L^{-1} of Hg(II) containing each of the various cations (2000 μg L^{-1}) were shaken with 16 μL of NPs suspension (~ 0.8 mg) for 1 hr at pH 6.0. The latter design would thus provide sufficient metals in the solution to potentially saturate the available binding sites that could be taken up by Hg(II) ions. In all cases, the mixture was separated via an external magnetic field and the final concentration of Hg(II) ions was determined by PSA Millennium Merlin AFS whereas the concentrations of the other metals were determined by atomic absorption spectroscopy (AAS). SH-SCMNPs were initially washed three times using deionised water to remove any metals that were loosely attached to the bottles or to the adsorbent itself. The SH-SCMNPs were then reacted with the test solution for 1 hr at 22.5˚C with shaking at 200 rpm. Then, the SH-SCMNPs were separated from the solution and used in a second adsorption cycle without any attempt to desorb any bound ions. This procedure was repeated for five cycles and the heavy metal ions were finally recovered after six cycles using concentrated hydrochloric acid (5 mL, 12.1 M HCl) as shown in Figure 3.6.

Similarly, the effects of interference by the coexisting anions of Cl^-, SO_4^{3-}, PO_4^{3-}, NO_3^- and F^- on the adsorption of Hg(II) were examined according to the procedure described above. The experiments were carried out in binary and multiplicity systems at the same mass concentrations that were used for various common cations.

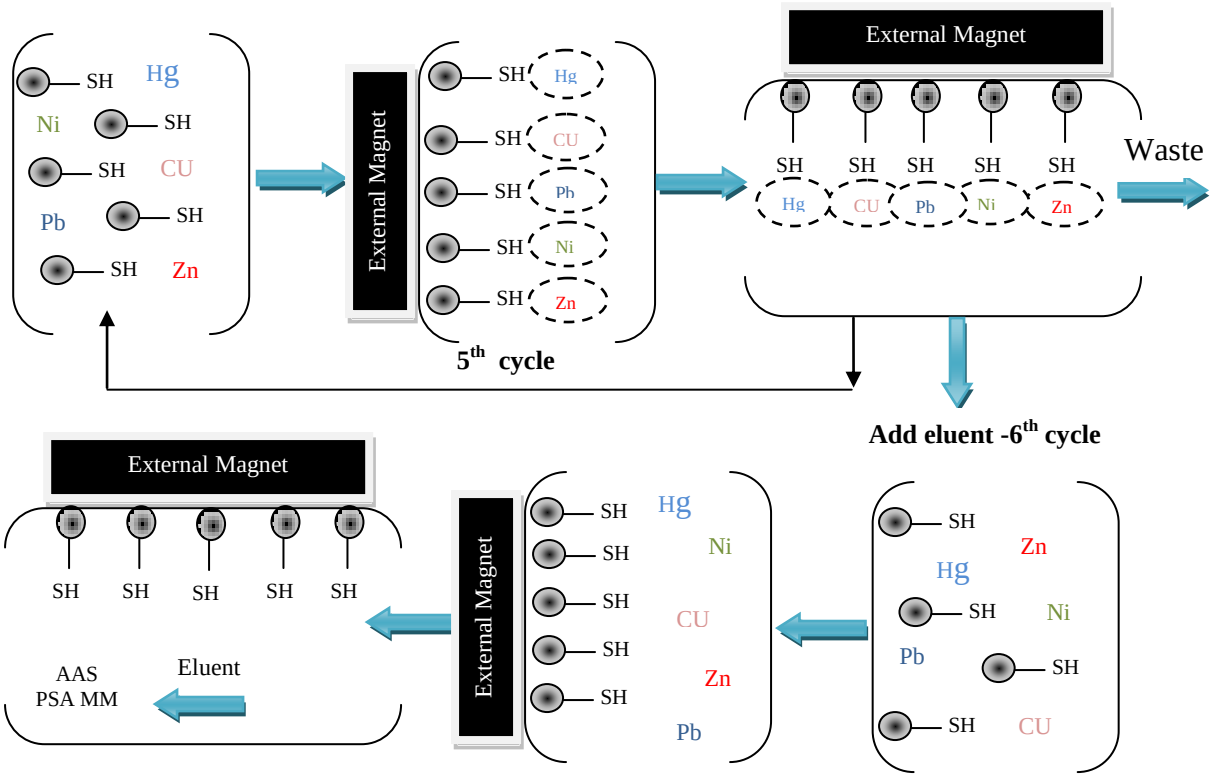

Figure 3.6: Schematic of the procedure used for studying the effect of cations on the adsorption process.

3.7 Recovery (Desorption) Studies

3.7.1 Desorption Process

Batch adsorption and desorption experiments were conducted with 8 mg L^{-1} SCMNPs and SH-SCMNPs with varying initial Hg concentrations (80, 120 and 20 µg L^{-1}) to determine sorbent efficiency. The desorption of Hg laden SCMNPs was then tested using 5 mL of HCl at concentrations ranging from 1.0 to 3.0 M with 30 min of reaction time to reach equilibrium. For Hg-adsorbed SH-SCMNPs, two eluents were used: HCl from 1.0 to 5.0 M and HCl at concentrations from 1.0 to 3.0 M mixed with 2 % (m/v) thiourea. Before this acid treatment, the magnetically recovered NPs were first washed three times with deionised water to remove Hg(II) which was loosely attached to the PET bottles or to the adsorbent itself. A 5 mL aliquot of the desorbent were then added and shaken for 1 hr. The NPs were separated magnetically from the desorbent and its mercury concentration was determined.

The control experiments were carried out in parallel using deionised water; the aim here was to determine whether deionised water affects the desorption of Hg. In these experiments, Hg laden SCMNPs or SH-SCMNPs and 20 mL of deionised water were placed in PET bottles. The mixture was allowed to equilibrate for 0.5, 1, 2, 6 and 24 hrs on an orbital shaker at 200 rpm and 22.5 ˚C. The NPs were then separated by an external magnetic field and PSA Millennium Merlin AFS was used to determine the supernatant.

3.7.2 Regeneration Process

Successive adsorption-desorption processes were carried out over five cycles. For each cycle, 0.4 mg NPs (SCMNPs or SH-SCMNPs) were mixed with 50 mL of 80, 120 and 200 μg L^{-1} of Hg(II) in PET bottles and the solution was then agitated at 200 rpm and 22.5˚C. After each adsorption process, the NPs were washed 3 times using deionised water. For the desorption processes, the magnetic NPs were separated using an external magnetic field and then 5 mL of the eluents were added to Hg(II) laden NPs and shaken for 1 hr. For each cycle, the NPs were washed completely with deionised water and used later in the succeeding adsorption cycle. Therefore, the regenerated NPs were subsequently mixed with 50 mL of 80 120 and 200 μg L^{-1} of Hg(II) solutions and the process was repeated. When equilibrium was reached, the magnetic NPs were separated by an external magnetic field and PSA Millennium Merlin AFS was used to determine the supernatant.

3.8 Data analysis (Adsorption and Desorption Efficiency)

The adsorption capacity was calculated according to the following equation

$$q_e = \frac{V(C_o - C_e)}{M} \quad (3.5)$$

where C_o is the initial mercury concentration in the solution, C_e is the equilibrium concentration (mg L^{-1}) after adsorption, V is the solution volume (l), and M is the mass of NPs adsorbent (g).

This equation does have a limitation. This happens when the initial metal concentration is low or the adsorbent concentration is high or in other words when the mass of metal is too limited compared with the adsorbent present. In this case, the residual metal

concentration can be as low as around zero, although the adsorbent has not reached its adsorption capacity.

The desorption efficiency was calculated based on following equation:

$$Desorption capacity = \frac{(C_{ed} - C_o)V_d}{q_e M} \times 100 \quad (3.6)$$

where C_{ed} is the equilibrium concentration (mg L^{-1}) after desorption, C_0 is the initial concentration of mercury in the eluent (mg L^{-1}), V_d is the volume of the eluent (l), q_e is the adsorption capacity obtained in the adsorption test and M is the mass of the NPs adsorbent (g).

3.9 Dissolution of Fe and Si (Dissolution Kinetics)

Initial dissolution studies were conducted at room temperature of 22.5˚C, pH of 2.0, and shaking speed of 200 rpm unless otherwise stated. 200 mL of 8 mg L^{-1} NPs solutions (Fe_3O_4 NPs and SH-SCMNPs) at pH 2.0 and 6.0 were shaken for time intervals up to a maximum of 240 minutes. 20 mL of sample were taken over the course of this period to measure the total amount of Fe and Si released. Further experiments used pH values of 2.0, 4.0, 6.0 and 8.0 and a sample volume of 50 mL containing 8 mg L^{-1} of NPs (Fe_3O_4 NPs and SH-SCMNPs) shaken for 2 hrs.

The effect of the eluent was also checked by mixing SH-SCMNP with 10 mL 3.0 M HCl containing 2% thiourea (m/v) and shaking at 200 rpm for 30 min at 22.5˚C.

In this experiments, 8 mg L^{-1} of 50 mg mL^{-1} NPs aqueous dispersion (described in Section 3.2.5) were used as reference material to check how various factors (pH, time and elution process) affected the dissolution of Fe and Si.

In all cases after the prescribed time interval the NPs were separated with an external magnetic field and the supernatant was collected to determine the total amount of Fe and Si in the solution using ICP.

3.10.1 Raman Spectroscopic Study

The bonding analysis between Hg(II) and SH-SCMNPs was conducted using Raman spectroscopy with Nanonics MultiView 4000 (Nanonics Imaging LTD.) in the range of 400–4000 cm^{-1}. Raman scattering was excited with a 632.8 nm line of internal, air-cooled, helium–neon laser. For sample preparation, a 20 µL drop of NPs suspension was deposited on the microscope slide and dried at room temperature. The samples were placed on the stage and then analysed by scanning 32 times in the spectral range with a spectral resolution of 4 cm^{-1}.

3.10.2 Zeta potential

Zeta potential (ZP) is a very suitable index to evaluate the level of interaction between colloidal particles. ZP measurements are used to assess the stability of colloidal systems. ZP measurements were obtained using a ME11 Zetasizer Nano ZS (Malvern Instruments Ltd, UK). The ZP results were based on the electrophoretic mobility of the NPs in an aqueous medium after applying Smoluchowski's equation. Electrophoretic mobility was obtained by subjecting the samples to electrophoresis and measuring the velocity of the particles using laser Doppler velocimetry (LDV). The ZPs of the NPs were performed using Folded Capillary cell (DTS1060), (Malvern Instrument Ltd, UK), at 25°C. The measurements were carried out at pH ranging from 2.0 to 8.0 and the pH was adjusted to these levels using 0.1 M HNO_3 and NaOH. Smoluchowski's equation was used to predict the ZP, (ξ), from the measured particle electrophoretic mobility, μ_e, as

$$\zeta = \frac{\eta}{\varepsilon}\mu_e \quad (3.7)$$

where η and ε are the viscosity and the dielectric constant of the dispersion medium, respectively. The reported ZP values are averaged over six measurements, each of which was obtained over 20 electrode cycles. The measurements were performed in triplicates and the averaged values were calculated with the data of six runs and presented with the standard deviation.

3.11 Semi - Continuous Adsorption System

All the results obtained from the batch test experiments were employed to develop a semi-continuous system for the removal and recovery of mercury from industrial wastewater using magnetite NPs. This system is expected to provide a simple, cost-effective and environmentally friendly technique compared with present techniques.

This technique will be described in detail in Chapter 7.

Chapter 4

Characterisation of Nanoparticles

4.1 Introduction

The characterisation of Fe_3O_4 NPs, SCMNPs and SH-SCMNPs used a combination of complementary and confirmative techniques to build up a picture of the surface composition, morphology, orientation and structure of the NPs. These included: X-ray diffractometer (XRD); transmission electron microscopy (TEM) and scanning electron microscopy (SEM). Specific surface area and pore volume distribution were determined from N_2 adsorption-desorption isotherm using the BET and BJH methods; vibrating sample magnetometer (VSM); thermo gravimetric analysis (TGA); Fourier transform infrared spectroscopy (FTIR); and nano-sizer for the particles size distribution and zeta potential.

4.2 Results and Discussion

4.2.1 XRD Technique

Pei et al. (2007) and Valenzuela et al. (2009) described the effect of increasing the temperature of the solution during the synthesis of Fe_3O_4 NPs by co-precipitation, and this can lead to a change in the type of iron oxide, its size, distribution, shape and morphology. Therefore, in this case, the Fe_3O_4 NPs could be transformed to another form of iron oxide such as hematite or goethite. In order to avoid the effect of decomposition temperature on particle properties, the reactor used for synthesis of Fe_3O_4 NPs was fitted with two thermometers: one is in a RB flask to adjust the temperature in the core of the reaction and the other is in the silicon bath to keep the temperature below 100˚C. Powder XRD was used to confirm that SCMNPs and SH-SCMNPs were the NPs of the pure magnetite (Fe_3O_4). Figure 4.1 shows the typical nanocrystaline peaks of the Fe_3O_4 NPs prepared from $FeCl_2 \cdot 4H_2O$ and $FeCl_3 \cdot 6H_2O$, the phase identification was

performed by comparing the measured diffraction pattern of the prepared materials with that of pure magnetite and the reported data of the Joint Committee on Powder Diffraction Standards (JCPDS), file no. 19-0629. The XRD diffraction patterns with six diffraction peaks (220, 311, 400, 442, 511 and 440) can be indexed to the inverse spinel structure of Fe_3O_4 (as indicated in Figure 4.1). No other crystalline phases were detected. The absence of lines 110 (d = 4.183 Å at 2θ =21.22˚) and 104 (d = 2.700 Å at 2θ = 33.15˚) indicates that both goethite and hematite were not formed and that the XRD pattern corresponds to pure magnetite (Itoh and Sugimoto, 2003).

The wide angle XRD patterns (Figure 4.1) of the SCMNPs and SH-SCMNPS shows that the mesoporous spheres have similar diffraction peaks to that of the Fe_3O_4 NPs, and therefore the results suggest that the magnetic core was well retained in the silica matrix. A low angle of XRD pattern of mesoporous SCMNPs is shown in Figure 4.2, with only a high intensity peak (100) at 2θ = 2.50˚. This suggests that the mesoporous structure becomes nonsymmetric and poorly ordered. Less order in the mesostructure silica matrix could be attributed to the embedding of Fe_3O_4 NPs (Huang et al., 2009).

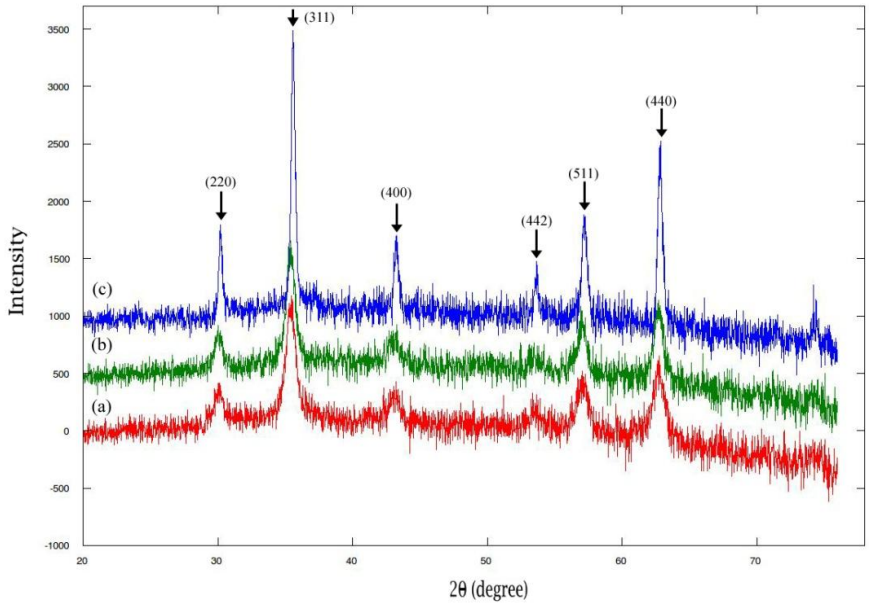

Figure 4.1: XRD pattern for (a) Fe_3O_4 NPs, (b) SCMNPs and (c) SH-SCMNPs.

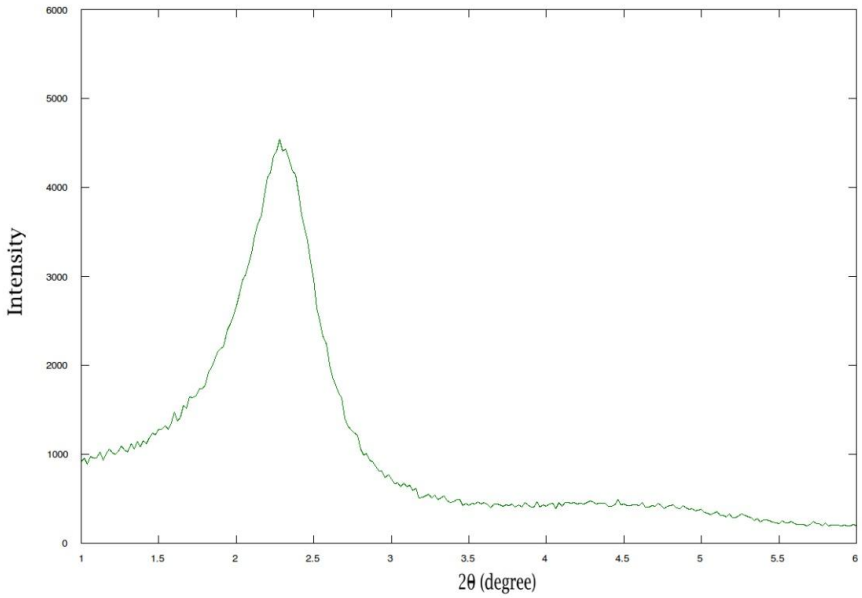

Figure 4.2: The low angle XRD pattern of SCMNPs.

4.2.2 Zeta Potential

The zeta potential of the Fe_3O_4 NPs, SCMNPs and SH-SCMNPs were all measured and showed that the magnitude decreased with increasing pH values. SH-SCMNPs showed good stability at a range of different pH values, with a maximum zeta potential of 43.60 mV. The magnitude, in general, decreased with pH but a moderate stability was still indicated at pH 4.0 when the zeta potential was 20.01 mV. At pH 2.0, however, the magnitude decreases significantly to 2.52 mV, corresponding to a less stable suspension. The surface charge of Fe_3O_4 NPs remained positive at pH values below 4.8. The isoelectric point (IEP) of Fe_3O_4 NPs was found to occur at pH 4.8. This value is significantly different from the IEP for the SCMNPs and SH-SCMNPs that occurred at pH 3.4 and 2.2, respectively. The negative surface charge of SCMNPs was to be expected due to the increased number of hydroxyl groups present on the surface of Fe_3O_4 NPs after silica coating; this was previously reported (Vaidya et al., 2011). In addition, the presence of silanol groups on the surface of SCMNPs (derived from TEOS) might play a key role in producing negative charges (Lee et al., 2011). A silanol group contains a hydrogen atom that can dissociate and produce a negative charge. Figure 4.3 shows that as the pH was decreased, more hydrogen ions were dissociated and produced negative zeta potentials. It was clearly noticeable that the zeta potential was changed after modifying SCMNPs with thiol groups. The obvious change in zeta potential further confirms the deposition of 3-MPTMS on the surface of the NPs. Similar to the silanol group, the thiol group of SH-SCMNPs contains a hydrogen atom that can dissociate and produce a negative zeta potential.

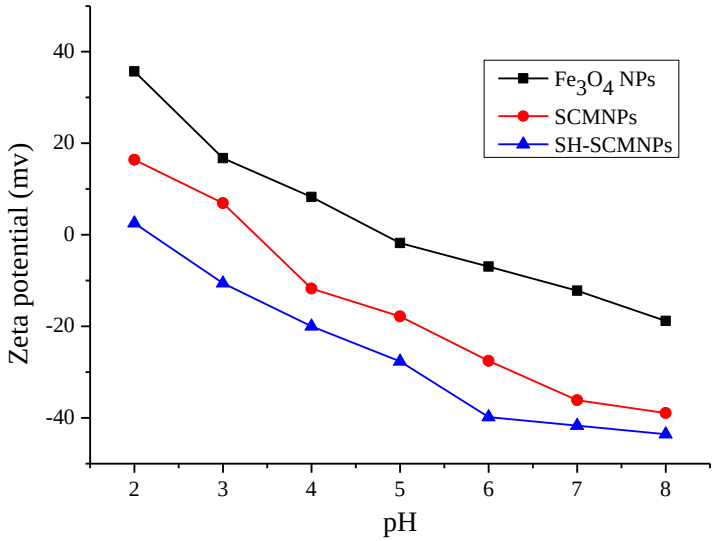

Figure 4.3: Zeta potentials of Fe_3O_4 NPs, SCMNPs and SH-SCMNPs.

4.2.3 Dynamic Light Scattering (DLS)

4.2.3.1 Particle size distribution

Several characteristics of the sample, such as solvent viscosity, solvent refractive index and sample temperature, can affect the DLS. The scattering intensity depends on the mass or size of the particles, solute particle concentration, and refractive index differences between the solute and solvent. The forming of aggregates via solute-solvent interactions should be avoided. In this study, the NPs suspensions were diluted to a concentration of approximately 8 mg L^{-1}. Low concentrations of salts such as NaCl and KCl have been described as good solvents to avoid a Coulombic interaction between charged systems (Polyelectrolytes) (Meunier et al., 2001; Ito et al., 2004). Therefore, these solvents were used as an index to compare with the results obtained using deionised water as the solvent. Air bubbles were removed by ultrasonication.

As shown in Figure 4.4, the measured hydrodynamic particle size distribution increased from an average diameter of ~75 nm for Fe_3O_4 NPs to ~105 nm after silica coating, and was found to be ~111 nm after 3-MPTMS functionalisation. It can be seen from Figure 4.4 that the size distribution of the three types of NPs is a unimodal size distribution. The results of the DLS measurements demonstrating only one peak suggest that the

particles are mostly isolated rather than being aggregated in the solution and that the prepared NPs are highly monodisperse in aqueous media.

Further experiments were performed to study the effect of the type of solvent on the hydrodynamic size distribution of the NPs using three different solvents: deionised water, 0.1 M NaCl and 0.1 M KCl. In all cases, the pH of the system was adjusted to pH 6.0 and measured directly before transferring the samples into folded capillary cells and mixing via bath sonication and vortexing. The DLS results for particle size in various types of solvents for NPs are presented in Table 4.1. Fe_3O_4 NPs, SCMNPs and SH-SCMNPs exhibited nearly the same size when dispersed in water, 0.1 M NaCl and 0.1 M KCl without any change or agglomeration size.

Table 4.1: Particle size and polydispersity index (Pdi) of NPs using various types of solvents.

Particles	**Media**	**DLS**	
		Average diameter (nm) (±SD)	**Pdi (±SD)**
Fe_3O_4 NPs	DW	75.52 (0.59)	0.14 (0.01)
	0.1M NaCl	75.60 (0.25)	0.16 (0.01)
	0.1M KCl	76.45 (0.52)	0.18 (0.02)
SCMNPs	DW	105.57 (0.45)	0.06 (0.02)
	0.1M NaCl	106.23 (0.74)	0.06 (0.03)
	0.1M KCl	106.20 (0.40)	0.05 (0.02)
SH-SCMNPs	DW	111.30 (0.61)	0.06 (0.01)
	0.1M NaCl	111.27 (0.55)	0.07 (0.02)
	0.1M KCl	111.20 (0.46)	0.06 (0.01)

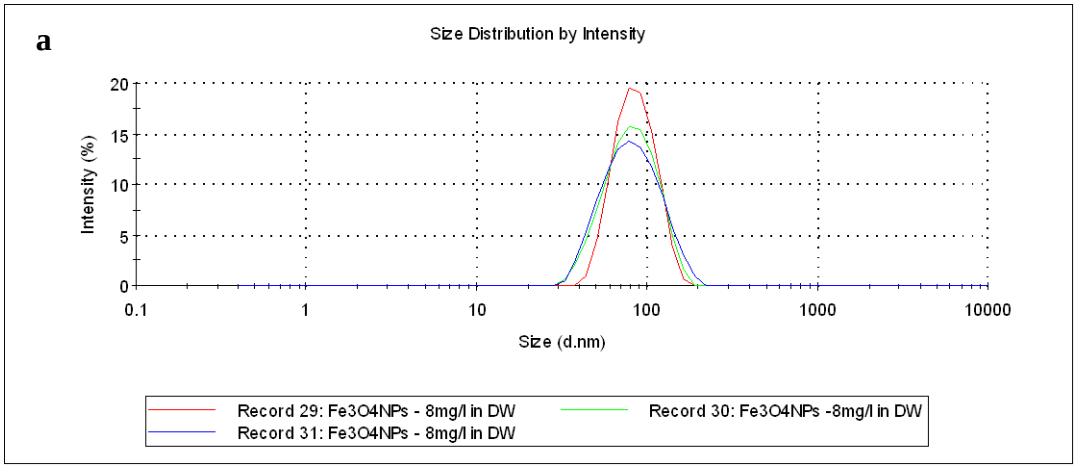

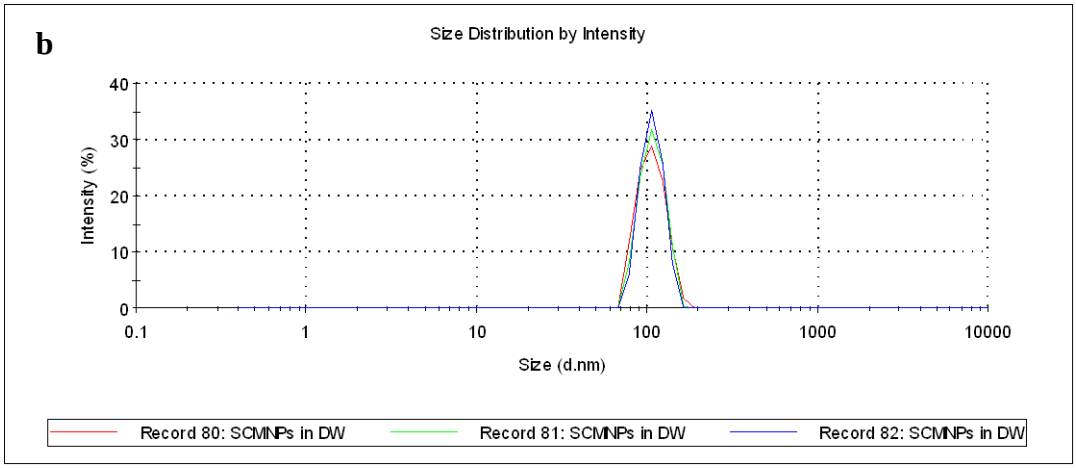

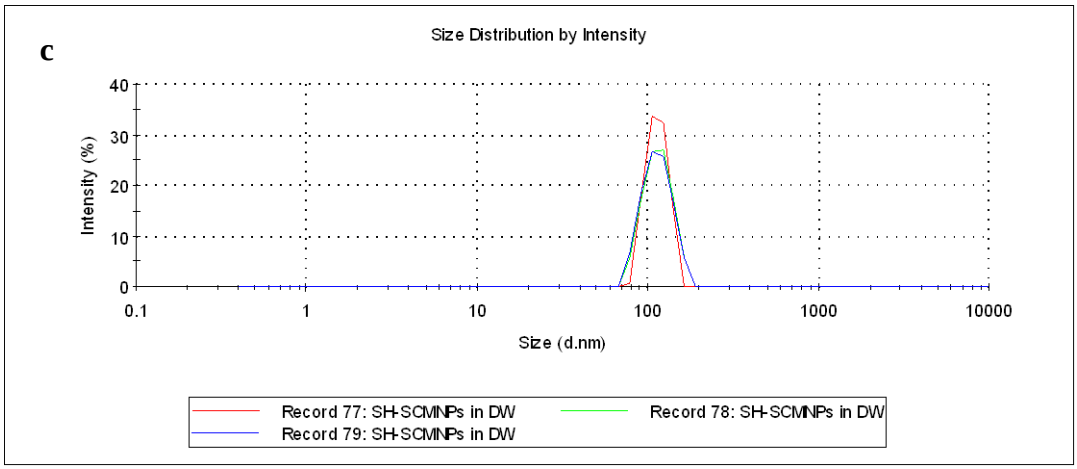

Figure 4.4: DLS plot for the particle size distribution of (a) Fe_3O_4 NPs, (b) SCMNPs, and (c) SH-SCMNPs in deionised water.

4.2.3.2 Stability tests

Stability tests were conducted by dispersing 8 and 32 mg L^{-1} of NPs (Fe_3O_4 NPs, SCMNPs and SH-SCMNPs) in deionised water at pH 6.0 and the stability of the suspensions were reviewed by measuring the size distribution of the NPs over time. As shown in Figure 4.5, the average particle size distribution remained essentially constant for 8 hours at different concentrations without obvious aggregation and without any significant deterioration in the hydrodynamic average size. All three types of particles remained suspended for a reasonable period of time after being well dispersed and this property is particularly suitable for target loading in industrial applications.

The hydrodynamic size distribution of SCMNPs and SH-SCMNPs was also measured across different pH ranges (2.0-9.0) and the measured average hydrodynamic size is shown in Figure 4.6. At pH 2.0, the average hydrodynamic size for SCMNPs and SH-SCMNPs was ~130.50 nm and ~149 nm, respectively but at pH 3.0, the average size decreased to ~125.20 nm for SCMNPs and to 136.90 nm for SH-SCMNPs. Changing the pH of the solution (4.0-9.0) did not significantly change the hydrodynamic size of either samples. Thus, SCMNPs and SH-SCMNPs are mostly isolated and are not aggregated across a range of pH values. The agglomeration of particles at pH 2.0-3.0 could be the result of coagulation that occurs when the zeta potential is above point zero of a charge (Lu et al., 2007). However, increasing the time of agitation easily breaks up loose agglomerates and the NPs could be re-suspended.

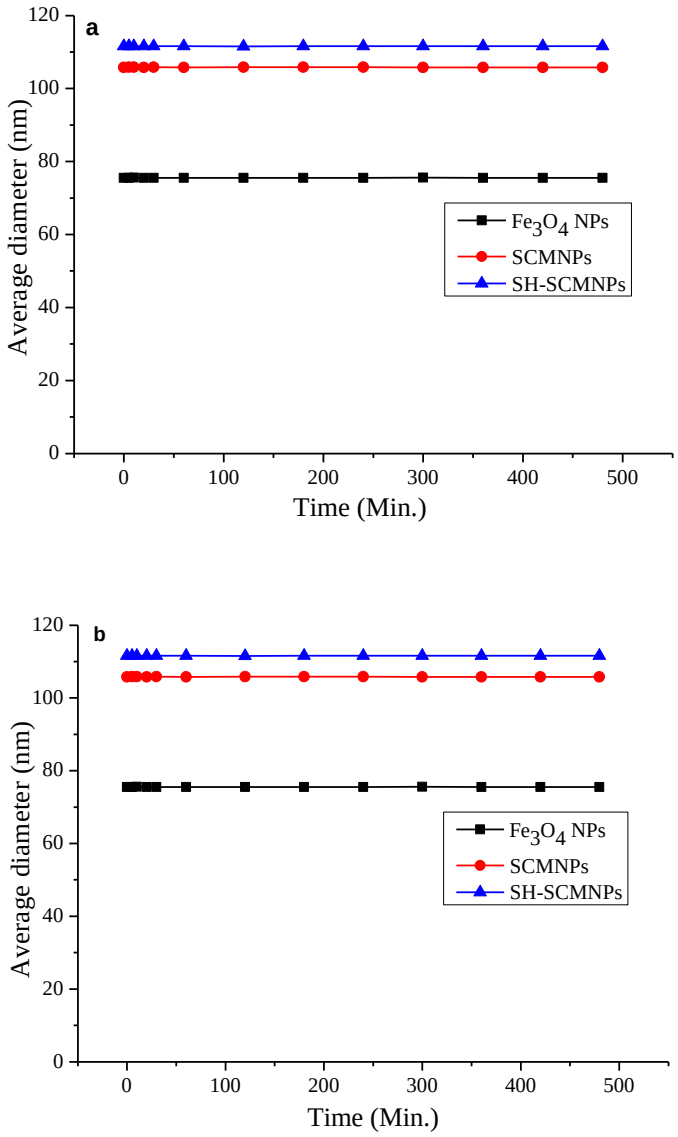

Figure 4.5: The time-dependent aggregation of Fe_3O_4 NPs, SCMNPs and SH-SCMNPS, (a) 8 mg L^{-1} and (b) 32 mg L^{-1}.

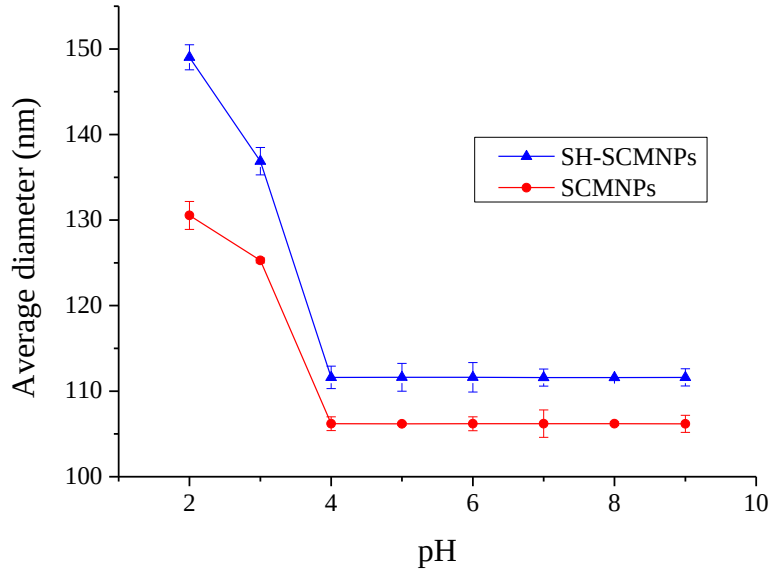

Figure 4.6: Variation of the hydrodynamic sizes of SCMNPs and SH-SCMNPs across a range of pH values.

4.2.4 Electron Microscopy

The size and morphology of prepared NPs was monitored during the various preparation steps using SEM and TEM. The results obtained are summarised below.

4.2.4.1 SEM

A typical SEM image for the Fe_3O_4 NPs is shown in Figure 4.7, and it can be seen that the particles are nearly spherical with a size range of between 30-100 nm. The particles appear to be aggregated which is due to the absence of any stabiliser in the reaction system during the course of formation of Fe_3O_4 NPs. This probably as a result of Fe_3O_4 NPs having a hydrophobic surface, and due to hydrophobic interaction between the particles, which causes the particles to agglomerate and form large clusters (Hamley, 2003).

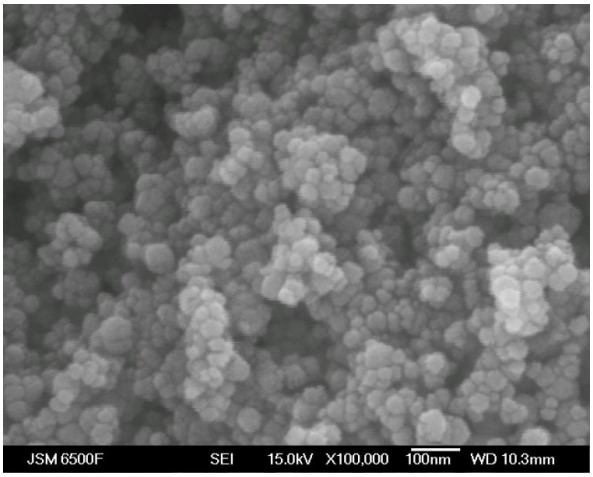

Figure 4.7: SEM micrograph of Fe_3O_4 NPs.

The NPs EDX spectrum (Figure 4.8) confirmed the composition of iron (68.5%) and oxygen (31.5%). The expected ratios of 72.4% iron and 27.6% oxygen were skewed due to the increased ratio of oxygen detected that likely included the presence of hydroxides.

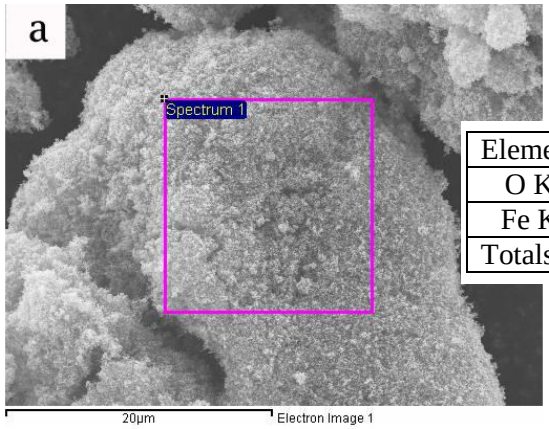

Element	Weight%	Atomic%
O K	31.52	61.64
Fe K	68.48	38.36
Totals	100.00	

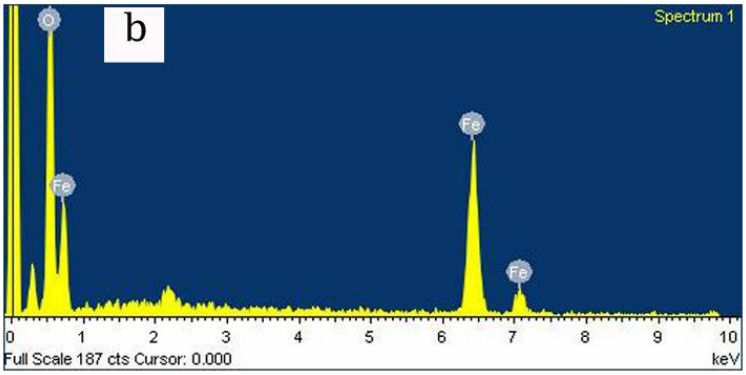

Figure 4.8: (a) Low magnification SEM micrograph (b) EDX spectra of Fe_3O_4 NPs.

The low magnification image of Fe_3O_4 NPs after silica coating is shown in Figure 4.9, where it can be seen in panel (b) that silicon was also detected together with Fe and O when using EDX to analyse SCMNPs.

To avoid aggregation of Fe_3O_4 NPs before coating stabilisers such as a surfactant or 'ligand' molecules are usually added at preparation (Gupta and Gupta, 2005). The structural properties of surfactants and micellar solutions played a key role during in the preparation of mesoporous SCMNPs (Chapter 3). In this research, the addition of CTAC aqueous solution as co-surfactants was used to alter the packing parameter, resulting in elongated CTAC micelles. CTAC aqueous solution adheres to the surfaces in a substrate specific manner and may cause a reduction in the curvature of the surfactant aggregates. However, these effects are complex and their evaluation is not within the scope of this research. Non-aggregated SH-SCMNPs are shown in Figure 4.10, which demonstrates many particles separated from each other.

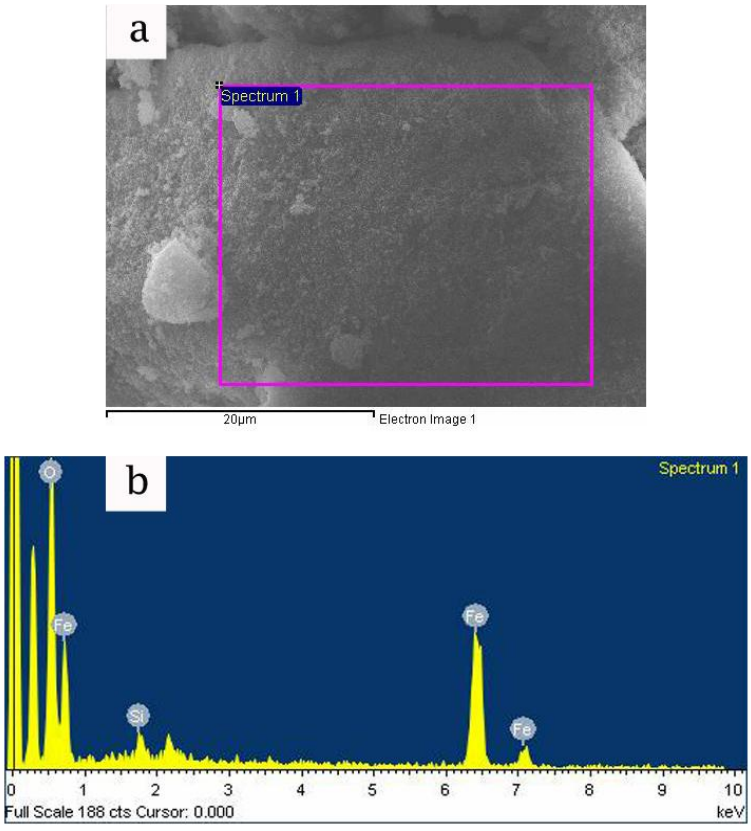

Figure 4.9: (a) Low magnification SEM micrograph (b) EDX spectra of SCMNPs.

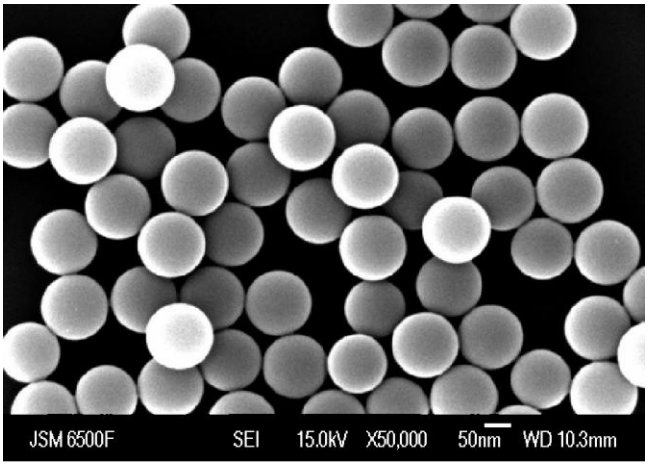

Figure 4.10: SEM micrograph of SH-SCMNPs.

The low magnification image of SCMNPs after thiol modification is shown in Figure 4.11. The exact composition was determined by EDX and the spectrum in panel (b) shows that a weak S peak is observed along with Fe, O and Si peaks. The presence of the S peak indicates that the functionalisation was successful.

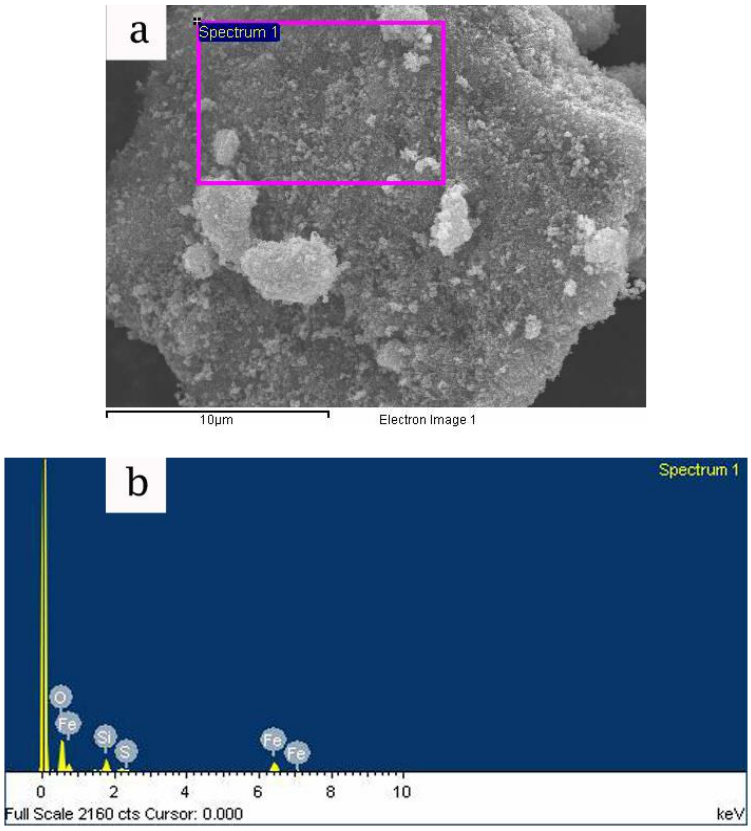

Figure 4.11: (a) Low magnification SEM micrograph (b) EDX spectra of SH-SCMNPs.

4.2.4.2 TEM

TEM gives visual information that can help identify the elemental composition of the material and also provide complementary information to other techniques such as X-ray diffraction.

A typical TEM image for Fe_3O_4 NPs is shown in Figure 4.12. It can be seen that the Fe_3O_4 NPs are nearly spherical with some demonstrating a hexagonal structure, as marked by the arrow. The mean particle size observed was in range of 30-80 nm. A high resolution TEM (HRTEM) image provided more structural information on the Fe_3O_4 NPs, and Figure 4.13a reveals that the Fe_3O_4 NPs show good face centered cubic (FCC) crystallinity with hexagonal intergrowth. Doves et al. (2007) suggested that FCC structures in a magnetite core are the result of oxygen forming FCC and Fe cations occupying the interstitial tetrahedral and octahedral sites. Here, the electrons can jump between Fe^{2+} and Fe^{3+} in the octahedral site. The presence of FCC crystallinity can be confirmed by visible lattice fringes corresponding to the (111) plane of Fe_3O_4, and the interlayer distance between the crystal faces was calculated to be ~0.19 nm. The power spectrum of the image (Figure 4.13b) further supports the presence of a FCC structure.

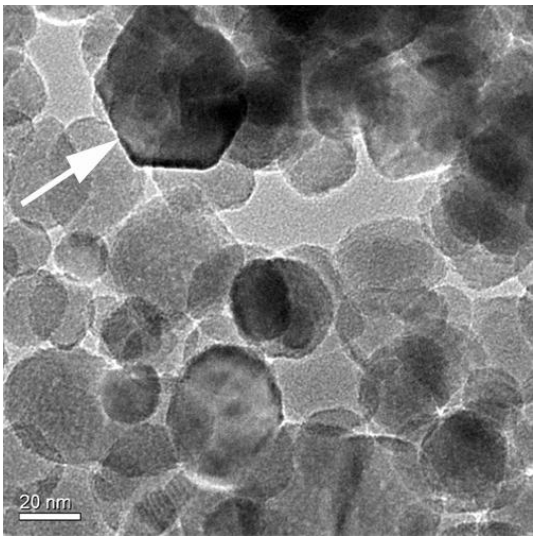

Figure 4.12: TEM micrograph of Fe_3O_4 NPs.

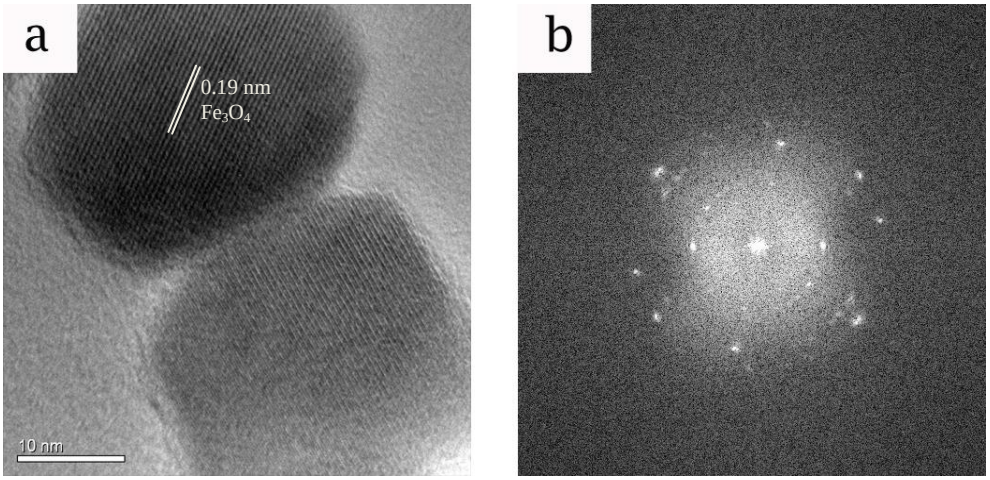

Figure 4.13: (a) HTREM image of Fe_3O_4 NPs and (b) power spectrum by Fourier transforming of the HRTEM image.

The electron diffraction (ED) pattern of Fe_3O_4 NPs shows that the NPs has a highly polycrystalline nature which can be indexed to the inverse spinel structure of Fe_3O_4 which is in agreement with the XRD results (Figure 4.14a), and the diffraction rings are consistent with Fe_3O_4 NPs reported in the literature (Sun et al., 2004; Yang et al., 2008). In the ED pattern, the rings/spots that were observed are an indication of the reflection of the FCC structure and this indicates the formation of crystalline Fe metal.

The ED pattern of some selected portions of the SH-SCMNPs (Figure 4.14b) shows that all the rings are clear and well defined. Zhou (2001) suggested that the clear diffraction rings in ED patterns reveals a nanocrystallinity of uniform crystallite size. The formation of uniform Fe_3O_4 particles could be attributed to the attachment of silica onto the surface of the particles. The existence of silica prevents the amalgamation of particles due to the repulsive interaction between the same charges on the silica. Thus, silica concentration plays an important role in modifying the particle and crystalline characteristics.

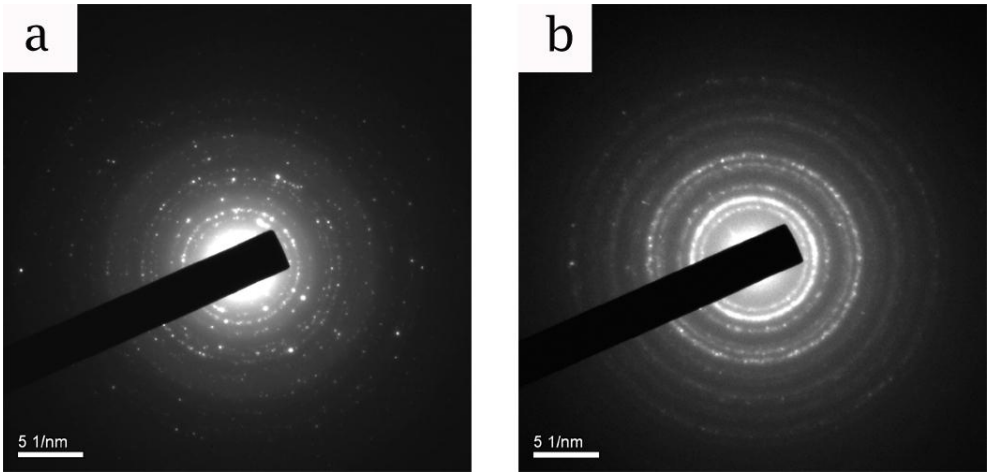

Figure 4.14: Electron diffraction patterns, (a) Fe_3O_4 NPs, (b) SH-SCMNPs.

A typical bright-field TEM image taken for SCMNPs is shown in Figure 4.15. SCMNPs retained their original shape with minimal aggregation between particles. A thin layer of silica (light shading) was observed in the Fe_3O_4 NPs, Figure 4.15a. The exact composition of the silica layer was determined by EDX and the spectrum is shown in Figure 4.15b. The spectrum showed two strong peaks that included Si and O, but a weak Fe peak was also observed.

The bright field high magnification TEM image of SCMNPs, Figure 4.16, shows that the lamellar mesostructure that interfered with the hexagonal structure was clearly obtained after calcination, this was determined when the electron beams were perpendicular to the axis of the channels. The inset panel of Figure 4.16 shows the well-defined mesoporous structure of the particles. The pore size is estimated to be ~ 2.1 nm and this was determined by direct electron beams parallel to the main axis of the pores.

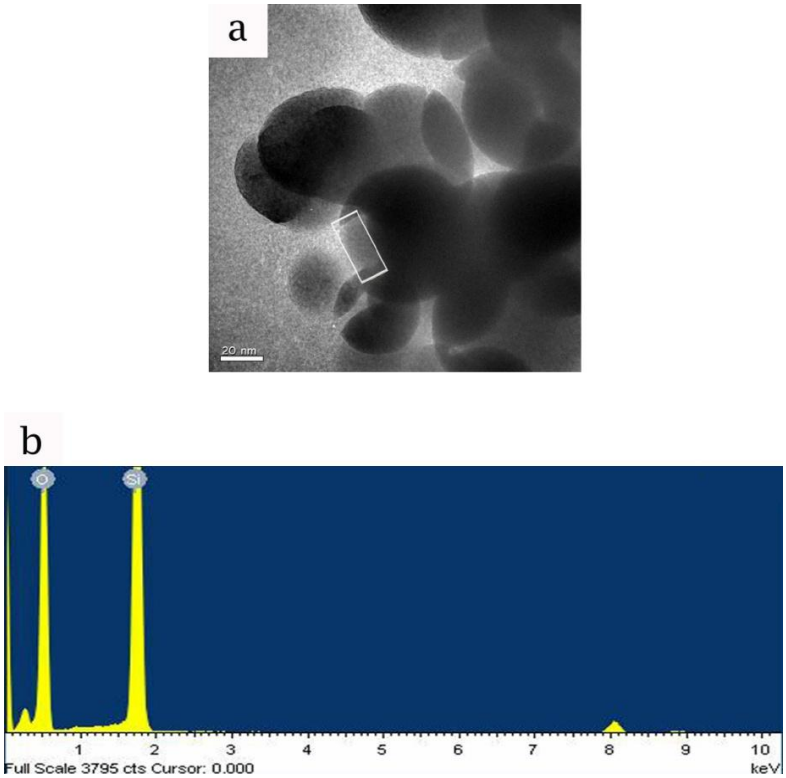

Figure 4.15: (a) high resolution image showing Fe_3O_4 NPs covered by silica and (b) EDX of silica layer around Fe_3O_4 NPs.

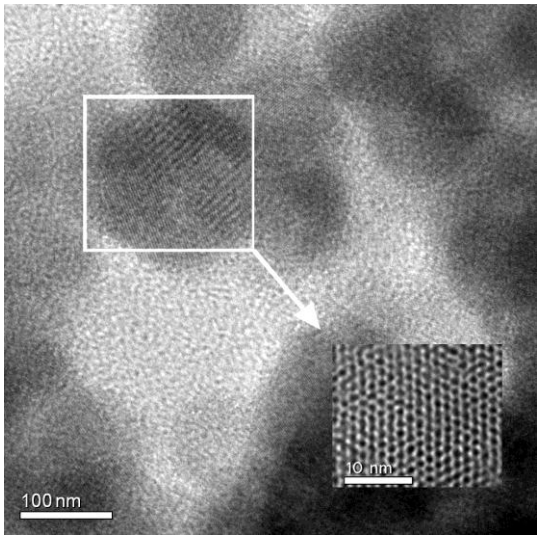

Figure 4.16: TEM image of one dimension of the mesoporous structure and the hexagonal arrangement of SH-SCMNPs.

4.2.5 TGA analysis

In order to confirm the anchoring of the thiol moiety to the surface of the SCMNPs, TGA analysis was undertaken. The TGA profiles of Fe_3O_4 NPs, SCMNPs and SH-SCMNPs are presented in Figure 4.17. The absolute weight loss of the uncoated Fe_3O_4

NPs is ~ 1.10 % for the whole temperature range and is due to the removal of the physically adsorbed water. For SCMNPs, three areas of weight loss were identified. The first region (I) from 50 °C to around 150 °C (~1.2% weight loss) is associated with removal of residual solvent and physically adsorbed water. The second weight loss of ~ 3 % over the temperature range of 200–600 °C (region II) is due to the removal of residual organic chemicals, and at temperatures above 600 °C (region III), a further slight weight reduction ~ 0.6 % is observed which corresponds to water losses due to condensation of the silanol groups to siloxane bonds (Brinker, 1988; Mureseanu et al., 2011). This weight loss of ~ 3.8 % is consistent with the findings of Dong et al., (2008) who used a sol-gel process for the synthesis of SCMNPs. A TGA curve of the SH-SCMNPs shows three main distinct weight loss steps. The first mass loss ~ 2 % in the temperature range of 50-200 °C corresponds to the removal of physically adsorbed water and remaining solvent, and the second weight loss of ~ 8 % is between 200 and 450°C is the result of a gradual oxidation of the organic groups from the surface of the silica. The last area of weight loss ~ 3.7 % is attributed to the complete oxidation of all organic materials. There was no significant weight loss observed for temperatures above 750 °C. The increased weight loss ~ 8.7 % demonstrated by SH-SCMNPs was a good indicator of the successful linkage between the silica surface and the thiol groups.

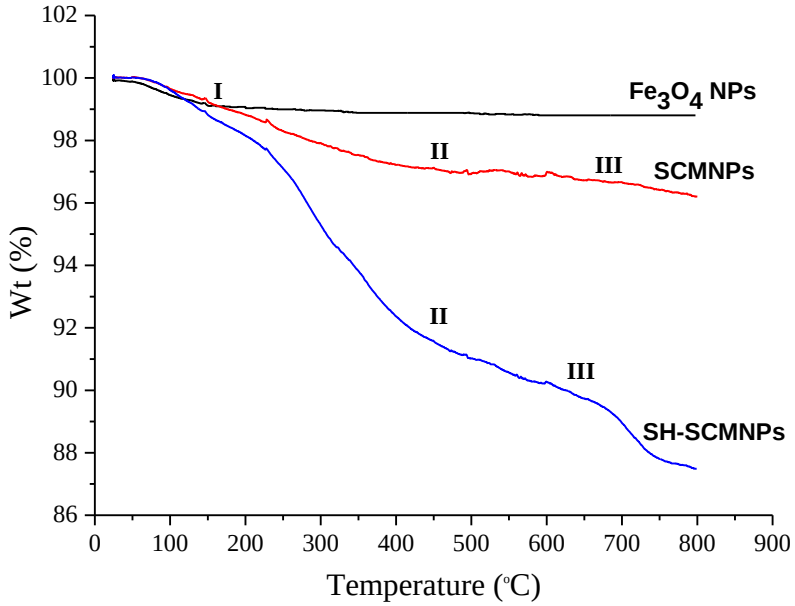

Figure 4.17: TGA Curves of Fe_3O_4 NPs, SCMNPs and SH-SCMNPs.

4.2.6 FTIR and Raman Spectroscopy

FTIR spectroscopy was used to confirm the presence of thiol groups, silica and other organic groups attached to the Fe_3O_4 NPs, SCMNPs and SH-SCMNPs (Figure 4.18). For the Fe_3O_4 NPs, the peaks at ~ 516.20 and 593.38 cm^{-1} can be attributed to the Fe-O bond vibration of Fe_3O_4 , while the peak at 1630.88 cm^{-1} also indicates the existence of a Fe-O bond. The FTIR spectrum of the SCMNPs shows strong absorption characteristics at the Si-O bands of 789.15 and 1082.49 cm^{-1}, and there is also a weak peak at 962.80 cm^{-1} corresponding to the Si-OH bending vibration. The absorption bonds at 582.57 cm^{-1} revealed the presence of a Fe-O-Si bond. The broad absorption band at 3421.33 cm^{-1} is attributed to the stretching of O-H bonds on the surface of the silanol groups with the hydrogen bond and the remaining adsorbed water molecules. Additional bands were observed at 2855.42 and 2964.29 cm^{-1} and these correspond to CH_3 and CH_2 vibrations respectively. S-H stretches were found at 2509.93 cm^{-1}; these are typically very weak and convoluted due to the contamination of the CO_2 stretching bands from the background. Generally, the S-H stretching band is characteristically weak and cannot be detected in the spectra of dilute solutions or thin films (Silverstein et al., 2005). However, the FTIR spectra showed that the surface of the SCMNPs contains an (-SH) group that results from the modification procedure with 3-MPTMS.

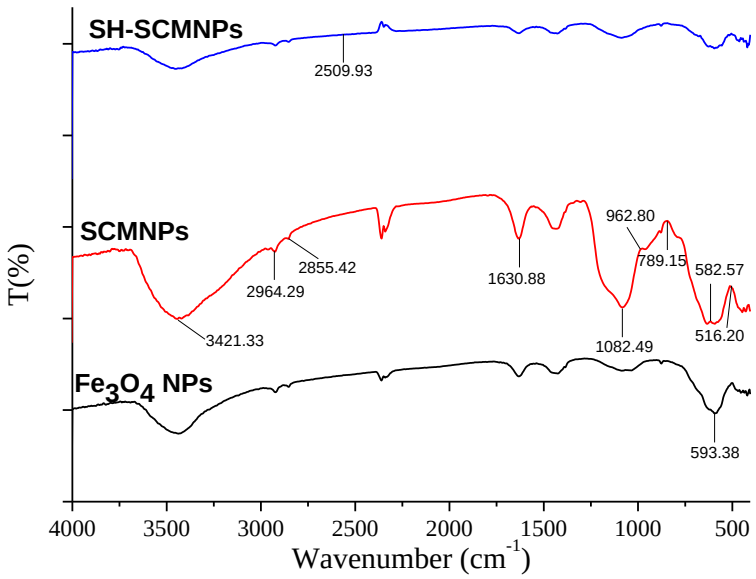

Figure 4.18: FTIR spectra of Fe_3O_4 NPs, SCMNPs and SH-SCMNPs.

Raman spectroscopy is a good technique to detect thiol groups on the surface of silica (Evangelista et al., 2007). Figure 4.19 shows the Raman spectra of SCMNPs and SH-SCMNPs obtained using a laser power of 10 Mw. For functionalised thiol on the surface of the silica, a band at 2512 cm^{-1} can be attributed to the S-H stretching vibration. It also indicates that thiol groups were attached to the silica-coated magnetite NPs. As observed in the FTIR spectroscopy, the peaks at ~ 493 and 506 cm^{-1} in the Raman spectroscopic investigation can also be attributed to the Fe-O bond vibration of Fe_3O_4. The observed peaks at 676 and 1750 cm^{-1} provide evidence of the presence of silica on the surface of Fe_3O_4, and these bands are assigned to Si-O stretching of the silanol group. The sharp band observed at 1680 cm^{-1} can be attributed to the stretching mode of siloxane (Si-O-Si), and a well defined peak at 2894 cm^{-1} can be assigned to C-H stretching of carbon, confirming the presence of organic groups attached to the surface of the silica (Prado et al., 2004). The band at 1383 cm^{-1} could be attributed to ring vibration.

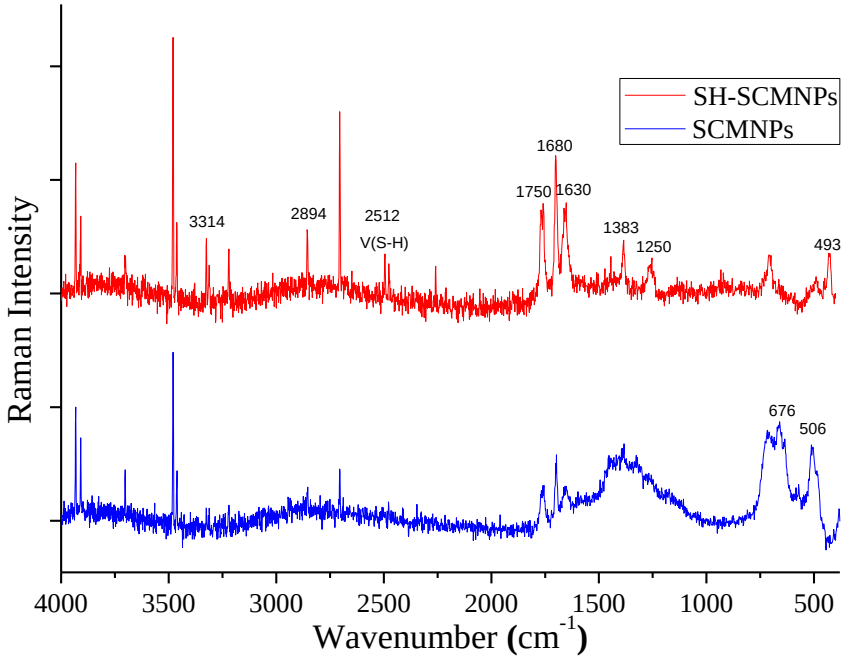

Figure 4.19: Raman spectra of SCMNPs and SH-SCMNPs.

4.2.7 Magnetic Properties

4.2.7.1 Vibrating sample magnetometer (VSM)

The magnetisation characteristics of synthesised magnetite NPs are significant in potential industrial applications. A strong magnetisation property is important in the collection of heavy metals from a complex system. The magnetisation curves for Fe_3O_4NPs, SCMNPs and SH-SCMNPs, as measured at room temperature, are shown in Figure 4.20. The saturation magnetisation curves show that no hysteretic loop was obtained for any of the samples. Typically, superparamagnetic NPs will exhibit no hysteresis and thus have zero magnetic coercivities and no remanence magnetisation, whereas blocked NPs will exhibit both (Lu et al., 2007). Therefore, the curves obtained indicated the superparamagnetic nature of the prepared magnetic NPs. The advantage of superparamagnetism behaviour is that large magnetisation is observed even under low magnetic fields (Ge et al., 2007). As can be seen, the Fe_3O_4 NPs possessed a very high saturation magnetisation (~ 0.60 emu); however, this saturation magnetisation decreased significantly to approximately 0.25 and 0.20 emu when the Fe_3O_4NPs were coated with silica and modified by thiol groups respectively. However, due to the presence of the nonmagnetic silica and the thiol groups, a reduction of magnetisation was expected. NPs in this study possessed superparamagnetic characteristics and high magnetisation values, and can quickly respond to an external magnetic field. In addition they can be re-dispersed without any significant aggregation when the external magnetic field is removed, a very important factor for Hg adsorption applications.

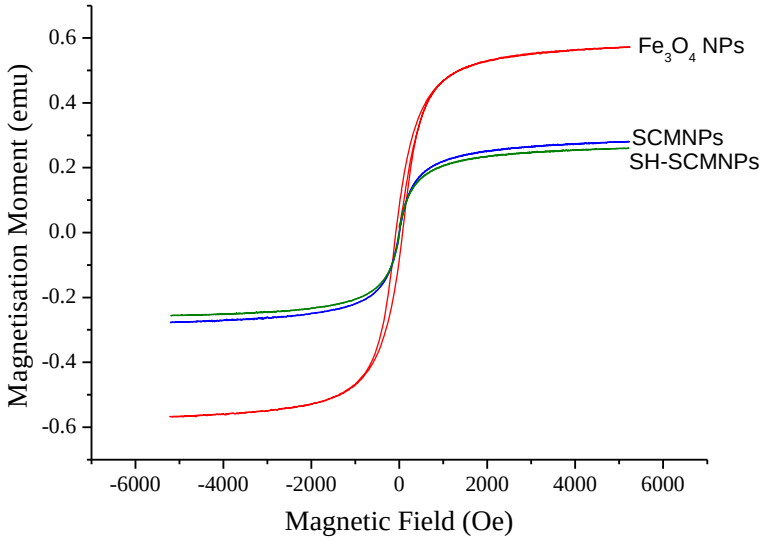

Figure 4.20: Room temperature magnetisation measurement of Fe_3O_4 NPs, SCMNPs and SH-SCMNPs.

4.2.7.2 NPs isolation

To investigate the separation of magnetite NPs from solution, SH-SCMNPs were used as they exhibit the weakest saturation magnetisation curve. A suspension of SH-SCMNPs was mixed according to the proportions used in the adsorption experiments and then a strong magnetic field was applied to isolate the NPs. Figure 4.21a shows that SH-SCMNPs were very well suspended following homogenisation by ultrasonication for 2 minutes and agitation for 1 hr at room temperature. As shown in Figure 4.21c, a permanent magnet that was placed adjacent to the suspension was able to visibly clarify the suspension within the space of one minute, and the total Fe in solution was below the sample detection limit of ICP-OES that is <0.19 mg L^{-1} (< 2.3% of the initial concentration). The magnetically separated SH-SCMNPs are not permanently magnetised and could be re-dispersed without any significant aggregation when the external magnetic field was removed (Figure 4.21d). The average hydrodynamic size of SH-SCMNPs was measured before and after separation and was found to be ~ 111.06 and 111.30 nm, respectively. Therefore, sorbents of magnetic NPs can be removed and regenerated in practice by magnetic separation.

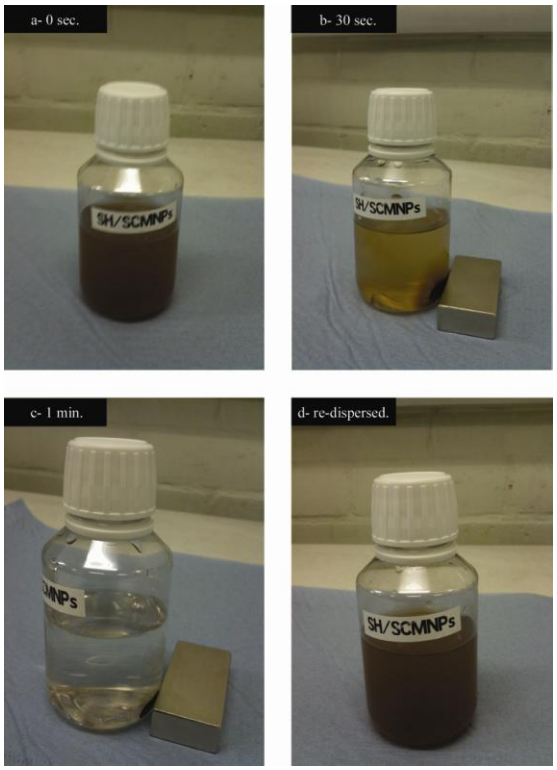

Figure 4.21: Demonstration of magnetic separation at (a) 0 sec., (b) 30 sec., (c) 1 min. and (d) re-dispersed.

To test the efficiency of this separation method, an UV/Vis scanning spectrophotometer (Ceceil 3000 series, Cecil Instruments Ltd., UK) was used to detect if there were any suspended solids still left in the solution after the specified time intervals, and the absorbance results for the wavelength of 520 nm are shown in Figure 4.22. It can be seen that for all types of NPs after applying the external magnetic field for 1 minute, the absorbance unit reading from the instrument dropped almost to its lowest level, which did not change significantly in the 10 minutes following the application of the magnet. Therefore, the separation time used after the adsorption and desorption experiments was fixed at 1 minute.

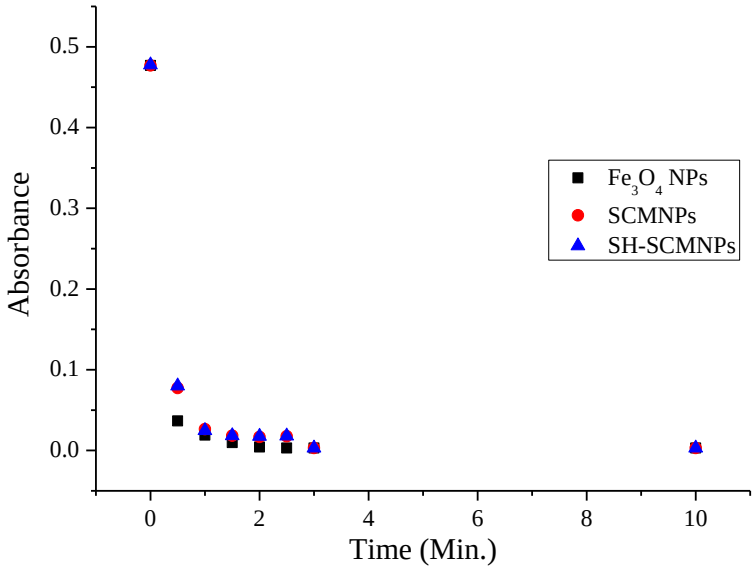

Figure 4.22: Absorbance unit reading of the residual suspended solids / colour after NPs removal at specific time intervals using UV/Vis spectrophotometer.

Intensive studies were performed to determine the pH effect on NPs solubility which might in turn affect the adsorption of Hg(II) and the reuse of NPs. ICP-OES was also applied to quantify the total Fe left in the solution after the magnetic separation of the NPs. The results of the dissolution of NPs at different conditions are discussed in Chapter 5.

4.2.8 BET Methods

The surface areas for the Fe_3O_4 NPs, SCMNPs and SH-SCMNPs are shown in Table 4.2. All the surface areas are in a range that is typically expected for magnetic NPs synthesised using sol-gel reactions and the method proposed by Wu et al. (2004) and Wu and Xu (2005); typically between 50-300 $m^2 g^{-1}$. The surface area increased from 79 $m^2 g^{-1}$ to 160 $m^2 g^{-1}$ due to the deposition of the mesoporous silica film on the magnetite cores. Dong et al. (2009) argued that the optimum surface area for coating mesoporous silica layers onto magnetite NPs is about 150 $m^2 g^{-1}$. The surface area might experience an increase in size of about 50 to 200% if the magnetite NPs were functionalised with organic groups. The surface area of the SCMNPs modified with 3-MPTMS was

measured as 250 m^2 g^{-1}. The higher specific surface area makes SH-SCMNPs an attractive candidate for targeted removal of heavy metals.

Table 4.2: Structural parameters derived from nitrogen adsorption data for Fe_3O_4 NPs, SCMNPs and SH-SCMNPs.

Sample	BET surface area (m^2 g^{-1})	Pore size (nm)	Total pore volume (cm^3 g^{-1})*
Fe_3O_4 NPs	79	---	0.17
SCMNPS	160	2.1-3.1	0.63
SH-SCMNPs	250	1.9-2.1	0.91

* Pore volume was calculated by the N_2 amount adsorbed at the highest P/P_0 (~ 0.99)

The N_2 adsorption-desorption isotherms of the SCMNPs and SH-SCMNPs, (Figure 4.23), exhibited a type–IV standard isotherm and also displayed the H3 hysteresis loop which confirms the typical isotherm associated with the presence of mesoporous structures based on the classifications of IUPAC (Zhang et al., 2007; Guo et al., 2009; Everett et al., 1985). The H3 hysteresis loop is usually found on solids consisting of aggregates or agglomerates of particles forming slit shaped pores (Leofanti et al., 1998). The isotherms determined in this study are consistent with those of other studies (Guo et al., 2009; Qu and Tie, 2009; Xia et al., 2011) that used sol-gel reactions for the preparation of silica-coated magnetic NPs.

The P/P_o position of inflection ranges is from 0.8 to 1.0 indicating the formation of the mesoporous structure on the Fe_3O_4 NPs. It is clear that the shape of the adsorption-desorption isotherm is affected by the non-porous cores of the Fe_3O_4 NPs. Moreover, the incorporation of non-porous Fe_3O_4 NPs of the size prepared in this study leads to a decrease in the amount of adsorbed nitrogen. The pore size for SCMNPs as calculated using the BJH method is shown in Figure 4.24, and the results suggest a bimodal pore distribution for the SCMNPs. The pore diameters for the SCMNPs and SH-SCMNPs are listed in Table 4.2. As expected, the presence of the Fe_3O_4 NPs leads to a decrease in both surface area and pore volume which is consistent with previous studies (Dong et

al., 2008; Nooney et al., 2002). The decrease of pore size after modification with thiol-groups might result in the collapse of the pores during modification with 3-MPTMS.

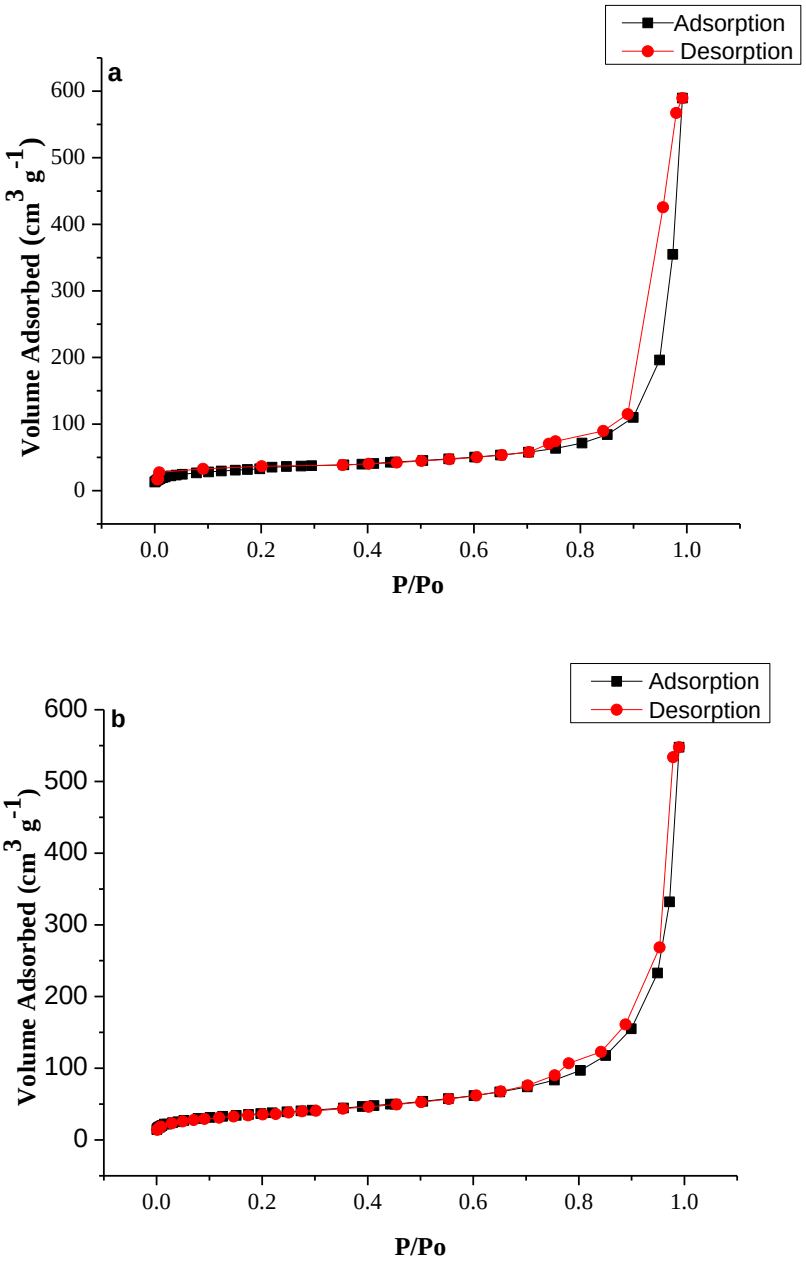

Figure 4.23: N_2 adsorption-desorption isotherm of (a) SCMNPs and (b) SH-SCMNPs.

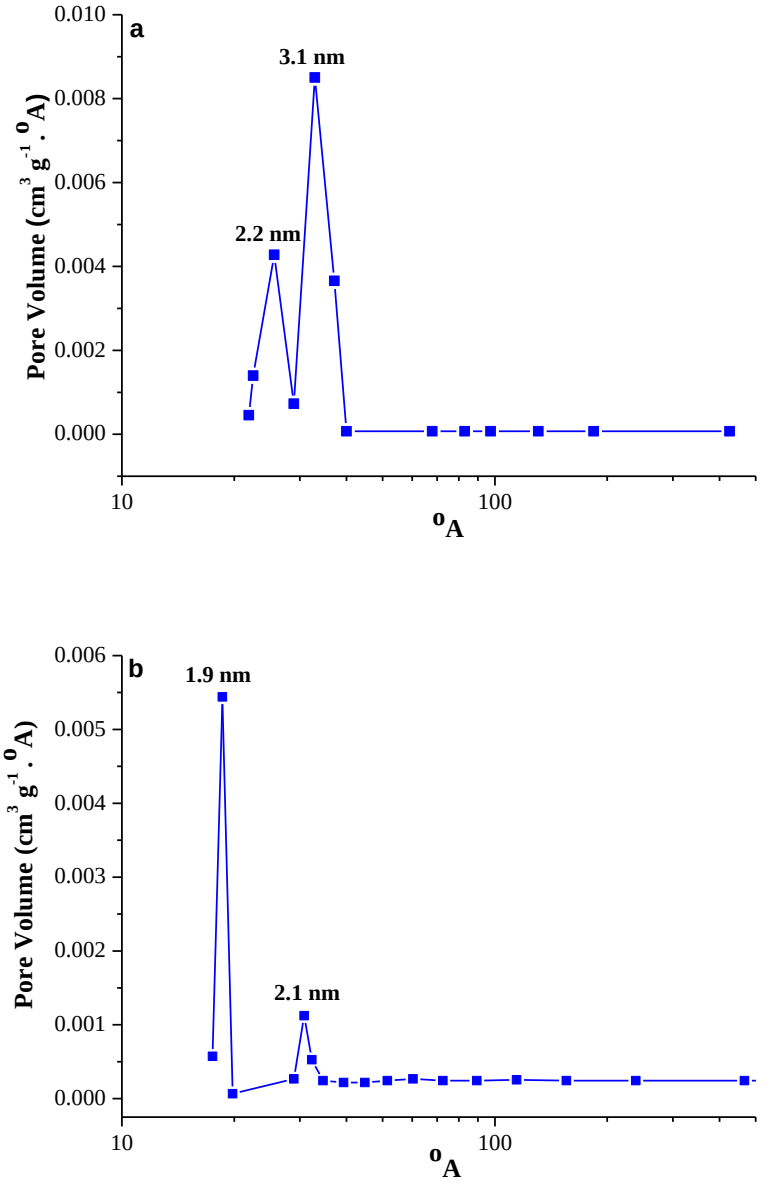

Figure 4.24: BJH pore size distribution curve of (a) SCMNPs and (b) SH-SCMNPs.

Chapter 5

Adsorption and Desorption of Hg

5.1 Introduction

The feasibility of using the nanoparticles (NPs) for the adsorption and desorption of Hg(II) from synthetic wastewater was tested. Batch experiments were performed to determine the optimal operational conditions for the maximum removal efficiency of Hg(II). Desorption and regeneration were also examined as the next step in progressing the application of this new type of adsorbents to more complex aqueous mixes containing other ions and dissolved species, typical of what might be found in natural and waste waters.

5.2 Control Experiments

5.2.1 NPs-free Control Experiments

Control experiments using PET bottle as reaction vessels were carried out at pH 6.0 using Hg(II) at a concentrations of 10 and 80 μg L^{-1} in the absence of nano-sorbents. Samples (10 mL) were taken in order to determine the total concentration of Hg before mixing via agitation for 24 hrs at room temperature (24˚C) and 200 rpm. The control experiments were replicated four times and the results are shown in Table 5.1. The average total Hg concentrations before shaking were 9.7 and 79.2 μg L^{-1}.

Table 5.1: Hg concentrations of the four replicate NPs-free control experiments; initial Hg concentrations were 10 and 80 µg L^{-1}.

	Hg con. (µg L^{-1}) Before shaking		Hg con. (µg L^{-1}) After shaking		Hg lost (%)	
	10	**80**	**10**	**80**	**10**	**80**
Replecate1	9.9	79.9	9.7	79.8	1.9	0.1
Replecate2	9.5	80.1	9.5	79.5	0.6	0.7
Replecate3	9.6	79.6	9.5	78.6	0.6	1.2
Replecate4	9.9	79.8	9.8	78.8	0.8	1.3
Average	9.7	79.8	9.6	79.2	1	0.8

Shaking 10 and 80 µg Hg L^{-1} for 24 hrs reduced the concentration of Hg(II) by 1% and 0.8% respectively, Table 5.1. A paired t-test indicated close to a significant effect of shaking for 24 hrs on Hg concentrations (P = 0.07 and 0.06 for the low and higher concentrations), Table 5.2. The small number of replicates (only 4) is inadequate to detect such small differences. However, the results are a good indicator that the PET bottles may be used as reaction vessels without any significant impact on the adsorption.

Table 5.2: Student's t-test calculations.

Paired sample test							
Hg Con. µg l^{-1}		**Paired Differences**					
		Mean	**95% conf. interval of the diff.**		**t**	**df**	***p*-value**
			lower	upper			
Pair 1	10- Pre - after	0.09	- 0.01	0.21	2.69	3	0.07
pair 2	80-Pre-after	0.66	- 0.04	1.37	2.97	3	0.06

5.2.2 Effect of NPs concentration on adsorption

The aim of this experiment was to assess the affinity of the NPs at different concentrations towards Hg. The initial concentration of NPs (Fe_3O_4 NPs, SCMNPs and SH-SCMNPs) was adjusted to be within the range of 2 to 40 mg L^{-1} in 80 µg L^{-1} Hg solution. Figure 5.1 shows that the residual values of Hg(II) ions decreases with higher

concentrations of adsorbents. The amount of Hg(II) adsorbed is greater for SCMNPs when compared to Fe_3O_4 NPs, and the greatest amount of Hg(II) adsorbed is achieved using the SH-SCMNPs. For all kinds of NPs, it is shown that the amount of adsorption increases with increasing the initial concentration of NPs. This might be attributed to the fact that with an increase in the initial concentration of NPs, more reaction sites are available for Hg(II) ions to be adsorbed. However, as the lowest concentration of Hg(II) ions was observed when the SH-SCMNPs concentration was 8 mg L^{-1} , therefore; batch adsorption tests were in general performed using 8 mg L^{-1} of adsorbents.

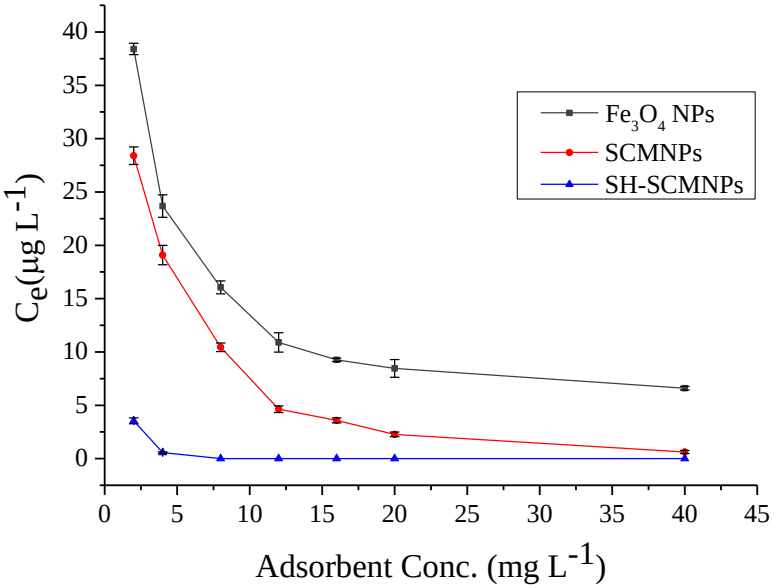

Figure 5.1: Effect of the initial concentration of NPs for the adsorption of Hg.

5.3 Kinetics Study

When choosing the adsorbents for a particular process, three main factors should be considered: the first is the affinity of the adsorbents towards the adsorbates, the second is the loading capacity, and the third is the speed at which the adsorbent can immobilise the adsorbate. Therefore, the equilibrium time is a significant operational factor for an economical wastewater treatment process (Amuda et al., 2009). Batch experiments were conducted to investigate the effect of time on the adsorption of Hg(II) ions from synthetic wastewater using different types of magnetic NPs.

Figure 5.2 shows that the rate of Hg(II) uptake using SH-SCMNPs was initially high, with about 90% of Hg(II) removed during the first 5 minutes. This was followed by a gradual reduction in the rate of removal leading to an equilibrium condition which was achieved within less than 15 minutes with 100% of the Hg(II) adsorbed. For the SCMNPs, the initial rate of adsorption was slower than the SH-SCMNPs as can be seen in Figure 5.2. About 80% of all the Hg(II) was adsorbed within 20 minutes followed by a much slower subsequent rate leading gradually to equilibrium conditions. The adsorption equilibrium was achieved within about 50 minutes, with 90% of the Hg(II) being adsorbed. Under the same conditions, the rate of Hg (II) removal using Fe_3O_4 NPs was initially very slow before it appreciably increased and attained about 85% of the adsorption capacity in 80 minutes.

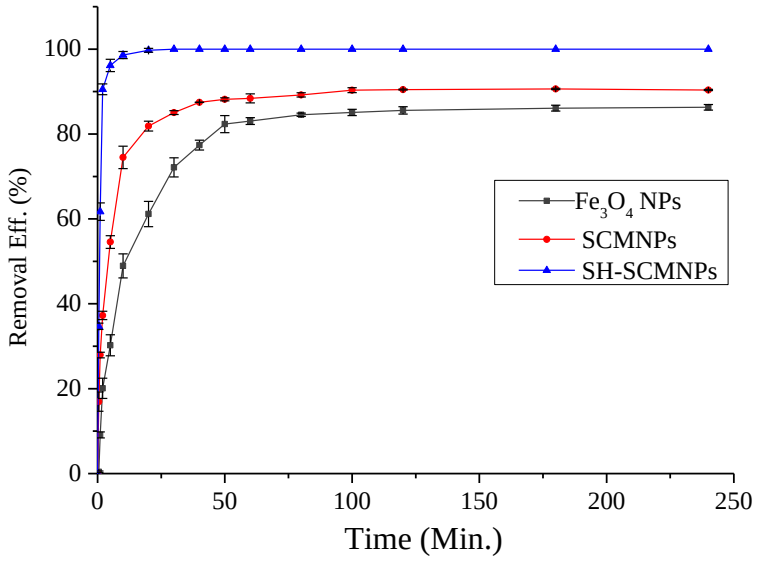

Figure 5.2: Kinetic adsorption experiments by Fe_3O_4 NPs, SCMNPs and SH-SCMNPs with 80 μg L^{-1} solution at an initial pH 6.0.

For the SH-SCMNPs, the rapid adsorption may be attributed to two factors: firstly, the SH groups of SH-SCMNPs binds Hg(II) ions effectively, Hg is characterised as a soft Lewis acid and can polarise to form strong covalent bonds with soft Lewis bases, such as SH (Pearson, 1968); and secondly, there is an electrostatic attraction between the external surface of the adsorbent and the metal ion. The rapid adsorption also indicates that the internal mesoporous structure is not a limiting factor for the diffusion of Hg(II)

into the interior of the SH-SCMNPs, a finding consistent with other studies that have used mesoporous structures for mercury removal (Brown et al., 1999; Mattigod et al., 2007; Wu et al., 2007; Bibby and Mercier, 2002). It was also found that the rate of Hg(II) uptake was relatively slow for SCMNPs without functionalisation. This can be attributed to the absence of the thiol groups and the decrease in the availability of active sites present on the surface. However, the high surface area (160 m^2 g^{-1}) and the increased number of hydroxyl groups after coating with silica, led to a faster adsorption rate than when Fe_3O_4 NPs were used. For Fe_3O_4 NPs, adsorption occurs only on the surface that explains the slower rate of adsorption. This trend suggests that only physisorption reactions occur on the surface, a finding in agreement with the conclusions of previous studies that have used unmodified Fe_3O_4 NPs for the removal of heavy metals (Hu et al., 2006; Tuutijärvi et al., 2009; Nassar, 2010).

All three kinds of magnetic NPs achieved a much shorter equilibrium time for the removal of Hg(II) compared with other conventional adsorbents such as activated carbon and fly ash. The adsorption using the Fe_3O_4 NPs was also faster than adsorption using functionalised mesoporous silica. Table 5.3 shows the equilibrium time determined for the removal of Hg(II) ions using some common adsorbents and non-magnetic functionalised mesoporous silica from previously published studies. The rapid adsorption of Hg by Fe_3O_4 NPs is perhaps attributed to the external surface adsorption. Since nearly all of the adsorption sites of Fe_3O_4 NPs exist in the exterior of the adsorbent, it is easy for the adsorbate to access the active sites and thereby a rapid approach to equilibrium compared to conventional methods. As discussed above, high and rapid uptake of Hg by SH-SCMNPs is attributed to the SH groups functionalised ordered mesoporous silica, demonstrating the ability of SH-SCMNPs to bind Hg ions quantitatively to each SH groups site in the adsorbent due to its uniform and large framework structure. This advantage belonging functionalised ordered mesoporous silica was not observed in common adsorbents or even with using non-ordered conventional adsorbents functionalised with same ligands because grafting such heterogeneous porous frameworks led to pore clogging resulting in decreasing the adsorption rate. The factor which could interpret fast adsorption rates of Hg onto mesoporous NPs is that mass

transfer kinetics are usually much faster than those in the corresponding amorphous grafted materials or in non-porous conventional adsorbents (Lee et al., 2001; Walcarius et al., 2003; Walcarius and Delacôte, 2005).

Table 5.3: The equilibrium time for Hg(II) removal by common adsorbents.

Sorbents	Equilibrium Time (hrs)	References
Activated carbon	2-8	Namasivayam and Periasamy (1993); Namasivayam and Kadirvelu (1999); Mahon et al., (2000); Rao et al.,(2009)
Clay	6-14	Viraraghavan and Kapoor,(1994); Say et al.,(2008); Senevirathna et al., (2011)
Fly ash	48-72	Rio and Delebarre,(2003)
MSiNPs	1-2	Aguado et al.,(2005); Mureseanu et al.,(2010)

5.4 Effect of Physical Environmental Factors on Adsorption

5.4.1 Temperature

The temperature of the adsorption medium has been shown to be an important factor when the mechanism of the metal-binding processes is energy dependent (Green-Ruiz, 2009). The removal efficiency of Hg (II) from 100 mL of a 160 µg L^{-1} Hg solution by SH-SCMNPs at a concentration of 6 mg L^{-1} was tested at 10, 22.5 and 35˚C. The results in Figure 5.3 show the removal of 93.48% of the Hg(II) at 10˚C, 93.76% at 22.5 ˚C and 82.99% at 35˚C. The uptake at 10 and 22.5˚C was almost the same, but then decreased between 22.5˚C and 35 ˚C. These results correspond well with those of Tsai et al. (2005) who suggested that in an exothermic adsorption process, the quantity of adsorbate taken up increases with a decrease in the adsorption temperature. This variation in adsorption may be the result of an enhanced escaping tendency of Hg(II) at increasing temperatures (Jeon and Ha Park, 2005). As the temperature was raised, the fraction of Hg that can escape from the surface increased and the amount adsorbed decreased, resulting in a reduction in boundary layer thickness. These observations are in agreement with those of Zhou et al. (2009) who used thiourea-modified magnetic chitosan microspheres for the adsorption of Hg(II).

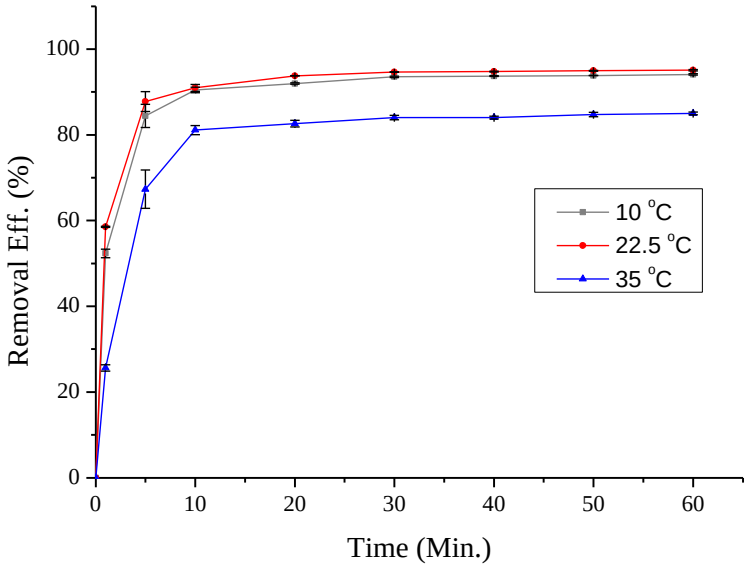

Figure 5.3: Effect of temperature on SH-SCMNPs with 160 µg L^{-1} Hg solution at an initial pH 6.0.

5.4.2 Shaking Speed

When performing batch processes, it is important to identify the relationship between the uptake rates of Hg and the agitation speed in order to find the optimal conditions for the adsorption process. As discussed in Section 5.3, the kinetics of the Hg uptake capacity of SH-SCMNPs showed that uptake starts with a rapid phase followed by a relatively slow one. The effect of the shaking speed on Hg(II) removal is shown in Figure 5.4. An experiment was conducted using a solution with a pH value of 6.0, an adsorption time of 60 minutes, an adsorption temperature of 22.5˚C, an adsorbent concentration of 8 mg L^{-1} and a Hg(II) concentration of 80 µg L^{-1}. These parameters were kept constant, while the shaking speed was varied from 50 to 200 rpm. The removal efficiencies of Hg(II) at a shaking speed of 50, 100 and 200 rpm were found to be 98.06%, 100% and 100 % respectively. As the shaking speed increases, it is believed that the thickness of the boundary layer decreases as well as reducing the film resistance to the mass transfer surrounding the adsorbent particles (El-Latif et al., 2010). This can reduce the time it takes the adsorbate to diffuse onto the surface of the particles. The results showed that the rate of Hg(II) removal was determined by the intensity of shaking as well as its duration. Figure 5.4 shows that 30 minutes contact of the adsorbent at a shaking speed of

50 rpm resulted in almost equal uptake to that observed at 100 and 200 rpm. So, even at a relatively low mixing rate, the limitations of mass transfer associated with the boundary layer surrounding the particles can be overcome given sufficient time. Once the shaker speed increased to 100 rpm, mixing was so complete that the effect of mass transfer became insignificant as can be seen by the similarity in adsorption rates at the higher shaker speeds. These results were in agreement with the work of Hu et al., (2007) and Zhang and Cheng (2011) who used mesoporous particles for the adsorption of heavy metals.

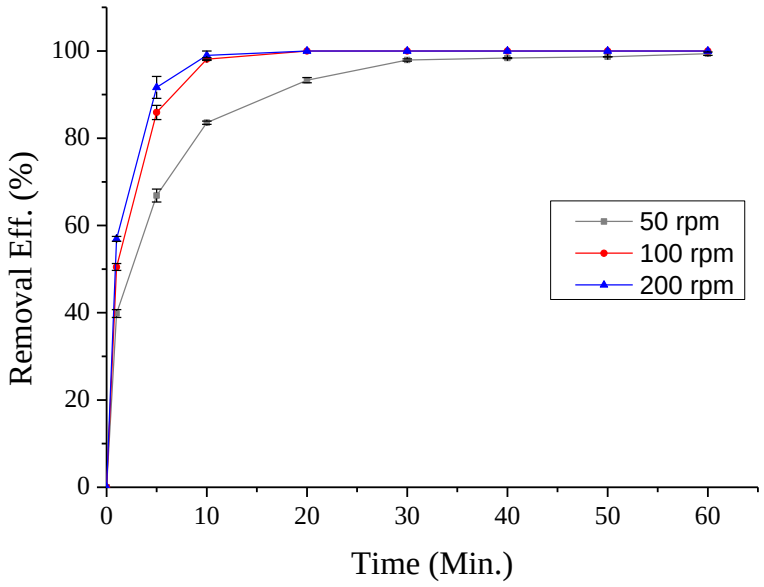

Figure 5.4: Effect of shaking speed on the removal of Hg solution by SH-SCMNPs with 80 µg L^{-1} solution at an initial pH 6.0.

5.5 Effect of Solution Matrix on Hg Adsorption

5.5.1 Water Type and the Presence of Coexisting Ions (Preliminary Investigation)

Initial experiments to assess the adsorption properties of the NPs were carried out with Hg (II) dissolved in deionised water and solutions with an initial Hg concentration of 80, 120, 160, 200, 400, 600, 800, 1000 µg L^{-1} were used. Figure 5.5 shows that the loading capacity of the SH-SCMNPs was found to be 113.7 mg Hg g^{-1} when applied to concentrations of 8 mg L^{-1} of adsorbent. However, practical applications would be for

the removal of very low concentrations of Hg(II) from natural water sources or during the treatment processes for potable water or wastewater. As a first step to assess any possible effects that an interaction between Hg(II) and dissolved ions in water could have on adsorption, tests were carried out using bottled (spring) water and tap water as the solute. The ion concentrations (mg L^{-1}) of the bottled and tap water used is shown in Table 5.4. The same initial Hg concentrations were used and the results of Figure 5.5 indicate that the influence of coexisted ions in the bottled water on the removal of Hg was small. The value of 111.9 mg Hg g^{-1} for bottled water, was approximately the same as when deionised water was used as the solute. However, the loading capacity of the SH-SCMNPs decreased to 98.5 mg Hg g^{-1} when tap water was used as the solute. It is evident that coexisted ions in natural water, such as Mg^{2+}, Ca^{2+} and Na^{+} might have influence on the adsorption efficiency of Hg. Southampton water contains concentration of Ca^{2+} (117 mg L^{-1}). It was addressed in literature (Mattigod et al., 1999; Herrero et al., 2005) that Ca^{2+} ions are found to significantly inhibit Hg removal. However, the presence of Mg^{2+} an Na^{2+} has no influence on Hg adsorption as the SH group cannot be coordinated well with the more abundant smaller, lighter metals such as Na and Mg (Ritchie et al., 2001).

Table 5.4: Concentration (mg L^{-1}) of anions and cations in bottled* and tap water**.

Water type	Cations Concentration (mg L^{-1})				Anions Concentration (mg L^{-1})					pH
	Mg^{2+}	Ca^{2+}	Na^{+}	K^{+}	SO_4^{-2}	Cl^{-}	NO_3^{-}	F^{-}	HCO_3^{-}	
Bottled water	26	80	6.5	1	12.6	6.8	3.7	0.16	360	7.08
Tap water	37	117	49	2.5	285	84	-	0.21	154	6.30

* According to information provided by supplier.
** According to information provided by Southern Water (SouthernWater, 2012).

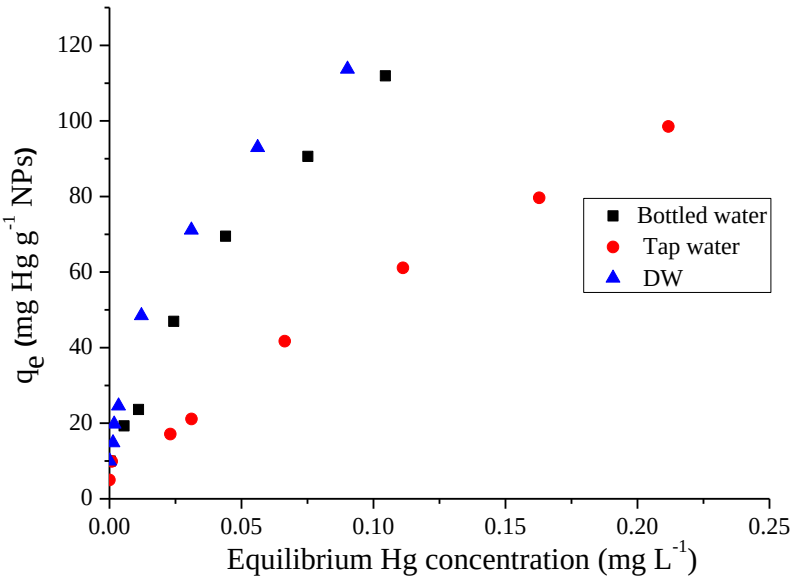

Figure 5.5: Adsorption curve for SH-SCMNPs with deionised, bottled and tap water matrix.

5.6 Effect of Potential Interfering Ions on Hg(II) Adsorption

5.6.1 Interference from Pb, Zn, Ni and Cu

5.6.1.1 Control experiments

Solutions prepared by diluting 1000 mg L^{-1} stock solutions of Pb(II), Zn(II), Cu(II) and Ni(II) to metal concentrations of 2 and 10 mg L^{-1} were then tested in the reaction vessels without adding NPs as an adsorbent. Each sample was shaken at 200 rpm for 24 hrs at 22.5˚C. The metal concentrations before and after shaking are presented in Table 5.5 and Figure 5.6. At an initial concentration of 2 mg L^{-1}, the percentage of Pb, Zn, Cu and Ni lost from solution were 1.84, 2.12, 1.54 and 2.10% respectively. Almost the same percentage was lost from the solution with an initial concentration of 10 mg L^{-1} and this change is not significant.

Table 5.5: Metals concentrations of four replicates of NPs-free control experiments; metals initial concentration 2 and 10 mg L^{-1}.

	Metals conc. (2 mg L^{-1})			Metals conc. (10 mg L^{-1})		
	Before shaking	**After shaking**	**Metals Lost (%)**	**Before shaking**	**After shaking**	**Metals Lost (%)**
Pb	2.04	2.0	1.84	10.09	9.95	1.51
Zn	2.03	1.98	2.12	10.02	9.86	1.59
Cu	2.05	2.02	1.54	10.05	9.91	1.38
Ni	2.02	1.97	2.10	10.01	9.87	1.35

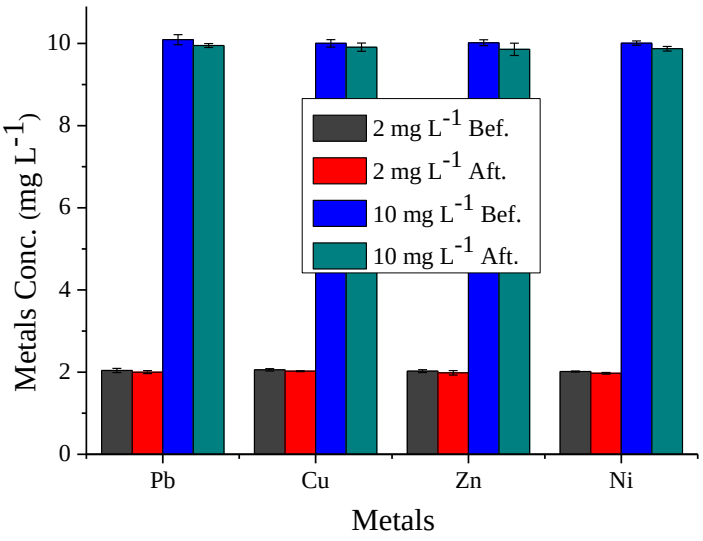

Figure 5.6: NPs-free control experiments.

The student's t-test was used to compare the means of the metal concentrations before and after shaking, Table 5.6. The results indicated that the sample means do not differ significantly as the *p*-value was greater than 0.05 for all the paired samples tested (before and after shaking for 24 hrs). Some of results were close to being significant as shown in Table 5.6. These could be significant differences but a sample of four replicates is too small to prove it. However, the *p*-values of Cu at 10 mg L^{-1} and Pb at low and high concentrations were non-significant ($p > 0.1$). In All cases, the initial

concentration at pH values of less than 8.0; therefore, metals ions were unlikely to have precipitated from solution.

Table 5.6: Student's t-test calculations.

Paired sample test							
Metals Con. mg L^{-1}		**Paired Differences**					
		Mean	**95% conf. interval of the diff.**		**t**	**df**	**p-value**
			lower	upper			
Pair 1-Pb	2 pre – 2 aft.	0.04	-0.02	0.10	2.20	3	0.115
pair 2-Pb	10 pre –10 aft.	0.14	-0.06	0.35	2.22	3	0.113
Pair 1-Zn	2 pre – 2 aft.	0.02	-0.01	0.06	2.67	3	0.076
pair 2-Zn	10 pre – 10 aft.	0.08	-0.01	0.17	2.92	3	0.061
Pair 1-Cu	2 pre – 2 aft.	0.04	-0.004	0.08	2.85	3	0.065
pair 2-Cu	10 pre – 10 aft.	0.05	-0.06	0.16	1.50	3	0.231
Pair 1-Ni	2 pre – 2 aft.	0.04	-0.01	0.09	2.65	3	0.077
pair 2-Ni	10 pre – 10 aft.	0.07	-0.02	0.16	2.74	3	0.090

5.6.1.2 Adsorption of competing metal ions on SH-SCMNPs

A preliminary study was undertaken to compare the affinity of SH-SCMNPs towards Hg(II), Pb(II), Cu(II), Zn(II) and Ni(II). These used solutions of the salts of the individual metals in isolation of each other with a fixed quantity of adsorbent and at different pH values. Figure 5.7 shows the results of individual metal adsorptions for 16 mg L^{-1} SH-SCMNPs at pH values of 2.0, 6.0 and 8.0 using 2 mg L^{-1} of each metal. Overall, Hg(II) showed a higher percentage of adsorption efficiency at pH 6.0 and 8.0 due to its high affinity towards thiol groups, followed by Pb(II). The highest adsorption efficiency of Pb(II) was seen at pH 2.0 (95.7 %), while the adsorption efficiency at pH 6.0 and 8.0 was almost the same. Minimal or no adsorption was observed for Cu(II), Zn(II) and Ni(II) at pH 2.0 as compared to the fair amount of Hg(II) and Pb(II) adsorbed at this value. At pH 6.0 and 8.0, the adsorption efficiency of Cu(II) was higher than that of Zn(II) and Ni(II), indicating a lack of affinity for these two metals by the thiol groups. The selectivity for various cations at selected pH values was divided into two groups and at pH 6.0 and 8.0; the order was Hg > Pb > Cu > Zn > Ni. At pH 2.0, Pb(II) was

removed more efficiently than Hg(II) followed by the other metals in same order as at pH 2.0. The results showed a lack of affinity for SH-SCMNPS towards Zn and Ni from solutions under acid conditions.

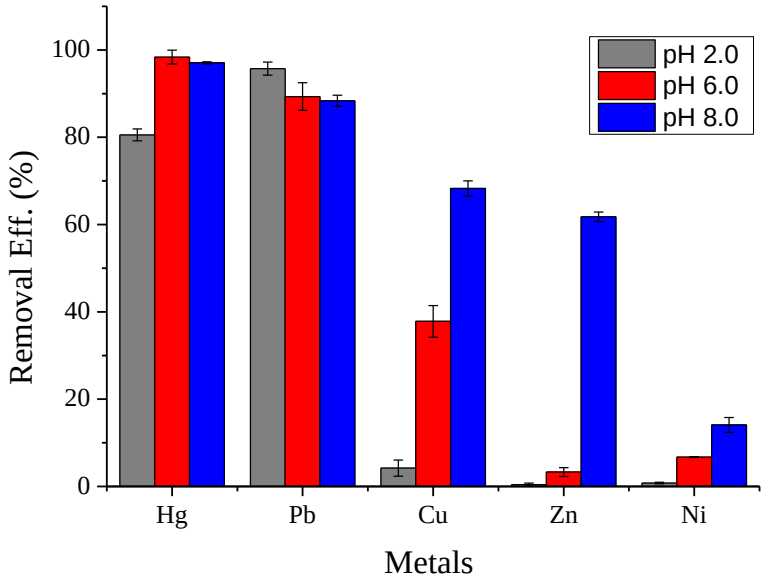

Figure 5.7: Adsorption efficiency of individual metals at different initial pH levels.

5.6.1.3 Assessment of the competition for binding sites on SH-SCMNPs using binary metal solutions

Adsorption experiments were carried out using mixed solutions of Hg(II) with, in each case, one other metal salt to evaluate how this affected the adsorption of the Hg(II) using SH-SCMNPs. Each experiment was carried out by mixing 200 µg L^{-1} of Hg(II) with each of Pb(II), Cu(II) and Ni(II) at a ratio of 1:10. Thus, the design would provide sufficient metals in the solution to potentially saturate the available binding sites that could be taken up by Hg(II) ions. Each experiment used 0.8 mg (16 mg L^{-1}) of SH-SCMNPs. These were initially washed three times using deionised water to remove any metals which were loosely attached to the bottles or to the adsorbent itself. They were then reacted with the test solution for 1 hr at 22.5˚ C with shaking at 200 rpm. Then, the SH-SCMNPs were separated from the solution and used in a second adsorption cycle without any attempt to desorp any bound ions. This procedure was repeated for up to five cycles in order to increase metal load and to provide the opportunity for ion exchange and therefore the release of the previously adsorbed metals back into the

solution. If this were to occur, it would be detected by an apparent negative adsorption value.

The results showed that, in general, there was a reduction in the adsorption efficiency after each successive cycle as shown in Figure 5.8. This may be due to the active sites being occupied by metals rather than being released from the adsorption sites between cycles. Figure 5.8a shows that the amount of Hg(II) and Pb(II) decreased with each successive cycle: 91.07% of Pb (II) was adsorbed during the first cycle and reached almost 1% at the end of third cycle. Hg(II) showed a similar trend, but with only 43.19% of Hg(II) being adsorbed by the end of last cycle. As a result of the saturation of the binding sites, the concentration of Pb(II) ions in the solution was increased. This saturation is due to the displacement of Pb(II) by Hg(II) ions. The release of Pb(II) into the solution suggests that as additional metals were added during each cycle, due to Hg's strong affinity for SH-SCMNPs, Hg(II) occupied the available sites during each addition and exchanged with Pb(II) ions causing their release back into solution.

Although the concentrations of Cu(II) and Zn(II) in the solution were more than ten times that of Hg(II), there were no effects on the adsorption of Hg(II). In competition between Hg(II) and Cu (II), 99.85% of Hg(II) was adsorbed at the end of the first cycle and this decreased to 72.79% at the end of the fifth cycle (Figure 5.8b). While in the case of the binary solution of Hg(II) and Zn(II), 99.92% of Hg(II) was adsorbed at the end of the first cycle and this decreased to 79.22% at the end of the fifth cycle (Figure 5.8c). In both cases, the amount of adsorbed Hg(II) decreased gradually, while Cu(II) and Zn(II) showed an initial adsorption in the first cycle (44.90 and 10.39% respectively). This decreased greatly and dropped to 12.63% for Cu(II) and to almost zero for Zn(II) by the end of the third cycle followed by a further very slow decrease. As a result of the weak affinity between Ni(II) and Cu(II) and SH-SCMNPS, the metal ions were not released back into the solution and the NPs were not exhausted.

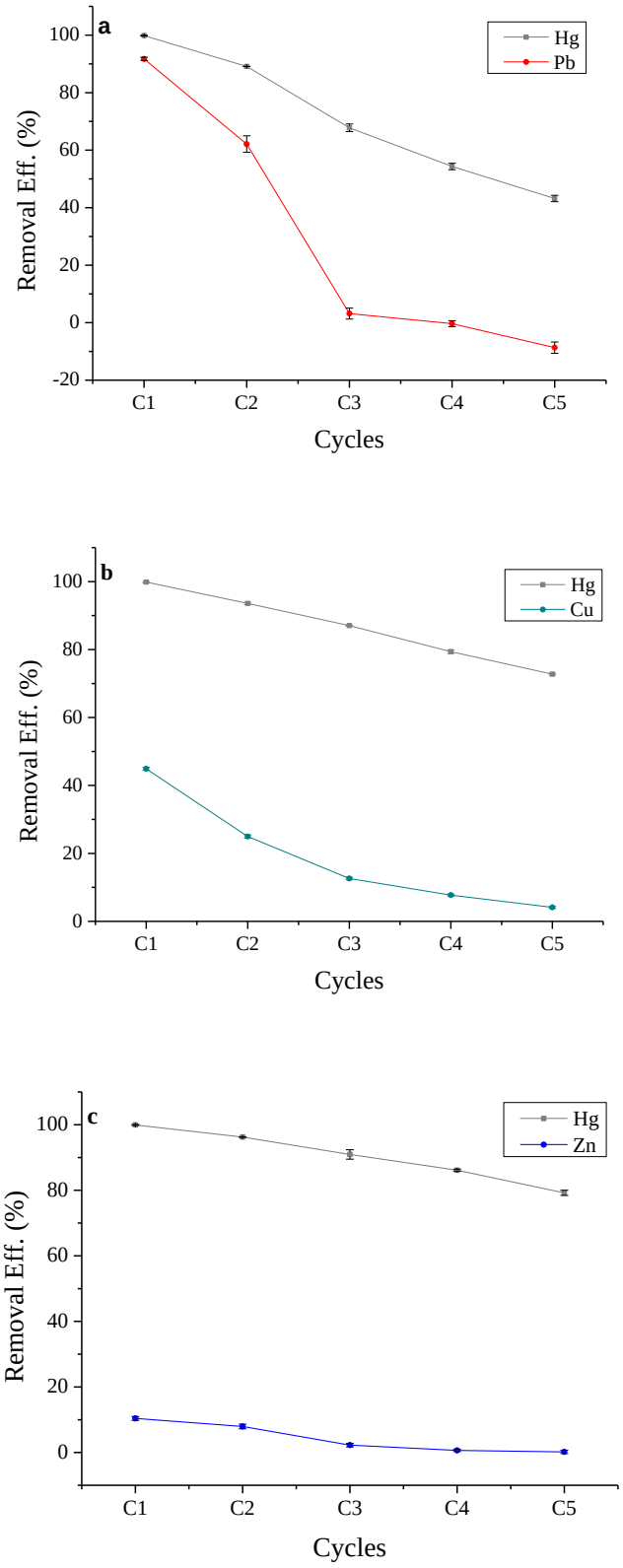

Figure 5.8: Five cycles binary-metals exhaustion at pH 6.0 using SH-SCMNPs.

It was noted that Pb and Hg showed the same trend of adsorption in the first and second cycles, the presence of Pb decreased the removal efficiency of Hg compared to other metals, indicating that they are equally competitive even though the concentration of Pb was ten times that of Hg. Therefore, another binary experiment was performed under different conditions as it was of particular interest to examine the competitive phenomena after the adsorption of metals onto SH-SCMNPs. In this experiment, the first two cycles were performed in the absence of Hg to allow other metals to bind to the available active sites. The experiment was carried out at a fixed mass concentration by mixing 1000 μg L^{-1} of Hg(II) with each of Pb(II), Cu(II) and Ni(II) at a ratio of 1:10. Figure 5.9a shows that 2100 μg L^{-1} (21.20%) of Pb were adsorbed in the first cycle which then decreased to 742.9 μg L^{-1}. Although SH-SCMNPs adsorbed a high amount of Pb, 835.10 μg L^{-1} (83.5 %) of Hg were adsorbed in the third cycle with a decreasing amount of Hg being adsorbed during each additional cycle. At the end of the fifth cycle, 198.2 μg L^{-1} of Pb were released into the solution with 232.9 μg L^{-1} of Hg being adsorbed. More Pb (153.4 μg L^{-1}) was released into the solution with a decreasing amount of Hg being adsorbed (13.3 μg L^{-1}) at the end of the sixth cycle. As expected for the first cycle, 1859.3 μg L^{-1} (18.6%) of Cu was adsorbed as shown in Figure 5.9b, followed by 1114.7 μg L^{-1} at the end of cycle two. The release of Cu occurred during the third cycle when 1000 μg L^{-1} of Hg was used for the adsorption process, resulting in 638.7 μg L^{-1} of Hg (63.86%) being adsorbed and displacing 555 μg L^{-1} of Cu. The amount of Cu displaced from SH-SCMNPs increased in the fourth cycle to 762 μg L^{-1} with the corresponding adsorption of 447.7 μg L^{-1} of Hg. The capacity of the SH-SCMNPs was exhausted by the fifth cycle and only 188.5 μg L^{-1} (18.86 %) of Hg was adsorbed with 138.8 μg L^{-1} of Cu being displaced. In the sixth cycle, 100.7 μg L^{-1} of Hg was adsorbed with the release of 184.8 μg L^{-1} of Cu into the solution. It can be noted from the previous discussions that SH-SCMNPs had only a weak affinity to Zn; therefore, as can be seen in Figure 5.9c, only 702.3 μg L^{-1} (7.02 %) of Zn was adsorbed in the first cycle followed by only 3.85% at the end of the second cycle. This gave Hg a chance to bind to the available active sites without any competition. During the fifth cycle, SH-SCMNPs exhibited a greater adsorption capacity and were exhausted resulting in the release of 14.4 μg L^{-1} of Zn into the solution.

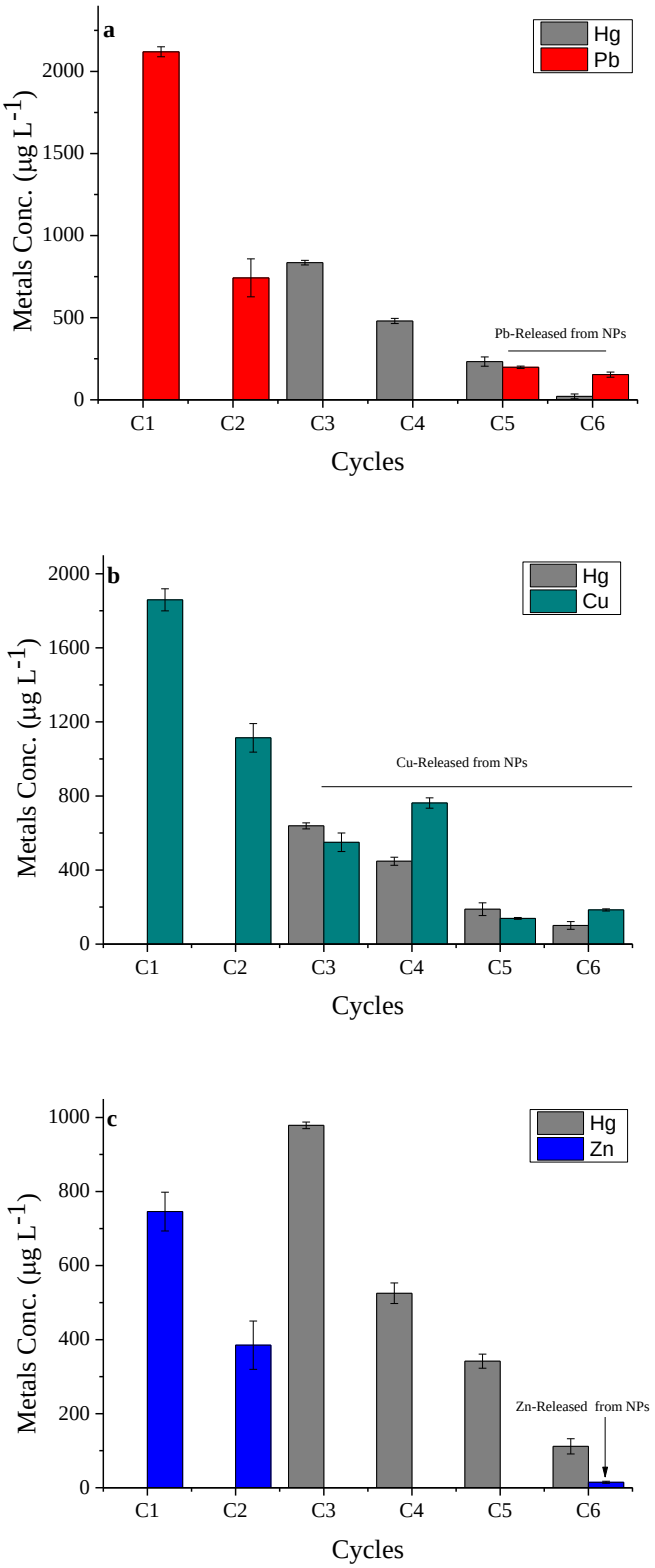

Figure 5.9: Binary-metals competition at pH 6.0 using SH-SCMNPs.

Hg ions exhibit a binding affinity towards thiol groups and Hg is characterised as a soft Lewis acid and can polarise to form strong covalent bonds with soft Lewis bases, notably sulphur (Pearson, 1968). According to the theory of Pearson, Pb(II) is classified as a soft Lewis acid while Cu(II) and Zn(II) are borderline Lewis acids that bind to thiol groups, especially in the absence of other competing ions. Therefore, the SH-SCMNPs adsorbent exhibited high complexation for the softer acid metal ions such as Pb(II), while exhibiting low complexation affinity for borderline metal ions such as Cu(II) and Zn(II). In the case of binary solutions with other metals, no competition was observed due to the high affinity of thiol groups for Hg(II) ions. As seen in Figure 5.8 and Figure 5.9, the high adsorption observed during the first two cycles in either the absence or presence of Hg can be attributed to the large available surface area and the abundance of available active sites.

Desorption experiments were performed on SH-SCMNPs to evaluate the reversibility of the adsorption for Hg, Pb, Cu and Zn. Concentrated hydrochloric acid (5 mL, 12.1 M HCl) solution desorbed metal laden SH-SCMNPs with nearly 100% elution efficiency as can be seen in Table 5.7.

Table 5.7: The recovery of metals laden with SH-SCMNPs using 12.1 M HCl.

Binary solution		Metals Removed (µg)	Metals Recovered (µg)	Metals Recovered %
Hg+Pb	Hg	158.5	158.6	100.1
	Pb	255.1	249.9	97.9
Hg+Cu	Hg	137.4	137.3	99.9
	Cu	123.8	120.9	97.7
Hg+Zn	Hg	196.2	195.6	99.7
	Zn	109.8	106.4	96.9

5.6.1.4 Assessment of the competition for binding sites on SH-SCMNPs using multi-metal solutions

Toxic metals rarely occur as single species in natural and wastewater, and the presence of a mixture of metals gives rise to interactive effects. The examination of the influence of multi-metals in various combinations is therefore more representative of actual environmental problems than single metal studies. Figure 5.10 shows the adsorption efficiency of multiple metals (Hg, Pb, Cu, Ni and Zn), where the concentration of each

metal in the mixed solution was 2000 µg L^{-1} and 200 µg L^{-1} of Hg mixed with 16 mg L^{-1} of SH-SCMNPs at pH 6.0. All the Hg (100 %) was adsorbed while most of the Pb (85 %) was also adsorbed. Although Pb demonstrated the greatest amount adsorbed from the individual and binary-metal solutions, the adsorbed Pb is likely to decrease due to the presence of other metals in the solution. As described in the previous section, the affinity of Cu, Ni and Zn for SH-SCMNPs was not as strong as that observed for Hg and Pb and the adsorption efficiency of Cu, Zn and Ni was 45.07 %, 13.75 % and 3.87 % respectively. When the metal ions were placed in a competitive situation in multi-species metal adsorption experiments, there was no effect on the adsorption of Hg even in the presence of high concentrations of other species (i.e. where the concentration is 10 times that of Hg).

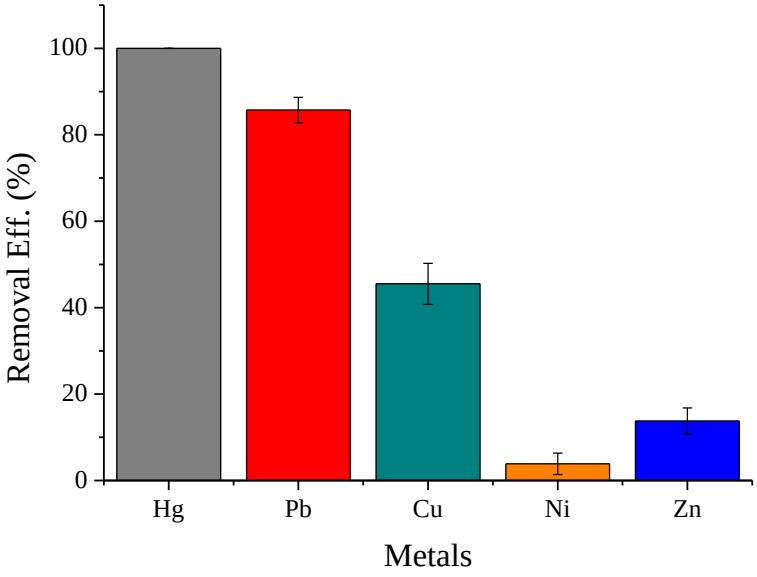

Figure 5.10: Multi-metals adsorption system by SH-SCMNPs at pH 6.0.

5.6.2 Effect of Common Anions

To observe the effect of different anions (F^-, Cl^-, NO_3^-, SO_4^{2-}, PO_4^{3-}) on the adsorption of Hg(II) by SH-SCMNPs, 50 ml of 200 µg L^{-1} Hg(II) were shaken with 100 mg L^{-1} of various anions. The results are shown in Figure 5.11, where it can be seen that the adsorption was inhibited in the order: NO_3^- < Cl^- (L) < SO_4^{2-} < PO_4^{3-} < F^- < Cl^- (H), depending on the coordination ability of different anions. The presence of NO_3^- had little influence and the corresponding removal efficiency was 97.19%. The influence of SO_4^{2-}

was also very small and decreased the removal efficiency to 92.93%. As Cl^- is a very common ion in chlor-alkali plants, high and low concentrations of this anion were examined. The presence of a low concentration of Cl^- had no influence on the adsorption of Hg(II), while the presence of a high concentration of Cl^- reduced the Hg(II) removal efficiency to 81.28%. Davies and Long (1968) reported that at lower chloride ion concentrations, $HgCl_2$ is the predominant species, while at higher chloride ion concentrations, Cl^- can react with Hg(II) to form stable $HgCl_4^{2-}$ which becomes the predominant species. The negatively charged chloro-complex $HgCl_4^{2-}$ would significantly affect the sorption behaviour of SH-SCMNPs, causing a substantial decrease in the removal of Hg(II). This result is in agreement with previous studies on the effect of Cl^- on the adsorption of Hg(II) (Walcarius and Delacôte, 2005; Bessbousse et al., 2008; Bessbousse et al., 2009). F^- ions have also been found to significantly inhibit Hg(II) removal and Namdeo and Bajpai (2008) attributed this to the fast diffusion of F^- ions towards the protonated positively charged surface of magnetite NPs. Since the size of F^- ions is much smaller than that of Hg(II), its diffusion through the pores of the sorbent particles is more rapid. This causes a decrease in the removal efficiency of Hg(II) in the presence of F^-. Further investigations are needed to study the effect of high concentrations of F^- on the adsorption of Hg(II). The presence of PO_4^{3-} causes a significant decrease in Hg(II) removal efficiency. PO_4^{3-} is a known inner-sphere complex-forming anion that is strongly adsorbed to metal oxide surfaces or is co-precipitated to form discrete solid phases on mineral surfaces (Jegadeesan et al., 2005). However, since the concentration of PO_4^{3-} in chlor-alkali effluents is less than 3 mg L^{-1} (Von Canstein et al., 1999) and since the initial concentration used in this experiment was 200 mg L^{-1}, PO_4^{3-} does not have any effect on the adsorption of Hg by SH-SCMNPs in real applications.

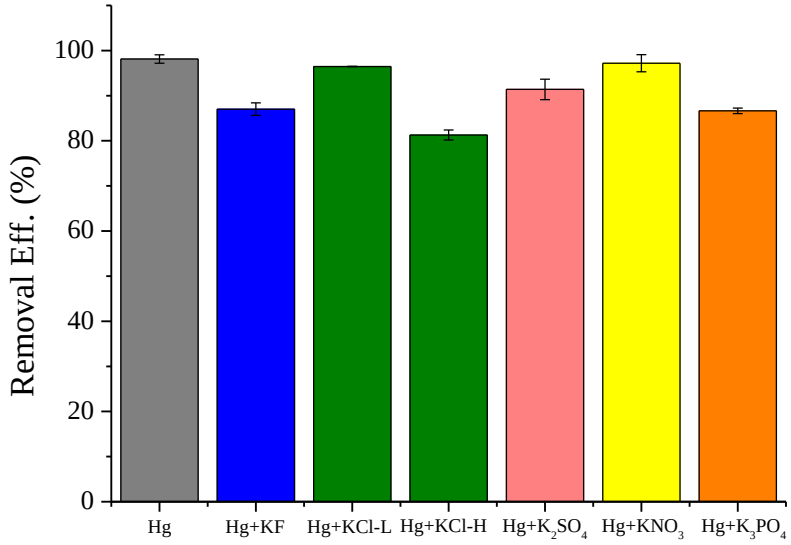

Figure 5.11: Adsorption efficiency of Hg(II) in competition with various anions.

5.7 Desorption and Regeneration Study

5.7.1 Effect of Type and Concentration of Eluent

In an effective treatment system, desorption and regeneration of the adsorbate are essential requirements. One of the key factors in this is the ability of the system to maintain adequate performance of the adsorbent during multi-cycle use (Dabrowski, 2001). The recovery of the adsorbate may be a secondary objective, and the more concentrated the adsorbate is in the desorption fluid, the more likely the process to succeed (Feng et al., 1997; Brown et al., 2000). The type and concentration of the eluent play a key role in the desorption process. Hydrochloric acid is commonly used for the elution of metal ions, including Hg(II), from adsorbents due to their high solubility, its common usage in industry and its relatively low cost (Naja and Volesky, 2010). Therefore desorption experiments were performed on SCMNPs and SH-SCMNPs to evaluate the reversibility of the adsorption of Hg. The effect of the type and concentration of the eluent on the desorption of Hg are also discussed.

In an attempt to highlight any potential desorption of Hg laden NPs using deionised water, Hg laden SCMNPs and SH-SCMNPs were tested using 20 mL of deionised water. This mixture was allowed to equilibrate for 0.5, 1, 2, 6 and 24 hrs on an orbital shaker at 200 rpm. Although the SCMNPs were reacted with deionised water up to 24 hrs, five cycle desorption experiments concluded that Hg at the three concentrations examined (80, 120 and 200 μg L^{-1} were irreversibly adsorbed to SCMNPs surfaces at pH 6.0 due to negligible desorption (< 1.3 %) of Hg after 24 hrs desorption, Table 5.8. Under the same conditions, the desorption efficiency of Hg laden SH-SCMNPs at initial concentrations of 80, 120, and 200 μg L^{-1} was found to be zero. Desorption results using deionised water indicated that Hg couldn't be released from these NPs over five cycles (up to 24 hrs of agitation). Therefore, SCMNPs and SH-SCMNPs could be used effectively for the permanent disposal of the adsorbent.

Table 5.8: Desorption efficiency of Hg(II) by SCMNPs and SH-SCMNPs using deionised water.

Adsorbent	Hg concentrations (μg L^{-1})	Adsorption efficiency (%)	Desorption efficiency (%) Time for reaction (hrs)				
			0.5	1	2	6	24
SCMNPs	80	90.06	0	0	0	0	0.86
	120	89.14	0	0	0	0	1.06
	200	88.02	0	0	0	0	1.26
SH-SCMNPs	80	100	0	0	0	0	0
	120	98.74	0	0	0	0	0
	200	97.56	0	0	0	0	0

As mentioned above, HCl was the chosen eluent as it is the most commonly used for the desorption of Hg (II). The possibility of the dissolution of Fe at a very low pH may occur and is discussed Section 5.8. Desorption of Hg laden SCMNPs was tested using 5 ml of HCl at concentrations of 1.0, 2.0 and 3.0 M, and the desorption results of bound Hg at initial concentrations of 80, 120, and 200 μg L^{1} are presented in Figure 5.12. As expected, the desorption efficiency increased with higher HCl concentrations. Using 3 M HCl, the desorption efficiency of Hg at initial Hg concentrations of 80, 120, 200 μg L^{-1} was 96.68, 89.86 and 90.75% respectively. The total Fe in the solution as measured by ICP-OES, was found to be below the sample detection limit of ICP-OES, which is less

than 0.19 mg L^{-1} (i.e., less than 2.3% of the initial concentration), indicating that there was insignificant decay of the SCMNPs when using 3.0 M HCl. At a 5.0 M HCl concentration, however, 15.9 % of the Fe incorporated in the NPs was dissolved, indicating that this strength of acid is not suitable as a regenerant even though it was capable of recovering more than 95% of the Hg.

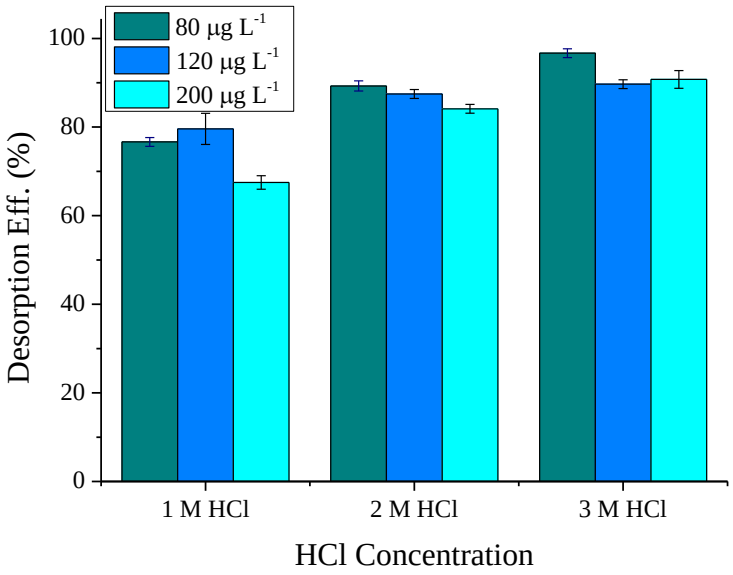

Figure 5.12: Desorption efficiency of adsorbed Hg(II) by SCMNPs using different concentrations of HCl.

For the efficient desorption of Hg laden SH-SCMNPs, varying concentrations of HCl from 1.0 to 5.0 M were tested. Figure 5.13 shows that the desorption efficiency decreases with a decreasing concentration of HCl, and that 5 mL of a 1.0 M HCl solution only lead to the recovery of a 10% of Hg(II). For the removal of Hg(II) from the functional thiol groups, as considered in the current work, acid alone is not effective and the addition of thiourea is required (Walcarius and Delacôte, 2005; Huang and Hu, 2008). Results of the subsequent tests which used a mixture of HCl and thiourea for desorption are also shown in Figure 5.13. These show that reducing the concentration of HCl from 5.0 to 1.0 M and adding 2 % thiourea gave a desorption efficiency of ~ 40 %. The addition of 5 mL 3.0 M HCl containing 2 % (m/v) thiourea as a complexing agent was able to recover 92.28, 88.48 and 87.29 % of Hg(II) at initial concentration of 80,

120 and 200 μg L^{-1}, respectively, from the solution. Figure 5.13 shows that more than 85% of the total adsorbed Hg(II) can be recovered during desorption.

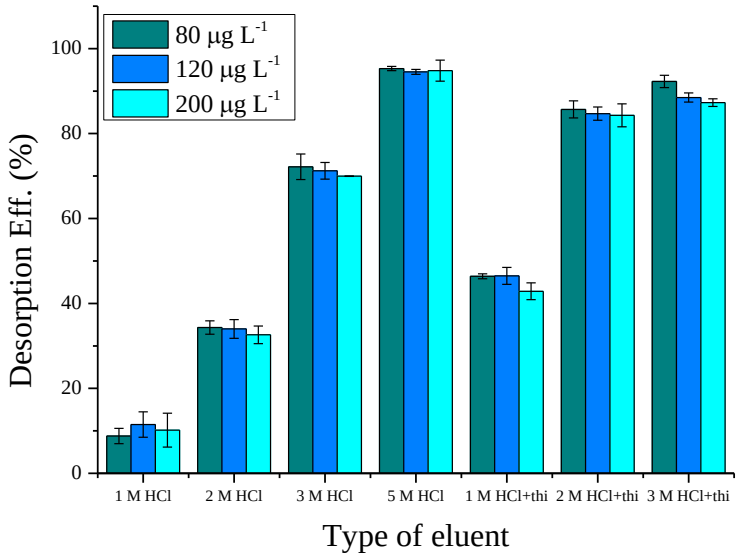

Figure 5.13: Desorption efficiency of adsorbed Hg(II) by SH-SCMNPs using different concentrations of HCl.

5.7.2 Desorption Kinetics

Based on the above discussions, 5 ml of 3.0 M HCl were used for the desorption of Hg laden SCMNPs and 3.0 M HCl containing 2% (m/v) thiourea were used for the desorption of Hg laden SH-SCMNPs. The desorption curves for SCMNP and SH-SCMNPs are shown in Figure 5.14. The rate of Hg desorption was initially fast and Hg-loaded SCMNPs and SH-SCMNPs desorbed 70.54 and 62.55 % respectively within 10 minutes. Hg laden SCMNPs and SH-SCMNPs both achieved their desorption equilibrium within 30 minutes. The desorption equilibrium of SCMNPs was quicker than the adsorption equilibrium and was reversed for SH-SCMNPs.

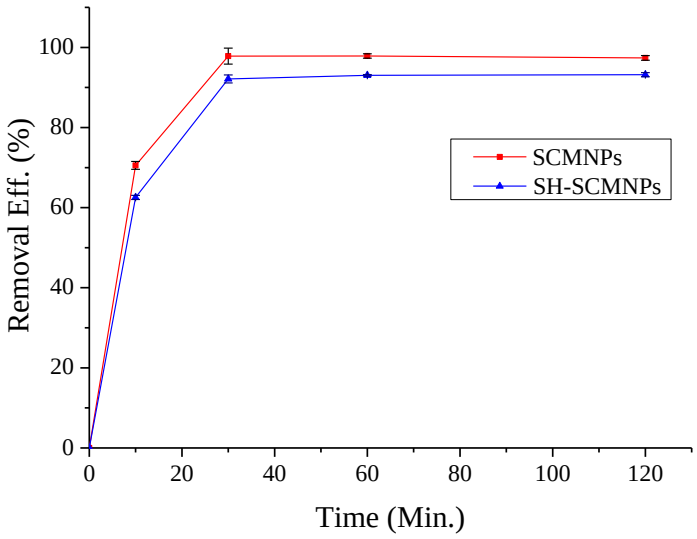

Figure 5.14: Desorption kinetic experiments using SCMNPs and SH-SCMNPs at initial Hg concentration of 80 µg L^{-1}.

5.7.3 Regeneration study

An adsorption-desorption cycle using the same NPs at a concentration of 8 mg L^{-1} was repeated 5 times, in each case using 50 ml of 80, 120, 200 µg L^{-1} Hg (II) solutions in the adsorption cycle and using 3.0 M HCl or 3.0 M HCl containing 2% (m/v) thiourea in the desorption cycle. The results are presented in Figure 5.15 and Table 5.9; these show that at the end of the fifth cycle, the SH-SCMNPs maintained adsorption efficiencies of 94.70, 92.68 and 92.94% for the Hg(II) solution concentrations of 80, 120 and 200 µg L^{-1}, respectively. As shown in Figure 5.16, the maximum removal efficiency of Hg(II) by SCMNPs decreased gradually from 89.97, 89.57 and 87.39 to 74.82, 67.70 and 72.38%, for the Hg(II) solution with concentrations of 80, 120 and 200 µg l^{-1} respectively, over five consecutive cycles, while the desorption efficiency decreased gradually to 81.60, 80.01 and 79.99% respectively. This gradual reduction in the adsorption efficiency may be due to Hg(II) not being fully released from the adsorption sites between cycles.

Both strong adsorption and resistant desorption are significant features of water treatment and solid waste disposal. Strong adsorption with no desorption would be ideal for the permanent disposal of metals, while bleed off or release of metals could be beneficial when considering the reuse and regeneration of the NP sorbents. Therefore, due to the strong sorption capabilities and good desorption efficiency observed in the

above experiments using 3.0 M HCl containing 2% (m/v) thiourea, SH-SCMNPs would offer significant advantages over current water and wastewater treatment and solid disposal adsorbents.

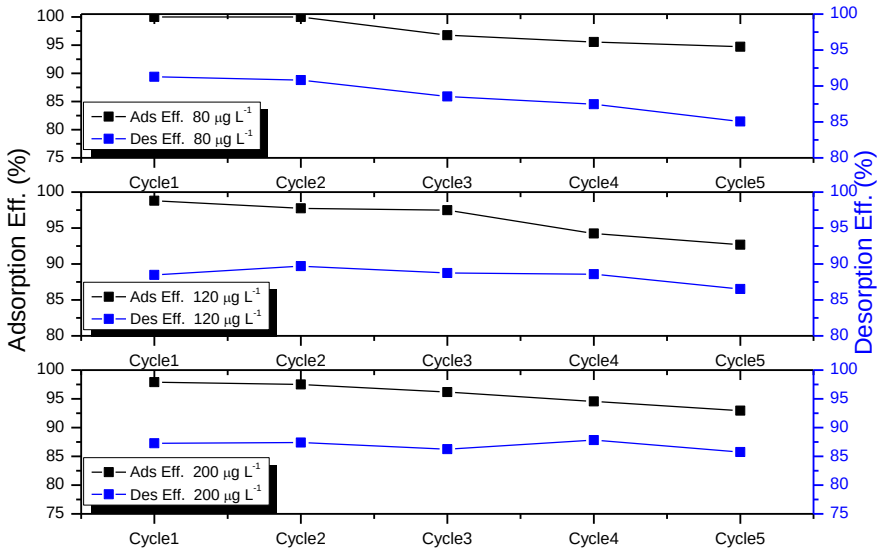

Figure 5.15: Percentage of Hg(II) adsorbed and desorbed during five adsorption /desorption cycles at initial concentrations of 80, 120 and 200 µg L^{-1} using SH-SCMNPs.

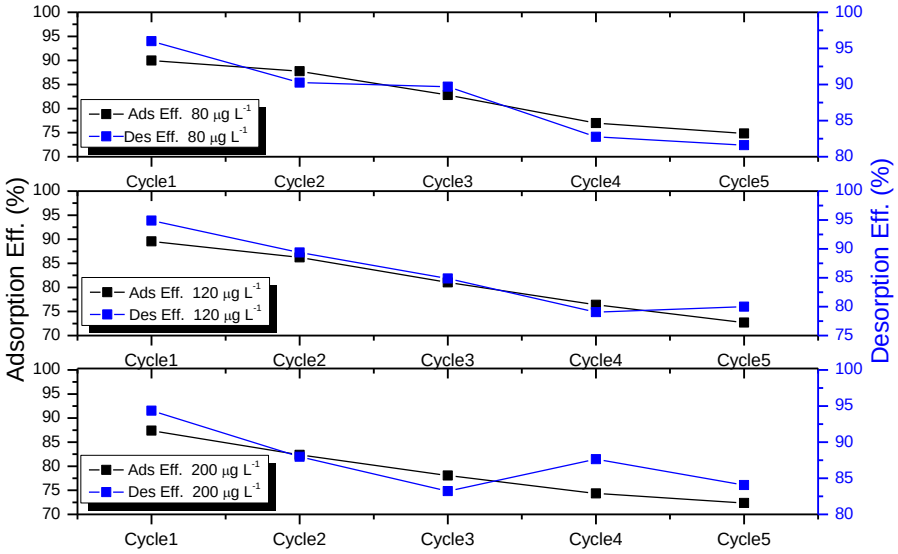

Figure 5.16: Percentage of Hg(II) adsorbed and desorbed during five adsorption /desorption cycles at initial concentrations of 80, 120 and 200 µg L^{-1} using SCMNPs.

Table 5.9: Adsorption and desorption efficiencies during successive adsorption and desorption cycles.

Cycle	Adsorption						Desorption					
	SCMNPs (%)			SH-SCMNPs (%)			SCMNPs (%)			SH-SCMNPs (%)		
	Hg concentrations (µg L^{-1})											
	80	120	200	80	120	200	80	120	200	80	120	200
1	89.97	89.57	87.39	100	98.80	97.91	96.00	94.90	94.37	91.66	88.66	87.19
2	87.76	86.24	82.36	100	97.75	97.49	90.26	89.38	87.99	90.81	89.71	87.41
3	82.80	81.03	78.06	96.49	97.49	96.18	89.71	84.88	83.22	88.55	88.74	86.24
4	77.00	72.38	74.35	95.50	94.25	94.55	82.76	79.06	78.66	87.64	88.59	87.38
5	74.82	67.70	72.38	94.70	92.68	92.94	81.60	80.01	79.99	85.07	86.52	85.47

The above results are encouraging and further suggest that SH-SCMNPs have a good ability to retain more than 92% of their original Hg(II) adsorption capacity over five cycles with a good reusability, since 3.0 M HCl containing 2% (m/v) thiourea was used effectively to desorp Hg from SH-SCMNPs. Nevertheless, the reasons behind the reduction in its performance require further investigation. As mentioned above, the decreased capacity of SH-SCMNPs can be attributed to a limited number of active sites which bind Hg(II) much more strongly onto SH-SCMNPs so that the 3.0 M HCl containing 2% (m/v) thiourea could not elute Hg from them. All these sites became saturated on their first exposure to Hg and were not available for further binding on subsequent exposures. Feng et al. (1997) and Brown et al. (2000) found that the recovery of Hg(II) from thiol functionalised particles was less than 60% of the original recovery values when using 12.1 M HCl as an eluting agent due to the strong Hg-S covalent bond which tends to support this argument. Another drawback is that each adsorption/desorption process must be performed with some treatment, including using acid to release the Hg(II) from the loaded nano-sorbent into the desorption medium, washing the SH-SCMNPs with deionised water three times at the end of each cycle to remove Hg(II) loosely attached to the PET bottles or to the adsorbent itself and the isolation of the nano-sorbent from the solution using an external magnetic field. All of these factors could decrease the apparent capacity for adsorption. TEM was used to investigate the effect of these processes on the NPs and the results are shown in Figure 5.17, Figure 5.18 and Figure 5.19. Figure 5.17 shows the second cycle of Hg(II) laden SH-SCMNPs with EDX analysis, and as can be seen, the particles display a spherical morphology. However, the morphology of these particles is slightly different to that of the particles before the adsorption process (see Chapter 4) and some particles are exhibiting aggregation. This means that the adsorption and desorption process of Hg has resulted in some changes to the NPs morphology. Although most Hg was evaporated under the electron beam, some Hg was detected in the EDX spectrum, Figure 5.17b. Therefore, the EDX analysis gives the direct detection of the presence of Hg adsorbates on SH-SCMNPs; sulphur from the thiol group was also detected. The EDX analysis confirms the presence of Hg on the surface of SH-SCMNPS. Most adsorption studies have determined Hg adsorption by measuring only the residual Hg concentration in the

supernatant, a method that does not directly prove the presence of Hg on the adsorbent. Moreover, sophisticated analytical methods give direct confirmation of the presence of metals sorption onto the adsorbent. Figure 5.18 shows the fourth cycle SH-SCMNPs after the elution process. The repeated washing and elution after each cycle has resulted in the deformation of the surface and the aggregation of the NPs. As described in Chapter 4, SH-SCMNPs demonstrated the existence of many open pores on their surface. The particles exhibiting a uniform distribution could facilitate the transport of molecules and provide free access without hindering the diffusion (Yoshitake et al., 2002). This feature leads to an increase in the adsorption rate and the available capacity. The TEM image, Figure 5.19a, of Hg(II) shows a significant reduction in the porous structure following adsorption and the pore structure is calculated by measuring the intensity through the line drawn between points a and b, Figure 5.19b, and found to be ~ 0.33 nm as shown in Figure 5.19c. This result indicated that some pores have been filled with Hg(II) during the adsorption process.

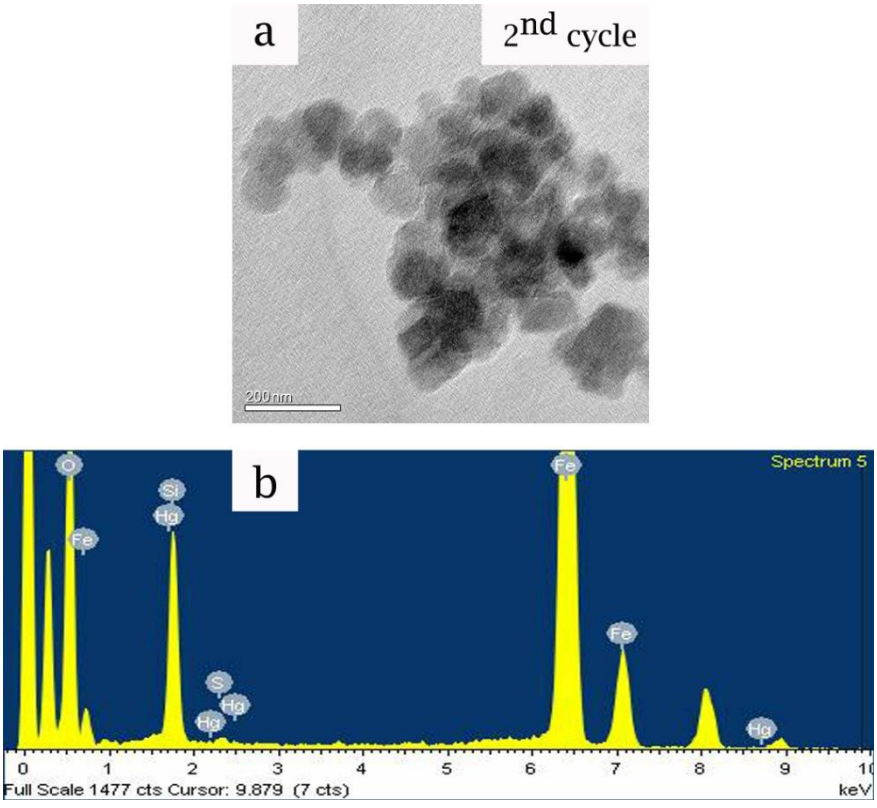

Figure 5.17: (a) TEM image of the second cycle of Hg (II) loaded SH-SCMNPs and (b) the corresponding EDX spectra.

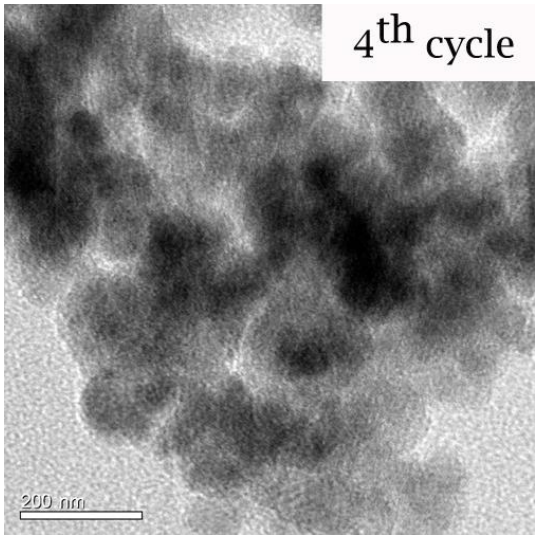

Figure 5.18: TEM image of the fourth cycle of SH-SCMNPs following elution treatment.

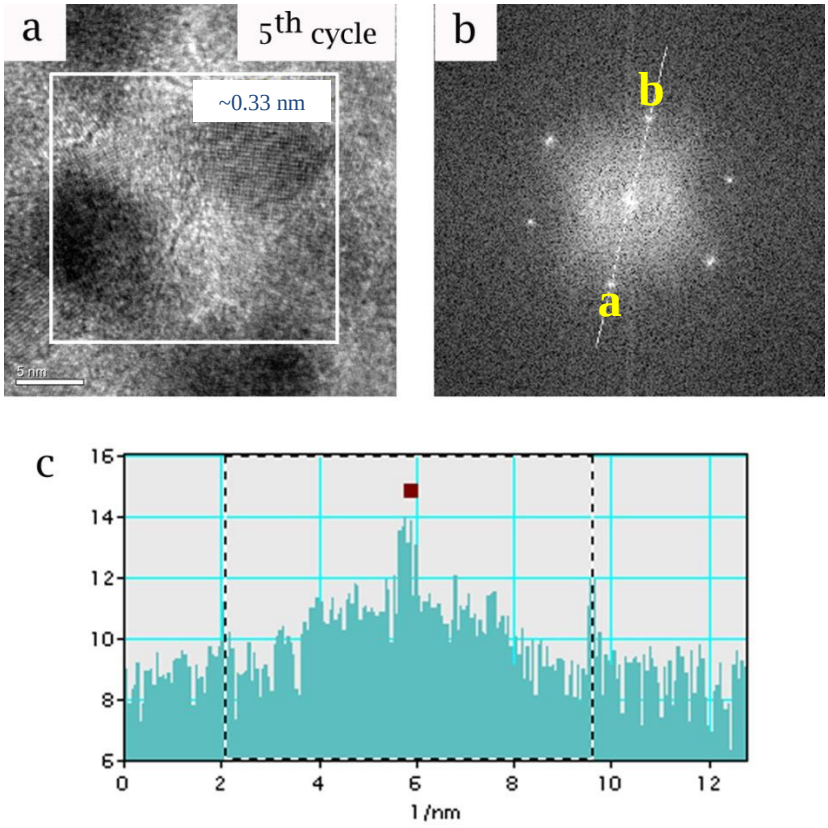

Figure 5.19: (a) HTREM image of the fifth cycle of SH-SCMNPs, (b) diffraction pattern of the fifth cycle of SH-SCMNPs, and (c) its intensity.

5.8 Further Studies on the Dissolution of Silica Coated NPs

Iron oxides are in general, compounds with very low solubility (Kraemer, 2004) and are readily attacked by acids (Schwertmann, 1991). Silicon oxide is relatively water insoluble compared to other minerals and the solubility of amorphous silicon oxide in water is dependent on the pH range and the relative concentration. The solubility of amorphous silica can be enhanced under alkaline conditions due to the formation of monomeric and multimeric silicate (Stumm et al., 1967; Guthrie and Reardon, 2008). The dissolution of iron and silica is governed by some factors that influence the rate of dissolution, such as the temperature, the composition of the solution phase (e.g., pH, ions, ligands and the concentration of acids), surface structure and structural modifications. In this study, the pH of the solution was investigated as a major factor in the dissolution of Fe and Si, and the contact time and effect of strong acids during the elution process were examined.

5.8.1 Dissolution Kinetics

5.8.1.1 Effect of contact time

The effect of the contact time on the dissolution of Fe_3O_4 NPs and SH-SCMNPs at pH 2.0 is shown Figure 5.20. The dissolution of the NPs was confirmed by measuring the total residual concentration of Fe in the supernatant after the NPs were isolated using an external magnetic field. The concentration of Fe released from the SH-SCMNPs was below the sample detection limit of the ICP-OES, which is less than 0.19 mg L^{-1}. The initial rate of dissolution of Fe_3O_4 NPs was low (0.22 mg L^{-1}, ~3.69 % of the initial concentration) and it approached an equilibrium condition in 30 minutes with the dissolution of 0.69 mg L^{-1} (~11.65 % of the initial concentration). The effect of the contact time on the dissolution of Fe_3O_4 NPs and SH-SCMNPs at pH 6.0 was negligible (data not shown). The concentration of iron from Fe_3O_4 NPs and SH-SCMNPs was less than 0.19 mg L^{-1}. As noted in Chapter 2, the aim of coating the Fe_3O_4 NPs with silica was to achieve high resistance to leaching in acidic media. The results confirmed that as the concentration of released Fe from the SH-SCMNPs was less than 0.19 mg L^{-1} at pH 2.0 and 6.0. There was no protection to the Fe_3O_4 NPs from dissolution in the acidic media in the absence of any metals dropped on the surface of the NPs.

Leaching of sorbent components into the treated water is unfavourable. However, the effluent discharge limit of Fe into municipal sewers is 2 mg L^{-1} (WHO, 2011) which is higher than the concentration of Fe released from the NPs.

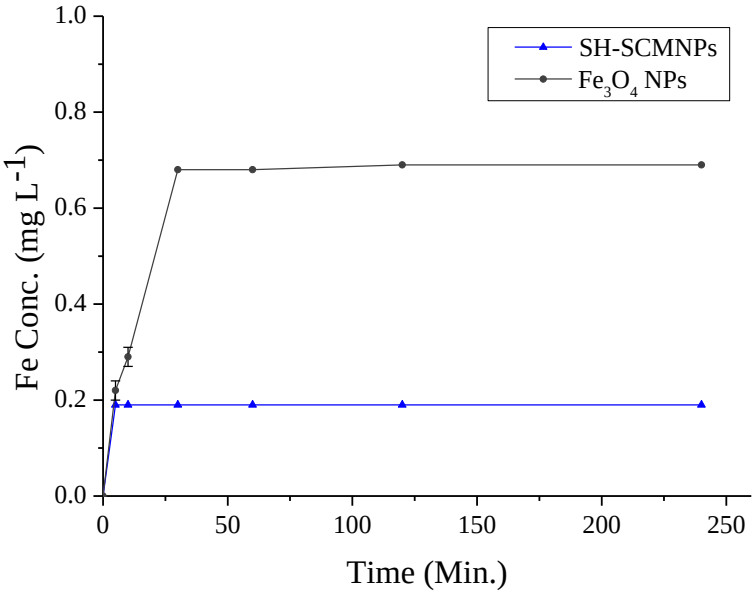

Figure 5.20: Effect of contact time on the dissolution of Fe_3O_4 NPs and SH-SCMNPs at pH 2.0.

5.8.1.2 Effect of pH

As discussed in Chapter 4, the pH of the solution is an important parameter for controlling the particle size of colloids because it affects the stability of the surface charge and particle interactions. The effect of pH on the dissolution of Fe_3O_4 NPs and SH-SCMNPs is shown in Figure 5.21, Figure 5.22 and Figure 5.23. The reference concentration of Fe and Si (8 mg L^{-1} of 50 mg mL^{-1} NPs aqueous dispersion) are also presented in Figure 5.21, Figure 5.22 and Figure 5.23. It was found that the Fe_3O_4 NPs are sensitive in the acidic media demonstrating the dissolution 0.63 mg L^{-1} (10.61 %) of Fe. The dissolution was negligible with increasing pH and the concentration of Fe was below the sample detection limit of ICP-OES. A small amount of Fe, less than 0.19 mg L^{-1} was detected over the pH range tested, which confirmed that the solution pH does not affect the dissolution of SH-SCMNPs as shown in Figure 5.22. An increasingly small amount of Si was dissolved into the solution as the pH values increased, as shown in Figure 5.23. At pH 8.0, the concentration of Si released from the SH-SCMNPs into

the solution was 116.5 μg L^{-1} (17.12%). This result agrees with the findings of previous researchers (Guthrie and Reardon, 2008; Pham et al., 2011) who confirmed that the presence of an alkaline environment markedly enhanced the dissolution rate of silica compared with neutral or acidic environments.

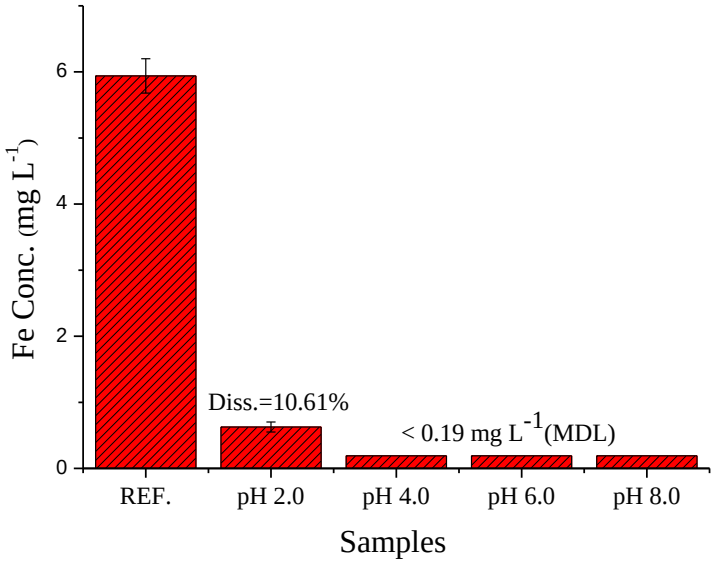

Figure 5.21: Effect of pH on the dissolution of Fe from Fe_3O_4 NPs.

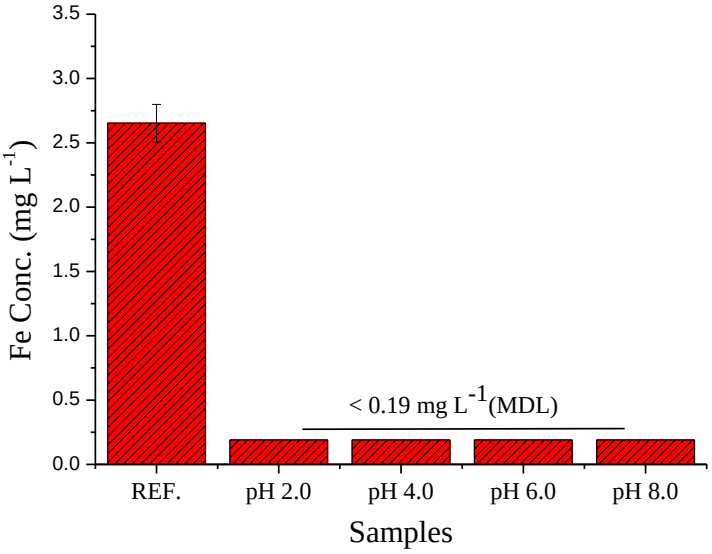

Figure 5.22: Effect of pH on the dissolution of Fe from SH-SCMNPs.

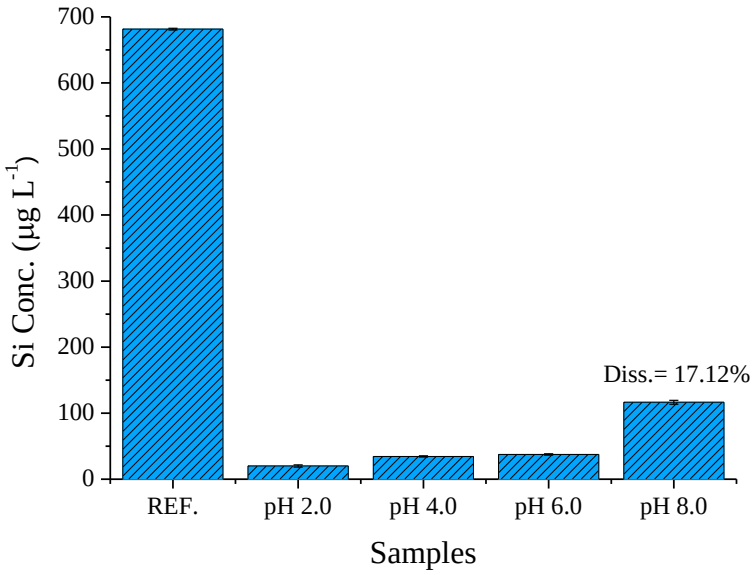

Figure 5.23: Effect of pH on the dissolution of Si from SH-SCMNPs.

5.8.1.3 Effect of elution process

This experiment was carried out by shaking 50 mL of 80 µg L^{-1} Hg(II) solution with 8 mg L^{-1} SH-SCMNPs at pH 4.0 and 6.0. After separating the SH-SCMNPs by a magnet, the effect of the elution process on the dissolution of the SH-SCMNPs was investigated by mixing SH-SCMNPs with 3.0 M HCl containing 2% thiourea (m/v) with a shaking speed of 200 rpm for 1 hr, and the results are presented in Table 5.10. Despite the eluent solution being highly acidic (pH 1.8), the dissolution of SH-SCMNPs was not affected in this case and the results were similar to those obtained in the previous section. The concentration of Fe was also below the sample detection limit of ICP-OES, indicating that the matrix in a very acidic solution only contributes to the release of very small amounts of Fe from the SH-SCMNPs. The results confirm that the well-sealed dense liquid silica coating on Fe_3O_4 NPs could prevent the substrate materials from leaching into the acidic environment. The amount of Si leached out by the elution process was less than 39 µg L^{-1} (5.71 %).

Table 5.10: Dissolved Fe and Si during the elution process.

Samples	ICP (mg L^{-1} Fe dissolved)*	ICP (µg L^{-1} Si dissolved)**
SH-SCMNPs-pH 4.0	<0.19	38.66 ±2.31
SH-SCMNPs-pH 6.0	<0.19	37.33 ± 2.08

* Total Fe in Reference Sample = 5.96 mg L^{-1}

** Total Si in Reference Sample = 683.12 µg L^{-1}

Chapter 6

Mechanism of Adsorption

6.1 Introduction

SH-SCMNPs as a tailored sorbent for the adsorption of Hg(II) ions were found to be a promising adsorbent for their high removal. As discussed in Chapter 5 and based on the competition between Hg(II) ions and other ions, the adsorption mechanism can be attributed to the complexation chemistry between the thiol groups and the metal ions, with the specificity of a thiol group towards Hg(II) ions being the result of a conventional acid base interaction between the two. The pH value affects adsorption as it determines the degree of protolysis or 'ionisation' of both the adsorbate and the adsorbent. Since hydrogen and hydroxide ions often interact with adsorbents commonly used in aqueous phase applications, the adsorption of Hg(II) ions may be strongly influenced by the pH of the solution. In this chapter, the zeta potential of the SH-SCMNPs and of the SH-SCMNPs that had been in contact with Hg(II) solutions at different concentrations were determined to measure the surface charge and to assess the effect of pH. Raman and FTIR spectroscopy were used to give detailed information relating to the mechanism of Hg(II) adsorption onto SH-SCMNPs. By using these techniques, the inner-from outer sphere mechanism and the monodentate attachment can be distinguished.

6.2 Adsorption Isotherm

The adsorption isotherm defines the equilibrium distribution of an adsorbate onto the adsorbent for the equilibrium concentration of the adsorbate in the solution at constant temperature. To derive data for the adsorption isotherm, initial concentrations of 40, 80, 120, 160, 200, 400, 600, 800 and 1000 μg Hg(II) L^{-1} were used with the Fe_3O_4 NPs, SCMNPs and SH-SCMNPs adsorbents at 8 mg L^{-1}, as shown in Table 6.1. The amount of Hg(II) ions adsorbed per unit mass of the Fe_3O_4 NPs, SCMNPs and SH-SCMNPs is shown in Figure 6.1. From plotting the adsorbed Hg(II) (q_e) against the equilibrium

concentration (C_e) at pH 6.0, the loading capacity of the Fe_3O_4 NPs, SCMNPs and SH-SCMNPs was found to be 42.3, 48.4 and 113.7 mg g^{-1}, respectively when applied at a concentration of 8 mg L^{-1}. However, it is clear from the isotherm curves, Figure 6.1, that the Hg(II) adsorption isotherm shows an increase in uptake of Hg with a change in the type of nano-sorbents. This may suggest that different mechanisms are responsible for the removal of Hg(II) ions from the solution. In an attempt to increase the maximum adsorption capacity in the same range of Hg initial concentration used in the above adsorption isotherm experiments, initial concentrations of 80, 160, 200, 400,600, 800 and 1000 µg Hg(II) L^{-1} were used with SH-SCMNPs adsorbents at 4 mg L^{-1}. As expected, the amount of Hg(II) ions adsorbed per unit mass of the SH-SCMNPs increased with the decreased weight of the adsorbent. Figure 6.1 shows that the loading capacity of the SH-SCMNPs was found to be 207.7 mg g^{-1}. Table 6.2 presents a comparison of the loading capacity with other adsorbents used for the adsorption of Hg(II) as reported in the literature, and it is clear that SH-SCMNPs have a higher adsorption capacity for Hg(II) when used under similar conditions. However, the highest adsorption capacity of Hg by SH-SCMNPS might be attributed to the amount functional group (-SH) present on the adsorbent surface and grafted hexagonal mesoporous structure, demonstrating the ability of SH-SCMNPs to bind to Hg ions.

The two parameter Langmuir and Freundlich isotherms were used to initially define surface adsorption processes because their predicated calculations were based on the observed data without parameter adjustments for optimization. The adsorption data were fitted to both the Langmuir and Freundlich isotherm models, which can be used to describe the equilibrium between Hg(II) ions adsorbed (q_e) and in solution (C_e) when at a constant temperature. The Langmuir isotherm describes a homogeneous surface with a uniform sorbate monolayer whereas the Freundlich isotherm describes solids with heterogeneous properties. The Freundlich adsorption constant K_f represents the extent of sorption or adsorption intensity, where larger K_f values indicate stronger attraction forces between the adsorbate surface and the adsorbate. The Freundlich exponent ‘n’ represents adsorbate change in affinity as adsorption density changes; values of $0.2 < 1/n < 0.8$ are considered good adsorbents, with smaller values indicating strong adsorbent bonds and

better adsorption (McCabe et al., 2005) and higher values indicating less heterogeneity (Sawyer et al., 2002). Langmuir parameters include Q_0, which is the Langmuir adsorbent maximum capacity for the adsorbate, the Langmuir constant b is a measure of affinity of the adsorbate for the adsorbent, and R^2 is the correlation. The adsorption affinity is represented by the initial slope of the isotherm curve and adsorption capacity is the position of the plateau.

The plots for C_e/q_e against C_e for both quantities of adsorbent are shown in Figure 6.2 with a linear regression line fitted. The values of the Langmuir constants Q_0 and b were calculated from the slope and intercept of this line and are shown in Table 6.3. The correlation coefficient (R^2) is > 0.97 for the data in the model indicating monolayer adsorption of the Hg (II) ions to the surface of the SCMNPs and SH-SCMNPs at the concentrations of adsorbent and adsorbate applied. However, this model did not fit particularly well with the Fe_3O_4 NPs data resulting in a correlation coefficient (R^2) of 0.93. The sorption capacity for Fe_3O_4 NPs and SCMNPs were 42.3 and 48.4 mg Hg g^{-1}, respectively. For SH-SCMNPs, the different quantities of adsorbent gave different sorption capacities of 113.7 and 207.7 mg Hg g^{-1}. A higher maximum capacity was achieved when the ratio of adsorbent to adsorbate was low, as the maximum capacity calculated from the Langmuir equation is not a constant but a function of this ratio. It is readily understood that the number of available adsorption sites increases by increasing the concentration of adsorbent and it, therefore, results in the increase of the amount of adsorbed Hg. The decrease in adsorption capacity with increase in the concentration of SH-SCMNPs is mainly because of unsaturation of adsorption sites through the adsorption process (Manohar et al., 2002; Jeon and Ha Park, 2005). Another reason could be attributed to the particle interaction (Yean et al., 2005; Illés and Tombácz, 2006), such as aggregation, resulting from high concentration of SH-SCMNPs.

The experimental data was also plotted in accordance with the Freundlich model (Figure 6.3) and the constants obtained are shown in Table 6.4. The correlation coefficients (R^2) between the experimental data and the model were 0.99 for Fe_3O_4 NPs and for SCMNPs it was 0.99 and 0.97 for the two different quantities of SH-SCMNPs utilised. The Freundlich isotherm model fitted the experimental data better than the Langmuir

isotherm model. The Freundlich isotherm model is therefore the most suitable model to characterise Hg(II) adsorption onto all three types of NPs in the solution conditions. The results in general suggest that heterogeneous conditions exist. As discussed in Chapter 3, hydroxide groups are present on the surface of the Fe_3O_4 NPs and the objective of using the sol-gel method for coating Fe_3O_4 NPs with silica was to increase the density of the hydroxyl group on the NPs. Therefore, it is best to describe the surface of the Fe_3O_4 NPs and SCMNPs as heterogeneous and adsorb Hg(II) ions to the present active sites. Due to the increase in surface area of the Fe_3O_4 NPs after coating with silica, SCMNPs have large adsorption capacities that result in more surface sites becoming exposed.

In the same manner, the Freundlich isotherm model produced an excellent fit to the experimental data for Hg ions for the two different quantities of adsorbent used, suggesting that heterogeneous conditions exist. It might therefore be the case that the SH-SCMNPs provide heterogeneity by virtue of having different functional groups present and a complex porous structure. The Freundlich parameter $1/n$ gave values of 0.73, 0.65, and 0.47 for Fe_3O_4 NPs, SCMNPs and SH-SCMNPs respectively, indicating that Hg ions can be effectively removed from aqueous solutions.

In summary, comparing the R^2 values for these two isotherms (Table 6.3 and 6.4), higher correlations were most often observed using the Freundlich isotherm which indicated the likelihood of heterogeneous surfaces. Therefore, the Freundlich isotherm is the correct equation to use to express the uptake of Hg onto three types of NPs. Although previous studies, suggest that the Hg(II) adsorption isotherm of thiol-functionalised mesoporous silica adsorbents usually exhibit typical Langmuir behaviour which are the characteristics of chemical adsorption (Chen et al., 1999; Brown et al., 2000; Aguado et al., 2005; Aguado et al., 2008). This observation suggests the adsorption of a monolayer on independent binding sites. In the present work, the results suggested the adsorption mechanism of Hg may involve not only metal ion chelation by thiol complexing of 3-MPTMS, it can be involved complexation by hydroxide groups, or likely to interact with silanol groups located on Fe_3O_4 NPs. However, this finding is consistent with those of previous studies using modified thiol groups with different types of materials for the adsorption of Hg, as shown in Table 6.5. These studies reported that

the Freundlich isotherm model correlated better than the Langmuir isotherm model, thereby suggesting heterogeneous adsorption.

Table 6.1: Results for the adsorption isotherm of Hg by 8 mg L^{-1} Fe_3O_4 NPs, SCMNPs and SH-SCMNPs using Hg(II) concentrations of 40-1000 µg L^{-1} at pH 6.0.

C_o	C_e	q_e	C_e/ q_e	C_e	q_e	C_e/ q_e	C_e	q_e	C_e/ q_e
µg L^{-1}	mg L^{-1}	mg g^{-1}	g L^{-1}	mg L^{-1}	mg g^{-1}	g L^{-1}	mg L^{-1}	mg L^{-1}	g L^{-1}
	Fe_3O_4 NPs			SCMNPs			SH-SCMNPs		
40	0.005	4.3	1.27	0.002	4.8	0.41	0.000	5	0.00
80	0.011	8.6	1.34	0.005	9.4	0.51	0.000	10	0.00
120	0.020	12.5	1.59	0.011	13.7	0.77	0.002	14.7	0.14
160	0.028	16.6	1.67	0.015	18.1	0.84	0.004	19.5	0.21
200	0.041	19.9	2.06	0.021	22.4	0.95	0.006	24.3	0.25
250							0.008	30.2	0.26
300	0.055	24.3	2.27	0.029	27.7	1.03	0.010	36.3	0.28
350							0.013	42.1	0.31
400	0.068	29	2.36	0.037	32.9	1.12	0.017	47.9	0.35
450							0.021	53.7	0.39
600	0.084	33.2	2.52	0.047	37.9	1.24	0.031	71.1	0.44
800	0.098	37.7	2.60	0.054	43.2	1.25	0.056	93	0.60
1000	0.011	42.3	2.63	0.063	48.4	1.30	0.090	113.7	0.79

Table 6.2: Comparison of the sorption capacities of adsorbents used for Hg (II) removal (mg g^{-1}).

Materials	Sorbent	Max capacity (mg g^{-1})	Max Hg conc. (µg L^{-1})	Adsorbent conc. (g L^{-1})	Final Hg con. (µg L^{-1})*	Reference
Nano-sorbents	**Thiol-modified magnetite beads-porous materials**	14.0	60000	1	46000	Dong et al. (2008)
	Magnetic NPs modified with 2-mercaptobenzothiazole	0.59	1000	1	410	Parham et al. (2012)
	Humic acid coating Magnetic NPs	97.7	5000	1	240	Liu et al. (2008)
	Thiol-modified magnetite NPs-non porous materials	19.8	560	0.01	21900	Song et al. (2011)
	Silica-graft dimethylaminoethyl methacrylate	8.1	30000	1	361.1	Zhao et al. (2011)
Conventional sorbents	**Zeolite**	57.5	470	2	200	Chojnacki et al. (2004)
	Clay	0.04	1000	12.50	500	Viraraghavan and Kapoor (1994)
		0.2	1500	28	856	Senevirathna (2011); Bailey et al. (1999)
	Peat moss	16.2	5000	5	844	
	Fly ash	2.5	10000	20	1000	Sen and De (1987)
	Activated carbon	109.9	200000	0.48	128000	Namasivayam and Kadirvelu (1999); Rao et al. (2009)
		22.3	140000	0.50	129000	
	SH-SCMNPs	207.7	1000	0.004	169	This study

* Some of the final Hg concentrations were not present in some references, but calculated according to other experimental parameters.

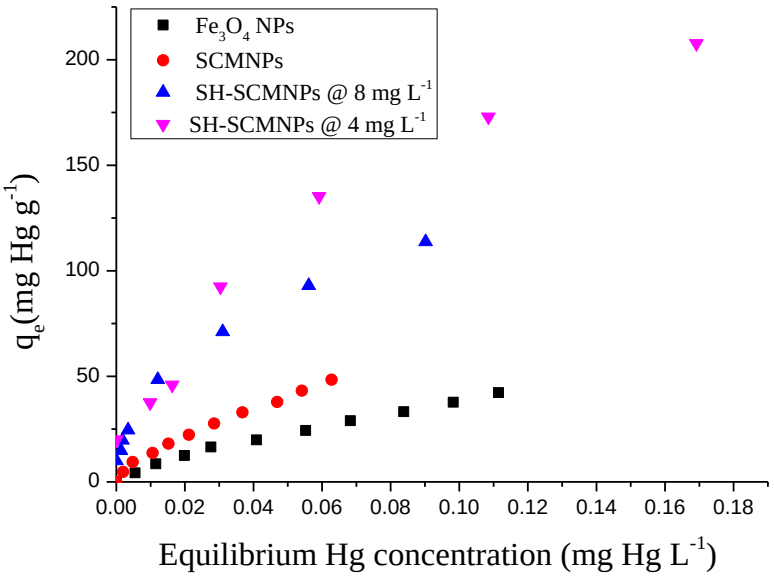

Figure 6.1: Comparison of adsorption isotherm curves by Fe_3O_4NPs, SCMNPs and SH-SCMNPs at an initial pH of 6.0.

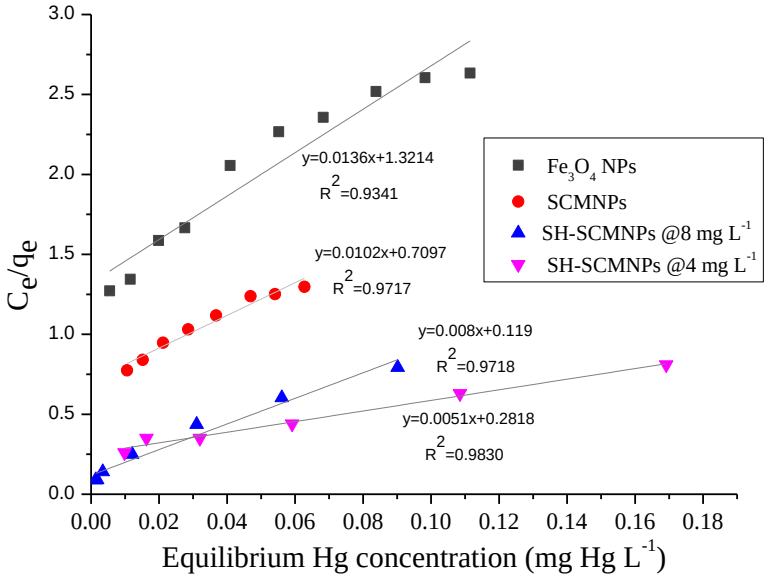

Figure 6.2: Langmuir isotherm approach for thermodynamics experiments of Hg(II) adsorption at pH 6.0.

Table 6.3: Estimated values of constants for the Langmuir model using Fe_3O_4 NPs, SCMNPs and SH-SCMNPs at pH 6.0.

Adsorbent	Langmuir Constant		R^2
	Q_0(mg g^{-1})	b(l mg^{-1})	
Fe_3O_4 NPs	42.3	0.01	0.93
SCMNPs	48.4	0.01	0.97
SH-SCMNPs @ 8 mg L^{-1}	113.7	0.07	0.97
SH-SCMNPs @ 4 mg L^{-1}	207.7	0.02	0.98

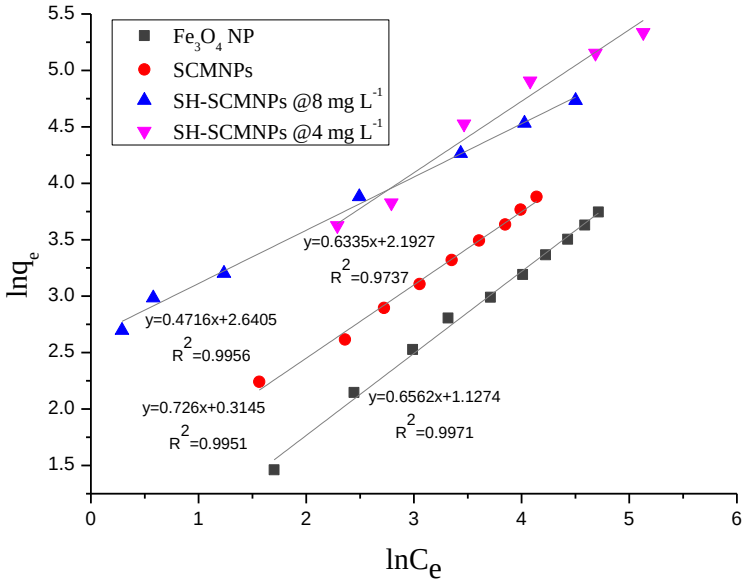

Figure 6.3: Freundlich isotherm approaches for thermodynamics experiments of Hg(II) adsorption at pH 6.0.

Table 6.4: Estimated values of constants for the Freundlich model using Fe_3O_4 NPs, SCMNPs and SH-SCMNPs at pH 6.0.

Adsorbent	Freundlich Constant		R^2
	K_f	1/n	
Fe_3O_4 NPs	1.37	0.73	0.99
SCMNPs	5.17	0.65	0.99
SH-SCMNPs @ 8 mg L^{-1}	14.03	0.47	0.99
SH-SCMNPs @ 4 mg L^{-1}	8.96	0.48	0.97

Table 6.5: Some examples of Freundlich isotherm as the correct model used to express the uptake of Hg onto thiol-functionalised materials.

Adsorbent	Reference
Thiol-grafted chitosan beads	Merrifield (2002)
Benzoylthiourea-modified mesoporous Silica particles	Antochshuk et al. (2003)
(Acetylacetone)-2-Thiol-Phenyleneimine particles	Kara (2005)
2-Mercaptobenzimidazole- Immobilized Organophilic Hydrotalcite	Anirudhan et al (2009)

6.3 Comparative Study on the Effect of Solution pH

6.3.1 Effect of pH and Electrophoretic Mobility (EM) Studies

The pH value affects adsorption as it determines the degree of protolysis or 'ionisation' of both the adsorbate and the adsorbent. Since hydrogen and hydroxide ions often interact with adsorbents commonly used in aqueous phase applications, the adsorption of Hg(II) ions may be strongly influenced by the pH of the solution (Walcarius and Delacôte, 2005). At concentrations higher than 50 mg L^{-1}, Hg(II) is likely to precipitate out from the solution. To mitigate this effect, the test used 50 ml aliquots of Hg (II) at concentrations of 80, 200, 500and 1000 µg L^{-1} mixed with NPs at a concentration of 8 mg L^{-1} for 1 hour in order to reach equilibrium. The test was carried out at pH values ranging from 2.0 to 9.0.

The effect of the solution pH on the removal of 50 ml 80 μg L^{-1} Hg(II) by Fe_3O_4 NPs, SCMNPs and SH-SCMNPs is shown in Figure 6.4. As far as the mercury is concerned, the removal efficiency was strongly pH-dependent. The uptake of Hg(II) ions by Fe_3O_4 NPs increased rapidly with increasing pH values, and the optimum removal efficiency was between pH 5.0 and 6.0. The adsorption efficiency decreased slightly when the pH of the solution was above this level. The removal efficiency of Fe_3O_4 NPs was 83.91% at a pH of 6.0, whilst only 12.32% of the Hg(II) ions were removed at pH 2.0. It can also be seen from Figure 6.4 that SCMNPs reached their optimum removal efficiency at pH 6.0 and had a maximum removal efficiency of 89.84%. SCMNPs showed a similar response at lower pH values with the removal of Hg(II) ions at only 71.18% at pH 2.0. The optimal removal efficiency was achieved at pH 5.0, 6.0 and 7.0 with the removal of 88.67, 89.84 and 88.36 % respectively. The removal efficiency decreased from 88.36 to 80.05% when increasing the pH from 7.0 to 9.0. There was no effect on the removal efficiency between pH 2.0-7.0 using SH-SCMNPs; however, it decreased by 6.95% when the pH rose to 9.0. Thus, the optimal Hg removal using these three types of NPs can be achieved by controlling the pH of the solution. To ensure that only the adsorption reaction occurs for Hg(II) ions, the operating pH is therefore suggested to be at 6.0 based on the above discussion.

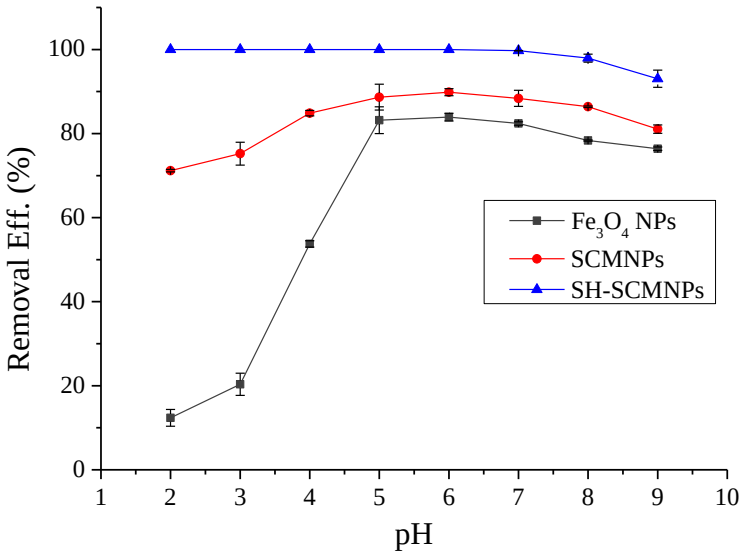

Figure 6.4: Effect of pH on the removal of Hg (II) ions by Fe_3O_4 NPs, SCMNPs and SH-SCMNPs with 80 μg L^{-1} solution.

As discussed above, at lower concentrations of the Hg(II) solution there was no effect on the removal efficiency between pH 2.0 and 7.0. Therefore another experiment was conducted to investigate the effect of pH at concentrations of 200, 500 and 1000 μg l^{-1} mixed with SH-SCMNPs at a concentration of 8 mg L^{-1} for 1 hour in order to reach equilibrium. The results showed that there was a decrease in the removal efficiency at all pH values tested with increasing concentration of the Hg(II) solution, Figure 6.5. At the 200 μg l^{-1} Hg(II) concentration, there was no effect on the removal efficiency between pH 2.0 and 7.0. However, there was a reduction in the removal efficiency at the higher Hg (II) concentrations and at the lower pH values. In addition, above pH 7.0 there was a small decrease in the efficiency of removal. These results support the findings of Walcarius and Delacôte (2005) who also showed an independence of the effects of pH on adsorbence when using -SH functional groups. The high selectivity and affinity for Hg by the thiol-functionalised group is a possible explanation for this (Mattigod et al., 2007). This affinity is predicted on the basis of the hard and soft acid base (HSAB) theory that directly correlates the degree of cation softness with the observed strength of interaction with base functionalities, such as –SH groups. The relatively large ionic size, low electro-negativity, and high polarisability (highly deformable bonding electron orbital) of Hg(II) are characteristics of a soft acid, and as the thiol group is a soft base, they have a high affinity to each other.

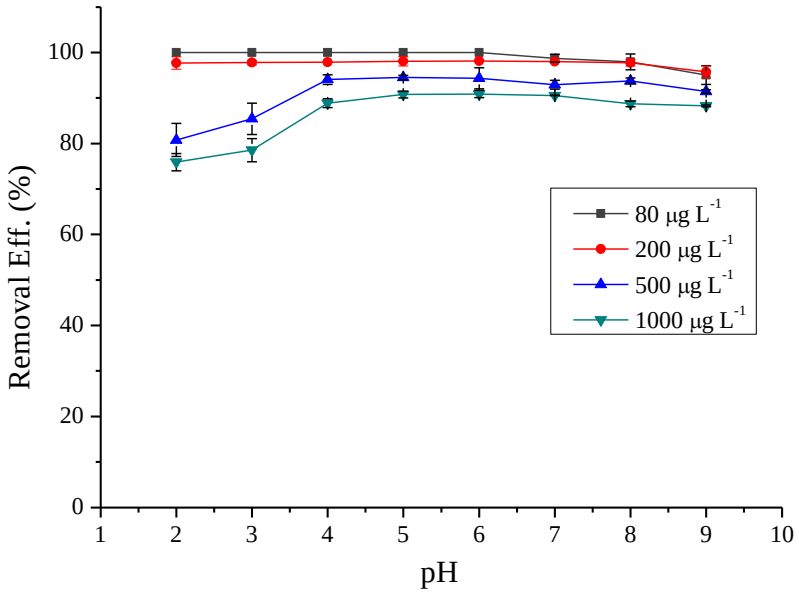

Figure 6.5: Effect of pH on the removal of Hg(II) ions by SH-SCMNPs at different initial Hg(II) concentrations.

To understand the adsorption mechanism it is important to determine the point of zero charge, pH_{pzc}, of the adsorbent. Zeta potential measurements were conducted in order to observe the shift in the isoelectric point of the system containing NPs (Fe_3O_4 NPs, SCMNPs and SH-SCMNPs) in suspension and various concentrations of Hg(II) ions. The surface charge of the NPs and of those that had been in contact with the Hg(II) solutions at different concentrations was studied by measuring their zeta potential at pH values ranging from 2.0-8.0.

For Fe_3O_4, the removal of Hg (II) ions was inefficient at pH values <4.0, and the pH_{pzc} for Fe_3O_4 NPs and Fe_3O_4 NPs at 80 μg L^{-1} occurred at 4.8 and 4.5 respectively, Figure 6.6. The removal efficiency can be attributed to the positive surface charge of Fe_3O_4 that declined the sorption of positive metals. Consequently, when the pH of the solution is below the pH_{pzc}, the adsorbent surface is positively charged, and anion adsorption simply occurred by electrostatic attraction. In contrast, when the pH of the solution is above the pH_{pzc} level, the adsorbent surface is negatively charged, and cation adsorption occurs. At pH values lower than the pH_{pzc}, adsorption of Hg should be reduced to nearly zero; however, this is not the case for Hg. Even at pH values lower than pH_{pzc}, a large amount of Hg was still adsorbed onto the Fe_3O_4 NPs. In this case, the result suggests that ion exchange between Hg (II) and H^+ ions may play a role within this pH range.

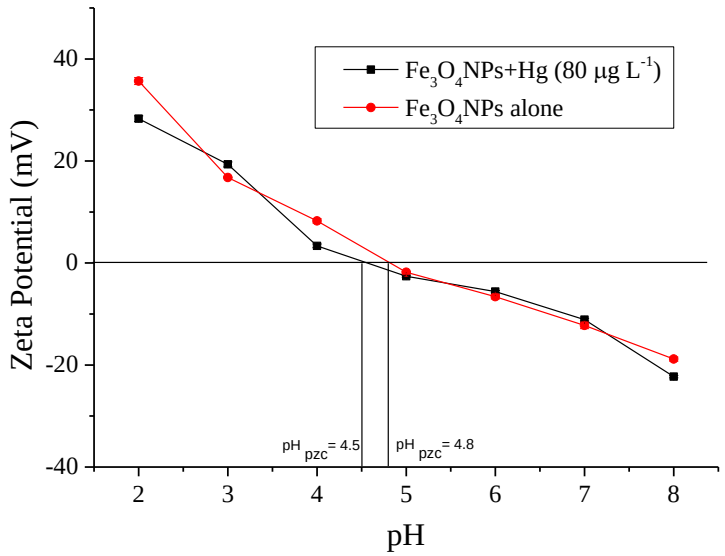

Figure 6.6: Zeta potential of Fe_3O_4 NPs at different pH values.

As shown in Figure 6.4, the optimal pH ranges for the removal of Hg(II) ions using SCMNPs was from 4.0 to 7.0 with an enhanced adsorption efficiency better than Fe_3O_4 NPs. The pH_{pzc} of SCMNPs was located at pH 3.3, (Figure 6.7). It clear that, at pH 2.0 and 3.0 the surface of the SCMNPs adsorbent should be positive, thereby adsorbing few Hg(II) ions due to the repelling electrostatic forces, whereas at pH 4.0 and above, the surface is strongly negatively charged and adsorbs Hg(II) ions through strong electrostatic forces.

As described in Chapter 4 (Section 4.2.6) the surfaces of the SCMNPs are generally covered with hydroxyl (OH) groups and silanol groups (Si–OH). Hydroxyl groups are attached to one silicon atom to build a vicinal or germinal silanol based on the number of silicon atoms (Jal et al., 2004). This new structure increases the density of the hydroxyl group on the NPs with large surface areas. Therefore, a possible explanation for the increase in Hg(II) ion removal using SCMNPs could be attributed to the following two reasons. The first mechanism is based on the change of physico-chemical properties of hydroxyl groups at different pH values. Aguado et al. (2008) reported that for pH values of less than 4.0, the oxygen and hydrogen atoms of the hydroxyl group were competitively bound by protons, causing a decrease in Hg adsorption. It is likely that the decreased adsorption of Hg was primarily ascribed to the competitive binding between protons and the Hg for the hydroxyl groups, although the columbic repulsion might also be responsible the decreased Hg adsorption at these low pHs. With increasing pH, protons are released from the hydroxyl groups, making more binding sites available for the adsorption of Hg(II) ions. The second reason is that the increase in surface area, after coating the Fe_3O_4 NPs with Si (160 $m^2 g^{-1}$), which is available for Hg(II) adsorption might explain the higher adsorption of Hg (II) ions onto SCMNPs. This reason can also be used to explain the higher levels of adsorption observed at the lower pH values, especially at the lower concentrations.

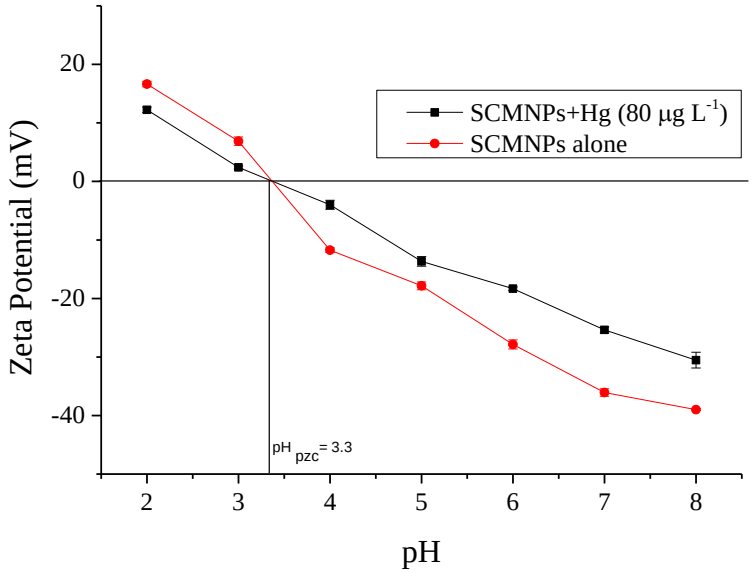

Figure 6.7: Zeta potential of SCMNPs at different pH values.

The mechanism of adsorption at different Hg(II) concentrations using SH-SCMNPs can be interpreted as follows. At a pH value below pH_{pzc}, Figure 6.8, adsorption by chemical binding should be nearly zero due to the positive surface charge of both SH-SCMNPs and the metal ions whilst at pH values above pH_{pzc}, the adsorbent surface is negatively charged and cation adsorption is expected. In the case of the test carried out at an initial concentration of Hg(II) > 500 µg L^{-1} however, some Hg was still adsorbed onto the SH-SCMNPs, suggesting that ion exchange between Hg(II) and H^+ ions might play a role in the pH range below pH_{pzc} by allowing some of the Hg to attach to the adsorbent. In the case of a lower initial concentration of Hg(II) ≤ 200 µg L^{-1}, all of the Hg was adsorbed at the lower pH as there were a sufficient number of protonated ligand sites available. At pH values above pH_{pzc}, adsorption of Hg was complete as expected. However, increasing the pH of the solution to above 7.0 also decreased the adsorption efficiency at all Hg concentration as shown in Figure 6.5. This can be attributed to the dissolution of Si with increasing pH values as discussed in Chapter 5.

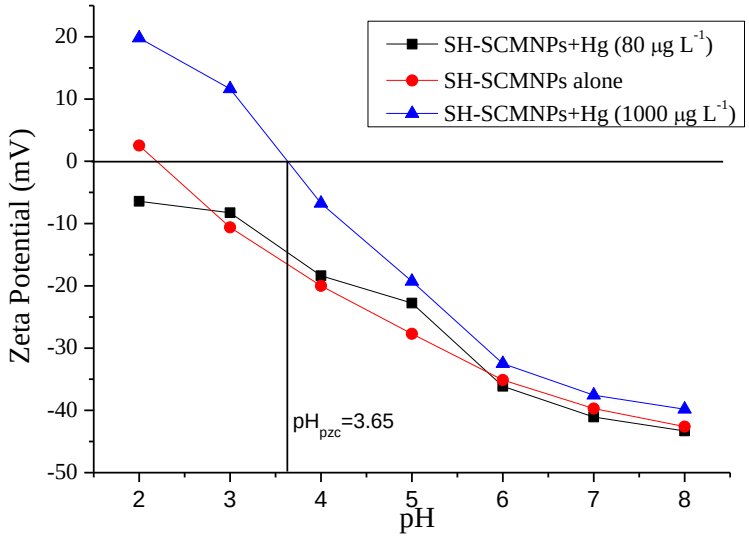

Figure 6.8: Zeta potential of SH-SCMNPs at different pH values.

In conclusion, the optimal pH value for the simultaneous adsorption of Hg from aqueous solution was at pH values of 5.0 and 6.0, while SH-SCMNPs showed that at the two lower concentrations of Hg(II) solution tested, there was no effect on the removal efficiency when the pH of the solution was between 2.0 and 7.0. There was a reduction in the removal efficiency at the higher Hg(II) concentrations at the lower pH values, and above pH 7.0 there was a small decrease in the removal efficiency. The –SH groups could be oxidised if stored for a long time in an acidic medium (Palmberger et al., 2008; Juntapram et al., 2011) leading to a lowered reactivity of the -SH groups. Based also on the dissolution study presented earlier in Chapter 5, the dissolution of Si increased with increasing pH values above 6.0. Therefore, a pH of 6.0 was selected for all subsequent experiments.

6.3.2 Effect of Ionic Strength

Ionic strength of the solution is one of the factors which could reduce the adsorption efficiency (Song et al., 2009). In general, as different kinds of salts are mixed in real wastewater, the ionic strength is high. At high ionic strength, adsorption sites are surrounded by counter ions that partially lose their charge, and this weakens the binding force due to electrostatic interactions (Jeon and Ha Park, 2005). Furthermore, a decrease

in ionic strength may enhance colloidal stability and promote lead transport, whereas an increase in ionic strength may promote colloidal aggregation (Brant et al., 2007).

The relationship between zeta potential and the ionic strength of a solution, and different values of pH and their effect on the adsorption of Hg(II) by SH-SCMNPs are presented in Figure 6.9 and Figure 6.10. The latter figures show that there was no effect of the adsorption of Hg(II) ions at a concentration of 80 μg L^{-1} with an ionic strength of 0.1 and 0.01M $NaNO_3$. At Hg concentration of 1000 μg L^{-1}, the surface of SH-SCMNPs adsorbent was positive at pH 2.0 and 3.0 (Figure 6.10), thereby adsorbing little Hg due to the repelling electrostatic forces, whereas at pH 4.0 and above, the surface charge was negative and Hg was adsorbed due to the strong electrostatic forces. However, the adsorption efficiency remained stable at pH ranging 4.0 to 7.0 until it reached above pH 7.0 when there was a small decrease in the efficiency of removal. These results are typical and were discussed in Section 6.3.1 where the amount of Hg(II) removal from the solution was not influenced by the presence of the electrolyte either with 0.01 or 0.1M $NaNO_3$.

There is no previous research that has demonstrated that thiol-functionalised NPs, either magnetite or non-magnetite particles, are stable at increased ionic strengths. Therefore, its study may help to investigate the stability of SH-SCMNPs in suspension by evaluating changes in the zeta potential as a function of pH, ionic strength and electrolyte species such as $NaNO_3$. The lack of effect of ionic strength on the adsorption efficiency and zeta potential of SH-SCMNPs could be attributed to a stabiliser covering the surface of the Fe_3O_4 NPs, either a surfactant or ligand molecules. The lack of effect of ionic strength is in agreement with previous studies that used stabilisers for coating NPs. For example, Badawy et al. (2010) used polyvinylpyrrolidone (PVP) to stabilise Ag NPs which were stable with increasing ionic strengths to 0.1M NaCl. Goals et al. (2010) used polymers to coat Fe_3O_4 NPs; however, this was undertaken at very low ionic strengths of up to 10 mM NaCl. Therefore, the effect of ionic strength on the removal efficiency and zeta potential in the presence of stabiliser materials is expected to be negligible. The lack of the effect of ionic strength may also be attributed to weak competition between Hg(II) and Na ions for active sites. However, the presence of thiol groups on the adsorbent surface and since the adsorption efficiency remained reasonably

unaffected at 0.01 and 0.1 M $NaNO_3$ ionic strength, then this can be attributed to the strong selectivity of thiol groups for Hg(II) ions over monovalent anions.

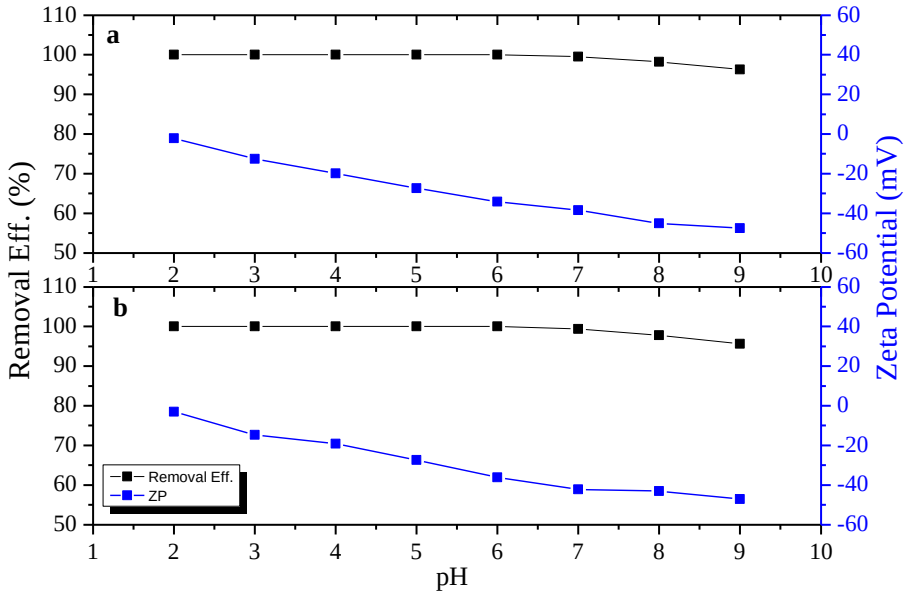

Figure 6.9: Effect of ionic strength of adsorption of Hg(II) ions by SH-SMNPS, (a) 80 µg L^{-1} Hg(II)+ 0.01M $NaNO_3$, and (b) 80 µg L^{-1} Hg(II)+ 0.1M $NaNO_3$.

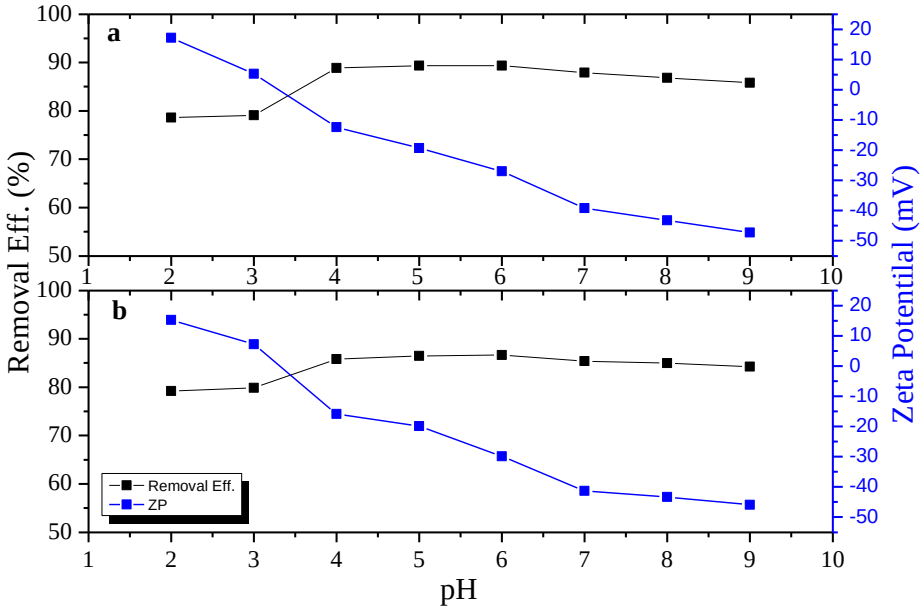

Figure 6.10: Effect of ionic strength of adsorption of Hg(II) ions by SH-SMNPS, (a) 1000 µg L^{-1} Hg(II)+ 0.01M $NaNO_3$, and (b) 1000 µg L^{-1} Hg (II)+ 0.1M $NaNO_3$.

6.4 Instrumentation Studies

6.4.1 XRD Study

XRD was used to characterise the surface of SH-SCMNPs after adsorption at pH 2.0 and 6.0. Figure 6.11 shows typical XRD peaks of a nanocrystaline matching with the results discussed in Chapter 4 and no other crystalline phase was detected. However, the XRD pattern does not show any Hg peaks either at pH 2.0 or 6.0. There are two possible reasons that might explain this observation. First, the initial concentration of Hg(II) ions used in the adsorption experiments was 200 μg L^{-1} and this small amount cannot be well defined in crystallinity, therefore leading to insufficient elastic scattering of the X-rays to give the characteristic peak. Secondly, the XRD patterns were obtained by step-scanning from 20˚ to 76˚ (2θ) for 2 hrs. Therefore, Hg could have been evaporated under high vacuum conditions. However, the result confirmed that the adsorption of Hg(II) onto SH-SCMNPs had no effect on the crystallinity of the SH-SCMNPs and they could be reused after eluent treatment without any change to the crystalline phase.

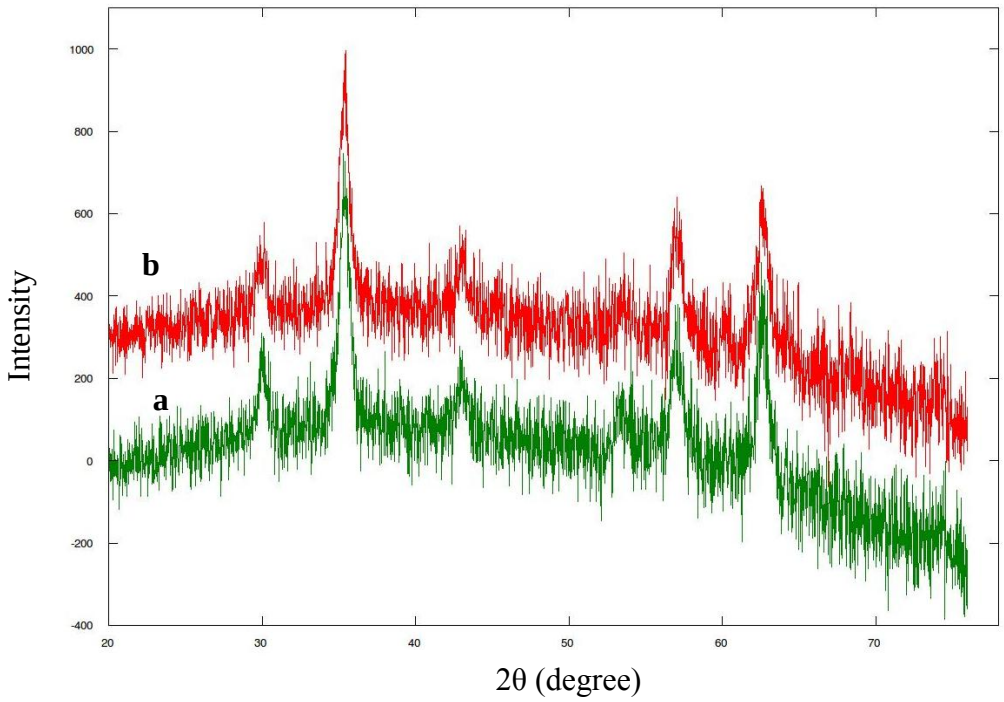

Figure 6.11: XRD pattern of SH-SCMNPs after Hg(II) adsorption, (a) at pH 2.0 and (b) at pH 6.0.

6.4.2 Raman Spectroscopic Study

Both Raman and FTIR spectra were collected from 200 μg L^{-1} of Hg(II) solution at pH values of 2.0, 4.0, 6.0 and 8.0. The Raman spectrum of SH-SCMNPs adsorbed with Hg(II) ions is shown in Figure 6.12. The observed Raman spectral frequencies are listed in Table 6.6 along with the suggested vibrational assignments. SH-SCMNPs free of Hg(II) ions exhibited a S-H stretch at 2512 cm^{-1} which was clearly observed and was discussed in Chapter 4. The absence of any bands at 510 cm^{-1} which are assigned to a S-S (disulphide formation) bond confirmed that no air oxidation had occurred during the modification process (Hoffmann et al., 2001). The appearance of broad bands at 380, 390 and 493 cm^{-1} revealed the presence of Fe_3O_4. The peak at 608 cm^{-1} can be attributed to the characteristics of maghemite (γ-Fe_3O_4) rather than magnetite (Fe_3O_4), and the laser heating appears to have converted the magnetite into maghemite (de Faria et al., 1997; Xi et al., 2008). The observed peaks at 1050, 1060 and 1270 cm^{-1} provide evidence of the presence of silica on the surface of Fe_3O_4, and these bands are assigned to Si-O stretching of the silanol group. The sharp band observed at 1670 cm^{-1} can be attributed to the stretching mode of siloxane (Si-O-Si). However, this band was not observed at pH 8.0 which confirmed the dissolution of Si in alkaline media. The absence of some groups of SH-SCMNPs might be attributed to the entrance of Hg(II) ions, forming metal complexes and resulting in a weakening, or even disappearance, of some related adsorption peaks (Li et al., 2009). A well-defined peak at 2850 cm^{-1} can be assigned to the C-H stretching of carbon, confirming the presence of organic groups attached to the surface of the silica. The stretching vibration of mercury thiolates (Hg-S) in solution occurs in the range 180-400 cm^{-1} and can be detected by Raman spectroscopy (Biscarini et al., 1984; Hoffmann et al., 2001). There are two factors which govern the position of the stretching vibration of mercury thiolate: the first factor is the coordination number of Hg to thiolate sulfur centres at a distance < 2.8 Å, while the second factor is the nature of the alkyl groups (Hoffmann et al., 2001). The strong Raman band at 710 cm^{-1} is assigned to the *v*(C=S) stretching mode formed by thioamides (Edwards et al., 1995). Additionally, this band is sensitive to the type of alkyl groups bonded to the sulfur atoms (Hoffmann et al., 2001). However, this peak did not appear in the IR spectra. The Hg-S and Hg-C bands observed using Raman spectroscopic studies are

summarised in Table 6.6. The Raman spectra (Figure 6.12a and b) showed bands at 180, 231, 280 and 297 cm^{-1}; these bands are attributed to the *v*(Hg-S) stretching vibration of mercury thiolates. These results are consistent with the work of Biscarini et al. (1984) who reported that these bands clearly indicate that the four observed bands should be assigned to the Hg-S stretching mode and do not involve the halogen atoms. However, the presence of the Hg-S stretching vibration suggests covalent bonding between Hg and S (Edwards et al., 1995). The absence of SH groups from the Raman spectra in Figure 6.12a and b which were observed before the adsorption of Hg(II) ions at 2512 cm^{-1}, confirm that all thiol groups in SH-SCMNPs remain connected to the Hg(II) species. The Raman band at 218 cm^{-1} is assigned to *v*(Hg-Cl), and this band is described as that of mercury-halogen groups (Biscarini et al., 1984). This band can also be used to confirm the presence of Hg(II) ions on the surface of SH-SCMNPs.

Table 6.6: Observed Raman spectral frequencies of SH-SCMNPs after Hg(II) ion sorption at pH 2.0, 4.0, 6.0 and 8.0.

pH 2.0	pH 4.0	pH 6.0	pH 8.0	Assignments description
180	231 and 297	231 and 297	280	Hg-S
-	218	218	218	Hg-Cl
380	390	390	-	Fe_3O_4
380	380	380	380	Fe_3O_4
493	493	493	-	Fe_3O_4
608	608	608	608	γ-Fe_3O_4
710	710	710	-	ν_s(C=S)
1050	1060	1270	1270	ν_s(Si-O-Si)
-	-	1670	-	Si-O
1790	1650 and 1800	-	-	CH_2
2850	2850	2850	2850	$\nu_s(CH_2)$

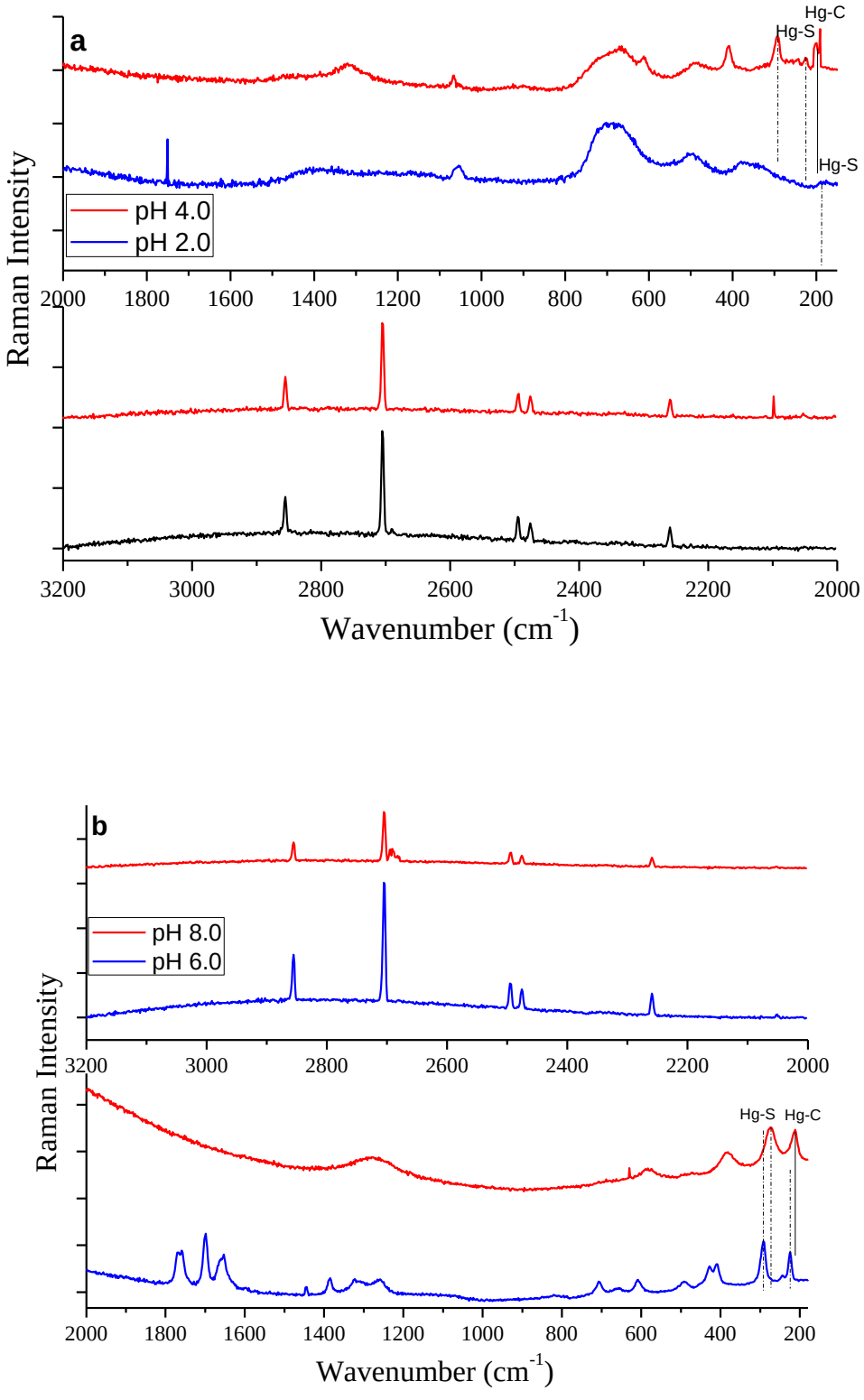

Figure 6.12: Raman spectra of SH-SCMNPs after adsorption at (a) pH 2.0 and 4.0, and (b) pH 6.0 and 8.0.

6.4.3 FTIR Spectroscopic Study

The FTIR technique was used to provide valuable information on the state of the adsorbed molecules, thereby shedding light on the adsorption mechanism. The FTIR spectra of the samples collected after Hg(II) adsorption onto SH-SCMNPs at pH 2.0, 4.0, 6.0 and 8.0 are shown in Figure 6.13. The observed IR spectral frequencies are listed in Table 6.7 along with the suggested vibrational assignments. The FTIR spectra of all the samples contained similar features for thiol-functionalised silica coated magnetite NPs as described in Chapter 4 (Section 4.2.6), such as a broad band at 675 attributed to the magnetite Fe_3O_4 in a consistent manner with that reported in Chapter 4 for FTIR of SH-SCMNPs before Hg(II) adsorption, the broad adsorption bands between 805-811 cm^{-1} belonging to the Si-O and the band at around 1083 cm^{-1} which can be attributed to the Si-O-Si stretching vibration. However, the presence of Si-O-Si stretching suggests that the thin silica film around Fe_3O_4 NPs remains unchanged after the adsorption process. This finding can be confirmed by the presence of Si after two cycles of the adsorption-desorption process as discussed in Chapter 5. The increase of the adsorption bands at around 1630 cm^{-1} is due to the deformation of Fe-O after adsorbing water molecules during the adsorption process. The bands at around 2883 and 2955 cm^{-1} are assigned to CH_3 and CH_2 vibrations respectively, and the peak between 3420- 3450 cm^{-1} is the O-H stretch vibration. All the samples with differing values of pH lost the SH band at 2509 cm^{-1} due to the SH being replaced with Hg(II). A new band appeared at 1384 cm^{-1} corresponding to the Cl-O stretching vibrations mode of $–Cl^-$. The presence of Cl^-, indicates that Cl^- ions were adsorbed onto the SH-SCMNPs together with Hg(II). The loss of –SH bands and the presence of Cl^- indicates that there is strong complexation of the adsorbed Hg (II) ions onto the surface of the SH-SCMNPs. A strong IR band in the region of 1350-1400 cm^{-1} often occurs in the presence of Cl^- (Silverstein et al., 2005). As previously described, Hg-S and Hg-C stretching complexes are located in the range 180 and 400 cm^{-1}, and the range scanned using this method was between 400-4000 cm^{-1}. Therefore, the surface thiolate ligands involved in the complexation of mercury were only evidenced by the absence of the SH band at ~ 2509 cm^{-1}.

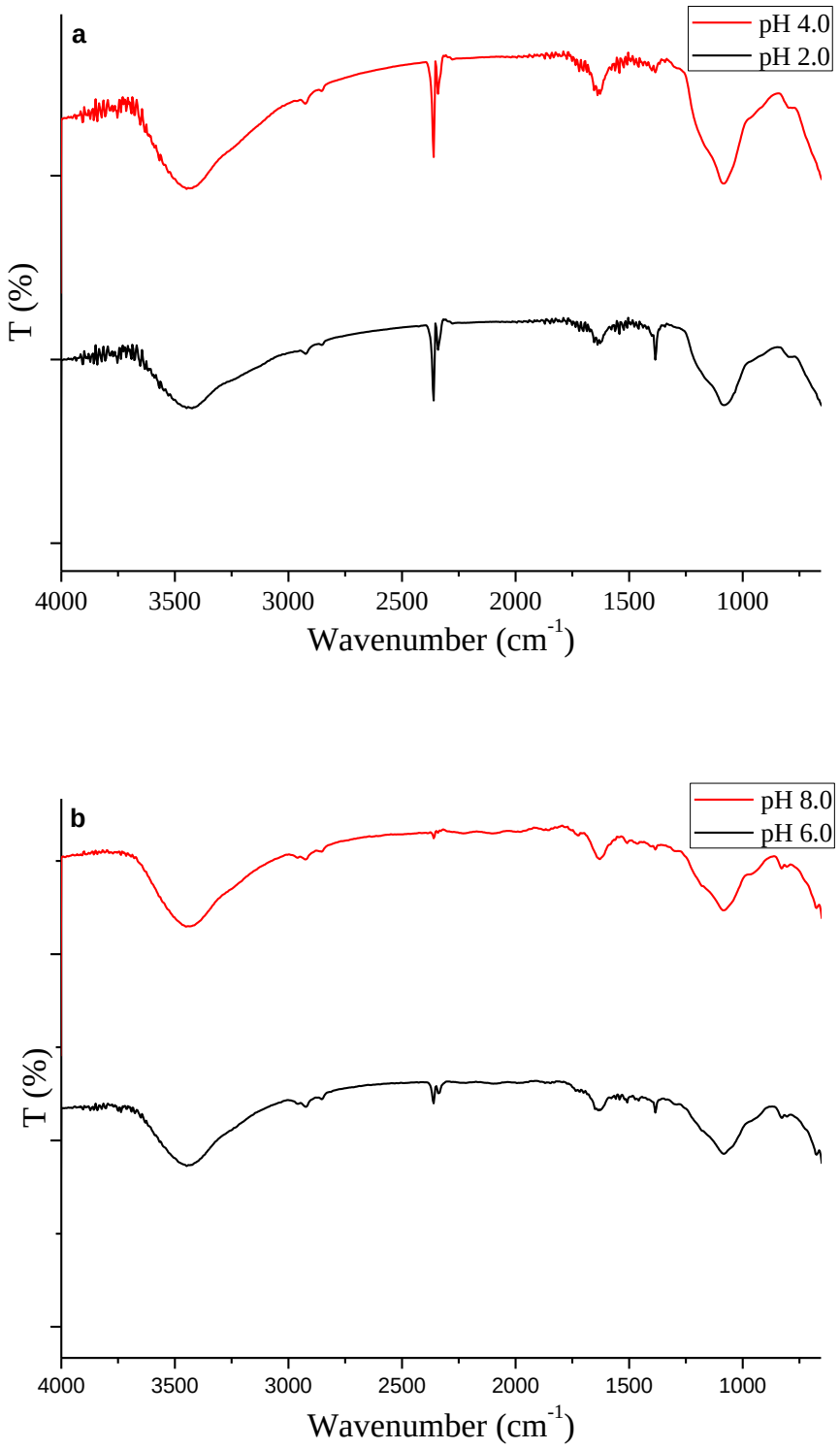

Figure 6.13: FTIR spectrum of Hg(II) loaded SH-SCMNPs, at (a) pH 2.0 and 4.0, and (b) pH 6.0 and 8.0.

Table 6.7: Observed IR spectral frequencies of SH-SCMNPs after Hg(II) sorption at pH 2.0, 4.0, 6.0 and 8.0.

pH 2.0	pH 4.0	pH 6.0	pH 8.0	Assignments description
-	-	675.02	675.23	Fe_3O_4
816.03	811.02	811.24	805.33	ν_s(Si-O)
1081.61	1084.02	1083.07	1084.74	ν_s(Si-O-Si)
1384.31	1384.67	1384.30	1384.35	ν_s(Cl-O)
1456.22	1459.31	1458.46	1463.49	ν_s(CH_2)
1626.88	1638.51	1635.69	1629.45	δ(Fe-O)
2854.01	2853.60	2853.55	2854.24	ν_s(CH_2)
2951.21	2952.69	2959.15	2959.87	ν_s(CH_3)
3424.37	3448.54	3424.37	3450.72	ν_s(OH)

vs= stretch, δ= deformation

Chapter 7

Semi-Continuous System for the Adsorption and Desorption of Hg(II) Ions

7.1 Introduction

As discussed in Chapter 5, the aim of the batch tests was to determine the optimum practical operating conditions for achieving the maximum Hg(II) adsorption from synthetic wastewater. SH-SCMNPs were also evaluated for the removal and recovery of Hg(II) ions from synthetic wastewater and they were found to be an effective adsorbent. In order for these findings to be implemented in industrial applications, all the operation conditions will be used to design a scaled-up semi-continuous system for the continual removal and recovery of Hg(II) ions from synthetic wastewater.

In this chapter, detailed designs for a scaled-up magnetic semi-continuous system will be given, followed by an investigation into the operating conditions to examine how a magnetic nano-sorbent can work in a semi-continuous system. The operating procedures, loss of adsorbents, adsorption and desorption of Hg(II) ions, retention time and interference effect on the adsorption of Hg(II) ions will all be investigated experimentally. It is expected that the results that will be obtained from the scaled-up system will not necessarily be as ideal as the batch test findings. However, the decrease in adsorption and desorption efficiency will be evaluated.

7.2 Apparatus Setup and Experimental Design

The semi-continuous system consisted of 40 litre feed tank (glass tank of 45 cm length and 30 cm width) fitted with teflon end caps, a NPs tank (2000 ml Borosilicate Erlenmeyer flask fitted with a rubber stopper with a hole), adsorption and desorption tanks (500 ml Borosilicate Erlenmeyer flasks), a treated water tank (5 litre glass container), PVC pipes and peristaltic pumps (Masterflex pump-7518-00 PSF/CRS).

The operating procedure, (Figure 7.1) for the whole process can be divided into five parts: 1) the synthetic Hg(II) or a cocktail solution of contaminated wastewater and a certain amount of SH-SCMNPs was charged into the adsorption tank using a peristaltic pump at the desired flow rate for the adsorption process; 2) The mixture then overflowed into the first magnetic separator and the SH-SCMNPs were separated from the treated water and deposited into the bottom of the separator unit using an external magnet field. The treated water was pumped into the treated water tank and the residual Hg from the effluent were determined using a PSA Millennium Merlin AFS; 3) the Hg-adsorbed SH-SCMNPs and 3.0 M HCl containing 2% thiourea (m/v) eluent were manually added into the desorption tank for the recovery of the Hg from the SH-SCMNPs; 4) the mixture then passed into the second magnetic separator tank for magnetic separation. The Hg recovered from the effluent was determined using a PSA Millennium Merlin AFS; 5) finally the regenerated SH-SCMNPs were placed in the NPs tank and then mixed with fresh wastewater from the feeding tank being pumped together into the adsorption unit for a further cycle. The operation parameters for the whole process are summarised in Table 7.1.

Table 7.1: Operational parameters for semi- continuous system.

Parameter	Wastewater - Feed tank	NPs- Feed tank
Flow rate (ml min^{-1})	3.2	1
Adsorbent Concentration (µg L^{-1})	-	3360*
Hg Concentration (µg L^{-1})	105**	-
Adsorbent density (g/cm^3)	-	2.25
Adsorbent particle size (nm)	-	~110

* The initial concentration of adsorbent used to study the effect of cations on the adsorption of Hg(II) ions was 10416 µg L^{-1} .
** The amount of the initial concentration of Hg(II) ions in the cocktail solution was 200 µg l^{-1} and other metals was 1000 µg L^{-1}.
- The pH value of synthetic Hg(II) contaminated wastewater was between 4.30 and 4.56 and was used without any adjustment.

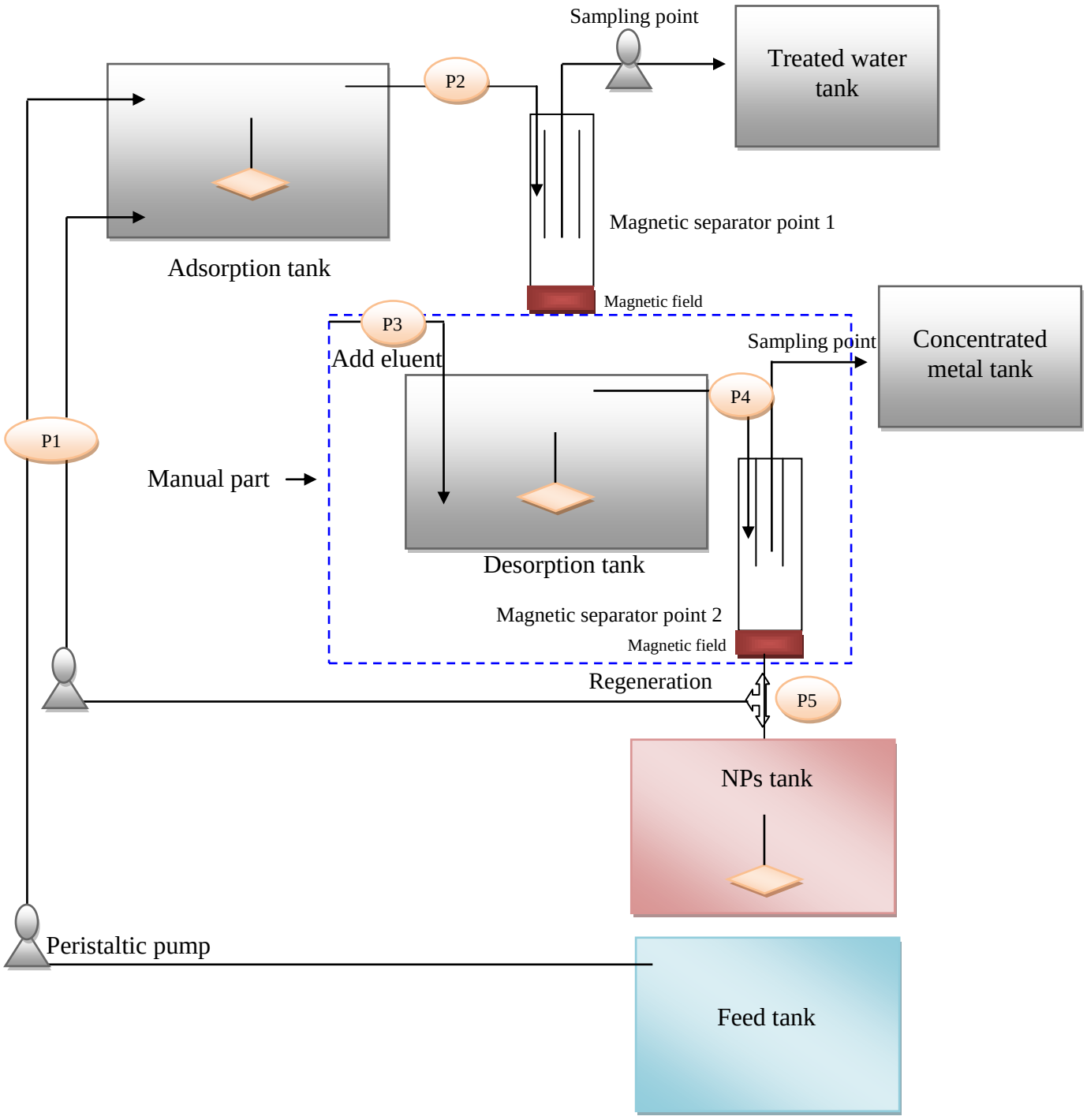

Figure 7.1: Schematic of the experimental set-up for the magnetic semi-continuous system.

7.3 Results and Discussion

7.3.1 Determination of Hg(II) Loss by Passive Adsorption or other Mechanisms

Control experiments were designed to show if any other factor other than the presence of SH-SCMNPs could be responsible for adsorption. Other potential factors that could lead to a reduction in concentration of adsorbate could be: precipitation, free metals attached to the feed and adsorption tanks, PVC pipes or present in the adsorbent. Five litres of a 105 µg L^{-1} Hg(II) solution at pH 6.0 were pumped into the adsorption and feed tank in the absence of SH-SCMNPs. The effluent from the system was checked for the concentration of Hg(II) ions over a period of 24 hrs and the results are shown in Figure 7.2. The loses of Hg(II) from the solution were 0.65%, an insignificant change indicating that the whole system can be used for the adsorption and desorption process without any significant loss of Hg(II) ions from the aqueous phase.

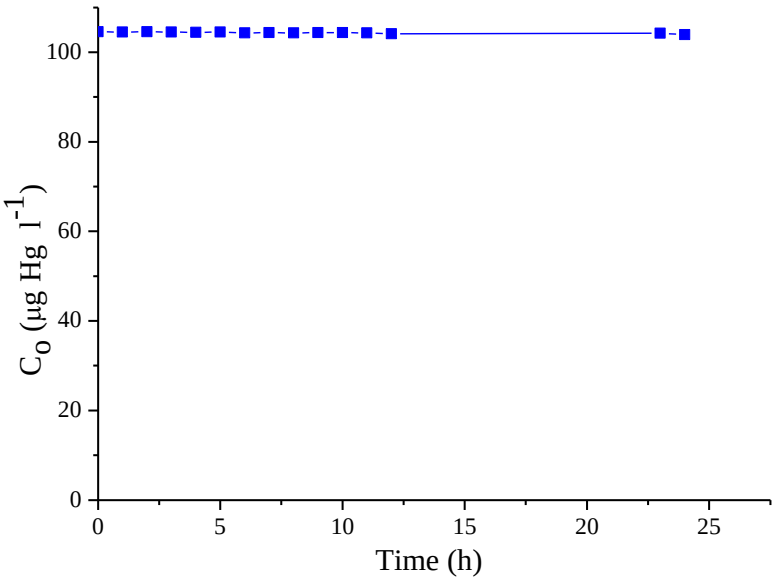

Figure 7.2: Control experiments of the semi-continuous system with a 105 µg L^{-1} Hg(II) solution at pH 6.0.

7.3.2 Determination of Optimal Retention Time

The optimal retention time was determined using different volumes of conical flasks (50, 100, 250 and 500 mL) as the adsorption tank. A flow of 4.2 mL min^{-1} was maintained

using two peristaltic pumps, one of which fed the Hg(II) solution at a rate of 3.2 mL min^{-1} from the feed tank and the second fed the NPs suspension at a rate of 1 mL min^{-1}. The mixture was then pumped from the adsorption into the separator tank. After separating the NPs using an external magnetic field, the final concentration of metal ions was determined using a PSA Millennium Merlin AFS. The control experiments were conducted in triplicates and the average values are presented in Figure 7.3. As discussed in Chapter 5, the rate of Hg(II) uptake using SH-SCMNPs had been found to be initially high, with about 90% of the Hg(II) ions being removed during the first 5 minutes and equilibrium being achieved within less than 15 minutes and 100% of the Hg(II) ions being adsorbed. However, in the semi-continuous system only 82.74% of the Hg(II) ions were removed at a retention time of 12 minutes and 88.27% at a retention time of 24 minutes. For the retention times of 60 and 120 minutes, 96.93 and 97.54% of the Hg(II) ions were removed respectively. Therefore, the retention time of 120 minutes was used in the later experiments.

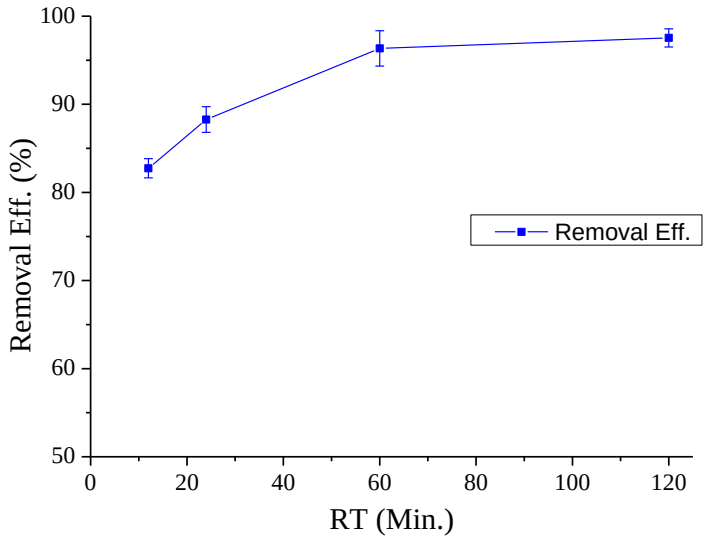

Figure 7.3: Optimal retention time in the control experiments with 105 µg L^{-1} Hg(II) solution.

7.3.3 System Testing

7.3.3.1 Adsorption and desorption of Hg(II) ions

The efficiency of the system using the operational parameters given in Table 7.1 was examined over eleven adsorption-desorption cycles. The results are given in Figure 7.4;

these show that 77 μg L^{-1} (97.53%) of the Hg(II) ions were adsorbed during the first cycle (2.5% less than obtained in batch tests), while the desorption efficiency was 92.52% (almost the same results as in the batch tests). A decrease of 10.8% of the sorption efficiency and 16.30% of the desorption efficiency was noted at the end of five cycles. These values are significantly higher than the ~ 5% loss in removal efficiency and 6.8% loss in desorption efficiency observed during the batch adsorption-desorption test.

In order to increase the adsorption and desorption efficiencies, 10.8% of a fresh SH-SCMNPs suspension was replaced at the end of 5^{th} cycle. As can be seen in Figure 7.4, 77 μg L^{-1} (96.81%) of Hg was adsorbed in the sixth cycle and the desorption efficiency increased to 87.67%. The same process was repeated at the end of the tenth cycle and this enhanced both the adsorption and desorption efficiencies. It was also noticed that the loss in efficiency (12.96%) was proportionally greater in the fifth cycle than during the previous 4 cycles. This was also the case for the ninth and tenth cycles compared to the sixth-eighth cycles. The reasons for the reduction in the capacity of the SH-SCMNPs and their desorption efficiency have been discussed in detail in Chapter 5 and are primarily due to the limited number of active sites which bind Hg(II) much more strongly onto SH-SCMNPs so that the 3.0 M HCl containing 2% (m/v) thiourea could not elute the Hg from them. The damaged physico-chemical structure of the SH-SCMNPs is also likely to have caused a decrease in the adsorption-desorption efficiency. All the previous studies have cited the weight loss of the biosorbent as the main reason for the decrease in the biosorbtion-desorption efficiency. For example, Puranik and Paknikar (1997) reported a reduced Cd biosorbtion efficiency which resulted in the loss of biomass during the filtration process. Other researchers have not given a direct reason for the loss of weight of the biomass (Yakup Arica et al., 2004; Kacar et al., 2002). The use of 3.0 M HCl containing 2% (m/v) thiourea as the desorbing agent has no effect on the dissolution of Fe and Si as shown in Figure 7.5.

From the results presented, it is clear that even a good adsorbent material can show a reduction in efficiency over repeated adsorption–desorption cycles. The partial replacement of adsorbent with new material was shown to be a good solution in overcoming this drawback.

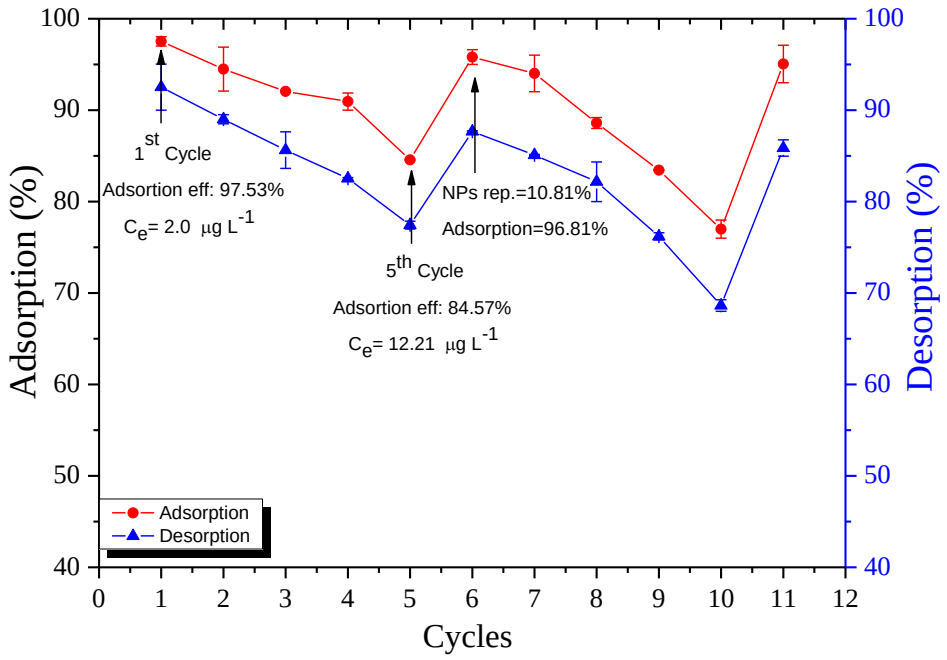

Figure 7.4: Percentage of Hg(II) ions adsorbed and desorbed during 11 adsorption-desorption cycles at an initial concentration of 80 µg L^{-1} using the semi-continuous system.

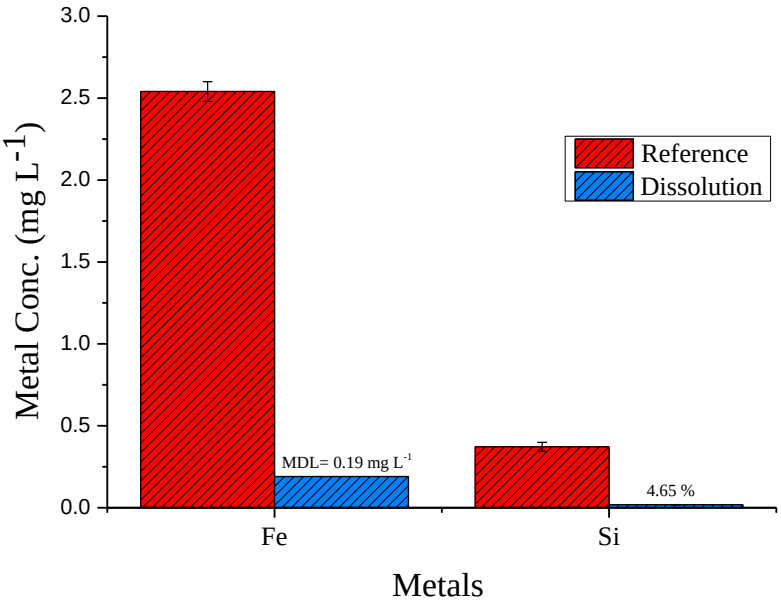

Figure 7.5: Dissolved Fe and Si during the elution process.

As discussed in Chapter 4, the coating of the Fe_3O_4 NPs with silica and ligand molecules provides enhanced stability due to combined electrostatic stabilisation. It was also noticed that aggregation of the SH-SCMNPs takes place at pH 2.0 and 3.0. Taking into account the practical application, the hydrodynamic diameters of SH-SCMNPs which were used over eleven cycles of adsorption-desorption in the semi-continuous system, were measured. However, the particles did not show any aggregation and remained suspended in the adsorption tank. It can be seen from Figure 7.6 that the average hydrodynamic size of the SH-SCMNPs was ~ 145 nm (increased by 31.53%) after intensive use in the adsorption-desorption process over eleven cycles. However, the aggregation of SH-SCMNPs did not have any effect on the magnetisation properties and SH-SCMNPs were quickly deposited at the bottom of the separator when an external magnetic field was applied. The saturation magnetisation was also measured and gave approximately 0.22 emu, Figure 7.7, typical of the results obtained before when using SH-SCMNPs for the adsorption-desorption process in the semi-continuous system. Therefore, the semi-continuous system with two magnetic separator points and an elution process had no effect on the magnetic properties of the SH-SCMNPs.

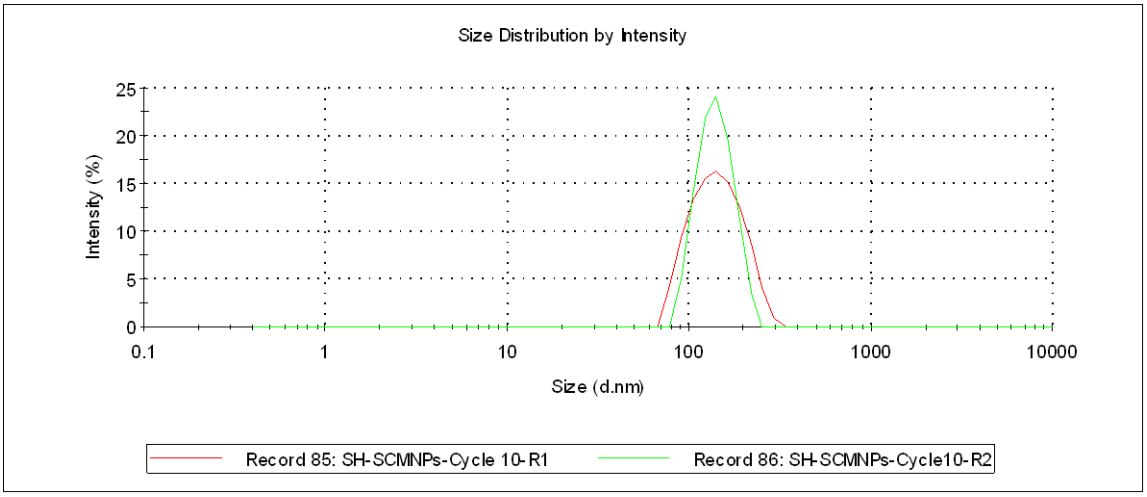

Figure 7.6: DLS plot for the particle size distribution after being used for eleven adsorption-desorption cycles.

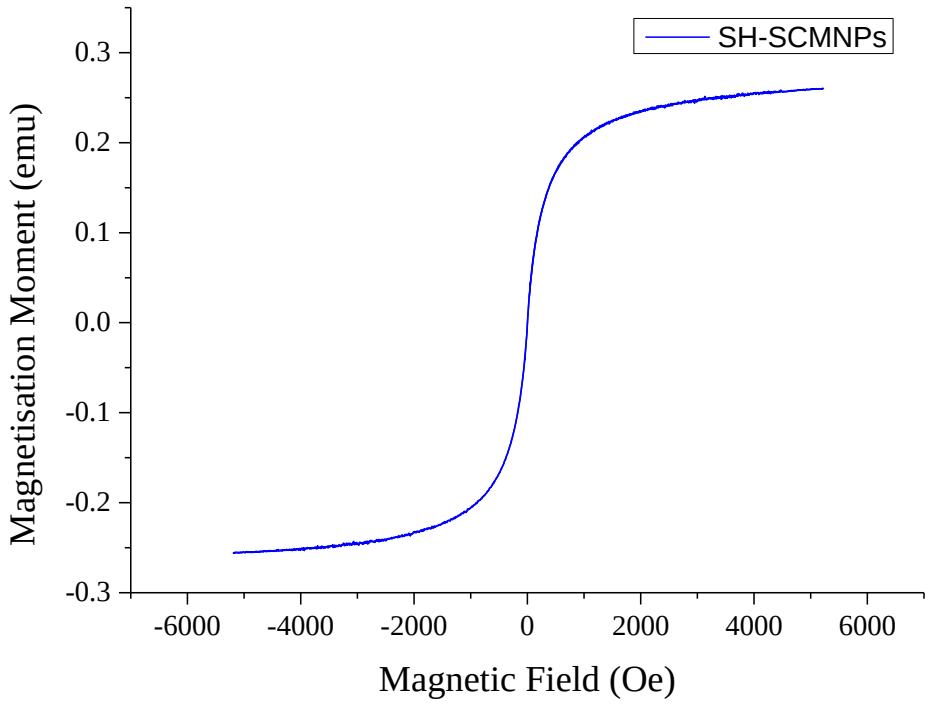

Figure 7.7: Room temperature magnetisation measurements of SH-SCMNPs after being used for eleven adsorption-desorption cycles.

7.3.3.2 Adsorption of Hg(II) ions in a semi continuous system competition with other cations

In order to determine if there was interference in the adsorption of Hg(II) caused by the presence of other cations, a solution was prepared by mixing 200 μg L^{-1} of Hg(II) with each of Pb(II), Cu(II) and Ni(II) at a ratio of 1:5. The aim was to provide sufficient metals in the solution to saturate the available binding sites which could affect the adsorption of Hg(II) ions. According to the theory of Pearson, Pb(II) is classified as a soft Lewis acid while Cu(II) and Zn(II) are borderline Lewis acids and therefore the presence of these metals might cause an effect on the adsorption of Hg(II) ions. The presence of these metals had no significant effect on the adsorption of Hg(II) ions by SH-SCMNPs in the semi-continuous system, as shown in Figure 7.8. Although the concentration of other metals in the solution were more than five times that of Hg(II), there were no effects on the adsorption of Hg(II), particularly in the first two cycles with

adsorption efficiencies of 94.85 and 92.53%, respectively. A decline of 16.90% in the adsorption efficiency and 17.04 % in the desorption efficiency were observed at the end of the fifth cycle. Following the addition of fresh nano-sorbents, the percentage adsorption and desorption of Hg(II) ions progressively increased to 91.65 and 86.52%, respectively.

The cations Ni, Cu and Pb in particular are present in high concentrations in industrial wastewater (EPA, 1990), and the findings point to a significant advantage in favour of SH-SCMNPs for the removal of Hg ions. It is likely that this type of system could be used in an industrial wastewater treatment plant instead of the conventional methods applied for the adsorption of Hg ions, but further tests would be necessary to confirm this.

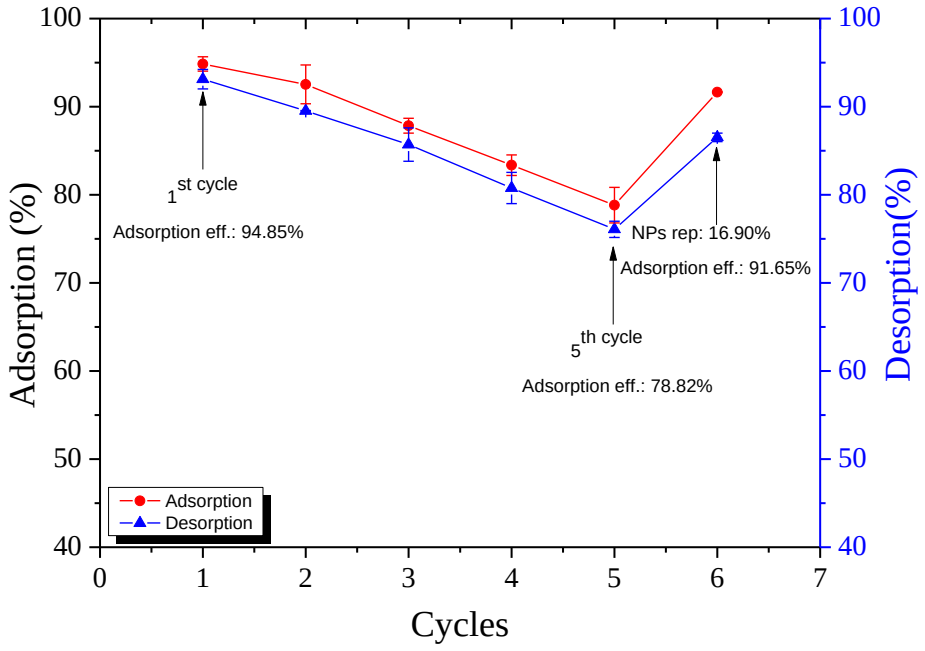

Figure 7.8: Percentage of Hg ions adsorbed and desorbed during five adsorption-desorption cycles in the presence of other cations using the semi-continuous system.

7.3.3.3 Adsorption of Hg in a semi continuous system in competition with selected anions

Interference effects from the anions F^-, Cl^-, SO_4^{2-}, PO_4^{3-} were tested using binary solutions containing 200 μg L^{-1} of Hg(II) mixed with 100 mg L^{-1} of the various anions. The semi-continuous system was operated according to the procedure described earlier. The results are shown in Figure 7.9, where it can be seen that the adsorption was inhibited in the following order: $Cl^- < SO_4^{2-} < PO_4^{3-} < F^-$, depending on the coordination ability of the different anions. The presence of Cl^- had little influence and the corresponding removal efficiency was 95.50%, which is almost the same as the results obtained (97.23%) in the absence of any anions. The influence of SO_4^{2-} was also very small and decreased the removal efficiency to 90.69%. The adsorption efficiency of Hg(II) ions in the presence of PO_4^{3-} and F^- was 85.07% and 84.76% respectively. The reasons for the decrease in Hg(II) uptake in the presence of PO_4^{3-} and F^- was discussed previously in Chapter 5. It can be concluded that the semi-continuous system was successful for the removal of Hg(II) ions by SH-SCMNPs under the selected conditions.

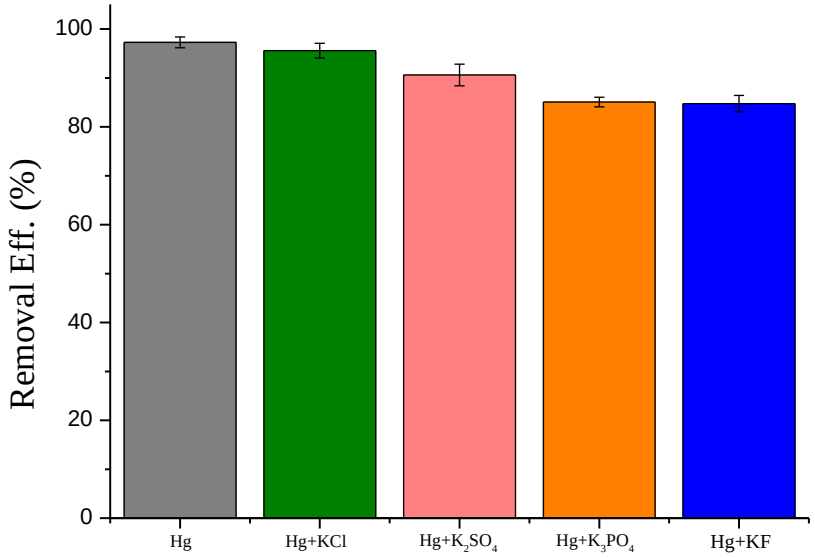

Figure 7.9: Adsorption of Hg(II) ions in the presence of other anions using the semi-continuous system.

Conclusions and Future Work

8.1 Conclusions

The main aim of this study was to evaluate the effectiveness of Fe_3O_4NPs, SCMNPs, and SH-SCMNPs for the removal and recovery of Hg(II) from synthetic wastewater. The project was divided into three parts. The first part focused on the preparation methods of these adsorbents coupled with an intensive study of their physical-chemical properties (particle size, shape, magnetic properties, surface area, and surface chemistries) using advanced analytical methods. The second part of the study examined the SH-SCMNPs as a potential adsorbent for Hg(II) adsorption from water compared with Fe_3O_4 NPs and SCMNPs in terms of kinetics and capacities. The reusability of SH-SCMNPs and the behaviour and mechanisms of Hg(II) sorption on SH-SCMNPs were examined. Finally, adsorption and desorption experiments were run in a semi-continuous system. This chapter will summarise the most important results presented in this thesis.

8.1.1 Synthesis and Characterisation

The magnetite (Fe_3O_4 NPs) was prepared via conventional co-precipitation methods. Mesoporous silica coatings were created on dense liquid-silica coated magnetite NPs (DLSC-Fe_3O_4 NPs) using cetyl-trimethyl-ammonium chloride (CTAC) as molecular templates followed by a sol-gel reaction. SCMNPs were functionalised with 3-MPTMS using the co-condensation method. Functionalisation of SCMNPs with this specific organic group was performed to enhance the selectivity of the magnetic NPs towards Hg(II). The NPs obtained via the co-precipitation methods were not monodispersed in size: their shape was spherical and approximately 75 nm in diameter. Through the co-condensation method, the obtained NPs were capped with nonpolar endgroups (thiol) on their surface that were approximately 111 nm in diameter, spherical in shape, and narrow in their distribution. The purity of the samples was characterised initially by

PXRD and the results confirmed that PXRD peaks of the nanocrystaline of Fe_3O_4 NPs matched well with standard Fe_3O_4. No other crystalline phases were detected.

In this study, to avoid possible aggregation occurring, Fe_3O_4 NPs were coated with silica and functionalised further with thiol organic groups. These methods impart excellent stability to magnetite NPs in an aqueous medium over a wide range of pH values with reasonable hydrodynamic size. The organic group bound magnetite NPs allowed these particles to circulate over a long time in aqueous system, and particle aggregation and sedimentation did not occur. The trend of decreasing zeta potential was observed after thiol grafted onto the surface of SCMNPs.

The SEM images showed that Fe_3O_4 NPs are nearly spherical and that particles appear to be aggregated. This is due to the absence of any stabiliser in the reaction system during the course of the Fe_3O_4 NP formation. The aggregation was minimised after using the CTAC aqueous solution as a surfactant stabiliser during the preparation process of mesoporous SCMNPs. EDX confirmed the presence of Si on the surface of Fe_3O_4 NPs; S was also determined by EDX, indicating that the functionalisation with 3-MPTMS was successful. Both FTIR and Raman spectroscopic studies also confirmed that the thiol groups were attached to the silica support.

In the present study, prepared magnetite NPs were evaluated for their use in the separation of NPs from the solution after the adsorption process. Fe_3O_4 NPs showed a relatively large magnetic moment of the NPs, which indicates that Fe_3O_4 NPs can be used effectively in adsorption applications. However, the decrease in the saturation magnetisation after coating Fe_3O_4 NPs with silica and modification with thiol groups did not affect their magnetic properties, and they could respond quickly to an external magnetic field. In addition, when the external magnetic field was removed, they could be re-dispersed without any significant aggregation.

8.1.2 Adsorption and Desorption of Hg(II)

Magnetite NPs are an alternative adsorbent for removing Hg(II) from water. These NPs have many favourable features that play a key role in the removal of Hg. For instance, a

high specific surface area results in a high number of silanol groups, which are found primarily on the surface of the SCMNPs and enable a high loading capacity. The magnetite NPs demonstrate strong magnetisation, allowing easy separation from a complex multiphase system, and the reactive site mesoporous structure functionalised with the thiol groups is tailored for Hg adsorption; all these unique properties make them ideal adsorbents over conventional adsorbents. Most research prior to this study had concentrated on uncovered magnetite NPs for the removal of organic constituents or heavy metals from water and wastewater. Most of these previous studies focused on the adsorption process for the removal of heavy metals from contaminated water, and limited research exists on factors leading to a decrease of adsorption, such as dissolution, types of eluents, and the effect of pH on these ideal sorbents. This research evaluated the potential of prepared NPs (Fe_3O_4 NPs, SCMNPs. and SH-SCMNPs) for Hg removal and recovery from synthetic wastewater. This work also looked at several parameters effecting Hg(II) adsorption onto these NPs, such as NPs concentration, ions commonly found in water, and environmental conditions, such as pH; other conditions, such as contact time, shaking speed, and temperature, were also examined. Research results have contributed to the development of good adsorbents for the removal and recovery of Hg from wastewater.

Results showed that the covalent binding between the –SH groups of SH-SCMPs and Hg provide high affinity for Hg adsorption in that 4 mg L^{-1} SH-SCMNPs are capable of reducing the initial concentration of 80 μg L^{-1} to below the WHO drinking water limit of 2 μg L^{-1}. SH-SCMNPS were also evaluated for their usefulness in removing Hg(II) in the presence of binary, multiple metals in solution. The results confirmed that SH-SCMNPs were highly efficiency in removing Hg from solutions in the present of other metals. The inner-sphere complex-forming PO_4^{3-} and F^- competed strongly with Hg(II) for adsorption sites, whereas other anions did not compete effectively due to weak adsorption via outer-sphere complexation.

The high surface area on SH-SCMNPs and the high affinity of its functional groups for Hg result in fast-binding kinetics. Conversely, a slower removal of Hg was observed when used Fe_3O_4 NPs was used.

An intensive study was carried for the desorption of Hg(II) from SH-SCMNPs and the results showed that Hg(II) ions adsorbed on SH-SCMNPs could be desorbed effectively using 3 M HCl containing 2 % (m/v) thiourea. This shows that the SH-SCMNPs could be regenerated and maintained at almost the same Hg(II) adsorption capacity. Further analysis was carried out using TEM to evaluate the effect of the desorption processes in decreasing the capacity of adsorption. The TEM and dissolution studies confirmed that (a) aggregation, (b) reduction in the porous structure, and (c) dissolution of the NPs along with the strong Hg-S covalent bond could play a key role in decreasing adsorption and desorption performance during five adsorption/desorption cycles. However, desorption and regeneration studies demonstrated that SCMNPs and SH-SCMNPs could be recovered efficiently for re-adsorption of the Hg ions and that Hg could be highly concentred and possibly considered for recycling.

In the present work, in order to enhance the adsorption of Hg(II) and inhibit the dissolution of Fe_3O_4 NPs, two ways for dissolution prevention involving dense liquid silica coated magnetite NPs (DLSC-Fe_3O_4 NPs) and silica coating Fe_3O_4 NPs via sol-gel reaction were developed. The increased efficiency of the silica in eliminating the pH dependence and enhancing the NP stability of SCMNPs and SH-SCMNPs in aqueous medium is noteworthy. On the other hand, the dissolution of Fe_3O_4 NPs was to found to be detrimental at pH 2.0 or had a long contact time.

8.1.3 Mechanism of Adsorption

The adsorption capacity of Fe_3O_4 NPs, SCMNPs, and SH-SCMNPs was found to be 42.3, 48.4, and 113.7 mg g^{-1}, respectively when 8 mg L^{-1} of different adsorbents was used. The loading capacity of the SH-SCMNPs was found to be 207.7 mg g^{-1} when applied at a concentration of 4 mg L^{-1}. The data of Hg(II) adsorption was modelled with the Langmuir and Freundlich isotherms. The Langmuir isotherm did not correlate well with the adsorption data of Fe_3O_4 NPs and SCMNPs; the Freundlich isotherm is the correct equation to use to express the Hg uptake onto the three types of NPs. Therefore, the adsorption mechanism for Hg(II) using SH-SCMNPs may involve not only the Hg chelation by SH complexing functions, but also the surface complexation by OH or Si-OH sites located on the Fe_3O_4 NPs.

The removal efficiency was highly pH dependant, and the optimal adsorption for Fe_3O_4 NPs and SCMNPs occurred at pH 5.0 and 6.0, respectively. The effect of pH on the adsorption of Hg(II) using SH-SCMNPs was highly dependent on the initial concentration of Hg(II).

In the present work, zeta potential measurements were carried out to interpret the adsorption mechanism. It was proposed that the adsorption of Hg(II) using Fe_3O_4NPs is due to the electrostatic attraction and ion exchange between Hg(II) and H^+ ions at pH values lower than the pH_{pzc}. On the other hand, the adsorption of Hg(II) using SCMNPs was controlled predominantly by the electrostatic attraction and the change of physico-chemical properties of the hydroxyl groups at different pH values. The increase of surface area after coating the NPs with Si could be also responsible for the higher adsorption of Hg(II) ions onto SCMNPs. This could be attributed to a stabiliser covering the surface of the Fe_3O_4 NPs. The Hg-binding mechanism for representative SH-SCMNPs was investigated by zeta potential measurements, FTIR, and Raman spectroscopy. According to the hard and soft acids and bases theory and the information analysed instrumentation methods, the adsorption mechanism of Hg(II) using SH-SCMNPs could be explained as a primary chemical adsorption and a secondary physical adsorption. The Raman results confirmed that the complexation of Hg centres by thiolate depends on the pH value. It was also noted that increasing the ionic strength did not show any effect on the adsorption of Hg(II) using SH-SCMNPs.

8.1.4 Semi-Continuous System Study

A magnetic semi-continuous system was carried out for the adsorption and desorption of Hg(II) and good results were obtained.

The presence of other cations in the solution other than Hg did not affect Hg adsorption in the first cycle. The adsorption efficiency deceased gradually in later adsorption cycles; therefore, fresh SH-SCMNPs suspensions were replaced after five adsorption/desorption cycles to increase the adsorption and desorption efficiencies in later cycles. Several anions found commonly in water were tested to determine their effect on Hg adsorption onto SH-SCMNPs. Among the anions tested, PO_4^{3-} and F^- had the largest effect on Hg adsorption. Regeneration experiments were performed using a

magnetic semi-continuous system, and Hg was eluted successfully with 3.0 M HCl containing 2% (m/v) thiourea. The results obtained using the semi-continuous system confirmed that this type of system could be used in an industrial wastewater treatment plant instead of the conventional methods applied for the adsorption of Hg ions, but further tests would be necessary to confirm this.

8.2 Future work

8.2.1 Adsorption Isotherm and X-ray Photoelectron Spectroscopy (XPS) Study

There are plenty of interests and scope for further work on adsorption isotherms to distinguish the correct isotherm. Although previous studies suggest that the Hg(II) adsorption isotherm of thiol-functionalised mesoporous silica adsorbents usually exhibits typical Langmuir behaviour, which are the characteristics of chemical adsorption, the results in this thesis show different uptakes of the Hg(II) by SH-SCMNPs and evidence of difference mechanisms. Therefore, the adsorption isotherm could be extended using a high initial concentration of Hg at different temperatures and different pH values. This study should be coupled with XPS measurements to study the elemental composition of a chemical oxidation state at the surface of SH-SCMNPs after adsorption.

8.2.2 Different Cycles of Elution

The desorption study showed that the recovery of Hg could be achieved gradually by increasing the molarity of HCl acid. In the same manner, the removal efficiency could be achieved in the later cycles of desorption using fresh elution. Therefore, further studies on this point should be performed to test how fresh elution could enhance the recovery of Hg.

8.2.3 Preparation of Dual and Multi Functional Groups on the Surface of Mesoporous SCMNPs

In this study, thiol-functionalised mesoporous silica coated magnetite nanoparticles were successfully prepared and used as an adsorbent for Hg(II). The experimental results

showed that this nano-sorbent have high adsorption efficiency in either batch tests or a semi-continuous system. Heavy metals are generally classified as soft or borderline acids according to HSAB principle of Pearson. It is obvious that the adsorption of heavy metals from aqueous phase onto a solid adsorbent relies on the affinity of the metal to the extracting group. Therefore, dual or multi functional groups could be used to enhance the selectivity of SCMNPs towards the target metal ions. This should be further investigated

8.2.4 Magnetic Continuous System for Adsorption and Desorption of Hg(II)

The results obtained from semi-continuous system (Chapter 7) confirmed that SH-SCMNPs could be used effectively for the removal and recovery of Hg(II) from an aqueous phase. The design of a larger scale continuous system for the adsorption and desorption of Hg(II) from wastewater with magnetic recovery of the nanoparticles was not possible. This should now be attempted and at a scale which will allow further design data to be derived, as any development of this system should go hand in hand with engineering considerations.

8.2.5 Application of SH-SCMNPs for Real Wastewater Treatment

The assessment of the application of SH-SCMNPs for the removal of Hg(II) from different water types , including wastewater, is necessary if the scope of the technology is to be fully assessed.

Most natural waters, and even more so, wastewater have complex properties. The effect that the water chemistry, including the presence of organic material that can interact with Hg ions by various reactions, needs to be more fully assessed than the present study has permitted. Other factors are: the high concentration and ionic strength of heavily contaminated or saline waters that may have a significant on the adsorbent as well as the adsorbate; different pH values, either acidic (pH 2.0) or alkaline (pH 13.0) which might lead to dissolve Fe and Si.

8.2.6 Removal of Pb(II) Using SH-SCMNPs

The experimental results showed that SH-SCMNPs have high adsorption efficiency for the removal of Pb(II) even in the presence of Hg(II). Most of the current research

focused on the adsorption of Hg(II) onto the thiol functionalised nano-materials. Future research could also pay more attention towards the use of SH-SCMNPs as an ideal sorbent for the removal and recovery of Pb(II). In doing this it will also be necessary to explore the behaviour and mechanism of Pb(II) adsorption on SH-SCMNPs.

References

ADEBAJO, M. O., FROST, R. L., KLOPROGGE, J. T., CARMODY, O. & KOKOT, S. 2003. Porous materials for oil spill cleanup: a review of synthesis and absorbing properties. *Journal of Porous Materials,* 10**,** 159-170.

ADENIJI, A., WASTE, U. S. E. P. A. O. O. S., RESPONSE, E. & OFFICE, U. S. E. P. A. T. I. 2004. *Bioremediation of arsenic, chromium, lead, and mercury,* US Environmental Protection Agency.

AGUADO, J., ARSUAGA, J. & ARENCIBIA, A. 2005. Adsorption of aqueous mercury (II) on propylthiol-functionalized mesoporous silica obtained by cocondensation. *Industrial & Engineering Chemistry Research,* 44**,** 3665-3671.

AGUADO, J., ARSUAGA, J. M. & ARENCIBIA, A. 2008. Influence of synthesis conditions on mercury adsorption capacity of propylthiol functionalized SBA-15 obtained by co-condensation. *Microporous and Mesoporous Materials,* 109**,** 513-524.

AGUADO, J., ARSUAGA, J. M., ARENCIBIA, A., LINDO, M. & GASCON, V. 2009. Aqueous heavy metals removal by adsorption on amine-functionalized mesoporous silica. *Journal of Hazardous Materials,* 163**,** 213-221.

ALBRIGHT, L. F. 2008. *Albright's chemical engineering handbook*, CRC.

ÁLVAREZ, P. M., JARAMILLO, J., LÓPEZ-PIÑERO, F. & PLUCINSKI, P. K. 2010. Preparation and characterization of magnetic TiO_2 nanoparticles and their utilization for the degradation of emerging pollutants in water. *Applied Catalysis B: Environmental,* 100**,** 338-345.

AMUDA, O. S., ADELOWO, F. E. & OLOGUNDE, M. O. 2009. Kinetics and equilibrium studies of adsorption of chromium(VI) ion from industrial wastewater using Chrysophyllum albidum (Sapotaceae) seed shells. *Colloids and Surfaces B: Biointerfaces*, 68**,** 184-192.

ANIRUDHAN, T., SUCHITHRA, P. & DIVYA, L. 2009. Adsorptive potential of 2-mercaptobenzimidazole-immobilized organophilic hydrotalcite for mercury (II) ions from aqueous phase and Its kinetic and equilibrium profiles. *Water, Air, & Soil Pollution,* 196**,** 127-139.

ANTOCHSHUK, V., OLKHOVYK, O., JARONIEC, M., PARK, I. S. & RYOO, R. 2003. Benzoylthiourea-modified mesoporous silica for mercury (II) removal. *Langmuir,* 19**,** 3031-3034.

ASAHI, R., MORIKAWA, T., OHWAKI, T., AOKI, K. & TAGA, Y. 2001. Visible-light photocatalysis in nitrogen-doped titanium oxides. *Science,* 293**,** 269.

ASTM 2006. Designation: E2456-06 standard terminology relating to nanotechnology.

ATWOOD, D. A. (ed.) 2006. *Recent Developments in Mercury Science*, New Yourk: SPringer.

AWWA 2005. Factsheet: Membrane Filtration. American Water Works Association.

BABEL, S. & KURNIAWAN, T. 2003. Low-cost adsorbents for heavy metals uptake from contaminated water: a review. *Journal of Hazardous Materials,* 97**,** 219-243.

BADAWY, A. M. E., LUXTON, T. P., SILVA, R. G., SCHECKEL, K. G., SUIDAN, M. T. & TOLAYMAT, T. M. 2010. Impact of environmental conditions (pH, ionic strength, and electrolyte type) on the surface charge and aggregation of

silver nanoparticles suspensions. *Environmental Science & Technology,* 44**,** 1260-1266.

BAES, A., OKUDA, T., NISHIJIMA, W., SHOTO, E. & OKADA, M. 1997. Adsorption and ion exchange of some groundwater anion contaminants in an amine modified coconut coir. *Water Science & Technology.,* 35.

BAILEY, S. E., OLIN, T. J., BRICKA, R. M. & ADRIAN, D. D. 1999. A review of potentially low-cost sorbents for heavy metals. *Water Research,* 33**,** 2469-2479.

BAKER, C., ISMAT SHAH, S., HASANAIN, S., ALI, B., SHAH, L., LI, G., EKIERT, T. & UNRUH, K. Year. Inert Gas Condensation of Iron and Iron-Oxide Nanoparticles. *In*, 2008. Cambridge Univ Press.

BARRETT, E. P., JOYNER, L. G. & HALENDA, P. P. 1951. The determination of pore volume and area distributions in porous substances. I. Computations from nitrogen isotherms. *Journal of the American Chemical Society,* 73**,** 373-380.

BAYRAMOĞLU, G. & ARICA, M. Y. 2007. Kinetics of mercury ions removal from synthetic aqueous solutions using by novel magnetic p(GMA-MMA-EGDMA) beads. *Journal of Hazardous Materials,* 144**,** 449-457.

BECK, J., VARTULI, J., ROTH, W., LEONOWICZ, M., KRESGE, C., SCHMITT, K., CHU, C., OLSON, D. & SHEPPARD, E. 1992. A new family of mesoporous molecular sieves prepared with liquid crystal templates. *Journal of the American Chemical Society,* 114**,** 10834-10843.

BESSBOUSSE, H., RHLALOU, T., VERCHÈRE, J.-F. O. & LEBRUN, L. 2009. Novel metal-complexing membrane containing poly(4-vinylpyridine) for removal of Hg(II) from aqueous solution. *The Journal of Physical Chemistry B,* 113**,** 8588-8598.

BESSBOUSSE, H., RHLALOU, T., VERCHÈRE, J. F. & LEBRUN, L. 2008. Sorption and filtration of Hg(II) ions from aqueous solutions with a membrane containing poly(ethyleneimine) as a complexing polymer. *Journal of Membrane Science,* 325**,** 997-1006.

BIBBY, A. & MERCIER, L. 2002. Mercury (II) ion adsorption behavior in thiol-functionalized mesoporous silica microspheres. *Chem. Mater,* 14**,** 1591-1597.

BILLINGE, S., MCKIMMY, E., SHATNAWI, M., KIM, H., PETKOV, V., WERMEILLE, D. & PINNAVAIA, T. 1997. Mercury binding sites in thiol-functionalized mesostructured silica. *Science (Washington, DC),* 276**,** 923-926.

BISCARINI, P., FORESTI, E. & PRADELLA, G. 1984. Organothiometallic compounds. Crystal structure and spectroscopic properties of (isopropylthio) mercury (II) chloride. *J. Chem. Soc., Dalton Trans.***,** 953-957.

BITTNER, A., ECHEVERRIA, D., WOODS, J., APOSHIAN, H., NALEWAY, C., MARTIN, M., MAHURIN, R., HEYER, N. & CIANCIOLA, M. 1998. Behavioral Effects of Low-Level Exposure to Hg^0 among dental professionals a cross-study evaluation of psychomotor effects. *Neurotoxicology and teratology,* 20**,** 429-439.

BLACK & CORPORATION, V. 2010. *Chlorine: History, Manufacture, Properties, Hazards, and Uses*, NJ, John Wiley & Sons, Inc.

BRANT, J., LABILLE, J., BOTTERO, J. Y. & WIESNER, M. R. 2007. Nanoparticle transport, aggregation and deposition. *Environmental Nanotechnology. Applications and Impacts of Nanomaterials. Eds. MR Wiesner and JY Bottero***,** 231-294.

References

BRIGATTI, M. F., COLONNA, S., MALFERRARI, D., MEDICI, L. & POPPI, L. 2005. Mercury adsorption by montmorillonite and vermiculite: a combined XRD, TG-MS, and EXAFS study. *Applied Clay Science,* 28**,** 1-8.

BRINKER, C. 1988. Hydrolysis and condensation of silicates: effects on structure. *Journal of Non-Crystalline Solids,* 100**,** 31-50.

BROWN, J., MERCIER, L. & PINNAVAIA, T. 1999. Selective adsorption of Hg^{2+} by thiol-functionalized nanoporous silica. *Chemical Communications,* 1999**,** 69-70.

BROWN, J., RICHER, R. & MERCIER, L. 2000. One-step synthesis of high capacity mesoporous Hg^{2+} adsorbents by non-ionic surfactant assembly. *Microporous and mesoporous materials,* 37**,** 41-48.

BROWN, P., GILL, S. & ALLEN, S. 2001. Metal removal from wastewater using peat. *Water Research,* 34**,** 3907-3916.

BRUCE, I., TAYLOR, J., TODD, M., DAVIES, M., BORIONI, E., SANGREGORIO, C. & SEN, T. 2004. Synthesis, characterisation and application of silica-magnetite nanocomposites. *Journal of Magnetism and Magnetic Materials,* 284**,** 145-160.

CADENA, F., RIZVI, R. & PETERS, R. W. Year. Feasibility studies for the removal of heavy metals from solution using tailored bentonite. *In:* Hazardous and Industrial Wastes - Proceedings of the Mid-Atlantic Industrial Waste Conference 1990. 77-94.

CAMPOS, D., EIC, M. & OCCELLI, M. 2000. Diffusion of high molecular weight hydrocarbons in mesostructured materials of the MCM-41 type. *Studies in Surface Science and Catalysis,* 129**,** 639-648.

CARPENTER, E. 2001. Iron nanoparticles as potential magnetic carriers. *Journal of Magnetism and Magnetic Materials,* 225**,** 17-20.

CELIS, R., HERMOSIN, M. & CORNEJO, J. 2000. Heavy metal adsorption by functionalized clays. *Environmental Science & Technology,* 34**,** 4593-4599.

CHEN, MCKIMMY, E. J., PINNAVAIA, T. J. & HAYES, K. F. 2004. XAS Study of Mercury(II) Ions Trapped in Mercaptan−Functionalized Mesostructured Silicate with a Wormhole Framework Structure. *Environmental Science & Technology,* 38**,** 4758-4762.

CHEN, C. Y., LI, H. X. & DAVIS, M. E. 1993. Studies on mesoporous materials:: I. Synthesis and characterization of MCM-41. *Microporous Materials,* 2**,** 17-26.

CHEN, X., FENG, X., LIU, J., FRYXELL, G. & GONG, M. 1999. Mercury separation and immobilization using self-assembled monolayers on mesoporous supports (SAMMS). *Separation Science and Technology,* 34**,** 1121-1132.

CHOJNACKI, A., CHOJNACKA, K., HOFFMANN, J. & GORECKI, H. 2004. The application of natural zeolites for mercury removal: from laboratory tests to industrial scale. *Minerals Engineering,* 17**,** 933-937.

CLARKSON, T. 1998. Human toxicology of mercury. *The Journal of Trace Elements in Experimental Medicine,* 11**,** 303-317.

COLVIN, V. 2003. The potential environmental impact of engineered nanomaterials. *Nature Biotechnology,* 21**,** 1166-1170.

COMMISSION, E. 2006. Directive 2006/11/EC of the European Parliament and of the Council of 15 February 2006 on pollution caused by certain dangerous substances discharged into the aquatic environment of the Community. *OJ L,* 4**,** 52-59.

References

COPELAND, D., FACER, M., NEWTON, R. & WALKER, P. 1996. Use of poly (ethylene terephthalate) plastic bottles for the sampling, transportation and storage of potable water prior to mercury determination. *The Analyst,* 121**,** 173-176.

CORMA, A. 1997. From microporous to mesoporous molecular sieve materials and their use in catalysis. *Chemical Reviews,* 97**,** 2373-2420.

CRINI, G. 2005. Recent developments in polysaccharide-based materials used as adsorbents in wastewater treatment. *Progress in Polymer Science,* 30**,** 38-70.

CUNDY, C. S. & COX, P. A. 2005. The hydrothermal synthesis of zeolites: Precursors, intermediates and reaction mechanism. *Microporous and Mesoporous Materials,* 82**,** 1-78.

CYR, P. J., SURI, R. P. S. & HELMIG, E. D. 2002. A pilot scale evaluation of removal of mercury from pharmaceutical wastewater using granular activated carbon. *Water research,* 36**,** 4725-4734.

DA'NA, E. & SAYARI, A. 2011. Effect of regeneration conditions on the cyclic performance of amine-modified SBA-15 for removal of copper from aqueous solutions: Composite surface design methodology. *Desalination***,** 277, 54-60.

DABROWSKI, A. 2001. Adsorption -- from theory to practice. *Advances in Colloid and Interface Science,* 93**,** 135-224.

DABROWSKI, A., HUBICKI, Z., PODKOSCIELNY, P. & ROBENS, E. 2004. Selective removal of the heavy metal ions from waters and industrial wastewaters by ion-exchange method. *Chemosphere,* 56**,** 91-106.

DAVIES, J. & LONG, D. 1968. The vibrational spectra of the halides and complex halides of the Group IIB elements. Part II. A Raman spectroscopic study of the systems HgX2–LiX (X= Cl, Br) in aqueous and tri-n-butyl phosphate solutions. *Journal of the Chemical Society***, A,** 2564-2568.

DAVIS, M. E. 2002. Ordered porous materials for emerging applications. *Nature,* 417**,** 813-821.

DE FARIA, D. L. A., VENÂNCIO SILVA, S. & DE OLIVEIRA, M. T. 1997. Raman microspectroscopy of some iron oxides and oxyhydroxides. *Journal of Raman Spectroscopy,* 28**,** 873-878.

DEERE, J., MAGNER, E., WALL, J. G. & HODNETT, B. K. 2002. Mechanistic and structural features of protein adsorption onto mesoporous silicates. *The Journal of Physical Chemistry B,* 106**,** 7340-7347.

DELACÔTE, C., GASLAIN, F. O. M., LEBEAU, B. & WALCARIUS, A. 2009a. Factors affecting the reactivity of thiol-functionalized mesoporous silica adsorbents toward mercury (II). *Talanta,* 79**,** 877-886.

DELACÔTE, C., GASLAIN, F. O. M., LEBEAU, B. & WALCARIUS, A. 2009b. Factors affecting the reactivity of thiol-functionalized mesoporous silica adsorbents toward mercury(II). *Talanta,* 79**,** 877-886.

DIALLO, M. & SAVAGE, N. 2005. Nanoparticles and water quality. *Journal of Nanoparticle Research,* 7**,** 325-330.

DIAS, J., ALVIM-FERRAZ, M., ALMEIDA, M., RIVERA-UTRILLA, J. & SȻNCHEZ-POLO, M. 2007. Waste materials for activated carbon preparation and its use in aqueous-phase treatment: A review. *Journal of Environmental Management,* 85**,** 833-846.

References

DIRECTIVE, E. C. N. 1998. Council Directive 91/676/EEC of 12 December 1991 concerning the protection of waters against pollution caused by nitrates from agricultural sources. *Official Journal L,* 375**,** 12.

DONG, J. & XU, Z. 2009. Synthesis of mesoporous silica coatings on magnetite particles for mercury removal application. *SME Annual conference.* Englewood, USA.

DONG, J., XU, Z. & WANG, F. 2008. Engineering and characterization of mesoporous silica-coated magnetic particles for mercury removal from industrial effluents. *Applied Surface Science,* 254**,** 3522-3530.

DONIA, A. M., ATIA, A. A. & ELWAKEEL, K. Z. 2008. Selective separation of mercury (II) using magnetic chitosan resin modified with Schiff's base derived from thiourea and glutaraldehyde. *Journal of Hazardous Materials,* 151**,** 372-379.

DOSEV, D., NICHKOVA, M. & KINNEDY, I. (eds.) 2007. *Nanomaterials Based in Environmental Sensors,* Singapore: Stallion Press.

DUJARDIN, M., CAZE, C. & VROMAN, I. 2000. Ion-exchange resins bearing thiol groups to remove mercury.: Part 1: synthesis and use of polymers prepared from thioester supported resin. *Reactive and Functional Polymers,* 43**,** 123-132.

EDWARDS, H., JOHNSON, A. & LAWSON, E. 1995. Structural determination of substituted mercaptothiadiazoles using FT-Raman and FT-IR spectroscopy. *Journal of Molecular Structure,* 351**,** 51-63.

EL-LATIF, M. M. A., IBRAHIM, A. M. & EL-KADY, M. 2010. Adsorption Equilibrium, kinetics and thermodynamics of methylene blue from aqueous solutions using biopolymer oak sawdust composite. *Journal of American Science,* 6.

EL-MOGAZI, D., LISK, D. & WEINSTEIN, L. 1988. A review of physical, chemical, and biological properties of fly ash and effects on agricultural ecosystems. *The Science of the Total Environment,* 74**,** 1.

EPA 1997. Fate and Transport of Mercury in the Environment. *Mercury Study Report Congress.*

EPA 2005. Mercury in Water by Cold Vapor Atomic Fluorescence Spectroscopy.

EPA 2007. Treatment technologies for Mercury in Soil, Waste and water, Remediation and technology Innovation. . Washington, DC.

EPA. 2009. *Environmental Effects of Mercury* [Online]. US. EPA. Available: http://www.epa.gov/mercury/eco.htm [Accessed 19 March 2009].

EPA, U. S. 1990. Environmental Pollution Control Alternatives: Drinking Water Treatment for Small Communities New York.

EPA, U. S. 1998. Office Research and Development. Capsules Report, Aqueous Mercury Treatment. EPA-625-R-97-004.

EPA, U. S. 2012. *Drinking Water Contaminants* [Online]. EPA, U. S. Available: http://water.epa.gov/drink/contaminants/index.cfm [Accessed 12 August 2012].

EVANGELISTA, S. M., DEOLIVEIRA, E., CASTRO, G. R., ZARA, L. F. & PRADO, A. G. S. 2007. Hexagonal mesoporous silica modified with 2-mercaptothiazoline for removing mercury from water solution. *Surface Science,* 601**,** 2194-2202.

EVERETT, D., HAUL, R., MOSCOU, L., PIEROTTI, R., ROUQUEROL, J. & SIEMIENIEWSKA, T. 1985. Reporting Physisorption Data for Gas Solid

Systems with Special Reference to the Determination of Surface-Area and Porosity (Recommendations 1984). *Pure and Applied Chemistry* 57**,** 603.

FADINI, P. & JARDIM, W. 2000. Storage of natural water samples for total and reactive mercury analysis in PET bottles. *The Analyst,* 125**,** 549-551.

FARAJI, M., YAMINI, Y. & REZAEE, M. 2010. Magnetic nanoparticles: synthesis, stabilization, functionalization, characterization, and applications. *Journal of the Iranian Chemical Society* 7**,** 1-37.

FARRÉ, M., GAJDA-SCHRANTZ, K., KANTIANI, L. & BARCELÓ, D. 2009. Ecotoxicity and analysis of nanomaterials in the aquatic environment. *Analytical and Bioanalytical Chemistry,* 393**,** 81-95.

FARRÉ, M., SANCHÍS, J. & BARCELÓ, D. 2011. Analysis and assessment of the occurrence, the fate and the behavior of nanomaterials in the environment. *TrAC Trends in Analytical Chemistry*.

FAUST, S. & ALY, O. 1998. *Chemistry of water treatment*, CRC Press.

FENG, X., FRYXELL, G. E., WANG, L. Q., KIM, A. Y., LIU, J. & KEMNER, K. M. 1997. Functionalized monolayers on ordered mesoporous supports. *Science,* 276**,** 923-926.

FIGUEIRA, P., LOPES, C., DANIEL-DA-SILVA, A., PEREIRA, E., DUARTE, A. & TRINDADE, T. 2011. Removal of mercury (II) by dithiocarbamate surface functionalized magnetite particles: Application to synthetic and natural spiked waters. *Water Research,* 45**,** 5773-5784.

FINSY, R. 1994. Particle sizing by quasi-elastic light scattering. *Advances in Colloid and Interface Science,* 52**,** 79-143.

GASLAIN, F., DELACÔTE, C., LEBEAU, B., MARICHAL, C., PATARIN, J. & WALCARIUS, A. 2007. Study of mercury (II) binding to thiol-modified ordered mesoporous silicas by analytical and electrochemical analyses: influence of the pore structure and the functionalization process. *Studies in Surface Science and Catalysis,* 165**,** 417-420.

GE, J., HU, Y., BIASINI, M., BEYERMANN, W. P. & YIN, Y. 2007. Superparamagnetic magnetite colloidal nanocrystal clusters. *Angewandte Chemie International Edition,* 46**,** 4342-4345.

GIRGINOVA, P. I., DANIEL-DA-SILVA, A. L., LOPES, C. B., FIGUEIRA, P., OTERO, M., AMARAL, V. S., PEREIRA, E. & TRINDADE, T. 2010. Silica coated magnetite particles for magnetic removal of Hg2+ from water. *Journal of Colloid and Interface Science,* 345**,** 234-240.

GOLAS, P. L., LOUIE, S., LOWRY, G. V., MATYJASZEWSKI, K. & TILTON, R. D. 2010. Comparative study of polymeric stabilizers for magnetite nanoparticles using ATRP. *Langmuir***,** 16890-16900.

GOLDSTEIN, J. 2007. *Scanning electron microscopy and X-ray microanalysis,* New York, Springer.

GREEN-RUIZ, C. 2009. Effect of salinity and temperature on the adsorption of Hg (II) from aqueous solutions by a Ca-montmorillonite. *Environmental Technology,* 30**,** 63-68.

GRINSTAFF, M., SALAMON, M. & SUSLICK, K. 1993. Magnetic properties of amorphous iron. *Physical Review B,* 48**,** 269-273.

GUERRA, D. L., VIANA, R. R. & AIROLDI, C. 2009. Adsorption of mercury cation on chemically modified clay. *Materials Research Bulletin,* 44**,** 485-491.

References

GUO, J., LOU, H., ZHAO, H., WANG, X. & ZHENG, X. 2004. Novel synthesis of high surface area MgAl 2 O 4 spinel as catalyst support. *Materials Letters,* 58**,** 1920-1923.

GUO, S., LI, D., ZHANG, L., LI, J. & WANG, E. 2009. Monodisperse mesoporous superparamagnetic single-crystal magnetite nanoparticles for drug delivery. *Biomaterials,* 30**,** 1881-1889.

GUPTA, A. K. & GUPTA, M. 2005. Synthesis and surface engineering of iron oxide nanoparticles for biomedical applications. *Biomaterials,* 26**,** 3995-4021.

GUTHRIE, C. P. & REARDON, E. J. 2008. Metastability of MCM-41 and Al-MCM-41. *The Journal of Physical Chemistry A,* 112**,** 3386-3390.

HAHN, K., KÄRGER, J. & KUKLA, V. 1996. Single-file diffusion observation. *Physical Review Letters,* 76**,** 2762-2765.

HAMLEY, I. 2003. Nanotechnology with soft materials. *Angewandte Chemie International Edition,* 42**,** 1692-1712.

HAN, S., KIM, M. & HYEON, T. 2003. Direct fabrication of mesoporous carbons using in-situ polymerized silica gel networks as a template. *Carbon,* 41**,** 1525-1532.

HARRIS, P. J. F., HERNÁNDEZ, E. & YAKOBSON, B. I. 2004. Carbon nanotubes and related structures: new materials for the twenty-first century. *American Journal of Physics,* 72**,** 415.

HE, F. & ZHAO, D. 2005. Preparation and Characterization of a New Class of Starch-Stabilized Bimetallic Nanoparticles for Degradation of Chlorinated Hydrocarbons in Water. *Environmental Science & Technology,* 39**,** 3314-3320.

HE, J., YANG, X., EVANS, D. & DUAN, X. 2003. New methods to remove organic templates from porous materials. *Materials Chemistry and Physics,* 77**,** 270-275.

HERRERO, R., LODEIRO, P., REY-CASTRO, C., VILARIÑO, T. & SASTRE DE VICENTE, M. E. 2005. Removal of inorganic mercury from aqueous solutions by biomass of the marine macroalga Cystoseira baccata. *Water research,* 39**,** 3199-3210.

HESTERBERG, D., CHOU, J. W., HUTCHISON, K. J. & SAYERS, D. E. 2001. Bonding of Hg (II) to reduced organic sulfur in humic acid as affected by S/Hg ratio. *Environmental Science & Technology,* 35**,** 2741-2745.

HISSLER, C. & PROBST, J. 2006. Impact of mercury atmospheric deposition on soils and streams in a mountainous catchment (Vosges, France) polluted by chlor-alkali industrial activity: The important trapping role of the organic matter. *Science of the Total Environment,* 361**,** 163-178.

HOFFMANN, G. G., BROCKNER, W. & STEINFATT, I. 2001. Bis(n-alkanethiolato)mercury(II) compounds, $Hg(SC_nH_{2n+1})2$ (n = 1 to 10, 12): Preparation methods, vibrational spectra, GC/MS investigations, and exchange reactions with diorganyl disulfides. *Inorganic Chemistry,* 40**,** 977-985.

HOYT, M. (ed.) 2007. *Analysis of nanopartcles in the environment,* New York: Taylor & Francis.

HOZUMI, A., YOKOGAWA, Y., KAMEYAMA, T., HIRAKU, K., SUGIMURA, H., TAKAI, O. & OKIDO, M. 2000. Photocalcination of mesoporous silica films using vacuum ultraviolet light. *Advanced Materials,* 12**,** 985-987.

HU, J., CHEN, G. & LO, I. 2005a. Removal and recovery of Cr (VI) from wastewater by maghemite nanoparticles. *Water Research,* 39**,** 4528-4536.

References

HU, J., CHEN, G. & LO, I. 2006. Selective removal of heavy metals from industrial wastewater using maghemite nanoparticle: Performance and mechanisms. *Journal of Environmental Engineering,* 132**,** 709.

HU, J., LO, I. & CHEN, G. 2004. Removal of Cr (VI) by magnetite nanoparticle. *Water science and technology: a journal of the International Association on Water Pollution Research,* 50**,** 139.

HU, J., LO, I. & CHEN, G. 2005b. Fast removal and recovery of Cr (VI) using surface-modified jacobsite (MnFe 2 0 4) nanoparticles. *Langmuir,* 21**,** 11173-11179.

HU, J., LO, I. & CHEN, G. 2007. Comparative study of various magnetic nanoparticles for Cr (VI) removal. *Separation and Purification Technology,* 56**,** 249-256.

HUANG, C. & HU, B. 2008. Silica-coated magnetic nanoparticles modified with [γ]-mercaptopropyltrimethoxysilane for fast and selective solid phase extraction of trace amounts of Cd, Cu, Hg, and Pb in environmental and biological samples prior to their determination by inductively coupled plasma mass spectrometry. *Spectrochimica Acta Part B: Atomic Spectroscopy,* 63**,** 437-444.

HUANG, S., FAN, Y., CHENG, Z., KONG, D., YANG, P., QUAN, Z., ZHANG, C. & LIN, J. 2009. Magnetic Mesoporous Silica Spheres for Drug Targeting and Controlled Release. *The Journal of Physical Chemistry C,* 113**,** 1775-1784.

ILLÉS, E. & TOMBÁCZ, E. 2006. The effect of humic acid adsorption on pH-dependent surface charging and aggregation of magnetite nanoparticles. *Journal of Colloid and Interface Science,* 295**,** 115-123.

ITO, T., SUN, L., BEVAN, M. A. & CROOKS, R. M. 2004. Comparison of nanoparticle size and electrophoretic mobility measurements using a carbon-nanotube-based coulter counter, dynamic light scattering, transmission electron microscopy, and phase analysis light scattering. *Langmuir,* 20**,** 6940-6945.

ITOH, H. & SUGIMOTO, T. 2003. Systematic control of size, shape, structure, and magnetic properties of uniform magnetite and maghemite particles. *Journal of Colloid and Interface Science,* 265**,** 283-295.

JAL, P., PATEL, S. & MISHRA, B. 2004. Chemical modification of silica surface by immobilization of functional groups for extractive concentration of metal ions. *Talanta,* 62**,** 1005-1028.

JEGADEESAN, G., MONDAL, K. & LALVANI, S. B. 2005. Arsenate remediation using nanosized modified zerovalent iron particles. *Environmental Progress,* 24**,** 289-296.

JEON, C. & HA PARK, K. 2005. Adsorption and desorption characteristics of mercury (II) ions using aminated chitosan bead. *Water Research,* 39**,** 3938-3944.

JÉRÔME ROSE, C. & BRANT, J. 2007. Methods for structural and chemical characterization of nanomaterials. *Environmental nanotechnology: applications and impacts of nanomaterials***,** 105.

JIANG, D., ZHANG, S. & ZHAO, H. 2007. Photocatalytic degradation characteristics of different organic compounds at TiO2 nanoporous film electrodes with mixed anatase/rutile phases. *Environmental Science & Technology,* 41**,** 303-308.

JUNTAPRAM, K., PRAPHAIRAKSIT, N., SIRALEARTMUKUL, K. & MUANGSIN, N. 2011. Synthesis and characterization of chitosan-homocysteine thiolactone as a mucoadhesive polymer. *Carbohydrate Polymers,* 87, 2399-2408.

KACAR, Y., ARPA, C., TAN, S., DENIZLI, A., GENC, O. & ARICA, M. Y. 2002. Biosorption of Hg (II) and Cd (II) from aqueous solutions: comparison of

biosorptive capacity of alginate and immobilized live and heat inactivated Phanerochaete chrysosporium. *Process Biochemistry,* 37**,** 601-610.

KAMARA, P., JACOB, S. & SRINIVASAN, D. 1989. Removal of heavy metals from waste water by sulphide precipitation technique. *Bull. Electrochem.,* 5**,** 572-574.

KANEL, S., MANNING, B., CHARLET, L. & CHOI, H. 2005. Removal of Arsenic (III) from Groundwater by Nanoscale Zero-Valent Iron. *Environmental science & technology,* 39**,** 1291-1298.

KANEL, S. & NEPAL, D. (eds.) 2008. *Nanoscale Porous materials for water Treatmenmt: davances and Challenges,* New York: ASSE.

KANG, Y., RISBUD, S., RABOLT, J. & STROEVE, P. 1996. Synthesis and Characterization of Nanometer-Size Fe_3O_4 and [γ]-Fe2O3 Particles. *Chem. Mater,* 8**,** 2209-2211.

KARA, D. 2005. Separation and Removal of Mercury (II) from Water Samples Using (Acetylacetone)-2-Thiol-Phenyleneimine Immobilized on Anion-Exchange Resin Prior to Determination by Cold Vapor Inductively Coupled Plasma Atomic Emission Spectroscopy. *Analytical Letters,* 38**,** 2217-2230.

KEMNER, K., FENG, X., LIU, J., FRYXELL, G. E., WANG, L. Q., KIM, A. Y., GONG, M. & MATTIGOD, S. 1999. Investigation of the local chemical interactions between Hg and self-assembled monolayers on mesoporous supports. *Journal of Synchrotron Radiation,* 6**,** 633-635.

KHAN, A. 2008. Preparation and characterization of magnetic nanoparticles embedded in microgels. *Materials Letters,* 62**,** 898-902.

KHATOON-ABADI, A., SHEIKH HOSEINI, A. & KHALILI, B. 2008. Effect of mercury on the human health and environment: an overview. *International Journal of Food Safety, Nutrition and Public Health,* 1**,** 33-50.

KIM, Y., LEE, B. & YI, J. 2003. Preparation of functionalized mesostructured silica containing magnetite (MSM) for the removal of copper ions in aqueous solutions and its magnetic separation. *Separation Science and Technology,* 38**,** 2533-2548.

KIM, Y. H. & CARRAWAY, E. R. 2000. Dechlorination of pentachlorophenol by zero valent iron and modified zero valent irons. *Environmental Science & Technology,* 34**,** 2014-2017.

KOMAROWSKI, S. & YU, Q. 1997. Ammonium ion removal from wastewater using Australian natural zeolite: Batch equilibrium and kinetic studies. *Environmental Technology,* 18**,** 1085-1097.

KRAEMER, S. M. 2004. Iron oxide dissolution and solubility in the presence of siderophores. *Aquatic Sciences-Research Across Boundaries,* 66**,** 3-18.

KRESGE, C., LEONOWICZ, M., ROTH, W., VARTULI, J. & BECK, J. 1992. Ordered mesoporous molecular sieves synthesized by a liquid-crystal template mechanism. *Nature,* 359**,** 710-712.

KU, Y. & CHEN, C. H. 1992. Kinetic study of copper deposition on iron by cementation reaction. *Separation science and technology,* 27**,** 1259-1275.

KUNDU, D., ZHOU, H. & HONMA, I. 1998. Thermally induced structural changes of lamellar and one-dimensional hexagonal mesoporous silica thin films. *Journal of Materials Science Letters,* 17**,** 2089-2092.

KURNIAWAN, T., CHAN, G., LO, W. & BABEL, S. 2006. Comparisons of low-cost adsorbents for treating wastewaters laden with heavy metals. *Science of The Total Environment,* 366**,** 409-426.

References

LANGMUIR, I. 1918. The adsorption of gases on plane surfaces of glass, mica and platinum. *Journal of the American Chemical Society,* 40**,** 1361-1403.

LARSON, K. & WIENCEK, J. 1992. Liquid ion exchange for mercury removal from water over a wide pH range. *Industrial & Engineering Chemistry Research,* 31**,** 2714-2722.

LECOANET, H. F., BOTTERO, J. Y. & WIESNER, M. R. 2004. Laboratory assessment of the mobility of nanomaterials in porous media. *Environmental Science & Technology,* 38**,** 5164-5169.

LEE, B., KIM, Y., LEE, H. & YI, J. 2001. Synthesis of functionalized porous silicas via templating method as heavy metal ion adsorbents: the introduction of surface hydrophilicity onto the surface of adsorbents. *Microporous and Mesoporous Materials,* 50**,** 77-90.

LEE, C. H., PARK, S. H., CHUNG, W., KIM, J. Y. & KIM, S. H. 2011. Preparation and characterization of surface modified silica nanoparticles with organo-silane compounds. *Colloids and Surfaces A: Physicochemical and Engineering Aspects*.

LEE, Y., LEE, J., BAE, C. J., PARK, J. G., NOH, H. J., PARK, J. H. & HYEON, T. 2005. Large-scale synthesis of uniform and crystalline magnetite nanoparticles using reverse micelles as nanoreactors under reflux conditions. *Advanced Functional Materials,* 15**,** 503-509.

LEOFANTI, G., PADOVAN, M., TOZZOLA, G. & VENTURELLI, B. 1998. Surface area and pore texture of catalysts. *Catalysis Today,* 41**,** 207-219.

LEOPOLD, K., FOULKES, M. & WORSFOLD, P. J. 2009. Preconcentration techniques for the determination of mercury species in natural waters. *TrAC Trends in Analytical Chemistry,* 28**,** 426-435.

LESAINT, C., FRÉBAULT, F., DELACÔTE, C., LEBEAU, B., MARICHAL, C., WALCARIUS, A. & PATARIN, J. 2005. Synthesis and characterization of mesoporous silicas functionalized by thiol groups, and application as sorbents for mercury (II). *In:* ABDELHAMID, S. & MIETEK, J. (eds.) *Studies in Surface Science and Catalysis.* Elsevier.

LEWINSKY, A. 2007. *Hazardous materials and wastewater: treatment, removal and analysis*, Nova Science Publishers.

LI, L., FAN, M., BROWN, R. C., LEEUWEN, J. V., WANG, J., WANG, W., SONG, Y. & ZHANG, P. 2006. Synthesis, properties, and environmental applications of nanoscale iron-based materials: A review. *Critical Reviews in Environmental Science and Technology,* 36**,** 405-431.

LI, X.-G., MA, X.-L., SUN, J. & HUANG, M.-R. 2009. Powerful Reactive Sorption of Silver(I) and Mercury(II) onto Poly(o-phenylenediamine) Microparticles. *Langmuir,* 25**,** 1675-1684.

LI, Y. H., WANG, S., LUAN, Z., DING, J., XU, C. & WU, D. 2003. Adsorption of cadmium (II) from aqueous solution by surface oxidized carbon nanotubes. *Carbon,* 41**,** 1057-1062.

LI, Y. H., WANG, S., WEI, J., ZHANG, X., XU, C., LUAN, Z., WU, D. & WEI, B. 2002. Lead adsorption on carbon nanotubes. *Chemical Physics Letters,* 357**,** 263-266.

LIANG, X., XU, Y., SUN, G., WANG, L., SUN, Y. & QIN, X. 2009. Preparation, characterization of thiol-functionalized silica and application for sorption of Pb^{2+}

and Cd^{2+}. *Colloids and Surfaces A: Physicochemical and Engineering Aspects,* 349**,** 61-68.

LIN, S. & JUANG, R. 2009. Adsorption of phenol and its derivatives from water using synthetic resins and low-cost natural adsorbents: A review. *Journal of environmental management,* 90**,** 1336-1349.

LIU, J. & DU, X. 2011. Fast removal of aqueous Hg (II) with quaternary ammonium-functionalized magnetic mesoporous silica and silica regeneration. *J. Mater. Chem.*

LIU, J., ZHAO, Z. & JIANG, G. 2008. Coating Fe_3O_4 magnetic nanoparticles with humic acid for high efficient removal of heavy metals in water. *Environ. Sci. Technol,* 42**,** 6949-6954.

LIU, Q., XU, Z., FINCH, J. & EGERTON, R. 1998. A novel two-step silica-coating process for engineering magnetic nanocomposites. *Chemistry of materials,* 10**,** 3936-3940.

LOGAR, N. Z. & KAUCIC, V. 2006. Nanoporous materials: from catalysis and hydrogen storage to wastewater treatment. *Acta Chimica Slovenica,* 53**,** 117.

LU, A., SALABAS, E. & SCHUTH, F. 2007. Magnetic nanoparticles: synthesis, protection, functionalization, and application. *Angewandte Chemie International Edition,* 46.

LU, M. & ZHAO, X. S. 2011. *Nanoporous Materials Science and Engineering,* Imperial College Press.

MALM, O., BRANCHES, F. J. P., AKAGI, H., CASTRO, M. B., PFEIFFER, W. C., HARADA, M., BASTOS, W. R. & KATO, H. 1995. Mercury and methylmercury in fish and human hair from the Tapajos river basin, Brazil. *Science of the Total Environment,* 175**,** 141-150.

MAMADOU, D., DUNCAN, J., SAVAGE, N., STREET, A. & SUSTICH, R. 2008. Nanotechnology Applications for Clean Water. *Micro & Nano Technologies***,** 700.

MANJU, G., ANOOP KRISHNAN, K., VINOD, V. & ANIRUDHAN, T. 2002. An investigation into the sorption of heavy metals from wastewaters by polyacrylamide-grafted iron (III) oxide. *Journal of Hazardous Materials,* 91**,** 221-238.

MANOHAR, D., ANOOP KRISHNAN, K. & ANIRUDHAN, T. 2002. Removal of mercury (II) from aqueous solutions and chlor-alkali industry wastewater using 2-mercaptobenzimidazole-clay. *Water Research,* 36**,** 1609-1619.

MATTIGOD, S., FRYXELL, G. & PARKER, K. 2007. *A Thiol-Functionalized Nanoporous Silica Sorbent for Removal of Mercury from Actual Industrial Waste,* New York, World Scientific Pub Co Inc.

MATTIGOD, S. V., FENG, X., FRYXELL, G. E., LIU, J. & GONG, M. 1999. Separation of complexed mercury from aqueous wastes using self-assembled mercaptan on mesoporous silica. *Separation science and technology,* 34**,** 2329-2345.

MAYO, J., YAVUZ, C., YEAN, S., CONG, L., SHIPLEY, H., YU, W., FALKNER, J., KAN, A., TOMSON, M. & COLVIN, V. 2007. The effect of nanocrystalline magnetite size on arsenic removal. *Science and Technology of Advanced Materials,* 8**,** 71-75.

References

MCBAIN, J. W. 1909. XCIX. The mechanism of the adsorption ("sorption") of hydrogen by carbon. *The London, Edinburgh, and Dublin Philosophical Magazine and Journal of Science,* 18**,** 916-935.

MCCABE, W. L., SMITH, J. C. & HARRIOTT, P. 2005. *Unit Operations of Chemical Engineering*, McGraw-Hill Book Company New York.

MERCIER, L. & PINNAVAIA, T. J. 1997. Access in mesoporous materials: Advantages of a uniform pore structure in the design of a heavy metal ion adsorbent for environmental remediation. *Advanced Materials,* 9**,** 500-503.

MERCIER, L. & PINNAVAIA, T. J. 1998a. A functionalized porous clay heterostructure for heavy metal ion (Hg^{2+}) trapping. *Microporous and Mesoporous Materials,* 20**,** 101-106.

MERCIER, L. & PINNAVAIA, T. J. 1998b. Heavy metal ion adsorbents formed by the grafting of a thiol functionality to mesoporous silica molecular sieves: factors affecting Hg (II) uptake. *Environmental Science & Technology,* 32**,** 2749-2754.

MERRIFIELD, J. D. 2002. *Synthesis and Characterization of Thiol-Grafted Chitosan Beads for Mercury Removal.* PhD thesis, The University of Maine.

MEUNIER, V., NICOLAI, T. & DURAND, D. 2001. Structure of aggregating κ-carrageenan fractions studied by light scattering. *International Journal of Biological Macromolecules,* 28**,** 157-165.

MIZUKOSHI, Y., SHUTO, T., MASAHASHI, N. & TANABE, S. 2009. Preparation of superparamagnetic magnetite nanoparticles by reverse precipitation method: Contribution of sonochemically generated oxidants. *Ultrasonics Sonochemistry,* 16**,** 525-531.

MME11ZS-NANO 2008. Zetasizer Nano series User Manual MAN0317 Issue 4.0. *Malvern Instruments Ltd., England.* Malvern Instruments Ltd.

MOHAN, D., GUPTA, V., SRIVASTAVA, S. & CHANDER, S. 2000. Kinetics of mercury adsorption from wastewater using activated carbon derived from fertilizer waste. *Colloids and Surfaces A: Physicochemical and Engineering Aspects,* 177**,** 169-181.

MURDOCK, R. C., BRAYDICH-STOLLE, L., SCHRAND, A. M., SCHLAGER, J. J. & HUSSAIN, S. M. 2008. Characterization of nanomaterial dispersion in solution prior to in vitro exposure using dynamic light scattering technique. *Toxicological sciences,* 101**,** 239-253.

MURESEANU, M., CIOATERA, N., TRANDAFIR, I., GEORGESCU, I., FAJULA, F. & GALARNEAU, A. 2011. Selective Cu^{2+} adsorption and recovery from contaminated water using mesoporous hybrid silica bio-adsorbents. *Microporous and Mesoporous Materials,*146, 141-150.

MURESEANU, M., REISS, A., CIOATERA, N., TRANDAFIR, I. & HULEA, V. 2010. Mesoporous silica functionalized with 1-furoyl thiourea urea for Hg(II) adsorption from aqueous media. *Journal of Hazardous Materials,* 182**,** 197-203.

NAJA, G. M. & VOLESKY, B. 2010. Treatment of Metal-Bearing Effluents: Removal and Recovery. *Handbook on Heavy Metals in the Environment, Taylor & Francis and CRC Press, Boca Raton, FL***,** 247-291.

NAKAYAMA, T. & YAMAMOTO, T. 1999. Synthesis and magnetic properties of nanocluster composite. *Ceramic Transactions (USA),* 108**,** 257-264.

NALEWAJSKI, R. F. 1984. Electrostatic effects in interactions between hard (soft) acids and bases. *Journal of the American Chemical Society,* 106**,** 944-945.

References

NAM, K., GOMEZ-SALAZAR, S. & TAVLARIDES, L. 2003. Mercury (II) adsorption from wastewaters using a thiol functional adsorbent. *Industrial & Engineering Chemistry Research* 42**,** 1955-1964.

NAMASIVAYAM, C. & KADIRVELU, K. 1999. Uptake of mercury (II) from wastewater by activated carbon from an unwanted agricultural solid by-product: coirpith. *Carbon,* 37**,** 79-84.

NAMASIVAYAM, C. & PERIASAMY, K. 1993. Bicarbonate-treated peanut hull carbon for mercury (II) removal from aqueous solution. *Water Research,* 27**,** 1663-1668.

NAMDEO, M. & BAJPAI, S. 2008. Investigation of hexavalent chromium uptake by synthetic magnetite nanoparticles. *EJEAFChe,* 7**,** 3082-3094.

NANOMAGNETIC. 2009. *Magnetic materals cahrcterzation techanique and instrument* [Online]. Nanomagnetic.org. Available: http://www.nano.gov.sa [Accessed May 2009].

NARITA, A., NAKA, K. & CHUJO, Y. 2009. Facile control of silica shell layer thickness on hydrophilic iron oxide nanoparticles via reverse micelle method. *Colloids and Surfaces A: Physicochemical and Engineering Aspects,* 336**,** 46-56.

NASSAR, N. N. 2010. Rapid removal and recovery of Pb (II) from wastewater by magnetic nanoadsorbents. *Journal of Hazardous Materials,* 184**,** 538-546.

NEMEROW, N. L. & AGARDY, F. J. 1998. *Strategies of industrial and hazardous waste management,* Wiley.

NG, E. P. & MINTOVA, S. 2008. Nanoporous materials with enhanced hydrophilicity and high water sorption capacity. *Microporous and Mesoporous Materials,* 114**,** 1-26.

NOLL, K., GOUNARIS, V. & HOU, W. 1991. *Adsorption technology for air and water pollution control,* CRC.

NOLL, K. E., HAAS, C., SCHMIDT, C. & KODUKULA, P. 1985. Recovery, recycle and reuse of industrial wastes.

NOONEY, R. I., KALYANARAMAN, M., KENNEDY, G. & MAGINN, E. J. 2000. Heavy metal remediation using functionalized mesoporous silicas with controlled macrostructure. *Langmuir,* 17**,** 528-533.

NOONEY, R. I., THIRUNAVUKKARASU, D., CHEN, Y., JOSEPHS, R. & OSTAFIN, A. E. 2002. Synthesis of Nanoscale Mesoporous Silica Spheres with Controlled Particle Size. *Chemistry of Materials,* 14**,** 4721-4728.

NORELL, M. A., MAKOVICKY, P. & CLARK, J. M. 1997. Porous silica via colloidal crystallization. *Nature,* 389**,** 447.

NÜßLEIN, F., FEICHT, E. A., SCHULTE-HOSTEDE, S., SELTMANN, U. & KETTRUP, A. 1995. Exposure analysis of the inhabitants living in the neighbourhood of a mercury-contaminated industrial site. *Chemosphere,* 30**,** 2241-2248.

O'NEILL, P. 1998. *Environmental Chemistry,* 199, Taylor & Francis Ltd

OBARE, S. & MEYER, G. 2004. Nanostructured materials for environmental remediation of organic contaminants in water. *Journal of Environmental Science and Health. Part A, Toxic/Hazardous Substances & Environmental Engineering,* 39**,** 2549-2582.

References

OLIVEIRA, L., RIOS, R., FABRIS, J., SAPAG, K., GARG, V. & LAGO, R. 2003. Clay-iron oxide magnetic composites for the adsorption of contaminants in water. *Applied Clay Science,* 22**,** 169-177.

OTTO, M. & BAJPAI, S. 2007. Treatment technologies for mercury in soil, waste, and water. *Remediation Journal,* 18**,** 21-28.

OZIN, G. A., ARSENAULT, A. C. & CADEMARTIRI, L. 2009. *Nanochemistry: a chemical approach to nanomaterials,* Royal Society of Chemistry.

PACHECO, S., MEDINA, M., VALENCIA, F. & TAPIA, J. 2006. Removal of inorganic mercury from polluted water using structured nanoparticles. *Journal of Environmental Engineering,* 132**,** 342.

PACYNA, E. G., PACYNA, J. M., SUNDSETH, K., MUNTHE, J., KINDBOM, K., WILSON, S., STEENHUISEN, F. & MAXSON, P. 2010. Global emission of mercury to the atmosphere from anthropogenic sources in 2005 and projections to 2020. *Atmospheric Environment,* 44**,** 2487-2499.

PAEZ-HERNANDEZ, M., AGUILAR-ARTEAGA, K., GALAN-VIDAL, C., PALOMAR-PARDAVE, M., ROMERO-ROMO, M. & RAMIREZ-SILVA, M. 2005. Mercury ions removal from aqueous solution using an activated composite membrane. *Environmental Science & Technology,* 39**,** 7667.

PALMBERGER, T. F., HOMBACH, J. & BERNKOP-SCHNÜRCH, A. 2008. Thiolated chitosan: development and in vitro evaluation of an oral delivery system for acyclovir. *International Journal of Pharmaceutics,* 348**,** 54-60.

PARHAM, H., ZARGAR, B. & SHIRALIPOUR, R. 2012. Fast and efficient removal of mercury from water samples using magnetic iron oxide nanoparticles modified with 2-mercaptobenzothiazole. *Journal of Hazardous Materials,* 205–206**,** 94-100.

PATTERSON, J. & STEIN, L. 1997. Capsule Report: Aqueous Mercury Treatment. *NASA.*

PEARSON, R. 1968. Hard and soft acids and bases, HSAB, part 1: Fundamental principles. *Journal of Chemical Education,* 45**,** 581.

PEARSON, R. G. 1963. Hard and soft acids and bases. *Journal of the American Chemical Society,* 85**,** 3533-3539.

PEI, W., KUMADA, H., NATUSME, T., SAITO, H. & ISHIO, S. 2007. Study on magnetite nanoparticles synthesized by chemical method. *Journal of Magnetism and Magnetic Materials,* 310**,** 2375-2377.

PÉREZ-QUINTANILLA, D., DEL HIERRO, I., CARRILLO-HERMOSILLA, F., FAJARDO, M. & SIERRA, I. 2006. Adsorption of mercury ions by mercapto-functionalized amorphous silica. *Analytical and bioanalytical chemistry,* 384**,** 827-838.

PERRY, R. H., GREEN, D. W. & MALONEY, J. O. 2008. *Perry's chemical engineers' handbook,* McGraw-Hill New York.

PHAM, A. L. T., DOYLE, F. M. & SEDLAK, D. L. 2011. Inhibitory Effect of Dissolved Silica on the H_2O_2 Decomposition by Iron (III) and Manganese (IV) Oxides: Implications for H_2O_2-based In Situ Chemical Oxidation. *Environmental Science & Technology,* 46**,** 1055-1062.

PILLONI, M., NICOLAS, J., MARSAUD, V., BOUCHEMAL, K., FRONGIA, F., SCANO, A., ENNAS, G. & DUBERNET, C. 2010. PEGylation and preliminary

biocompatibility evaluation of magnetite–silica nanocomposites obtained by high energy ball milling. *International Journal of Pharmaceutics,* 401**,** 103-112.

PIPPAN, R., SCHERIAU, S., TAYLOR, A., HAFOK, M., HOHENWARTER, A. & BACHMAIER, A. 2010. Saturation of fragmentation during severe plastic deformation. *Annual Review of Materials Research,* 40**,** 319-343.

PIRRONE, N., CINNIRELLA, S., FENG, X., FINKELMAN, R. B., FRIEDLI, H. R., LEANER, J., MASON, R., MUKHERJEE, A. B., STRACHER, G. & STREETS, D. G. 2009. Global mercury emissions to the atmosphere from natural and anthropogenic sources. *Mercury Fate and Transport in the Global Atmosphere***,** 1-47.

PRADO, A. G. S., SALES, J. A. A., CARVALHO, R. M., RUBIM, J. C. & AIROLDI, C. 2004. Immobilization of 5-amino-1, 3, 4-thiadiazole-thiol onto silica gel surface by heterogeneous and homogeneous routes. *Journal of Non-Crystalline Solids,* 333**,** 61-67.

PURANIK, P. & PAKNIKAR, K. 1997. Biosorption of lead and zinc from solutions using Streptoverticillium cinnamoneum waste biomass. *Journal of Biotechnology,* 55**,** 113-124.

QU, L. & TIE, S. 2009. Mesoporous silica-coated superparamagnetic magnetite functionalized with CuO and its application as a desulfurizer. *Microporous and Mesoporous Materials,* 117**,** 402-405.

QU, S., YANG, H., REN, D., KAN, S., ZOU, G., LI, D. & LI, M. 1999. Magnetite nanoparticles prepared by precipitation from partially reduced ferric chloride aqueous solutions. *Journal of Colloid and Interface Science,* 215**,** 190-192.

RAM, A., ROKADE, M., ZINGDE, M. & BOROLE, D. 2009. Post-depositional memory record of mercury in sediment near the effluent disposal site of a chlor-alkali plant in Thane Creek–Mumbai Harbour, India. *Environmental technology,* 30**,** 765-783.

RAMAN, N., ANDERSON, M. & BRINKER, C. 1996. Template-based approaches to the preparation of amorphous, nanoporous silicas. *Chemistry of Materials* 8**,** 1682-1701.

RANDTKE, S. 1988. Organic contaminant removal by coagulation and related process combinations. *Journal American Water Works Association,* 88**,** 40-56.

RAO, M., REDDY, D., VENKATESWARLU, P. & SESHAIAH, K. 2009. Removal of mercury from aqueous solutions using activated carbon prepared from agricultural by-product/waste. *Journal of Environmental Management,* 90**,** 634-643.

RENGARAJ, S., KIM, Y., JOO, C. K. & YI, J. 2004. Removal of copper from aqueous solution by aminated and protonated mesoporous aluminas: kinetics and equilibrium. *Journal of Colloid and Interface Science,* 273**,** 14-21.

REZAEE, A., DERAYAT, J., MORTAZAVI, S., YAMINI, Y. & JAFARZADEH, M. 2005. Removal of mercury from chlor-alkali industry wastewater using Acetobacter xylinum cellulose. *American Journal of Environmental Sciences,* 1**,** 102-105.

RIO, S. & DELEBARRE, A. 2003. Removal of mercury in aqueous solution by fluidized bed plant fly ash. *Fuel,* 82**,** 153-159.

RITCHIE, S. M. C., KISSICK, K. E., BACHAS, L. G., SIKDAR, S. K., PARIKH, C. & BHATTACHARYYA, D. 2001. Polycysteine and other polyamino acid

functionalized microfiltration membranes for heavy metal capture. *Environmental Science & Technology,* 35**,** 3252-3258.

RODRIGUES, A., LE VAN, D. & DORDRECHT, D. 1989. *Adsorption, science and technology,* Buston, Kluer academic Puplisher.

RUTHVEN, D. 1984. *Principles of adsorption and adsorption processes,* Wiley-Interscience.

RYE, R. O. 2010. *Evolution of Ore Deposits and Technology Transfer Project: Isotope and Chemical Methods in Support of the US Geological Survey Science Strategy, 2003-2008,* US Geological Survey.

SANCHEZ-LOPEZ, J., JUSTO, A., FERNANDEZ, A., CONDE, C. & CONDE, A. 1997. Preparation and thermal evolution of vapour-condensed nanocrystalline iron. *Philosophical Magazine B,* 76**,** 663-667.

SAWYER, C. N., MCCARTY, P. L. & PARKIN, G. F. 2002. *Chemistry for Environmental Engineering and Science,* McGraw Hill Higher Education.

SAY, R., BIRLIK, E., ERDEMGIL, Z., DENIZLI, A. & ERSÖZ, A. 2008. Removal of mercury species with dithiocarbamate-anchored polymer/organosmectite composites. *Journal of Hazardous Materials,* 150**,** 560-564.

SCHNEIDER, M., TECHNIQUE, E., LEE, K., WU, P., BRAND, L., LEE, Y. & ISSAQ, H. 1998. Handbook of Instrumental Techniques for Analytical Chemistry. *Journal of Liquid Chromatography & Related Technologies,* 21**,** 3072-3076.

SCHUTTE, C. & FOCKE, W. 2007. Evaluation of nanotechnology for application in water and wastewater treatment and related aspects in South Africa. *Water Research Commission Report,* 195**,** 071-23.

SCHWERTMANN, U. 1991. Solubility and dissolution of iron oxides. *Plant and Soil,* 130**,** 1-25.

SEADER, J. & HENLEY, E. J. 2012. *Separation process principles,* New York, John Wiley & Sons, Inc.

SEN, A. K. & DE, A. K. 1987. Adsorption of mercury(II) by coal fly ash. *Water Research,* 21**,** 885-888.

SENEVIRATHNA, W., ZHANG, H. & GU, B. 2011. Effect of carboxylic and thiol ligands (oxalate, cysteine) on the kinetics of desorption of Hg (II) from kaolinite. *Water, Air, & Soil Pollution,* 215**,** 573-584.

SHAHBAZI, A., YOUNESI, H. & BADIEI, A. 2010. Functionalized SBA-15 mesoporous silica by melamine-based dendrimer amines for adsorptive characteristics of Pb (II); Cu (II) and Cd (II) heavy metal ions in batch and fixed bed column. *Chemical Engineering Journal,* 168, 505-518.

SHAN, G., SURAMPALLI, R. Y., TYAGI, R. D. & ZHANG, T. C. 2009. Nanomaterials for environmental burden reduction, waste treatment, and nonpoint source pollution control: a review. *Frontiers of Environmental Science & Engineering in China,* 3**,** 249-264.

SHAN, G. B., XING, J. M., ZHANG, H. Y. & LIU, H. Z. 2005. Biodesulfurization of dibenzothiophene by microbial cells coated with magnetite nanoparticles. *Applied and environmental microbiology,* 71**,** 4497-4502.

SHARMA, D. & FORSTER, C. 1993. Removal of hexavalent chromium using sphagnum moss peat. *Water research,* 27**,** 1201-1208.

References

SHIPLEY, H. J., YEAN, S., KAN, A. T. & TOMSON, M. B. 2009. Adsorption of arsenic to magnetite nanoparticles: Effect of particle concentration, pH, ionic strength, and temperature. *Environmental Toxicology and Chemistry,* 28**,** 509-515.

SILVERSTEIN, R. M., BASSLER, G. C. & MORRILL, T. C. 2005. *Spectroscopic Identification of Organic Compounds,* New Yourk, John Wiley and Sons.

SING, K., EVERETT, D., HAUL, R., MOSCOU, L., PIEROTTI, R., ROUQUEROL, J. & SIEMIENIEWSKA, T. 1985. Reporting physisorption data for gas/solid systems with special reference to the determination of surface area and porosity. *Pure and Applied Chemistry* 57**,** 603–619.

SKUBAL, L. & MESHKOV, N. 2002. Reduction and removal of mercury from water using arginine-modified TiO_2. *Journal of Photochemistry & Photobiology, A: Chemistry,* 148**,** 211-214.

SONG, B. Y., EOM, Y. & LEE, T. G. 2011. Removal and recovery of mercury from aqueous solution using magnetic silica nanocomposites. *Applied Surface Science,* 257**,** 4754-4759.

SONG, G., BO, J. & GUO, R. 2004. The characterization and property of polystyrene compounding of α-Fe_2O_3 in the nano-scale. *Colloid & Polymer Science,* 282**,** 656-660.

SONG, Z., CHEN, L., HU, J. & RICHARDS, R. 2009. NiO (111) nanosheets as efficient and recyclable adsorbents for dye pollutant removal from wastewater. *Nanotechnology,* 20**,** 275707.

SOUTHERNWATER 2012. H502-Water Supply Zone (18233). Southampton.

SPIEGEL, S. J. & VEIGA, M. M. 2010. International guidelines on mercury management in small-scale gold mining. *Journal of Cleaner Production,* 18**,** 375-385.

STAFIEJ, A. & PYRZYNSKA, K. 2007. Adsorption of heavy metal ions with carbon nanotubes. *Separation and Purification Technology,* 58**,** 49-52.

STIRK, W. & STADEN, J. 2002. Desorption of cadmium and the reuse of brown seaweed derived products as biosorbents. *Botanica marina,* 45**,** 9-16.

STOBER, W., FINK, A. & BOHN, E. 1968. Controlled growth of monodisperse silica spheres in the micron size range. *Journal of Colloid and interface Science,* 26**,** 62-69.

STUMM, W., HUPER, H. & CHAMPLIN, R. L. 1967. Formulation of polysilicates as determined by coagulation effects. *Environmental Science & Technology,* 1**,** 221-227.

STUMM, W. & MORGAN, J. J. 1996. *Aquatic chemistry: chemical equilibria and rates in natural water,* Wiley-Interscience.

SU, C. & PULS, R. W. 2001. Arsenate and arsenite removal by zerovalent iron: kinetics, redox transformation, and implications for in situ groundwater remediation. *Environmental Science & Technology,* 35**,** 1487-1492.

SUN, S., ZENG, H., ROBINSON, D. B., RAOUX, S., RICE, P. M., WANG, S. X. & LI, G. 2004. Monodisperse MFe_2O_4 (M = Fe, Co, Mn) Nanoparticles. *Journal of the American Chemical Society,* 126**,** 273-279.

SUS-RYSZKOWSKA, M., WEJRZANOWSKI, T., PAKIELA, Z. & KURZYDLOWSKI, K. 2004. Microstructure of ECAP severely deformed iron and its mechanical properties. *Materials Science & Engineering A,* 369**,** 151-156.

References

TAWABINI, B., AL-KHALDI, S., ATIEH, M. & KHALED, M. 2010. Removal of mercury from water by multi-walled carbon nanotubes. *Water science and technology: a journal of the International Association on Water Pollution Research,* 61**,** 591.

TCHOBANOGLOUS, G., BURTON, F. & STENSEL, H. 2003. *Wastewater engineering: treatment and reuse*, McGraw-Hill Science/Engineering/Math.

TCHOUNWOU, P., AYENSU, W., NINASHVILI, N. & SUTTON, D. 2003. Review: Environmental exposure to mercury and its toxicopathologic implications for public health. *Environmental Toxicology,* 18, 149-175.

THERON, J. 2008. Nanotechnology and Water Treatment: Applications and Emerging Opportunities. *Critical Reviews in Microbiology,* 34**,** 43-69.

THOMAS, W. J. & CRITTENDEN, B. D. 1998. *Adsorption Technology and Design*, Elsevier

TIWARI, D., BEHARI, J. & SEN, P. 2008. Application of Nanoparticles in Waste Water Treatment. *World Applied Sciences Journal,* 3**,** 417-433.

TRATNYEK, P. & JOHNSON, R. 2006. Nanotechnologies for environmental cleanup. *Nano Today,* 1**,** 44-48.

TSAI, W. T., HSIEN, K. J., CHANG, Y. M. & LO, C. C. 2005. Removal of herbicide paraquat from an aqueous solution by adsorption onto spent and treated diatomaceous earth. *Bioresource Technology,* 96**,** 657-663.

TUUTIJÄRVI, T., LU, J., SILLANPÄÄ, M. & CHEN, G. 2009. As (V) adsorption on maghemite nanoparticles. *Journal of hazardous materials,* 166**,** 1415-1420.

ULLRICH, S., ILYUSHCHENKO, M., KAMBEROV, I. & TANTON, T. 2007. Mercury contamination in the vicinity of a derelict chlor-alkali plant. Part I: Sediment and water contamination of Lake Balkyldak and the River Irtysh. *Science of the Total Environment,* 381**,** 1-16.

ULLRICH, S., TANTON, T. & ABDRASHITOVA, S. 2001. Mercury in the aquatic environment: a review of factors affecting methylation. *Critical Reviews in Environmental Science and Technology,* 31**,** 241-293.

ULUDAG, Y., ÖZBELGE, H. & YILMAZ, L. 1997. Removal of mercury from aqueous solutions via polymer-enhanced ultrafiltration. *Journal of Membrane Science,* 129**,** 93-99.

VAIDYA, S., THAPLYAL, P. & GANGULI, A. 2011. Enhanced functionalization of Mn_2O_3@ SiO_2 core-shell nanostructures. *Nanoscale Research Letters,* 6**,** 1-6.

VALENZUELA, R., FUENTES, M., PARRA, C., BAEZA, J., DURAN, N., SHARMA, S., KNOBEL, M. & FREER, J. 2009. Influence of stirring velocity on the synthesis of magnetite nanoparticles (Fe_3O_4) by the co-precipitation method. *Journal of Alloys and Compounds,* 488, 227-231.

VEIGA, M. M., MEECH, J. A. & OÑATE, N. 1994. Mercury pollution from deforestation. *Nature,* 368**,** 816-817.

VIJAYAKUMAR, R., KOLTYPIN, Y., FELNER, I. & GEDANKEN, A. 2000. Sonochemical synthesis and characterization of pure nanometer-sized Fe3O4 particles. *Materials Science & Engineering A,* 286**,** 101-105.

VIRARAGHAVAN, T. & KAPOOR, A. 1994. Adsorption of mercury from wastewater by bentonite. *Applied Clay Science,* 9**,** 31-49.

VON CANSTEIN, H., LI, Y., TIMMIS, K., DECKWER, W. D. & WAGNER-DÖBLER, I. 1999. Removal of Mercury from Chloralkali Electrolysis

Wastewater by a Mercury-Resistant Pseudomonas putidaStrain. *Applied and Environmental Microbiology,* 65**,** 5279-5284.

WAGNER-DÖBLER, I. 2003. Pilot plant for bioremediation of mercury-containing industrial wastewater. *Applied Microbiology and Biotechnology,* 62**,** 124-133.

WAGNER-DOBLER, I., VON CANSTEIN, H., LI, Y., TIMMIS, K. & DECKWER, W. 2000. Removal of mercury from chemical wastewater by microoganisms in technical scale. *Environmental Science & Technologyl,* 34**,** 4628-4634.

WALCARIUS, A. & DELACÔTE, C. 2003. Rate of access to the binding sites in organically modified silicates. 3. effect of structure and density of functional groups in mesoporous solids obtained by the co-condensation Route. *Chemistry of Materials,* 15**,** 4181-4192.

WALCARIUS, A. & DELACÔTE, C. 2005. Mercury(II) binding to thiol-functionalized mesoporous silicas: critical effect of pH and sorbent properties on capacity and selectivity. *Analytica Chimica Acta,* 547**,** 3-13.

WALCARIUS, A., ETIENNE, M. & LEBEAU, B. 2003. Rate of Access to the binding sites in organically modified silicates. 2. ordered mesoporous silicas grafted with amine or thiol groups. *Chemistry of Materials,* 15**,** 2161-2173.

WALCARIUS, A. & MERCIER, L. 2010. Mesoporous organosilica adsorbents: nanoengineered materials for removal of organic and inorganic pollutants. *J. Mater. Chem.,* 20**,** 4478-4511.

WANG, H., ZHANG, J. & HSU, T. 2004. Internal friction associated with phase transformation of nanograined bulk Fe–25 at.% Ni alloy. *Materials Science and Engineering: A,* 380**,** 408-413.

WANG, J., HUANG, P., HAMMER, U. & LIAW, W. 1985. Influence of selected cation and anion species on the adsorption of mercury (II) by montmorillonite. *Applied clay science,* 1**,** 125-132.

WANG, P. & LO, I. M. C. 2009. Synthesis of mesoporous magnetic γ-Fe2O3 and its application to Cr(VI) removal from contaminated water. *Water Research,* 43**,** 3727-3734.

WANG, X. S., LI, F. Y., HE, W. & MIAO, H. H. 2010a. Hg (II) Removal from Aqueous Solutions by Bacillus subtilis Biomass. *CLEAN–Soil, Air, Water,* 38**,** 44-48.

WANG, X. S., LU, H. J., ZHU, L., LIU, F. & REN, J. J. 2010b. Adsorption of Lead (II) Ions onto Magnetite Nanoparticles. *Adsorption Science & Technology,* 28**,** 407-417.

WARHURST, A. M., MCCONNACHIE, G. L. & POLLARD, S. J. T. 1997. Characterisation and applications of activated carbon produced from Moringa oleifera seed husks by single-step steam pyrolysis. *Water research,* 31**,** 759-766.

WARNER, M. G., WARNER, C. L., ADDLEMAN, R. S. & YANTASEE, W. 2009. Magnetic Nanomaterials for Environmental Applications.

WEE, K. & BAI, R. (eds.) 2008. *Nanoparticles as Sorbents for Removal of Heavy Metals Ions from Aqueous Solution,* New York: ASCE.

WHO 1991. *Environmental health criteria: Inorganic mercury*, World Health Organzation.

WHO 2006. *Guidelines for drinking-water quality: First addendum to volume* Geneva, World Heath Organization.

WHO 2011. Guidelines for drinking-water quality. Fourth ed.

References

WIGGINS, J., CARPENTER, E. & O'CONNOR, C. 2000. Phenomenological magnetic modeling of Au: Fe: Au nano-onions. *Journal of Applied Physics,* 87**,** 5651.

WILLIAMS, R. 1994. *Colloid and surface engineering: Applications in the process industries,* Butterworth-Heinemann UK.

WRIGHT, J. & SOMMERDIJK, N. 2001. *Sol-gel materials: chemistry and applications,* CRC.

WU, P. & XU, Z. 2005. Silanation of nanostructured mesoporous magnetic particles for heavy metal recovery. *Ind. Eng. Chem. Res,* 44**,** 816-824.

WU, P., ZHU, J. & XU, Z. 2004. Template-assisted synthesis of mesoporous magnetic nanocomposite particles. *Advanced Functional Materials,* 14**,** 345-351.

WU, W., XIAO, X., ZHANG, S., REN, F. & JIANG, C. 2011. Facile method to synthesize magnetic iron oxides/TiO_2 hybrid nanoparticles and their photodegradation application of methylene blue. *Nanoscale Research Letters,* 6**,** 533.

WU, X., MA, H., LI, J., ZHANG, J. & LI, Z. 2007. The synthesis of mesoporous aluminosilicate using microcline for adsorption of mercury (II). *Journal of Colloid and Interface Science,* 315**,** 555-561.

XI, G., WANG, C. & WANG, X. 2008. The Oriented Self-Assembly of Magnetic Fe_3O_4 Nanoparticles into Monodisperse Microspheres and Their Use as Substrates in the Formation of Fe3O4 Nanorods. *European Journal of Inorganic Chemistry,* 2008**,** 425-431.

XIA, M., CHEN, C., LONG, M., CHEN, C., CAI, W. & ZHOU, B. 2011. Magnetically separable mesoporous silica nanocomposite and its application in Fenton catalysis. *Microporous and Mesoporous Materials,* 145**,** 217-223.

XIAO, S., MA, H., SHEN, M., WANG, S., HUANG, Q. & SHI, X. 2011. Excellent copper (II) removal using zero-valent iron nanoparticle-immobilized hybrid electrospun polymer nanofibrous mats. *Colloids and Surfaces A: Physicochemical and Engineering Aspects*.

XU, Z. & DONG, J. 2008. Synthesis, characterization, and application of magnetic nanocomposites for the removal of heavy metals from industrial effluents. *Emerging Environmental Technologies***,** 105-148.

XU, Z., LIU, J., CHOUNG, J. W. & ZHOU, Z. 2003. Electrokinetic study of clay interactions with coal in flotation. *International Journal of Mineral Processing,* 68**,** 183-196.

XUE, X. & LI, F. 2008. Removal of Cu (II) from aqueous solution by adsorption onto functionalized SBA-16 mesoporous silica. *Microporous and Mesoporous Materials,* 116**,** 116-122.

YAKUP ARICA, M., BAYRAMOLU, G., YILMAZ, M., BEKTA, S. & GENC, O. 2004. Biosorption of Hg^{2+}, Cd^{2+}, and Zn^{2+} by Ca-alginate and immobilized wood-rotting fungus Funalia trogii. *Journal of hazardous materials,* 109**,** 191-199.

YAMAUCHI, Y., SUZUKI, N., SATO, K., FUKATA, N., MURAKAMI, M. & SHIMIZU, T. 2009. Active Mercury (II) Ion Removal: Stoichiometrically Controlled Thiol-Functionalized Mesoporous Silica by a Mass Production Spray Dry System. *Bulletin of the Chemical Society of Japan,* 82**,** 1039-1043.

YANG, R. T. 2003. Adsorbents: fundamentals and applications.

References

YANG, T. I., BROWN, R. N. C., KEMPEL, L. C. & KOFINAS, P. 2008. Magneto-dielectric properties of polymer-Fe_3O_4 nanocomposites. *Journal of Magnetism and Magnetic Materials,* 320**,** 2714-2720.

YEAN, S., CONG, L., YAVUZ, C., MAYO, J., YU, W., KAN, A., COLVIN, V. & TOMSON, M. 2005. Effect of magnetite particle size on adsorption and desorption of arsenite and arsenate. *Journal of Materials Research,* 20**,** 3255-3264.

YOSHITAKE, H., YOKOI, T. & TATSUMI, T. 2002. Adsorption of chromate and arsenate by amino-functionalized MCM-41 and SBA-1. *Chemistry of Materials,* 14**,** 4603-4610.

YUE, Z. & ECONOMY, J. 2005. Nanoparticle and nanoporous carbon adsorbents for removal of trace organic contaminants from water. *Journal of Nanoparticle Research,* 7**,** 477-487.

ZHANG, D. & CHENG, Y. 2011. Synthesis of Nano-Strontium Titanate Immobilised on the Silica Gel G and its Application in Removal of Heavy Metal Ions from Water. *Advanced Materials Research,* 194**,** 751-754.

ZHANG, L. X., LI, P. C., LIU, X. H., DU, L. W. & WANG, E. K. 2007. The Effect of Template Phase on the Structures of As-Synthesized Silica Nanoparticles with Fragile Didodecyldimethylammonium Bromide Vesicles as Templates. *Advanced Materials,* 19**,** 4279-4283.

ZHANG, W. 2003. Nanoscale Iron Particles for Environmental Remediation: An Overview. *Journal of Nanoparticle Research,* 5**,** 323-332.

ZHANG, X., WANG, Z. & GU, X. 1991. Simple combination of biodegradation and carbon adsorption—the mechanism of the biological activated carbon process. *Water research,* 25**,** 165-172.

ZHAO, L., SUN, J., ZHAO, Y., XU, L. & ZHAI, M. 2011. Removal of hazardous metal ions from wastewater by radiation synthesized silica-graft-dimethylaminoethyl methacrylate adsorbent. *Chemical Engineering Journal,* 170**,** 162-169.

ZHOU, L., WANG, Y., LIU, Z. & HUANG, Q. 2009. Characteristics of equilibrium, kinetics studies for adsorption of Hg(II), Cu(II), and Ni(II) ions by thiourea-modified magnetic chitosan microspheres. *Journal of Hazardous Materials,* 161**,** 995-1002.

ZHOU, Z., WANG, J., LIU, X. & CHAN, H. 2001. Synthesis of Fe_3O_4 nanoparticles from emulsions. *Journal of Material Chemistry,* 11**,** 1704-1709.